

UNIVERSITY  
OF SOUTHERN  
QUEENSLAND



*NUMERICAL INVESTIGATION OF STABILITY  
AND SETTLEMENT OF TUNNELS IN  
UNDRAINED CLAY*

A thesis submitted by

**Mathew S. Sams**

For the award of

**Master of Engineering Research**

2016

Australia



## ABSTRACT

This thesis describes the development, verification and use of a numerical model for investigating circular tunnels in cohesive soils. Using this model, important problems relating to tunnel construction can be studied. In particular, it studies the stability and settlement problems that arise during the construction of single and twin tunnels using tunnel-boring machines (TBM's). The developed numerical model simulates the movement and relaxation of the soil around the shield and tail void that occurs due to overcutting and the time delay to lining installation and back grouting. Using this numerical model, a parametric study is conducted which covers most of the practical range. Settlement and stability data is collected for single and twin tunnels.


The settlement data is analysed using a regression of the commonly used Gaussian equation on the settlement data. This approach allows a settlement parameter ( $i_x$ ) to be estimated reliably and accurately for each case. The results of this study are quite positive, settlement results compare well with previous experimental and observational results. Design charts using dimensionless ratios have therefore been presented, which allow the prediction of a settlement profile based on geometry, volume loss, and material properties.

Stability is analysed using the widely used Broms-Bennermark stability number ( $N$ ). This approach allows an  $N$  to be calculated for each case, which defines the differential between surface and internal pressure. By determining the collapse stage during the relaxation method, an envelope for the critical  $N$  is developed. This stability envelope is then compared to the rigorous upper and lower bound solutions computed by the finite-element limit analysis approach developed by the University of Newcastle Geotechnical group. The results are quite positive, with the stability results from this study remaining within 5% of the upper and lower bound solutions. Design charts using dimensionless ratios have therefore been presented. These calculated stability numbers are also considered with the settlement results, which allows some correlation between  $N$  and volume loss.

## CERTIFICATION OF THESIS

This dissertation is the result of my own work and includes nothing that is the outcome of work done in collaboration except where specifically indicated in the text. It has not been previously submitted, in part or completely, to any university of institution for any degree, diploma, or other qualification.

In accordance with the University of Southern Queensland guidelines, this thesis does not exceed 40,000 words in the main text.

Signed:  \_\_\_\_\_

Date: 27 June 2016 \_\_\_\_\_

Mathew S. Sams - BEng (Hons), GradIEAust

University of Southern Queensland

## ACKNOWLEDGEMENTS

Thank you to Dr Jim Shiau, my supervisor, who guided me through the technical challenges of the research degree, and encouraged me to gain as much academic experience as possible for its duration. The *FLAC* numerical model, particularly the pressure relaxation code, is Dr Shiau's development, which has been modified as required for this study. He also assisted me greatly with some of the non-technical challenges of helping me to begin my career in the geotechnical engineering discipline.

Thank you also to my family who heavily supported me through this period. This allowed me to pursue this research degree full time with a minimum of distraction.

Thank you to Kayla Friedman and Malcolm Morgan of the University of Cambridge, UK for producing the Microsoft Word thesis template used to produce this document.

## PUBLICATIONS DURING THESIS

These papers have been published over the duration of the degree.

### Conference Papers

Shiau, J. S., Sams, M. S., & Kemp, R. J. (2014). Physical modelling and PIV analyses of an underground tunnel heading. *Geotechnical Aspects of Underground Construction in Soft Ground*, 61-65.

Shiau, J. S., Sams, M. S., Zhang, J. & Kemp, R. J. (2014). Settlement Analyses of Underground Circular Tunneling in Soft Clay. *Geotechnical Aspects of Underground Construction in Soft Ground*, 347-352.

Lobwein, J., Sams, M., and Shiau, J. (2015). Finite Element Limit Analysis of Undrained Twin Circular Tunnels. In *Proceedings of Fifth International Conference of GEOMATE*. pp 66-71

Sams, M., and Shiau, J. (2015). Relating the Tunnel Settlement Parameter with Volume Loss. In *Proceedings of Fifth International Conference of GEOMATE*. pp 72-77

### Journal Papers

Shiau, J. Sams, M. and Lamb, B. (2016). INTRODUCING ADVANCED TOPICS IN GEOTECHNICAL ENGINEERING TEACHING – TUNNEL MODELLING, *International Journal of GEOMATE*, volume 10, issue 19, pp 1698-1705

Shiau, J., Lamb, B., and Sams, M. (2016). THE USE OF SINKHOLE MODELS IN ADVANCED GEOTECHNICAL ENGINEERING TEACHING, *International Journal of GEOMATE*, volume 10, issue 20, pp 1718-1724

Shiau, J., Sams, M., and Chen, J. (2016). STABILITY CHARTS FOR A TALL TUNNEL IN UNDRAINED CLAY, *International Journal of GEOMATE*, volume 10, issue 20, pp 1764-1769

Shiau, J., Buttling, S., and Sams, M. (2015) Developing a Project Based Learning Assignment for Geotechnical Engineering. In *Electronic Journal of Geotechnical Engineering*, volume 20, bundle 17, pp 10113-10121

# TABLE OF CONTENTS

<b>1 INTRODUCTION</b> .....	<b>15</b>
1.1 BACKGROUND .....	15
1.2 RESEARCH PROBLEM .....	16
1.3 AIMS AND OBJECTIVES.....	16
1.4 SCOPE OF WORK.....	17
1.5 ORGANISATION OF THESIS .....	17
<b>2 LITERATURE REVIEW</b> .....	<b>19</b>
2.1 INTRODUCTION .....	19
2.2 TUNNEL CONSTRUCTION.....	20
2.2.1 <i>Tunnel boring machines</i> .....	21
2.3 STABILITY DURING CONSTRUCTION .....	26
2.4 GREENFIELD SETTLEMENT.....	30
2.4.1 <i>Empirical Methods</i> .....	32
2.4.2 <i>Twin tunnel settlement</i> .....	35
2.4.3 <i>Sub surface settlement</i> .....	37
2.4.4 <i>Analytical methods</i> .....	38
2.4.5 <i>Longitudinal settlement</i> .....	40
<b>3 NUMERICAL MODELLING AND <i>FLAC</i></b> .....	<b>42</b>
3.1 INTRODUCTION .....	42
3.2 REVIEW OF NUMERICAL METHODS FOR SOFT SOIL .....	43
3.2.1 <i>Finite Element Method (FEM)</i> .....	43
3.2.2 <i>Finite Difference Method (FDM)</i> .....	44
3.2.3 <i>Boundary Element Method</i> .....	44
3.2.4 <i>Limit Analysis (FELA)</i> .....	45
3.3 REVIEW OF MODELLING TUNNEL PROCESSES .....	45

3.3.1	<i>The Gap Method</i> .....	46
3.3.2	<i>The Convergence-Confinement Method</i> .....	46
3.3.3	<i>The Strength Reduction Method</i> .....	47
3.3.4	<i>The Volume Loss Control Method</i> .....	47
3.4	FLAC.....	47
3.5	PRESSURE RELAXATION METHOD.....	50
<b>4</b>	<b>SINGLE TUNNEL SETTLEMENT</b> .....	<b>55</b>
4.1	INTRODUCTION.....	55
4.2	PROBLEM DEFINITION.....	56
4.3	METHOD OF ANALYSIS .....	58
4.4	RESULTS – AT COLLAPSE.....	60
4.5	RESULTS – PRE-COLLAPSE.....	65
4.5.1	<i>Practical Example – Predicting Settlement Profile</i> .....	75
4.6	CONCLUSION.....	76
<b>5</b>	<b>SINGLE TUNNEL STABILITY</b> .....	<b>78</b>
5.1	INTRODUCTION.....	78
5.2	PROBLEM DEFINITION.....	79
5.3	RESULTS – AT COLLAPSE.....	80
5.3.1	<i>Practical Examples</i> .....	82
5.3.2	<i>Failure Mechanism</i> .....	84
5.4	RESULTS – PRE-COLLAPSE.....	85
5.4.1	<i>Practical Example</i> .....	90
5.5	CONCLUSION.....	90
<b>6</b>	<b>TWIN TUNNEL SETTLEMENT</b> .....	<b>92</b>
6.1	INTRODUCTION.....	92
6.2	PROBLEM DEFINITION.....	93
6.3	METHOD OF ANALYSIS .....	95



6.4 RESULTS - AT COLLAPSE .....	99
6.4.1 Method 1 – Fully Merged Profiles.....	99
6.4.2 Method 2 – Partially Merged Profiles .....	102
6.4.3 Method 3 – Separate profiles.....	105
6.5 RESULTS – PRE-COLLAPSE.....	105
6.5.1 Method 1 – Fully Merged Profiles.....	106
6.5.2 Method 2 – Partially Merged Profiles .....	110
6.5.3 Method 3 – Separate Profiles.....	114
6.5.4 Practical Example .....	114
6.6 CONCLUSION .....	115
<b>7 TWIN TUNNEL STABILITY.....</b>	<b>116</b>
7.1 INTRODUCTION .....	116
7.2 PROBLEM DEFINITION.....	117
7.3 RESULTS – AT COLLAPSE .....	118
7.3.1 Practical Examples .....	123
7.3.2 Failure Mechanism.....	124
7.4 RESULTS – PRE-COLLAPSE.....	126
7.4.1 Practical Examples .....	131
7.5 CONCLUSION .....	132
<b>8 CONCLUSIONS AND RECOMMENDATIONS.....</b>	<b>133</b>
8.1 SUMMARY .....	133
8.2 FUTURE WORK AND CLOSING COMMENTS.....	137
<b>REFERENCES.....</b>	<b>140</b>
<b>APPENDIX 1 .....</b>	<b>148</b>
A1 MATLAB SURFACE FITS.....	148

# LIST OF FIGURES

FIGURE 2-1 DEPICTION OF THAMES TUNNEL CONSTRUCTION PROCEDURE .....	20
FIGURE 2-2 THAMES TUNNEL AS PART OF THE MODERN LONDON TUNNEL NETWORK IN 2010..	21
FIGURE 2-3 PHOTOGRAPH OF TBM USED IN MADRID METRO CONSTRUCTION (COURTESY OF <i>HERRENKNECHT</i> ).....	22
FIGURE 2-4 CUTAWAY DEPICTION OF A TBM OPERATING UNDERNEATH AN URBAN AREA (COURTESY OF <i>HERRENKNECHT</i> ).....	22
FIGURE 2-5 LONGITUDINAL SECTION OF A SLURRY SHIELD TBM (WHITTAKER AND FRITH, 1990) .....	23
FIGURE 2-6 SCHEMATIC DIAGRAM OF AN EARTH PRESSURE BALANCE TBM (WHITTAKER AND FRITH, 1990) .....	24
FIGURE 2-7 TYPICAL EXTRACTION ENVELOPE FOR A TBM.....	25
FIGURE 2-8 DIAGRAM OF TBM ILLUSTRATING THE OVERCUTTING PROBLEM.....	26
FIGURE 2-9 DEFINITION OF TUNNEL PROBLEM .....	28
FIGURE 2-10 ILLUSTRATION OF SETTLEMENT CONCEPT (ATTEWELL AND WOODMAN, 1982) ..	30
FIGURE 2-11 DIAGRAM SHOWING WHERE SETTLEMENT OCCURS DURING EXCAVATION (SUGIYAMA ET AL, 1999).....	31
FIGURE 2-12 PROFILE GIVEN BY GAUSSIAN EQUATION.....	32
FIGURE 2-13 CHART FOR $I_x/D$ BY PECK (1969).....	34
FIGURE 2-14 CHART SHOWING $I_x/D$ LINEARLY RELATED TO DEPTH (MAIR AND TAYLOR, 1997) .....	34
FIGURE 2-15 CHART SHOWING $I_x/D$ LINEARLY RELATED TO DEPTH (ADDENBROOKE AND POTTS, 2001).....	36
FIGURE 2-16 MINDLIN'S PROBLEM NO. 1 APPLIED TO TUNNELLING.....	38
FIGURE 2-17 3D MODELLING OF LONGITUDINAL TUNNELLING (HAJJAR ET AL, 2014).....	40
FIGURE 3-1 BASIC CALCULATION CYCLE IN <i>FLAC</i> .....	49
FIGURE 3-2 2D PLANE STRAIN DEFINITION OF THE TUNNEL PROBLEM.....	50
FIGURE 3-3 - TYPICAL MESH OF THE SINGLE TUNNEL SCRIPT .....	51

FIGURE 3-4 - MAX UNBALANCED FORCE HISTORY ( $C/D=3, \Gamma D/S_U=4, E/S_U=200$ ).....	52
FIGURE 3-5 - PLASTICITY PLOT (LEFT) AND VELOCITY PLOT (RIGHT) .....	53
FIGURE 3-6 - INPUTS SECTION OF THE PRESSURE RELAXATION SCRIPT FOR <i>FLAC</i> .....	54
FIGURE 4-1 TYPICAL DIAGRAM OF A SINGLE TUNNEL.....	56
FIGURE 4-2 TYPICAL SETTLEMENT INDUCED BY A SINGLE TUNNEL.....	57
FIGURE 4-3 A TYPICAL REGRESSION OF THE GAUSSIAN EQUATION TO THE <i>FLAC</i> SETTLEMENT DATA .....	59
FIGURE 4-4 SETTLEMENT PROFILES AT VARYING STAGES DURING RELAXATION ( $C/D=4, \Gamma D/S_U =$ $2, E/S_U=400$ ).....	59
FIGURE 4-5 TYPICAL SETTLEMENT PROFILES WITH RESPECT TO $C/D$ .....	60
FIGURE 4-6 TYPICAL SETTLEMENT PROFILES WITH RESPECT TO $\Gamma D/S_U$ .....	61
FIGURE 4-7 TYPICAL SETTLEMENT PROFILES WITH RESPECT TO $E/S_U$ .....	61
FIGURE 4-8 $E/S_U$ VERSUS $I_x/D$ WITH RESPECT TO $\Gamma D/S_U$ .....	62
FIGURE 4-9 $E/S_U$ VERSUS $I_x/D$ WITH RESPECT TO $C/D$ .....	62
FIGURE 4-10 RESULTS OF REGRESSION ANALYSIS, WITH RESULTING NORMALISED SETTLEMENT PARAMETER ( $K$ ) .....	63
FIGURE 4-11 RELATIONSHIP BETWEEN $K$ AND $\Gamma D/S_U$ .....	64
FIGURE 4-12 RESULTS COMPARISON WITH OTHER SUGGESTED EQUATIONS.....	64
FIGURE 4-13 SETTLEMENT PROFILES WITH VARYING $C/D$ ( $\Gamma D/S_U = 3, E/S_U=200, 50\%$ PoC)	66
FIGURE 4-14 SETTLEMENT PROFILES WITH VARYING $\Gamma D/S_U$ ( $C/D = 3, E/S_U=400, 50\%$ PoC)	66
FIGURE 4-15 SETTLEMENT PROFILES WITH VARYING $E/S_U$ ( $C/D = 3, \Gamma D/S_U = 3, 50\%$ PoC) ...	67
FIGURE 4-16 IMPACT OF $\Gamma D/S_U$ ON PROFILE INFLECTION POINT ( $C/D = 1, E/S_U=200$ ).....	68
FIGURE 4-17 IMPACT OF $C/D$ ON PROFILE INFLECTION POINT ( $\Gamma D/S_U = 2, E/S_U=200$ ).....	68
FIGURE 4-18 IMPACT OF $E/S_U$ ON PROFILE INFLECTION POINT ( $C/D=1, \Gamma D/S_U = 2$ ).....	69
FIGURE 4-19 COMPARISON WITH PREVIOUS RESULTS .....	69
FIGURE 4-20 RESULTS OF THIS STUDY WITH O'REILLY AND NEW'S EQUATION (EQ. 6).....	70
FIGURE 4-21 EQUATION FOR PRACTICAL ESTIMATION OF $K$ , IGNORING VOLUME LOSS EFFECTS ...	71

FIGURE 4-22 CONTOUR PLOT OF $K$ FOR $rD/s_u=1.5$ .....	72
FIGURE 4-23 CONTOUR PLOT OF $K$ FOR $rD/s_u=2$ .....	73
FIGURE 4-24 CONTOUR PLOT OF $K$ FOR $rD/s_u=3$ .....	73
FIGURE 4-25 CONTOUR PLOT OF $K$ FOR $rD/s_u=4$ .....	74
FIGURE 4-26 CONTOUR PLOT OF $K$ FOR $rD/s_u=5$ .....	74
FIGURE 4-27 CONTOUR PLOT OF $K$ FOR $rD/s_u=6$ .....	75
FIGURE 4-28 SETTLEMENT PROFILES OF EXAMPLE TUNNEL PROBLEM ( $H/D=3$ , $rD/s_u=3$ , $E/s_u=300$ ).....	76
FIGURE 5-1 SINGLE TUNNEL PROBLEM DEFINITION.....	80
FIGURE 5-2 COMPARISON OF STABILITY NUMBER AT COLLAPSE WITH WILSON ET AL (2011) ...	81
FIGURE 5-3 STABILITY NUMBERS AT THE POINT OF COLLAPSE DESIGN CHART .....	82
FIGURE 5-4 SHEAR STRAIN RATE (SSR) AND VELOCITY PLOT FOR $C/D=1$ AND $rD/s_u=1$ .....	84
FIGURE 5-5 SHEAR STRAIN RATE (SSR) AND VELOCITY PLOT FOR $C/D=1$ AND $rD/s_u=5$ .....	84
FIGURE 5-6 SHEAR STRAIN RATE (SSR) AND VELOCITY PLOT FOR $C/D=3$ AND $rD/s_u=1$ .....	85
FIGURE 5-7 SHEAR STRAIN RATE (SSR) AND VELOCITY PLOT FOR $C/D=3$ AND $rD/s_u=5$ .....	85
FIGURE 5-8 STABILITY NUMBER $N$ VERSUS VOLUME LOSS % FOR VARYING $rD/s_u$ BUT CONSTANT $C/D=1$ .....	86
FIGURE 5-9 STABILITY NUMBER $N$ VERSUS VOLUME LOSS % FOR VARYING $C/D$ BUT CONSTANT $rD/s_u=2$ .....	87
FIGURE 5-10 STABILITY NUMBERS AND VOLUME LOSS DESIGN CHART FOR $C/D=1$ .....	87
FIGURE 5-11 STABILITY NUMBERS AND VOLUME LOSS DESIGN CHART FOR $C/D=2$ .....	88
FIGURE 5-12 STABILITY NUMBERS AND VOLUME LOSS DESIGN CHART FOR $C/D=3$ .....	88
FIGURE 5-13 STABILITY NUMBERS AND VOLUME LOSS DESIGN CHART FOR $C/D=4$ .....	89
FIGURE 5-14 STABILITY NUMBERS AND VOLUME LOSS DESIGN CHART FOR $C/D=5$ .....	89
FIGURE 6-1 DEMONSTRATION OF THE DIFFERENT CATEGORIES USED IN THIS STUDY (NOT TO SCALE) .....	93
FIGURE 6-2 DEMONSTRATION OF THE DIFFERENT CATEGORIES USED IN THIS STUDY .....	95

FIGURE 6-3 DEMONSTRATION OF THE DIFFERENT CATEGORIES USED IN THIS STUDY.....	96
FIGURE 6-4 CONTOUR PLOT FOR $C/D=1$ WHICH INDICATES THE METHOD OF SETTLEMENT ANALYSIS TO USE.....	97
FIGURE 6-5 CONTOUR PLOT FOR $C/D=2$ WHICH INDICATES THE METHOD OF SETTLEMENT ANALYSIS TO USE.....	97
FIGURE 6-6 CONTOUR PLOT FOR $C/D=3$ WHICH INDICATES THE METHOD OF SETTLEMENT ANALYSIS TO USE.....	98
FIGURE 6-7 CONTOUR PLOT FOR $C/D=4$ WHICH INDICATES THE METHOD OF SETTLEMENT ANALYSIS TO USE .....	99
FIGURE 6-8 CONTOUR PLOT FOR $C/D=5$ WHICH INDICATES THE METHOD OF SETTLEMENT ANALYSIS TO USE.....	99
FIGURE 6-9 SETTLEMENT PROFILES WITH VARYING $C/D$ FOR A TYPICAL METHOD 1 CASE .....	100
FIGURE 6-10 SETTLEMENT PROFILES WITH VARYING $\Gamma D/S_U$ FOR A TYPICAL METHOD 1 CASE...	100
FIGURE 6-11 $I_x/D$ VS $H/D$ WITH VARYING $\Gamma D/S_U$ FOR ALL METHOD 1 DATA.....	101
FIGURE 6-12 $I_x/D$ VS $S/D$ WITH VARYING $C/D$ FOR ALL METHOD 1 DATA .....	102
FIGURE 6-13 SETTLEMENT PROFILES WITH VARYING $C/D$ FOR A TYPICAL METHOD 2 CASE .....	103
FIGURE 6-14 SETTLEMENT PROFILES WITH VARYING $\Gamma D/S_U$ FOR A TYPICAL METHOD 2 CASE...	103
FIGURE 6-15 $I_x/D$ VS $H/D$ WITH VARYING $\Gamma D/S_U$ FOR ALL METHOD 2 DATA.....	104
FIGURE 6-16 $I_x/D$ VS $S/D$ WITH VARYING $C/D$ FOR ALL METHOD 2 DATA .....	105
FIGURE 6-17 $I_x/D$ VS $H/D$ WITH VARYING $\Gamma D/S_U$ FOR ALL METHOD 1 DATA.....	107
FIGURE 6-18 $I_x/D$ VS VOLUME LOSS % WITH VARYING $S/D$ FOR $C/D=1$ METHOD 1 DATA .....	107
FIGURE 6-19 $I_x/D$ VS VOLUME LOSS % WITH VARYING $S/D$ FOR $C/D=5$ METHOD 1 DATA .....	108
FIGURE 6-20 $I_x/D$ VS $S/D$ WITH VARYING $C/D$ FOR ALL METHOD 1 DATA .....	108
FIGURE 6-21 $I_x/D$ VS VOLUME LOSS % WITH VARYING $C/D$ FOR ALL METHOD 1 DATA (ALL $S/D$ ) .....	109
FIGURE 6-22 DESIGN CHART FOR $I_x/D$ AGAINST VL% WITH VARYING $C/D$ FOR ALL METHOD 1 DATA (ALL $S/D$ ).....	109
FIGURE 6-23 $I_x/D$ VS $H/D$ WITH VARYING $\Gamma D/S_U$ FOR ALL METHOD 2 DATA (ALL $S/D$ ).....	110

FIGURE 6-24 $I_x/D$ VS VOLUME LOSS % WITH VARYING $S/D$ FOR $C/D=1$ METHOD 2 DATA.....	111
FIGURE 6-25 $I_x/D$ VS VOLUME LOSS % WITH VARYING $S/D$ FOR $C/D=5$ METHOD 2 DATA.....	112
FIGURE 6-26 $I_x/D$ VS $S/D$ WITH VARYING $C/D$ FOR ALL METHOD 2 DATA.....	112
FIGURE 6-27 $I_x/D$ VS VOLUME LOSS % WITH VARYING $C/D$ FOR ALL METHOD 2 DATA ( <i>ALL S/D</i> ) .....	113
FIGURE 6-28 DESIGN CHART FOR $I_x/D$ AGAINST VL % WITH VARYING $C/D$ FOR ALL METHOD 2 DATA ( <i>ALL S/D</i> ) .....	113
FIGURE 7-1 TYPICAL SCHEMATIC DIAGRAM OF THE PROBLEM.....	117
FIGURE 7-2 COMPARISON OF RESULTS WITH WILSON ET AL (2014) FOR $rD/s_u=2$ .....	119
FIGURE 7-3 COMPARISON OF RESULTS WITH WILSON ET AL (2014) AND OSMAN (2010) FOR $rD/s_u=3$ .....	119
FIGURE 7-4 COMPARISON OF RESULTS WITH WU AND LEE (2003) FOR $S/D=1.5$ .....	120
FIGURE 7-5 DESIGN CHART FOR THE CRITICAL STABILITY NUMBER N FOR $C/D=1$ .....	121
FIGURE 7-6 DESIGN CHART FOR THE CRITICAL STABILITY NUMBER N FOR $C/D=2$ .....	121
FIGURE 7-7 DESIGN CHART FOR THE CRITICAL STABILITY NUMBER N FOR $C/D=3$ .....	122
FIGURE 7-8 DESIGN CHART FOR THE CRITICAL STABILITY NUMBER N FOR $C/D=4$ .....	122
FIGURE 7-9 DESIGN CHART FOR THE CRITICAL STABILITY NUMBER N FOR $C/D=5$ .....	123
FIGURE 7-10 SSR PLOT (LEFT) AND VELOCITY VECTORS (RIGHT) AT THE POC ( $C/D=1, rD/s_u=2, S/D=2$ ).....	124
FIGURE 7-11 SSR PLOT (LEFT) AND VELOCITY VECTORS (RIGHT) AT THE POC ( $C/D=1, rD/s_u=5, S/D=2$ ).....	124
FIGURE 7-12 SSR PLOT (LEFT) AND VELOCITY VECTORS (RIGHT) AT THE POC ( $C/D=1, rD/s_u=2, S/D=8$ ).....	125
FIGURE 7-13 SSR PLOT (LEFT) AND VELOCITY VECTORS (RIGHT) AT THE POC ( $C/D=1, rD/s_u=5, S/D=8$ ).....	125
FIGURE 7-14 SSR PLOT (LEFT) AND VELOCITY VECTORS (RIGHT) AT THE POC ( $C/D=3, rD/s_u=2, S/D=2$ ).....	125

FIGURE 7-15 SSR PLOT (LEFT) AND VELOCITY VECTORS (RIGHT) AT THE POC ( $C/D=3, rD/s_u=5, S/D=2$ ) .....	125
FIGURE 7-16 SSR PLOT (LEFT) AND VELOCITY VECTORS (RIGHT) AT THE POC ( $C/D=3, rD/s_u=2, S/D=8$ ) .....	126
FIGURE 7-17 SSR PLOT (LEFT) AND VELOCITY VECTORS (RIGHT) AT THE POC ( $C/D=3, rD/s_u=5, S/D=8$ ) .....	126
FIGURE 7-18 CHART SHOWING $N$ WITH RESPECT TO VOLUME LOSS % FOR VARIOUS $rD/s_u$ ( $C/D=1, ALL S/D$ ).....	127
FIGURE 7-19 CHART SHOWING $N$ WITH RESPECT TO VOLUME LOSS % FOR VARIOUS $rD/s_u$ ( $C/D=5, ALL S/D$ ).....	127
FIGURE 7-20 CHART SHOWING $N$ WITH RESPECT TO VOLUME LOSS % FOR VARIOUS $C/D$ ( $rD/s_u =2, ALL S/D$ ).....	128
FIGURE 7-21 DESIGN CHART FOR $N$ WITH RESPECT TO VOLUME LOSS % AND $rD/s_u$ ( $C/D=1$ ) .....	129
FIGURE 7-22 DESIGN CHART FOR $N$ WITH RESPECT TO VOLUME LOSS % AND $rD/s_u$ ( $C/D=2$ ) .....	129
FIGURE 7-23 DESIGN CHART FOR $N$ WITH RESPECT TO VOLUME LOSS % AND $rD/s_u$ ( $C/D=3$ ) .....	130
FIGURE 7-24 DESIGN CHART FOR $N$ WITH RESPECT TO VOLUME LOSS % AND $rD/s_u$ ( $C/D=4$ ) .....	130
FIGURE 7-25 DESIGN CHART FOR $N$ WITH RESPECT TO VOLUME LOSS % AND $rD/s_u$ ( $C/D=5$ ) .....	131
FIGURE 10-1 TYPICAL <i>MATLAB</i> SURFACE FIT FOR SINGLE TUNNEL SETTLEMENT AT PRE-COLLAPSE ( $rD/s_u=2$ ) .....	149
FIGURE 10-2 <i>MATLAB</i> SURFACE FIT FOR SINGLE TUNNEL CRITICAL STABILITY NUMBER AT COLLAPSE.....	150
FIGURE 10-3 TYPICAL <i>MATLAB</i> SURFACE FIT FOR SINGLE TUNNEL STABILITY AT PRE-COLLAPSE ( $C/D=2$ ) .....	151
FIGURE 10-4 <i>MATLAB</i> SURFACE FIT FOR METHOD 1 TWIN TUNNEL SETTLEMENT AT PRE-COLLAPSE.....	152

FIGURE 10-5 *MATLAB* SURFACE FIT FOR METHOD 2 TWIN TUNNEL SETTLEMENT AT PRE-COLLAPSE .....153

FIGURE 10-6 TYPICAL *MATLAB* SURFACE FIT FOR TWIN TUNNEL STABILITY AT PRE-COLLAPSE ( $C/D=5$ ).....154



## LIST OF TABLES

TABLE 3-1 RECOMMENDED USE OF NUMERICAL MODELLING VS. AMOUNT OF DATA.....	43
TABLE 4-1 PARAMETERS OF VOLUME LOSS GENERAL EQUATION.....	72

# 1 INTRODUCTION

## 1.1 Background

The demand for tunnels and underground infrastructure has increased over the last few decades due to population growth and development of both existing and emerging urban regions. There are more than 100 cities globally that have underground transport, and with the global population projected to be 8.5 billion by 2030 (UN WPP report, 2015), this trend of development is set to continue. For this reason, continuing research into this area is of utmost importance.

Tunnelling in particular for transport and water supply infrastructure has become a preferred solution due to limited space for expansion at the surface, and the underground space being often under-utilized. They can also be financially beneficial in the long term due to reduced maintenance, in some ways environmentally superior due to reducing trip times, and storing this infrastructure underground allows more recreational space for humans, thereby increasing the standard of living.

The rapid development computers and simulation software coupled with advances of tunnelling techniques and machinery means that tunnels are now safer, cheaper, and more time-efficient than ever concerning operation and construction. As stated by Pelizza (1996), “going underground is no longer an unfortunate obligation, but actually a reasonable and effective solution”.

## 1.2 Research Problem

The primary problems for the geotechnical engineer during tunnelling construction as stated by Peck (1969), Ward and Pender (1980), and Mair and Taylor (1997) are stability of the tunnel heading and annulus, surface and sub-surface settlement, and determination of lining forces for the structural design. This research aims to address the problems of surface settlement and annulus stability during construction.

These two problems are in some ways connected – if the stability at the tunnel face during tunnel construction is mismanaged, larger settlements will occur. However, even in the case of ‘perfect’ stability control, an amount of settlement will inevitably occur. This is just a fundamental limitation of modern tunnelling machines and a fundamental result of the stress-strain mechanics of soil. This settlement can have substantial impacts on surface structures.

The stability problem refers to the pressure being applied to the inside of the cutting face as it is progressed forwards. This pressure must be substantial enough to prevent the soil from falling in to the tunnel but not so much as to cause the soil to be pushed forwards away from the cutting face, as this will cause heaving at the surface.

## 1.3 Aims and Objectives

The primary objective of this thesis is to develop a numerical model that accurately simulates the internal pressure of a boring machine and the ground relaxation and movements that occur during tunnel construction. As stated, the research problems being studied are surface settlement, and annulus stability.

For the settlement problem, the empirical method remains the most widely used for tunnel settlement analysis. Therefore, the aim of studying this problem in this research is to provide a comprehensive system to enable the use of this empirical equation for settlement based purely on soil and geometry parameters; this will allow prediction of the settlement profile.

The stability problem is most commonly defined using the Broms-Bennermark approach. This has again been adopted in this research with the aim of producing a system which can be used to provide an estimate of the collapse condition, and also

provide estimated ground movement as a percentage of the tunnel area (volume loss) based on respective stability number.

## 1.4 Scope of Work

These research problems are studied using a parametric investigation which has been implemented using dimensionless ratios which describe tunnel geometry, soil parameters, and volume loss. Studying the problem in this way allows a large practical range to be covered. A 2D plane strain finite difference analysis is conducted using a pressure relaxation method with homogenous undrained clay using the Tresca soil model. Both single and parallel twin tunnels have been analysed using this approach (twin tunnels are treated as bored simultaneously). Thus, this research covers single and twin tunnel settlement and stability.

Settlement has been studied with particular emphasis on the widely used empirical method and improving the estimation of the trough width parameter. This is done at both a collapse stage and at a pre-collapse working conditions stage. Stability has also been analysed simultaneously by the commonly used Broms-Bennermark stability number, which is then used to produce collapse bounds, and also to relate stability to volume loss. This could be very useful for the designer to bracket the problem, and also provide an estimation of the tunnelling machines ground loss performance.

## 1.5 Organisation of Thesis

### **Chapter 2 – Tunnelling in Soft Ground**

In this chapter, the design and construction methods of tunnels in soft ground are discussed. This includes construction methods, particularly shield machines and TBM's, and the geotechnical design criteria for tunnels. This chapter also has a review of the literature and past research in regards to stability analysis and settlement prediction.

### **Chapter 3 – Numerical Modelling and *FLAC***

This chapter houses a discussion of the different types of computer modelling techniques that are commonly used in the geotechnical area, in particular those used to analyse tunnels. This is followed with an in-depth discussion of the methodology

and approach taken in this research; that is the finite difference method of *FLAC* and the pressure relaxation method.

#### **Chapter 4 – Single Tunnel Settlement**

This chapter comprises the analysis of the settlement results from the single tunnel case. This includes both the critical ‘point of collapse’ stage and also the pre-collapse working conditions which analyses ground movements more similar to those during construction.

#### **Chapter 5 – Single Tunnel Stability**

This chapter discusses and analyses the stability results from the single tunnel cases. It focusses on the commonly used stability number, which has been calculated at the collapse stage and also at pre-collapse stages. This chapter is split as such – with the collapse bounds, and with the working condition stability numbers correlated to volume loss.

#### **Chapter 6 – Twin Tunnel Settlement**

This chapter comprises the analysis of the settlement results from the twin tunnel case. This includes both the critical ‘point of collapse’ stage and also the pre-collapse working conditions which analyses ground movements more similar to those during construction.

#### **Chapter 7 – Twin Tunnel Stability**

This chapter discusses and analyses the stability results from the twin tunnel cases. It focusses on the commonly used stability number, which has been calculated at the collapse stage and also at pre-collapse stages. This chapter is split as such – with the collapse bounds, and with the working condition stability numbers correlated to volume loss.

#### **Chapter 8 – Conclusion**

This chapter provides a finishing summary of the completed work, some of the key points in the discussion of the results, the future work following from this study to improve the results and industry usability and, and some closing comments on the justification of this study and tunnel research in general.

# 2 LITERATURE REVIEW

## 2.1 Introduction

This chapter will be a general review of modern tunnelling including a brief history, construction techniques with particular emphasis on the process involved with tunnel boring machines (TBM's). The advantages of these machines are outlined, as well as the key drawbacks that lead to inevitable ground movement. This chapter will also be a review of the research literature regarding stability and settlement analysis of tunnel excavations with particular focus on performance evaluation and prediction.

With the development of tunnel boring machines (TBM's) over the past few decades, tunnels can now be produced under very difficult ground conditions, such as very soft ground. In such conditions where the soil mechanics are more critical, responsibility increasingly falls to the geotechnical engineer (Terzaghi, 1950). These responsibilities include three main design and analysis objectives as stated in multiple state of the art reports by Peck (1969), Ward and Pender (1980), Mair and Taylor (1997), and Mair (2008). These include analysis of stability during construction, prediction and monitoring of long and short-term settlement, and determination of lining structural loading. This research focusses on the stability and settlement problems at the construction stage, thus the review will focus on them.

## 2.2 Tunnel construction

While tunnels in stiff ground and rock have a somewhat extensive history, tunnels in soft ground are relatively recent, with some of the first being built in the mid-19<sup>th</sup> century using basic cut and cover excavation methods, and unshielded underground excavation. These were almost all built above the water table. The first concept of tunnelling underneath one is widely credited to Sir Marc Brunel, for the first tunnel under the Thames River in London. Constructed over two decades in 1830-1850, it was hand excavated and made use of some of the first shield technology. However, withholding water from the excavation was still a severe problem. This led to the development of having the underground construction pressurised using compressed air. Further development of shielded underground excavations led to the first mechanized tunnelling machine in 1897, which was then used for parts of the London central railway line (Guglielmetti et al 2008).

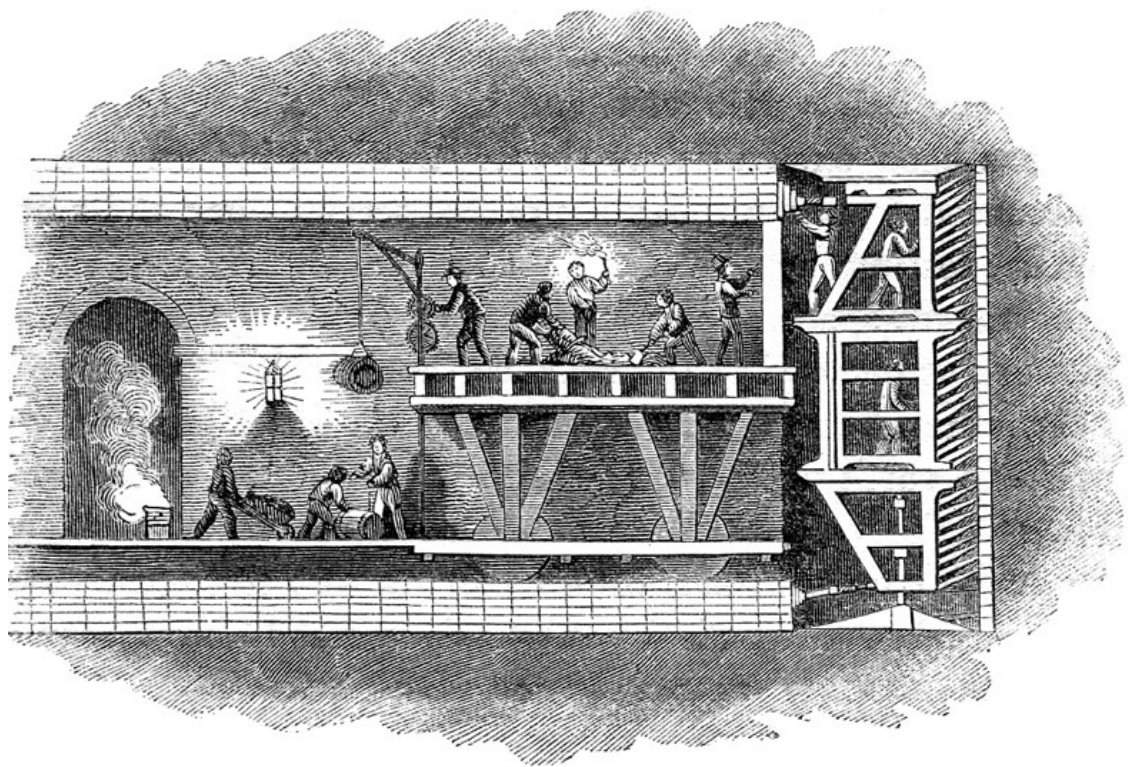


**Figure 2-1** Depiction of Thames tunnel construction procedure

In the mid-1950s, observations of health problems for workers in the tunnel, as well as poor performance for large diameter tunnels led to this becoming undesirable; improvements were needed. This led to the development of other more advanced methods such as NATM (Leca et al, 2000), and fully shielded boring machines capable of maintaining a face pressure only at the exposed face. These have evolved

into the modern boring machines that are used for the majority of urban tunnelling. (Guglielmetti et al, 2008)



**Figure 2-2 Thames tunnel as part of the modern London tunnel network in 2010**

Cities where tunnelling was once not considered a viable options due to geological complexity and sensitivity of buildings are now being undertaken due to advances in TBM technology. This allows much better control over the excavation speed; they allow strict control of face pressure and much better control of settlement because of the rapid installation of the lining and back grouting. Soft soils require this level of control and construction workmanship. In particular, soft clay in undrained soils conditions is considered one of the more difficult profiles to control stability and surface settlement and is the focus of this research.

### 2.2.1 Tunnel boring machines

Tunnel boring machines (TBM's) are defined as fully shielded machines that employ full closed-face excavation, such as the ones shown in figure 2-3 and 2-4. This implies that the cutting head covers the entire diameter of the tunnel, as opposed to partial excavation where the cutter-head is boom-mounted and moves independently inside the shield. TBM's are used for both rock and soft ground



tunnelling, with the significant difference being the degree of shielding (Chapman et al, 2010).

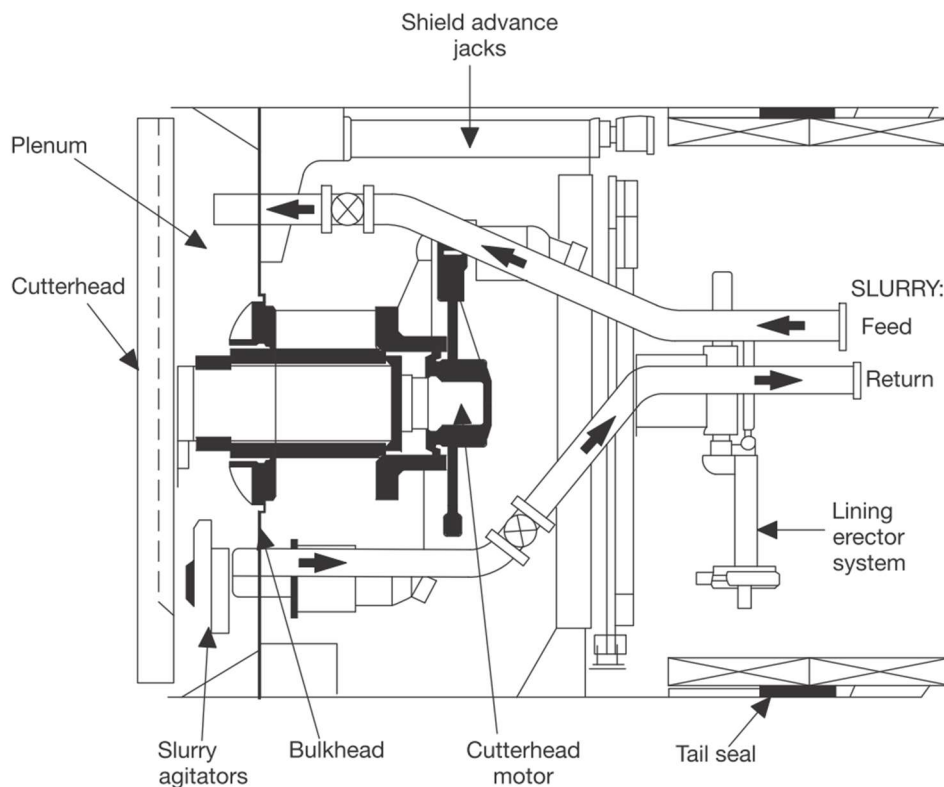


Figure 2-3 Photograph of TBM used in Madrid metro construction (courtesy of *Herrenknecht*)



Figure 2-4 Cutaway depiction of a TBM operating underneath an urban area (courtesy of *Herrenknecht*)

The principle of these machines is that pressure is maintained at the front of the shield and this provides stability to the tunnel face. In addition, this can be used to control water flow into the tunnel. These machines use a rotating cutterhead to excavate the ground. The cutter head can contain either picks or discs, or a combination of both. There are two basic types of pressurized closed face tunnelling systems, slurry-tunnelling machines (STMs) and earth pressure balance machines (EPBMs). STMs were initially developed for use specifically with cohesionless ground that contains a very low percentage of fines. EPBMs were developed for use in soft cohesive soils. However, due to the rare occurrence of pure cohesive and cohesionless soils in practice, both machines have been developed such that there is a large overlap in their capabilities (FHWA, 2009)



**Figure 2-5 Longitudinal section of a slurry shield TBM (Whittaker and Frith, 1990)**

STMs use a pressurised fluid to stabilize the face during excavation of the ground. The slurry does not only stabilize the face, but also mixes with the excavated material to allow it to be transported out of the machine. The liquid is pumped to the face, where it mixes with the excavated material. This mixture is then pumped out of the excavation chamber through a slurry line where it is conveyed to a separation plant, where the excavated material is taken out, and the fluid is pumped back to the cutting face.

If the ground condition is quite fine (i.e. clayey, silty), then the fluid is often just water. However, for frictional materials (sand, gravel), bentonite is introduced, which allows it to be much more easily pumped (Chapman et al, 2010). A typical schematic of a STM is shown in figure 2-5.

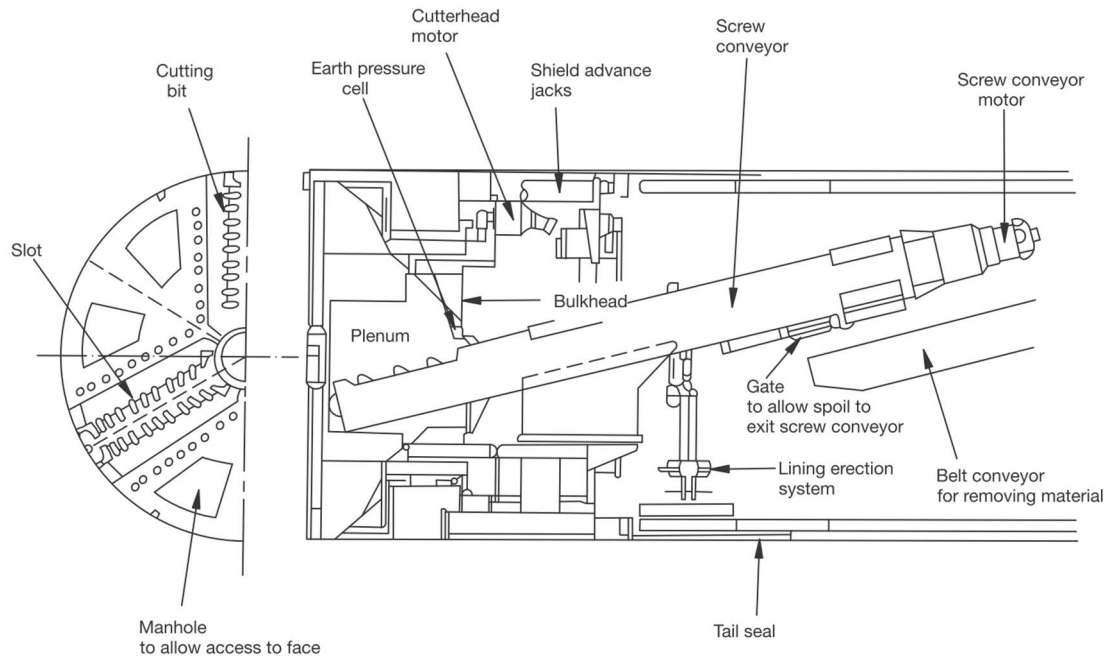


**Figure 2-6 Schematic diagram of an earth pressure balance TBM (Whittaker and Frith, 1990)**

EPBMs use the excavated material to support the tunnel face during excavation of the ground. The excavated material enters the plenum by extruding through the openings of the cutterhead in a fluid or plasticized state usually after having been mixed with a conditioning agent such as water, bentonite, or polymer foams. The plasticized spoil is removed from the plenum by using a screw conveyor, as shown in figure 2-6. The screw conveyor is used to remove the excavated material in a very controlled manner so that pressure is maintained in the plenum. At the same time, the pressure at the other end of the screw conveyor is atmospheric, i.e. there is a pressure drop from one end to the other. This means that the plasticized spoil in the screw conveyor needs to form a plug to help maintain this pressure differential.

The pressure in the plenum needs to be high enough to satisfy global stability requirements. It is controlled by the machine thrust on the cutterhead and the revolution speed of the screw conveyor, which also needs to be matched against the rate of advance of the tunnel machine, to manage volume loss. The requirement for the material in the plenum to behave plastically, to enable control of the delicate

pressure balance mechanism, limits its applicability to cohesive soils, but significant progress has been made with more advanced conditioning agents that allow EPBMs to be used with coarser grained materials.

As the cutting wheel is rotated, hydraulic jacks mounted onto the installed lining sections (or initially into the side of the excavation), force the TBM through the soil. Pressure at the face is maintained within specified limits to prevent collapse and to control volume loss at the face. After enough advance has occurred, a permanent lining is installed under the protection of the shield. When the TBM is not advancing, the cutting face can also be forced against the soil to provide additional support.

During advance, the quantity of soil recovered from the screw conveyor is carefully monitored. The soil is weighed on conveyors and mud skips counted (if used) to gather information on the amount of soil that is being excavated. This provides critical information to determine if the soil excavation rate at the face is within tolerable limits, as illustrated in figure 2-7. For example, if the excavation rate is higher than expected, then there will be excessive volume loss. If this were the case, operations would need to halt, and reconfigure the machine to be inside the extraction envelope (Kuesel et al, 2012).

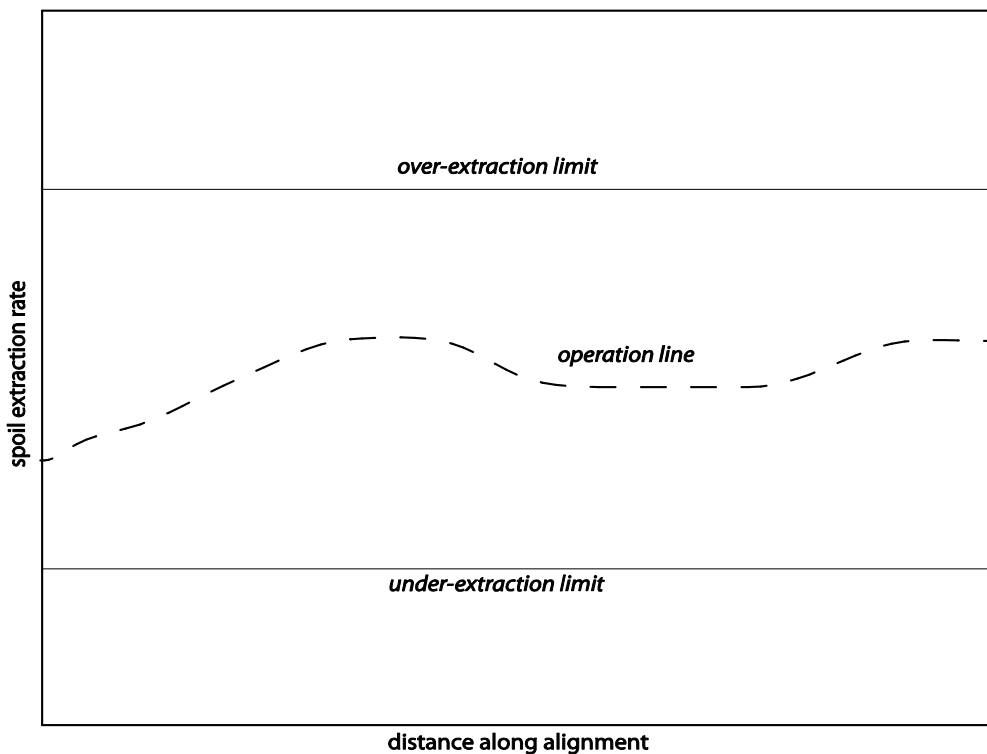


**Figure 2-7 Typical extraction envelope for a TBM**

However, TBMs are very good at managing this problem. The main source of ground loss problems arise in modern tunnel boring machines because of some unavoidable operational realities. Namely, the cutting head is always a slightly larger diameter than the shield, as shown in figure 2-8 to allow steering and to reduce movement friction. This overcutting problem is always in combination with an inevitable delay between when a tunnel advance is bored, and when the lining and the back grouting is installed. This overcutting and construction delay problem allows some soil relaxation at the tail.

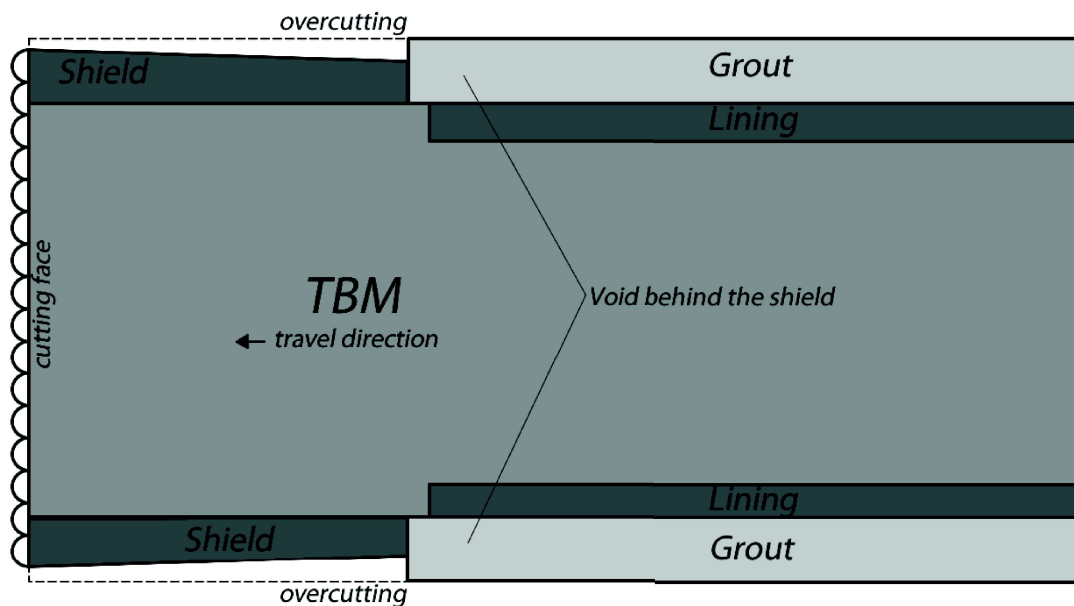


**Figure 2-8 Diagram of TBM illustrating the overcutting problem**

In the case of driving a TBM in a perfectly horizontal alignment (i.e. no pitching and snaking), then the radial displacement would be limited by the physical gap between the cutter head and lining. However, contributing to volume loss is the quality of workmanship and includes excess pitching, to avoid the tendency of the TBM to diving, and snaking, the irregular motion of the TBM moving from side to side when advancing. While the maximum excess pitch can be prescribed by the design engineer, snaking is dependent on the quality of the workmanship. Volume loss behind the face therefore occurs because of soil relaxing into the void from overcutting at the cutter face and the lining and quality of workmanship.

### 2.3 Stability during construction

In geotechnical engineering, stability analysis is used to predict the maximum load that can be supported by a geotechnical structure without inducing failure. This

collapse load can then be used to bound the working conditions, and set a maximum allowable load using a factor of safety. The conservativeness of the factor depends on the application and its associated serviceability requirements. However, in tunnelling, particularly with TBMs, the problem is a little different.

In conventional stability analysis, the 'destabilising' load is increased until the failure point is found. However, in tunnel stability analysis, there is usually both a 'stabilising' internal pressure ( $\sigma_t$ ) as well as a 'destabilising' surcharge pressure ( $\sigma_s$ ). Thus, many combinations of these two pressures that will cause the active failure (collapse) and many will cause the passive failure (blowout). Analysing tunnel stability during tunnel construction is essential for this reason, over estimating with the internal pressure can cause problems just the same as under estimating (Ng et al, 2004).

This difficulty of having the two pressures was realised by Broms and Bennermark (1967), who created a stability number  $N$ , as in equation 2.1, which combines the two into one convenient number. Their research was a pilot study of the plastic flow of clay soil in vertical openings of retaining walls. It was discovered that similar soil behaviour was observed when the difference between  $\sigma_t$  or  $\sigma_s$  remained constant, regardless of their respective magnitudes. In this equation,  $\gamma$  is the soil unit weight,  $H$  is the depth to axis, and  $s_u$  is the undrained shear strength of the soil, as shown in a schematic definition for the problem in figure 2-9.

$$N = \frac{\sigma_s + \gamma H - \sigma_t}{s_u} \quad (2.1)$$

Following this important research, many physical modelling studies of tunnel stability were carried out. These included a comprehensive study of deep excavations and tunnelling by Peck (1969), a study of collapse mechanisms by Atkinson and Cairncross (1973), a study of pore pressure effects by Seneviratne (1979), a comprehensive description of soil factors and behaviour around tunnels by Clough and Schmidt (1977) and centrifugal modelling of tunnelling in soft ground by Mair (1979). Early discussion on correlating stability number with settlement and safety factor can be found in Romo and Diaz (1981). An excellent early review of some of this research and some detailed discussion on theoretical soil mechanics relating to tunnels is also in Atkinson and Mair (1981).

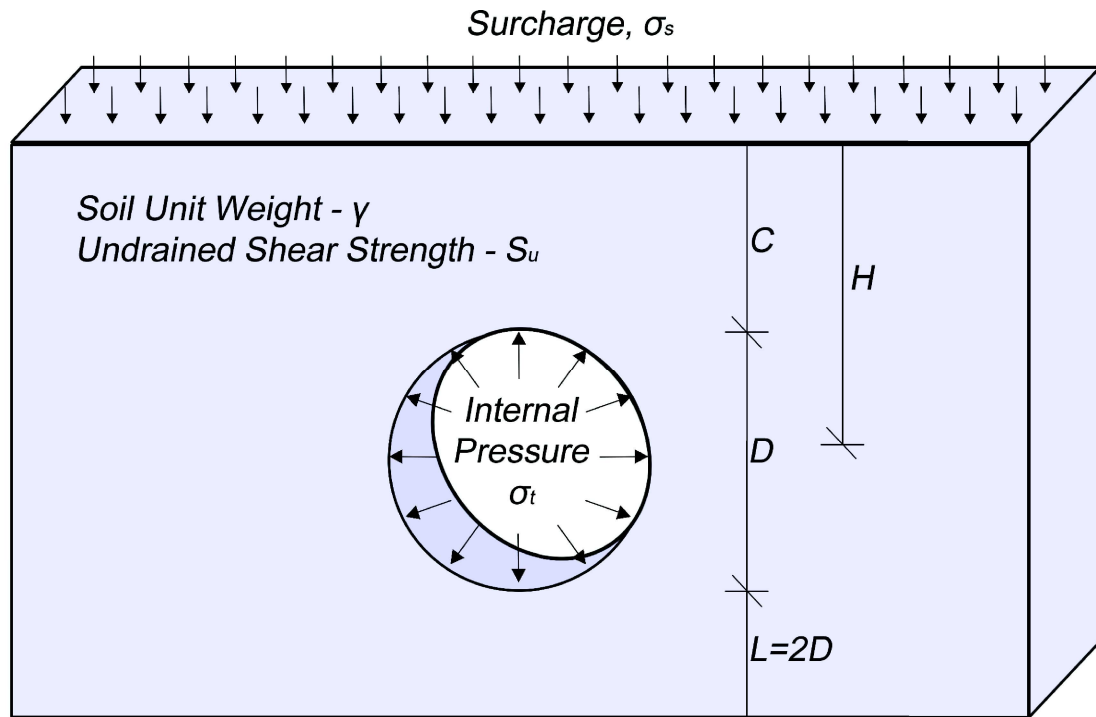


**Figure 2-9 Definition of tunnel problem**

Davis et al. (1980) built upon the earlier definition of stability ratio and approached the upper and lower bound solutions of the problem using a number of dimensionless parameters. The problem was regarded as to find the limiting value of a pressure ratio  $(\sigma_s - \sigma_t)/S_u$  that is a function of the independent parameters such as the depth ratio  $C/D$  and the strength ratio  $\gamma D/S_u$  as indicated in equation 2.2. This approach to the problem has been continued and expanded in the finite element limit analysis (FELA) research by the University of Newcastle geotechnical research group.

$$N = \frac{\sigma_s - \sigma_t}{s_u} = f\left(\frac{C}{D}, \frac{\gamma D}{s_u}\right) \quad (2.2)$$

The FELA approach uses finite elements to discretise the problem domain, but uses limit analysis to solve two optimisation problems. The first is based on the principle of finding the highest loaded scenario that is still statically admissible – this will be lower bound. The second is to find the lowest loaded scenario that is still kinematically admissible – this will be the upper bound (Sloan, 2013). Further detail on the development of this method can be found in chapter 3.2.4.

Following this development, a large number of research papers have been subsequently published in the areas of tunnel stability. Assadi and Sloan (1991)

published undrained stability of square tunnels followed by Sloan and Assadi (1991) published on similar topic but with the soil strength increasing with depth. This approach was then extended for stability of circular tunnels in Sloan and Assadi (1993), and plan strain headings in Sloan and Assadi (1994). In Lyamin and Sloan (2000), stability of circular tunnels in cohesive-frictional soils was considered. In Augarde et al (2003), the plane strain heading problem was reconsidered following significant developments with the limit analysis approach (non-linear programming).

The most recent papers are based on this new approach and further developments (conic programming) and papers have been produced on stability of circular tunnels in cohesive-frictional soil under surcharge loading (Yamamoto et al, 2011), in undrained soil where strength increases with depth (Wilson et al, 2011). Square and rectangular tunnels have also been considered in Wilson et al (2013) and Abbo et al (2013) respectively. As well as this, twin tunnel configurations of both square and circular tunnels have also analysed in Wilson et al (2008), Yamamoto (2013), and Wilson et al (2014).

There have also been other analytical solutions to the stability upper and lower bound problem. Leca and Dormieux (1990) calculated upper and lower stability bounds for circular tunnels in frictional material. Their approach led to comparison physical studies by Chambon and Corte (1994) and Anagnostou and Kovari (1996), who showed good agreement with the failure mechanism and results. Further analytical developments have also been developed for three dimensions by Soubra (2000) and Soubra et al (2008). A probabilistic approach by the same research group has been developed by Mollon et al (2009a) and Mollon et al (2009b); this allows for variation in the shear strength parameters of the soil.

More recent centrifugal and numerical modelling has been done by Lee et al (2006) which was an analysis of both stability and settlement. A recent review of physical modelling of tunnels in soft ground has been done by Meguid et al (2008), which reviews a number of papers from the early 2000s. After this time, Li et al (2009) apply a upper and lower bound method to a tunnel stability problem involving a large slurry machine that was used for the Shanghai Yangtze river tunnel. Osman (2010) has done small scale 1g twin tunnel model tests in clay to study both stability and settlement, and has varied spacing ratio and soil strength.



In this study, stability is analysed using an approach similar to that used in the FELA studies, the stability number (as in equation 2.2) is a variable dependant on  $C/D$ ,  $\gamma D/s_u$ , and in twin tunnels  $S/D$ .

## 2.4 Greenfield Settlement

Ground movements are an inevitable consequence of excavating and constructing a tunnel. Tunnel excavation causes relaxation of in-situ stress, which is only partially restricted by the insertion of the tunnel support. This is due to the time delay between excavation and installation of the support. In fact, it is not possible to create a void instantaneously and provide an infinitely stiff lining to fill it exactly. Hence, a certain amount of the deformation of the ground will take place at the tunnel depth. This will trigger a chain of movements, resulting in settlements at the ground surface, which become more significant with shallower tunnels as the movements at tunnel depth are able to reach the surface with less diffusion. This concept can be visualised and understood with figure 2-10.

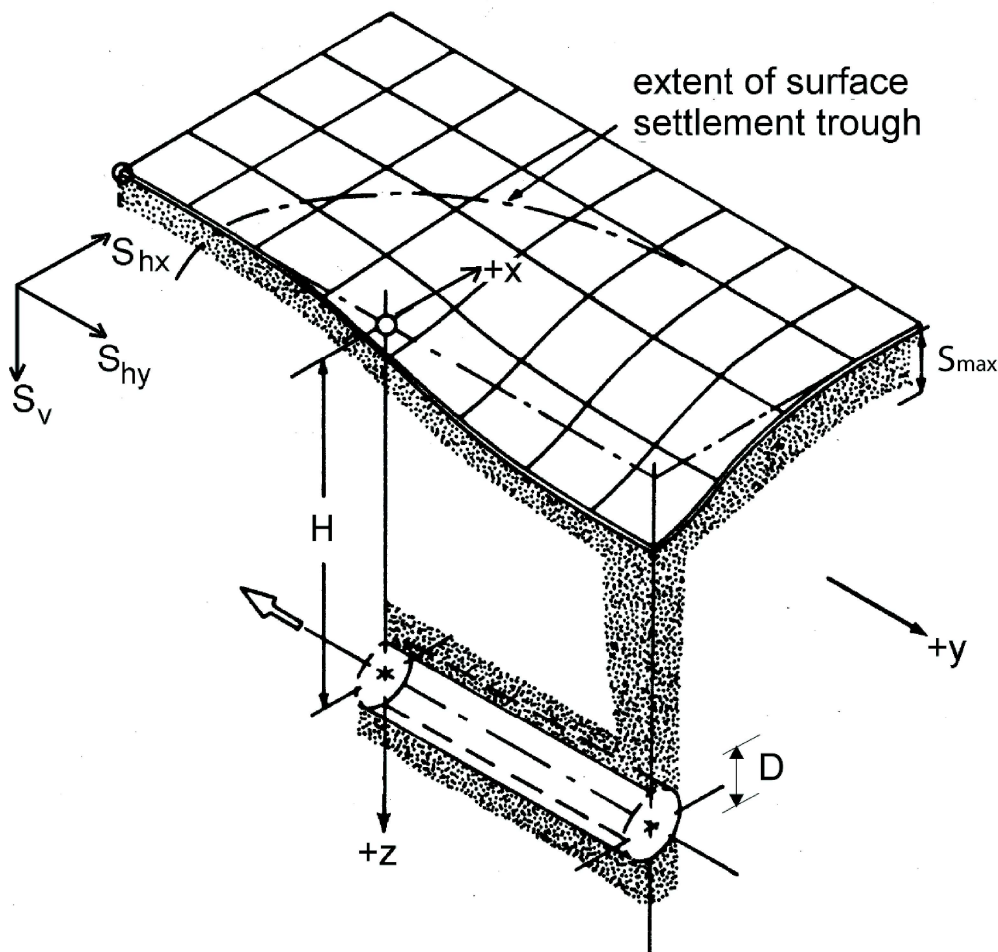


Figure 2-10 Illustration of settlement concept (Attewell and Woodman, 1982)

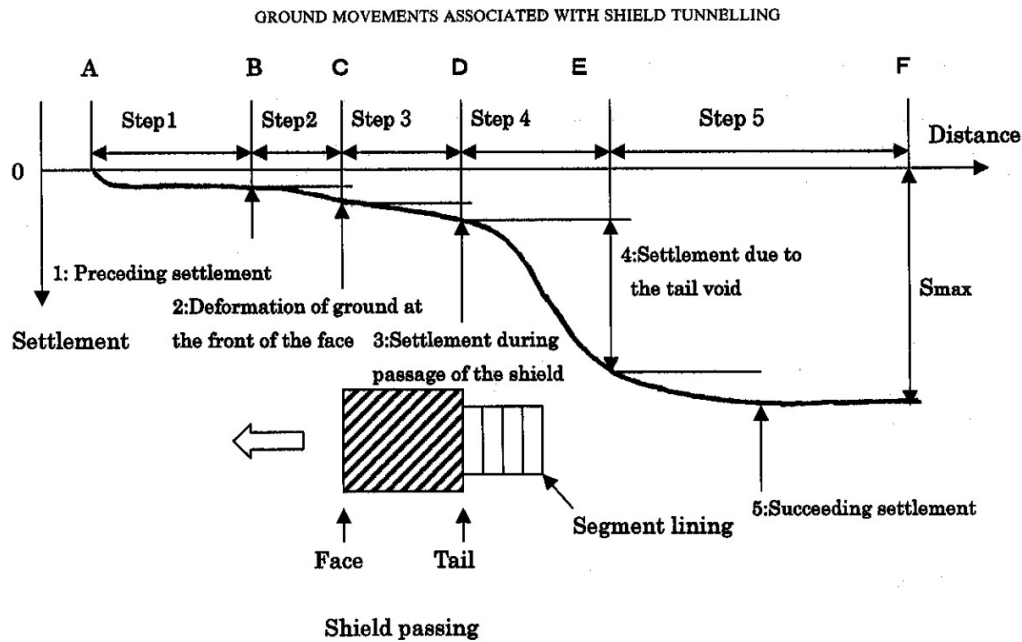


Figure 2-11 Diagram showing where settlement occurs during excavation (Sugiyama et al, 1999)

There are a few main causes for settlement during construction, as shown in figure 2-11 by Sugiyama (1999). Steps 1-3 occur before the shield has passed – they are caused by ground movement towards the excavated part of the tunnel, and stress relief as soil is removed near the cutting face (Bartlett and Bubbers, 1970). The majority of the settlement occurs in step 4 which is the aforementioned overcutting problem occurs, where there is temporarily unsupported soil in the gap above the shield as the lining and grout is installed (Fattah et al, 2013). A practical guide for managing settlement in soft ground is by Leca and New (2007) who comprehensively describe these problems.

Surface settlement induced by tunnelling is a complex phenomenon that is dependent on many factors such as soil and groundwater conditions, tunnelling dimensions and construction techniques. Therefore, much modern tunnelling research has been given to predict the soils response to changes in stress resulting from tunnel construction. With the rapid development of computer technology, numerical modelling using finite element or finite difference methods has become the preferred method for geotechnical design and analysis of tunnels.

In many cases however, empirical and semi-empirical methods are still applicable, and indeed quite capable for preliminary prediction and in cases that match the assumptions of the empirical method (greenfield or close to greenfield). For tunnel

settlement in particular, the empirical method is still widely used, due to its suitability and ease of use (Gunn, 1993 and Taylor, 1998). This research focusses on transverse settlement, which corresponds to the settlement profile perpendicular to the tunnel axis, as shown in figure 2-10. Other areas of tunnel settlement including analytical methods, sub-surface settlement will be briefly overviewed.

### 2.4.1 Empirical Methods

The empirical method for estimating surface settlement of tunnels generally follows a Gaussian distribution curve, as in equation 3. This approach was first suggested by Martos (1958), who observed that it matched settlement patterns of deep excavations for mining remarkably well. For the particular application to tunnels, research by Peck (1969) indicated a close fit with experimental and observational results. This equation is given in equation 2.3 and its typical form is shown in figure 2-12.

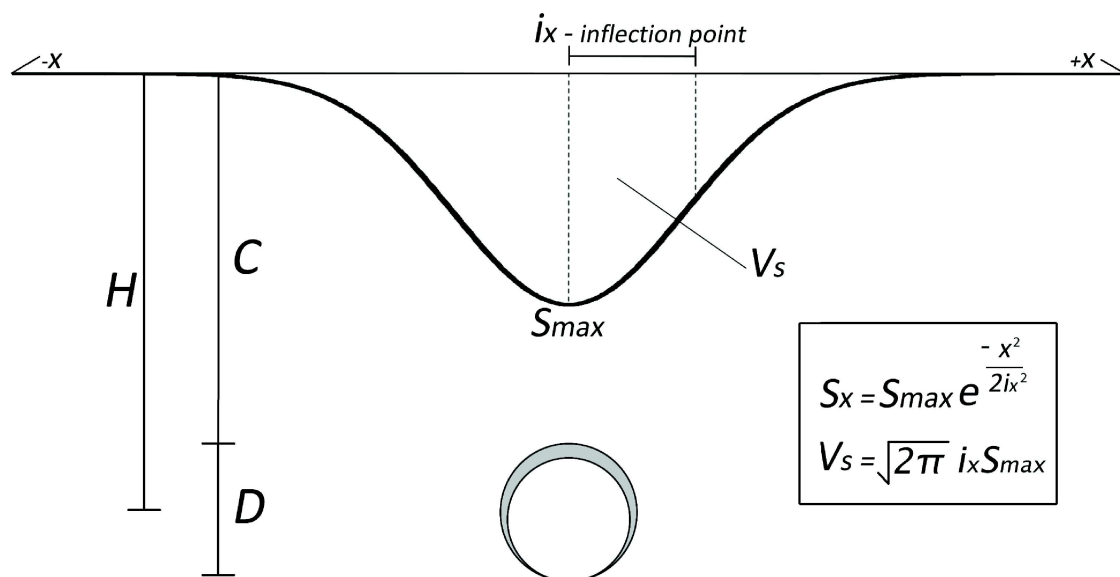


**Figure 2-12 Profile given by Gaussian Equation**

This method requires the input of a trough parameter ( $i_x$ ) which influences the physical width of the profile, and relates the volume loss and the maximum settlement, as in equation 2.4 (Mair et al, 1982). The surface settlement area and the volume loss at the tunnel can be directly equated in clay because there is no/very little change in volume/dilation (Peck, 1969 and Eisentein et al, 1981).

$$S_x = S_{\max} e^{\frac{x^2}{2i_x^2}} \quad (2.3)$$

$$V_s = \sqrt{2\pi} \cdot i_x \cdot S_{\max} \quad (2.4)$$

Further examination of this method has been extensive. Physical modelling has been one of the main methods used to test its adequacy. Results from Atkinson and Potts (1977), Mair (1979), Mair and Taylor (1997), Taylor (1998), Gran and Taylor (2000), Wu and Lee (2003), Osman et al. (2006a), and Ahmed and Iskander (2010) coming out in favour of this empirical method. It has also been extensively compared with measurements from constructed tunnels in Attewell and Farmer (1974), Cording & Hansmire (1975), O'Reilly and New (1982), Rankin (1988), Phienwej (1997), Devriendt (2010) reporting positive comparisons with the Gaussian equation.

Numerical modelling from Lee and Rowe (1990a and b), an early 3D finite element study of longitudinal and transverse tunnel settlement, reported a positive comparison with the Gaussian equation for the latter. More recently, Fattah et al (2013) compared numerical results against analytical and empirical methods and found the best agreement with the empirical method. Chakeri et al (2013 and 2014) compared 3D modelling with analytical, empirical, and measurement results. By doing this, they were able to highlight the most important parameters, generate an equation for  $S_{\max}$ , and conclude the empirical method is very appropriate, particularly considering its ease of use.

With this then established, one of the most important parts of this method is the trough parameter ( $i_x$ ) which requires careful selection, as it is relatively sensitive. Estimations of the inflection point parameter ( $i_x$ ) have been attempted by many researchers. In the initial study, Peck (1969) proposed a chart for  $i_x/D$  with respect to the material and the depth ratio, as shown in figure 2-13. Further notable research by Clough and Schmidt (1981) yielded equation 2.5, Mair and Taylor (1997) in equation 2.6, and Lee et al. (1999) in equation 2.7. However, these only take into account the geometry of the system, volume loss and soil strength are not definable parameters.

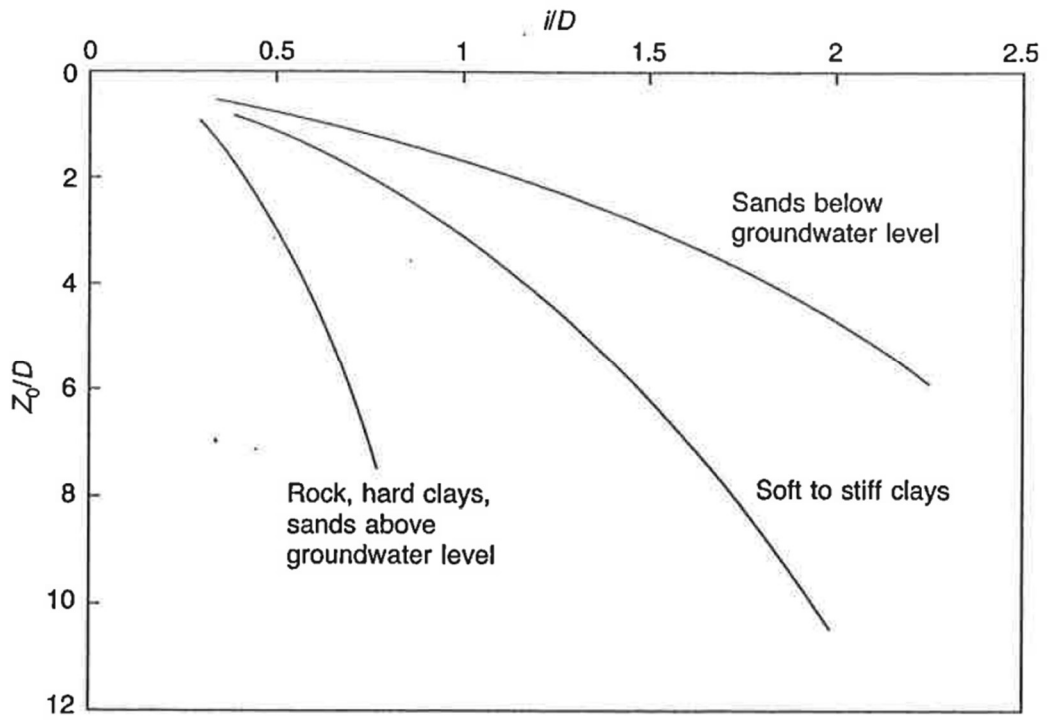


Figure 2-13 Chart for  $i_x/D$  by Peck (1969)

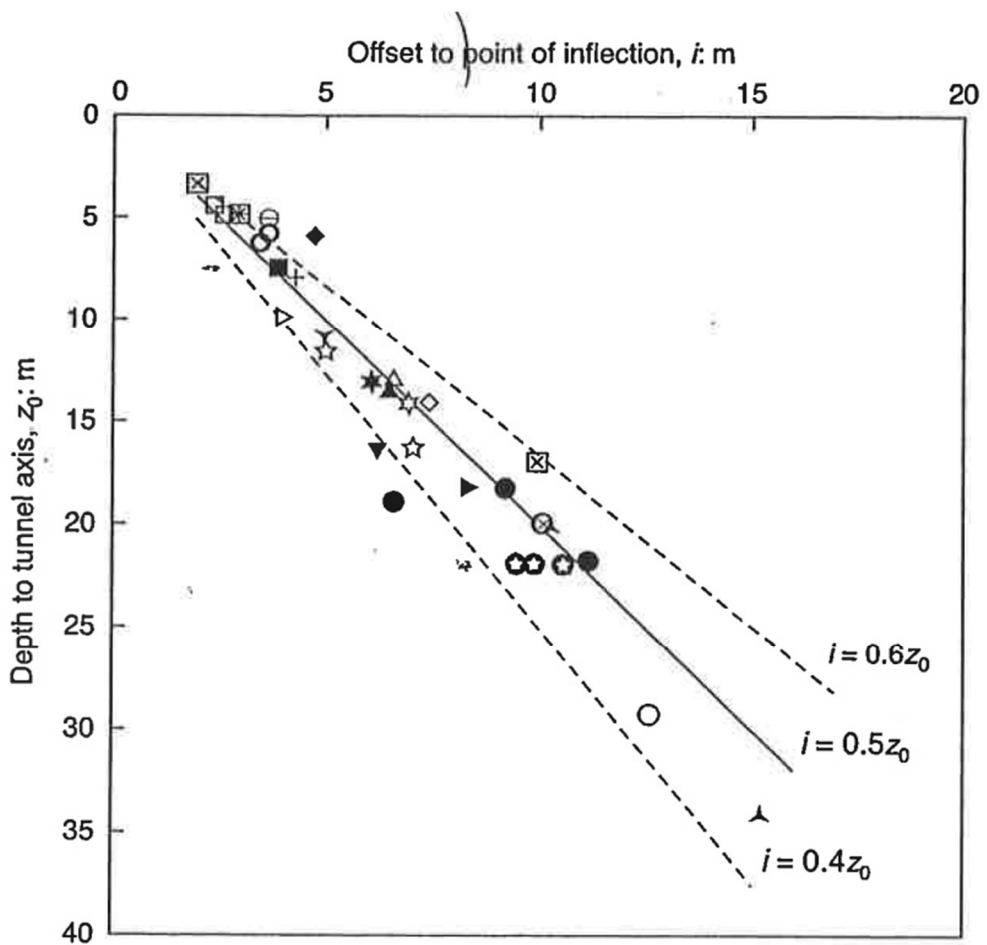


Figure 2-14 Chart showing  $i_x/D$  linearly related to depth (Mair and Taylor, 1997)

The most widely used method is the one suggested by O'Reilly and New (1982), which through analysing data collected from tunnels in London suggested that  $i_x$  is linearly proportional to the to-axis tunnel depth,  $H$ , as in equation 2.8. Further research by Mair and Taylor (1997) with centrifugal modelling seems to confirm this, as shown in figure 2-14. However, equation 2.8 is not suitable for very shallow cases ( $C/D < 1$ ), as the diameter would become a more dominant parameter. However, this equation allows the coefficient of proportionality ( $k$ ) to vary with other parameters such as volume loss and soil type. Commonly assumed values of  $k$  range from 0.4 for stiff clays to approximately 0.7 for soft clays (Guglielmetti, 2008).

$$i_x = 0.5D^{0.2}H^{0.8} \quad (2.5)$$

$$i_x = 0.75D\left(\frac{C}{D}\right)^{0.8} \quad (2.6)$$

$$i_x = 0.29\left(\frac{H}{D}\right) + 0.5 \quad (2.7)$$

$$i_x = kH \quad (2.8)$$

However, these have not been thoroughly defined using dimensionless parameters. It is thus the aim of this study to investigate the variation of this  $k$  parameter with respect to the aforementioned dimensionless parameters: depth ratio  $C/D$ , soil strength ratio  $\gamma D/s_u$ , Young's Modulus ratio  $E/s_u$ , volume loss %.

## 2.4.2 Twin tunnel settlement

While analysis of single tunnels is very significant research wise, in practice, it is common to have two parallel tunnels for major rail and road infrastructure. Having the additional tunnel adds complexity to the problem due to the added variable of spacing, and also the issue of construction timing – are they being built simultaneously, sequentially with time delay, or from opposite directions. However, it is still critically important to be able to predict settlement. O'reilly and New (1982) proposed a simple and elegant idea, to simply assume superposition and suggest the double Gaussian equation, as shown in equation 2.9 where  $s$  is the centre

to centre spacing between the tunnels (as seen in figure 6-1). This configuration of the equation also assumes that  $x=0$  is exactly between the two tunnels.

$$S_x = S_{\max} \left( e^{-\frac{(x-0.5s)^2}{2i_x^2}} + e^{-\frac{(x+0.5s)^2}{2i_x^2}} \right) \quad (2.9)$$

However, this equation is symmetric, and it has become apparent that this equation in this form is suitable only for cases where the tunnels are bored simultaneously and where the settlement will be symmetric (New and O'Reilly, 1991). Research by Ghaboussi and Ranken (1977), Kim et al (1998) about twin tunnel interactions indicated significant differences in the lining forces between the first and second tunnels. They concluded that the design process needs to reflect this, and suggested that settlement for sequential twin tunnels may also need further investigation.

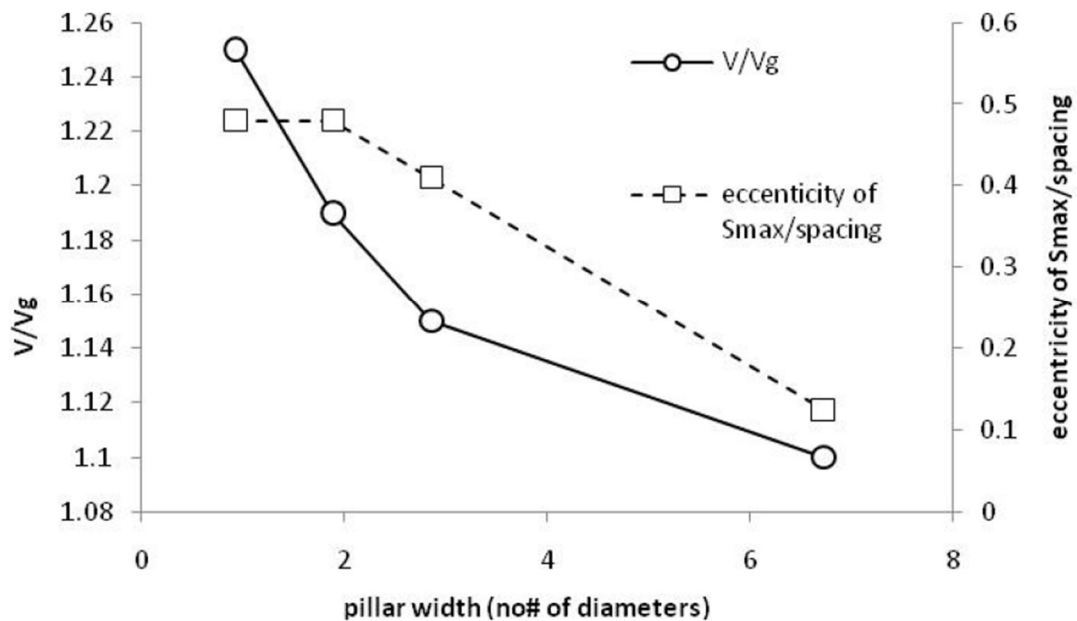


**Figure 2-15 Chart showing  $i_x/D$  linearly related to depth (Addenbrooke and Potts, 2001)**

Addenbrooke and Potts (2001) first suggested that a simple modifier could be applied to the settlement equation for the second tunnel. A design chart was produced indicating the increase of volume loss ( $V/V_g$  times more) that occurs for the second tunnel over the first tunnel, as shown in figure 2-15 where the pillar width is equivalent to the spacing between the tunnels. Other conclusions were that the amount of time delay was insignificant and that the  $i_x$  value of the second tunnel

remained virtually constant even though the magnitude of settlement was changing. Another approach has also been suggested by Chapman et al (2004) who suggested that the settlement by the second tunnel should be subject to a modification factor dependent on the magnitude of the 'overlapping zone', as in equation 2.10. In this equation, A is the multiple of the trough width parameter (2.5-3),  $k_A$  is the value of  $k$  for the first tunnel (as derived from equation 2.8), and M is the maximum modification factor described in Chapman et al (2007).

$$S_{\text{mod}} = FS_v \quad (2.10)$$

$$F = 1 + \left[ M \left( 1 - \frac{|s + x_A|}{Ak_A H} \right) \right] \quad (2.11)$$

Other modification factors following this premise have been done by Suwansawat and Einstein (2007) and Ocak (2014) who developed an approach based on measurement data. Do et al (2015) has also developed an approach based on these studies, and includes the effect that the second tunnel has on the first. Following this, research by Ercelbi et al (2011), Chen et al (2012), Chakeri et al (2015), and Divall and Goodey (2015) have examined twin tunnel settlement by combining and comparing these approaches with numerical and other measurement data. The overall conclusion is that the empirical method can still be used for sequential twin tunnels using these modifications.

However, as this is the first research into twin tunnel settlement by the author using the developed method, this study will be assuming simultaneous bored tunnels with consequently symmetric settlement profiles. Therefore, equation 2.9 will be of primary interest, and sequential tunnels are to be future work.

### 2.4.3 Sub surface settlement

Predicting subsurface movements is becoming increasingly important as more and more below ground structures are being built. Tunnels, pipelines, deep foundations, below ground basements etc. can be influenced by subsoil movements and need to be quantified to analyse sub-surface structure loading and possible damage. The common empirical formulas mentioned in previous sections cannot be directly applied. While subsurface has a similar pattern to surface settlement, as is



reasonable, it has been found that the shape parameter ( $i_x$ ) requires adjustment depending on the depth (Mair et al, 1993). According to this research, this can be easily done by using equation 2.12, where  $H$  is the tunnel axis depth,  $k$  is the value being used for the surface, and  $H_y$  is the subsurface depth being considered, which can be between zero, meaning at the surface, and  $H$ , which would mean at the tunnel depth. Further examination of this by Moh et al (1996) led to the development of equation 2.13, where  $m$  is a material factor ( $m=0.4$  for sand,  $m=0.8$  for clay).

$$i_x = k(H - H_y) \quad (2.12)$$

$$i_x = \left(\frac{D}{2}\right) \left(\frac{H}{D}\right)^{0.8} \left(\frac{H - H_y}{H}\right)^m \quad (2.13)$$

#### 2.4.4 Analytical methods

Closed form solutions have been calculated starting from an Elasticity Solution derived from Mindlin's problem no. 1, shown in figure 2-16. The elastic surface settlement solution is given in equation 2.14, where the settlement over the tunnel is given by  $\delta_z$ .  $D$  is diameter,  $G$  is the shear modulus of soil,  $x$  is the horizontal distance from tunnel centre,  $z$  is the depth from tunnel centre.

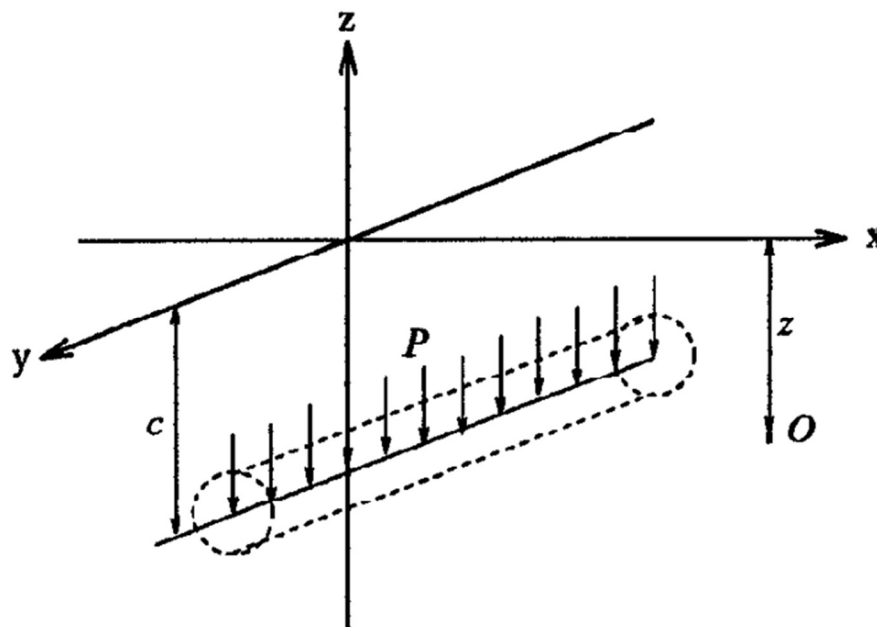


Figure 2-16 Mindlin's Problem no. 1 applied to tunnelling

$$\delta_z = -\frac{\gamma D^2 z^2}{8G(x^2 + z^2)} \quad (2.14)$$

Another approach, which has become the dominant method for analytical estimation of tunnel settlement, is based on the work by Sagaseta (1987). This assumes that for simple soil models such as isotropic incompressible conditions, strain fields can be calculated independent of stresses, and that the soil will completely move into the void. This method for settlement is given in equation 2.15, where  $R$  is the tunnel radius.

$$\delta_z = -\frac{\gamma R^2 z^2}{G(x^2 + z^2)} + \frac{\gamma D^2 z^2}{4G(x^2 + z^2)} \quad (2.15)$$

Further developments by Verruijt and Booker (1996) allow compressible material and ovalisation of the tunnel. The equation representing settlement is given in equation 2.16, where now  $S_x$  represents surface settlement at  $x$  distance from the tunnel axis. Poisson's ratio is given by  $\nu$ , radial contraction is  $\varepsilon$ , and  $\delta$  is the ovalisation constant. The depth to axis of the tunnel is  $z_0$  and  $R$  is the tunnel radius.

$$S_x = 4(1-\nu)\varepsilon R^2 \frac{z_0}{z_0^2 + x^2} - 2\delta R^2 \frac{z_0(x^2 - z_0^2)}{(x^2 + z_0^2)^2} \quad (2.16)$$

Loganathan and Poulos (1998) showed that the formula can be expressed as in equation 2.17, where  $\varepsilon$  is given by equation 2.18, and  $g$ , the gap parameter, is given by equation 2.19 (Lee et al, 1992). Note that with TBM's, the  $u_{3d}^*$  parameter is taken as 0 (Chi et al, 2001).

$$S_x = 4(1-\nu)\varepsilon R^2 \left( \frac{z_0}{z_0^2 + x^2} \right) e^{\left( \frac{-1.38x^2}{(H+R)^2} \right)} \quad (2.17)$$

$$\varepsilon = \frac{4gR + g^2}{4R^2} \quad (2.18)$$

$$g = G_p + u_{3D}^* + \omega \quad (2.19)$$

$G_p$  is the physical gap that represents the difference between maximum outside diameter of the tunnelling machine and the outside diameter of the lining for a circular tunnel (equation 2.20) (Park, 2005). The thickness of the TBM tailpiece is  $\Delta$ , and  $\delta$  is the required clearance for lining installation. The workmanship parameter,  $\omega$  takes into account quality of construction, and is taken as the minimum of  $0.6G_p$  and  $0.33u_i$  (Chou and Bobet, 2002). This additional parameter  $u_i$  is the elasto-plastic strain displacement at the crown and is calculated from equation 2.21.  $N$  is the stability number and  $s_u$  is the undrained shear strength of the soil.

$$G_p = 2\Delta + \delta \quad (2.20)$$

$$\frac{u_i}{R} = 1 - \sqrt{\frac{1}{1 + \left(\frac{2(1+\nu)s_u}{E}\right) e^{\left(\frac{N-1}{2}\right)^2}}} \quad (2.21)$$

#### 2.4.5 Longitudinal settlement

The problem of longitudinal settlement has relatively little research attention. Probable reasons for this are that field data is hard to get/expensive as it has limited practical worth (Tan and Ranjith, 2003). It is also a true 3D problem as shown in figure 2-17, which immediately makes it less attractive to researchers, and it also has an unavoidable dynamic component, as accurate models need to simulate machine movement with time.

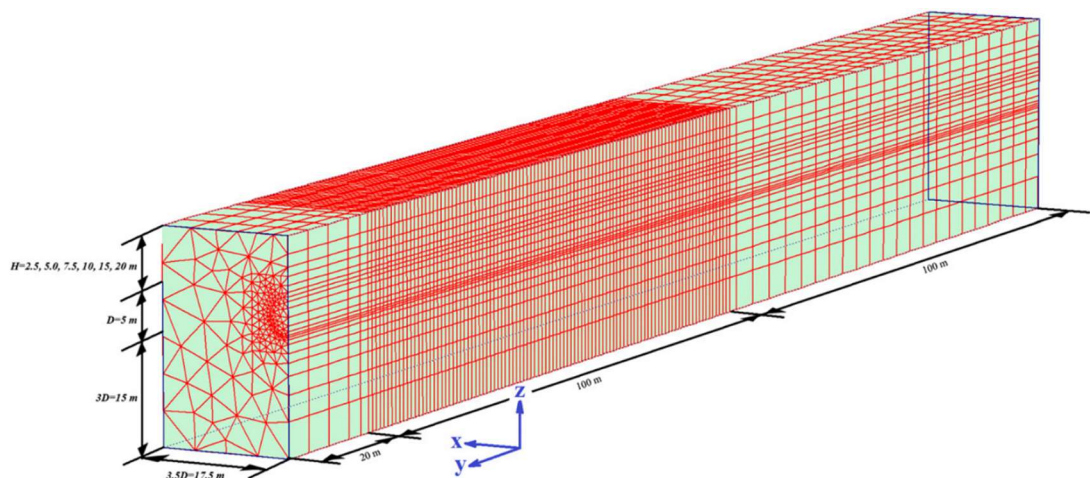


Figure 2-17 3D modelling of longitudinal tunnelling (Hajjar et al, 2014)

According to Attewell et al (1986), it is possible to use a cumulative probability curve to represent the settlement. Sagaseta (1987) proposed equation 2.22 for the distribution of longitudinal settlement, where  $V_s$  is volume loss,  $H$  is the depth to axis, and  $y$  is the longitudinal distance from the tunnel heading.

$$U_z = \frac{V_s}{2\pi H} \left( 1 + \frac{y}{\sqrt{y^2 + H^2}} \right) \quad (2.22)$$

# 3 NUMERICAL MODELLING AND *FLAC*

## 3.1 Introduction

This chapter will firstly provide a brief overview of the development of numerical methods and modelling techniques for simplifying the behaviour of a tunnel excavation. Secondly, the numerical methods being used in this research will be introduced and discussed. This includes the commercial program *FLAC*, and the pressure relaxation method used in this research.

Over the past three decades, the development of computers has led to an incredible change in the way engineering is done. This has been particularly true in the geotechnical field, where a significant portion of the design and analysis is done, and indeed expected to be completed using software (Gioda and Swoboda, 1999). It has also had a big impact on the research area (Lee, 2008). Achieving an accurate numerical model allows studies that are more comprehensive and in a more timely manner. However, this achievement of ‘accuracy’ is not easy, and for this reason of verification and validation, physical modelling is still and will continue to be very widespread for research purposes.

The modelling of geo-engineering processes requires some considerably different considerations and procedures than that of fabricated materials. There is usually relatively little site data for the design and analyses. Material data can and will vary largely, and the soil profiles, rock strata, and possible discontinuities are only ever

partially known. Because of this, numerical models are best used to study mechanisms and the effect of parameters, as illustrated in table 3-1. This has been the objective in this research – an extensive study of parameters leading to some simple design charts.

**Table 3-1 Recommended use of numerical modelling vs. amount of data**

Typical situation	Complicated geology; inaccessible; no testing budget	← ..... →	Simple geology; \$\$\$ spent on site investigation
Data	NONE	← ..... →	COMPLETE
Approach	Investigation of mechanisms	← • Bracket field behavior by parameter studies • →	Predictive (direct use in design)

## 3.2 Review of Numerical Methods for Soft Soil

Numerical methods used for geotechnical engineering in soft soil will be discussed in this section. Many methods were developed over the past decades, but the most popular and generally, the best are finite element, finite difference and boundary element methods. These are technically quite different, and each offer their own advantages and disadvantages, but their operation is consistent.

In these methods, the majority of the subsurface is modelled as a continuous block of material. Discontinuities such as structures can be modelled individually. Each method involves discretization of the problem domain by computer analysis. Geometry, Boundary, initial, groundwater, and material conditions need to be specified. Modelling instructions need to be given, then the program is run, and the dynamic and constitutive equations can be approximately solved to equilibrium or otherwise. The last and possibly most important step is for the user to interpret the results.

### 3.2.1 Finite Element Method (FEM)

The problem is discretized into a limited number of elements connected at nodal points. Changes in the geomechanics are induced by changing the original conditions, for example introducing a tunnel excavation.

The problem is analysed by solving the system of equations, which relates the unknown quantities to the known quantities using a global stiffness matrix. The concept to solve for unknown values at all points at one time like this is referred to as the implicit approach. One of the great advantages for this approach is that it presents an associated solution, meaning that both stress and strain are calculated together, which allows accurate modelling of stability and ground movement.

The founding mathematical concepts can be found in Zienkiewicz et al (1971) and Zienkiewicz et al (1977). More recent reviews and information can be found in Potts, D.M., and Zdravković (2001) and Hughes (2012).

### 3.2.2 Finite Difference Method (FDM)

This method discretises the domain similar to the FEM; elements and nodes are used. The main difference is the approach used to solve the unknown parameters. This method uses an explicit approach that works on the principle that a disturbance in the mesh will only be felt at adjacent nodes if a small enough time step is used.

This approach is mainly used for dynamic problems, but can be used as a quasi-static method if dampening is applied to the dynamic problem. This approach allows analysis of the solution procedure with time, which allows observation of movement after each individual step, a significant advantage over FEM. No matrices are generated which means that much less computer memory is required, and also that required computer power isn't linked with the size of displacements. This method is also associated, and can be used to simulate stability and settlement problems together. See Cundall (1976) for founding mathematics.

### 3.2.3 Boundary Element Method

This method is relatively new, particularly for modelling tunnels. It is different from FEM and FDM in that only the boundaries are discretised into elements, and the rest of the continuum is estimated using linear partial differential equations. For this reason, this method is most commonly used for homogenous formations with no or very few discontinuities. However, to overcome some of these shortcomings it is common to introduce internal boundaries to increase accuracy, and address changes in materials and structure interfaces like tunnels. This method requires comparably much less calculations than other methods and can be very efficient.

However, scenarios with complicated geometry and soil profiles may be inappropriate for this method. See Crouch, Starfield, and Rizzo (1983) for founding mathematics and Ang (2007) for a more recent review and introduction to this method.

### 3.2.4 Limit Analysis (FELA)

Finite Element Limit analysis is theoretically very different from displacement finite element analysis (conventional FEM). Both methods use elements in a mesh to form a discrete formation. However, the problem formulation is very different. In FELA, the solution is obtained by optimising two conditions, a lower bound and an upper bound. The lower bound is found on the principle that any set of loads supported by a statically admissible stress field will underestimate the true collapse load. The upper bound is found on the principle that any kinematically admissible velocity field will provide an unsafe solution to the true collapse load. The true solution can therefore be bracketed between these lower and upper bounds. This approach is particularly good for analysing stability, but won't be particularly good for accurate assessment of ground movement.

A full detailed description of the theory and development of this method has been done by Sloan (2013). The initial developments using linear programming are in Sloan (1988 and 1989). The newer developments are based on a much faster non-linear programming formulation by Lyamin and Sloan (2002a and 2002b). Even newer developments by Krabbenhoft et al (2005 and 2007) allow geometry and loading conditions that are more complex. Publications using this method particularly in tunnelling have been discussed in chapter 2.

## 3.3 Review of Modelling Tunnel Processes

Tunnel excavation is a three dimensional engineering process. While recognising that three-dimensional analysis is becoming possible in the work place, still two-dimensional modelling dominates. This is because there are practical limits on cost and computer resources, which, when performing analyses sufficiently sophisticated to handle all the complexities of tunnelling, restrict users to two-dimensional modelling. If multiple shallow tunnels are to be analysed, or if the ground surface response is key to the analysis then a plane strain representation of the transverse section is required. If a single deep tunnel is to be investigated, and



surface effects are not of prime interest, then an axially symmetric approximation may be appropriate and heading advance can be studied. For the reviewed subsections on Tunnel Excavation Modelling below, see also Potts and Zdravkovic (2001).

### 3.3.1 The Gap Method

This method was introduced by Rowe et al. (1983). A predefined void is introduced into the finite element mesh which represents the total ground loss expected. In this way the out of plane and in plane ground losses are incorporated together with additional losses to allow for miss-alignment of the shield, the quality of workmanship, and the volume change due to soil remoulding. It is clear therefore, how one can account for the different tunnel construction methods outlined above by varying the size of the void. For example, if modelling an EPB machine, the out of plane component of the total ground loss could be reduced.

The void is placed around the final tunnel position, and allows the user to locate the soil boundary prior to excavation. This is achieved by resting the invert of the tunnel on the underlying soil and prescribing the gap parameter at the crown. The gap parameter is the vertical distance between the crown of the tunnel and the initial position before tunnelling. The analysis proceeds by removing boundary tractions at the perimeter of the opening and monitoring the resulting nodal displacements. When the displacement of a node indicates that the void has been closed and the soil is in contact with the predefined lining position, soil/lining interaction is activated at that node. The soil and the lining are actually treated as separate bodies, related only by nodal forces (Rowe et al, 1978).

### 3.3.2 The Convergence-Confinement Method

Another approach to modelling excavation is the  $\lambda$  or convergence-confinement method (Panet and Guenot, 1982), in which the proportion of unloading before lining construction is prescribed, so volume loss is a predicted value. An internal force vector,  $(1 - \lambda)\{F_0\}$ , is applied at the nodes on the tunnel boundary ( $\{F_0\}$  being equivalent to the initial soil stresses  $\{\sigma_0\}$ ).  $\lambda$  is initially equal to 0 and is then progressively increased to 1 to model the excavation process. At a prescribed value  $\lambda_d$  the lining is installed, at which point the stress reduction at the boundary is  $\lambda_d\{\sigma_0\}$ .

The remainder of the stress reduction is applied to create the lining stress. The stress reduction with the lining in place is then  $(1 - \lambda)\{\sigma_0\}$ .

### 3.3.3 The Strength Reduction Method

The strength reduction or progressive softening method is very common in slope stability analysis, and in engineering practice. In this method, the shear strength of the soil is gradually reduced until a failure condition is triggered. The factor of safety at this point can then be calculated as the ratio of the actual shear strength to the virtual shear strength at collapse. This method will provide a good estimate for analysis of stability, but will not produce reliable results for settlement prediction as the soil's properties are being changed during the modelling process. It is also very applicable for parametric studies. This method is also built into many commercial FEM and FDM software, and is therefore quite user friendly.

### 3.3.4 The Volume Loss Control Method

This method is similar to the convergence-confinement method, but instead of prescribing the proportion of unloading prior to lining construction, the analyst prescribes the volume loss that will result on completion of excavation. This method is therefore applicable to predictive analyses of excavation in soil types for which the expected volume loss can be confidently (and conservatively) determined for the given tunnelling method. It is also invaluable for worthwhile back analysis of excavations for which measurements of volume loss have been made. This method is very good for settlement analysis, as the material isn't being manipulated during the solution process.

## 3.4 *FLAC*

*FLAC* (short for Fast Lagrangian Analysis of Continua) is an explicit finite difference scheme for engineering mechanics, and is usually associated with geotechnical engineering and geomechanics (Itasca, 2003). It features Lagrangian analysis, a fully dynamic equation of motion, and built-in constitutive models. The method is similar to the Finite Element Method in that the subsurface is modelled as a continuum that is divided into a number of elements, which are interconnected at their nodes. The primary difference lies in the approach used to solve the unknown

parameters. In contrast to the implicit approach of the Finite Element Method, the Finite Difference Method (FDM) uses an explicit approach.

Finite differences are one of the oldest numerical techniques for solving differential equations and initial conditions. In this method, every derivative is replaced by an algebraic expression in terms of the variables – stress, displacement, etc, like in equations 3.1, 3.2, and 3.3. This is done for an arbitrary number of discrete points in the problem space – and at least initially, these variables will be undefined. The explicit method builds on the idea that for a small enough time step, a disturbance at a given mesh point is experienced only by its immediate neighbours. This implies that the time step is smaller than the time that the disturbance takes to propagate between two adjacent points. The objective for FDM is then to iterate until a solution is found with minimal unbalanced force and therefore minimal acceleration. This indicates an equilibrium. This is in contrast with the implicit approach of the finite element method, which requires each of the variables to for each element to be initially specified, with the objective of the formulation to minimize error.

For most Finite Difference programs, this time step is automatically determined such that numerical stability is ensured. Initially conceived as a dynamic, i.e. time related, computation approach the Finite Difference method can be used to solve static problems by damping the dynamic solution. Then, "time step" does not refer to a physical but rather to a problem solution (time) step. Analysed velocities relate to displacement in length per time step.

Forward Difference

$$\Delta_h f(x) = f(x+h) - f(x) \quad (2.23)$$

Backward Difference

$$\Delta_h f(x) = -f(x-h) + f(x) \quad (2.24)$$

Central Difference

$$\Delta_h f(x) = f(x+0.5h) - f(x-0.5h) \quad (2.25)$$

The solution scheme is given in figure 3-1, which shows the iteration cycle between the constitutive and the dynamic simulation. The separate solution for individual mesh points implies that no matrices need to be formed. For each time step an

individual solution is obtained for each mesh point. The calculation cycle leading to the solution involves Newton's law of motion and the constitutive law of the in situ material. The acceleration solved for a mesh point is integrated to yield the mesh point velocity, which in turn is used to determine the strain change. Subsequently, strains determine the corresponding stress increments which in turn generate forces on the surrounding mesh points. These are summed to determine the resulting out-of-balance force that relates to the acceleration that started the calculation cycle. The method is described in more detail by Cundall and Board (1988).

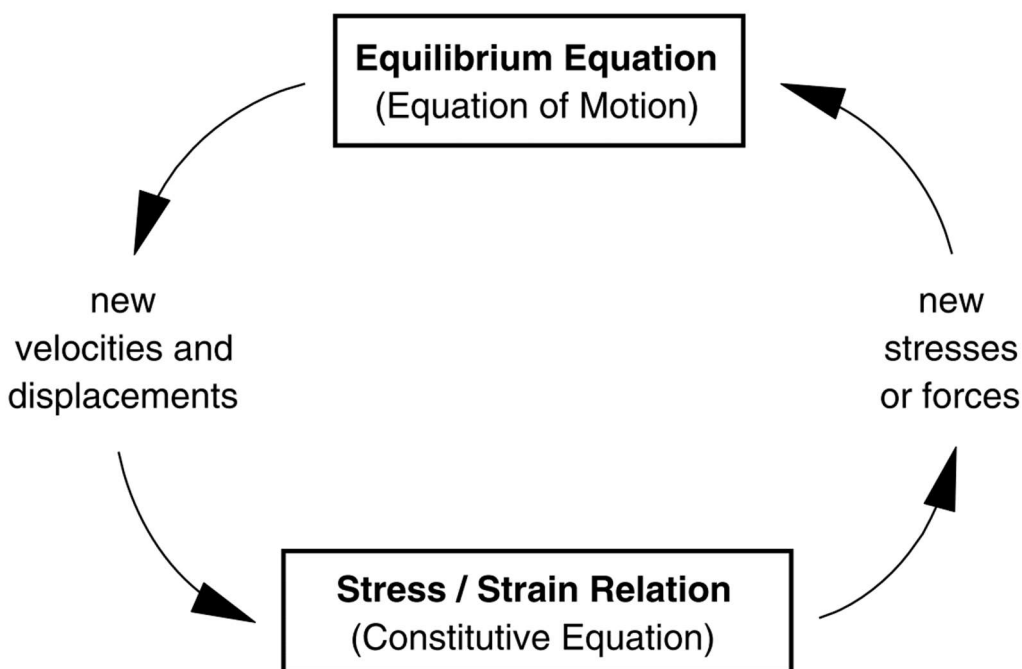


**Figure 3-1 Basic calculation cycle in *FLAC***

The general equation of motion in a continuous solid body is given in equation 3.4. This equation relates the two simulations (constitutive and dynamic), and allows calculation of element velocities from stresses.

$$\rho \frac{\partial \dot{u}_i}{\partial t} = \frac{\partial \sigma_{ij}}{\partial x_j} + \rho g_i \quad (2.26)$$

The strain rates are then calculated from these velocities using equation 3.5.

$$\dot{\epsilon}_{ij} = \frac{1}{2} \left[ \frac{\partial \dot{u}_i}{\partial x_j} + \frac{\partial \dot{u}_j}{\partial x_i} \right] \quad (2.27)$$

Strain rates are then used to recalculate element stresses using the constitutive simulation, of which a general form is given in equation 3.6.

$$\sigma_{ij} := M(\sigma_{ij}, \dot{\epsilon}_{ij}, \kappa) \quad (2.28)$$

### 3.5 Pressure relaxation method

With the development of powerful computers over the last two decades, numerical modelling has proceeded to become a dominant technique for problem resolution. This study uses a pressure relaxation method developed with the built-in program language of *FLAC* (*FLACish* or *FISH*). An approach such as this was first developed by Panet and Guenot (1983), whereby the internal tunnel pressure ( $\sigma_t$ ) is gradually reduced to zero from a starting amount equalling the equivalent in-situ soil pressure.

In this study, the soil is considered as a homogenous undrained clay following the Mohr-Coulomb (MC) model, i.e. a Tresca material. This is despite the fact that other soil models, such as the modified cam-clay model may give a more accurate simulation of ground movements (Brinkgreve, 2005). However, the MC model has the clear practical advantages of fewer input parameters, and greater familiarity for engineering practitioners. The system will be described in terms of dimensionless ratios such as  $C/D$ ,  $S/D$ ,  $\gamma D/S_u$ , and  $E/S_u$ .

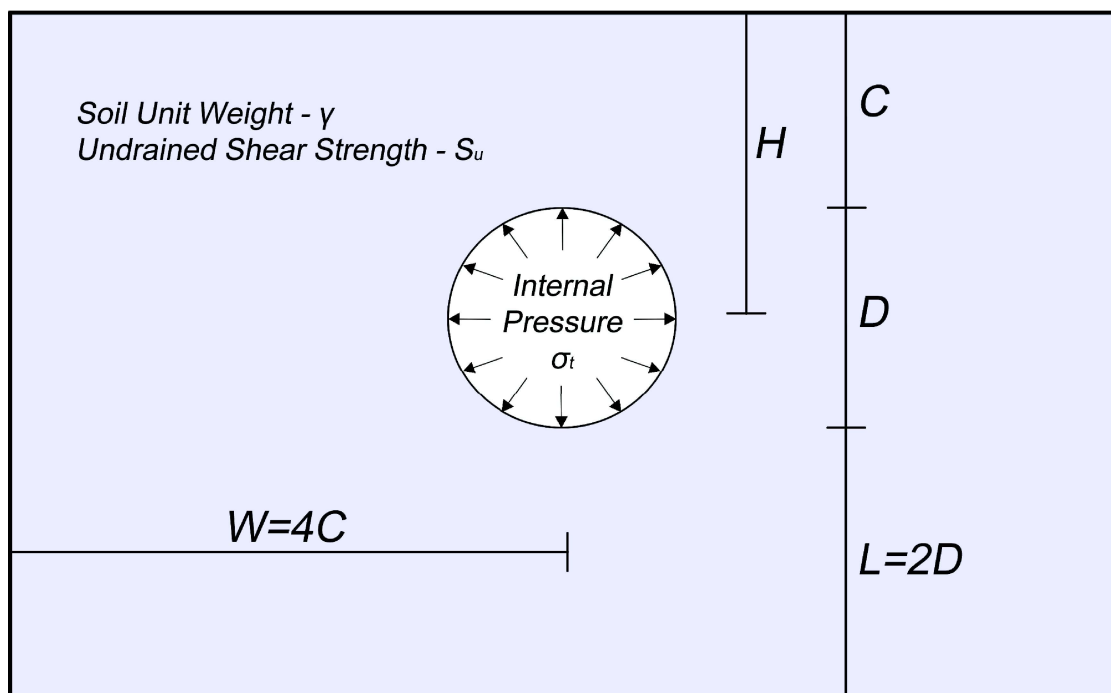
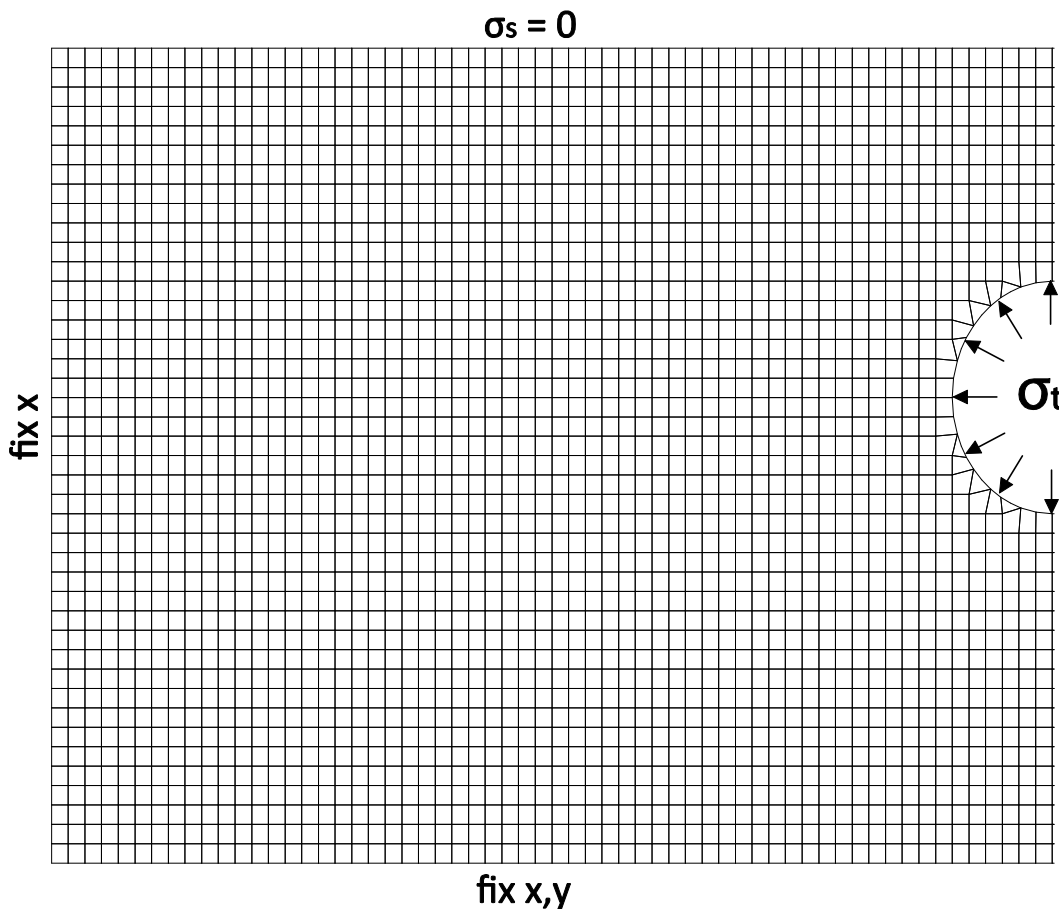


Figure 3-2 2D plane strain definition of the tunnel problem

Using this approach, the results can be studied methodically, and practical design charts employing these ratios can be produced that should cover a practical range. The circular tunnel problem is shown in Figure 3-2. In this study, only greenfield settlement has been analysed, thus the surcharge load ( $\sigma_s$ ) is set to 0 kPa.

The problem is modelled using 2D plane strain conditions in *FLAC* despite the fact that tunnelling is a three-dimensional activity. It has been found that the transverse settlement problem (cross-section) under greenfield conditions can be modelled quite accurately with this simplification (Ghaboussi et al, 1978), as long as the tunnel is considered as 'long'.



**Figure 3-3 - Typical mesh of the single tunnel script**

A typical finite difference mesh of the problem in this study is shown in figure 3-4. The boundary conditions are set to standard fixities and the domain is made large enough such that the soil mass is modelled accurately despite using a finite mesh. Using figure 3-2,  $L = 2D$  and  $W = 4C$  are adopted in all analyses of the thesis, which has been found to work well, with very little boundary interference.

After defining boundary conditions, soil properties and tunnel geometry, the developed model slowly reduces the internal supporting pressure from the at-rest pressure, at each relaxation step. In this study, the model was set to fully relax from 100% in-situ pressure to 0% in 1% increments. At each of these relaxation steps, the surface settlement data is recorded, and the stability number is calculated for later analysis.

The internal pressure  $\sigma_t$  is reduced by multiplying the at-rest pressure, where no movement occurs, by a reduction factor, which is based on the number and range of relaxation steps. At each subsequent relaxation step, the internal pressure is less than the at-rest pressure, and consequently the soil moves into the tunnel void until the internal forces in the soil reach equilibrium, balanced or otherwise.

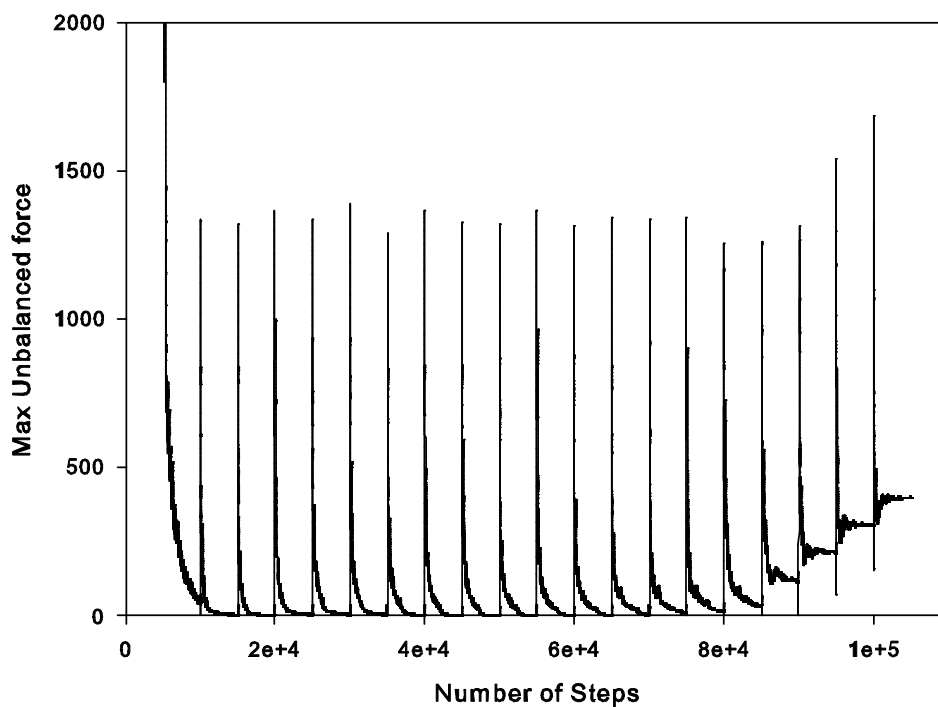


**Figure 3-4 - Max unbalanced force history ( $C/D=3$ ,  $\gamma D/s_u=4$ ,  $E/s_u=200$ )**

In the elastic state, internal forces have reached a balanced state (total unbalanced force in *FLAC* approaches zero), no more movement takes place and the circular tunnel is considered stable. Once the internal pressure is reduced to the extent where the internal forces are no longer sufficient to retain the earth pressures, total unbalanced forces will never approach zero and the tunnel is considered unstable.

This failure point or point of collapse (PoC) is quite abrupt and can be identified relatively easily by observing the unbalanced force history such as in figure 3-4. In

this figure, the number of steps is on the x-axis and the maximum unbalanced force is on the y-axis. In this study, 5000 iteration steps are used for each relaxation stage. Therefore, every 5000 steps in this figure where there is a 'jump' in max unbalanced force is the start of a new relaxation stage where the internal pressure has been slightly reduced (by 1% increment). With this in mind, it can be seen that an equilibrium is successfully found after approximately 80,000 steps when the max unbalanced force won't go to zero - this is the PoC. This point can also be clearly observed using plasticity indicator and velocity plots such as in figure 3-5.

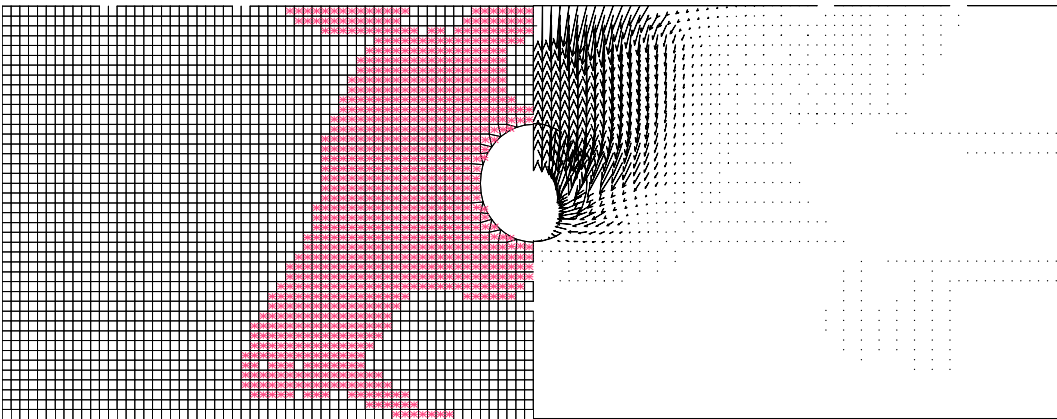


**Figure 3-5 - Plasticity plot (left) and velocity plot (right)**

A screenshot of the inputs section of the *FLAC* script is shown in figure 3-6. The developed script is quite user friendly, and given *FLAC*'s ability to queue jobs, it is very efficient and time effective to set up and run parametric studies.



```

; -----Developed by Dr. Jim Shiau, PhD(Newcastle)↓
; -----@ University of Southern Queensland, Toowoomba, QLD, 4350, Australia↓
;call c:\0\Circular_Stability_Settlement.txt↓
    new↓
    set echo on↓
    set plot emf↓
    config extra=10; ↓
    set overwrite on↓
    set replot on; "off" to add to the existing plot↓

↓
def para_meter↓
; :::::CHANGE the following parameters to suit your need:::::↓
; -----Set up all the parameters of the model↓
; -----This is the place you can change problem geometry↓
; ----- and material property↓
    pathname = 'F:\z\CD1\2\100c'      ; files will be saved here!!↓
    Save_or_not = 'YES'              ; "YES" - save all files (*.sav and *.emf)↓

↓
    Start_from_p = 0                 ;increment start from ??? %↓
    end_at_p = 100                   ; only Save at ??? % relaxatio↓

↓
    C = 6                             ; Height of overburden soil (m)↓
    D = 6                             ; Diameter must be 2 or above (m)↓

↓
    SOIL_DEN = 1631                  ; Soil density↓
    SOIL_COH = 48000                 ; A small 5 Pa to improve numerical stability↓
    SOIL_FRI = 0                    ; zero for clay↓
    SOIL_DIL = 0                    ; ** watch this value very carefully**↓
    SOIL_TENS = 10e10                ; very limited soil tension(N/m2, Pa)↓
    SOIL_Young = 4.8E6              ; Youngs Modulus ↓
    SOIL_poisson = 0.45             ; Poisson's ratio↓

↓
    Set_grav = 1*9.81               ; centrifuge model -more g required for clay↓
; -----surface pressure set to zero in most cases (in pascal, N/m2)-----↓
    Sigma_s = 0                     ; For soft cases, better set sigma_s=0 (N/m2, Pa)↓
; -----For strong cases, non-zero sigma_s is required to fail the soil.↓

↓
    No_step= 5000                   ; no of steppings for each relaxation↓
    No_relax = 101                  ; e.g. 21, 31, 51,101 ... etc↓
    XElementSize = 0.5              ; (m), element size;divide equally with B↓
    YElementSize = 0.5              ; (m), for coarse- use "0.5"; fine - "0.1"↓
; :::::CHANGE the above parameters to suit your need:::::↓

```

Figure 3-6 - Inputs section of the pressure relaxation script for *FLAC*

# 4 SINGLE TUNNEL SETTLEMENT

## 4.1 Introduction

This chapter describes the verification and use of a numerical model for investigating the settlement of single circular tunnels in cohesive soils at the point of collapse, and at preceding stages. The model aims to simulate the movement and relaxation of the soil around the shield and lining annulus that occurs due to the overcutting and grouting of the tunnel void by a tunnel-boring machine (TBM). To achieve this, the model uses a pressure relaxation technique that progressively reduces the tunnel support pressure from an initial condition until any points of interest, such as the point of collapse. At these stages, the surface settlement data is exported for analysis. In this chapter, data is exported for the collapse stage, and three previous pre-collapse 'working condition' stages.

The surface settlement data from these stages is exported for analysis using a regression of the commonly used Gaussian equation on the settlement data. Doing this allows accurate determination of  $i_x$  values for each case. This is done for a number of geometry and soil ratios, which will cover the most practical range for soft cohesive soils. The results of this study are quite positive, settlement results compare well with previous experimental and observational results. Design charts using dimensionless ratios have therefore been presented.

## 4.2 Problem Definition

Surface settlement induced by tunnelling is a complex phenomenon that is dependent on many factors such as soil and groundwater conditions, tunnelling dimensions and construction techniques. Therefore, much modern tunnelling research has been given to provide more accurate predictions of the soils response to tunnel construction.

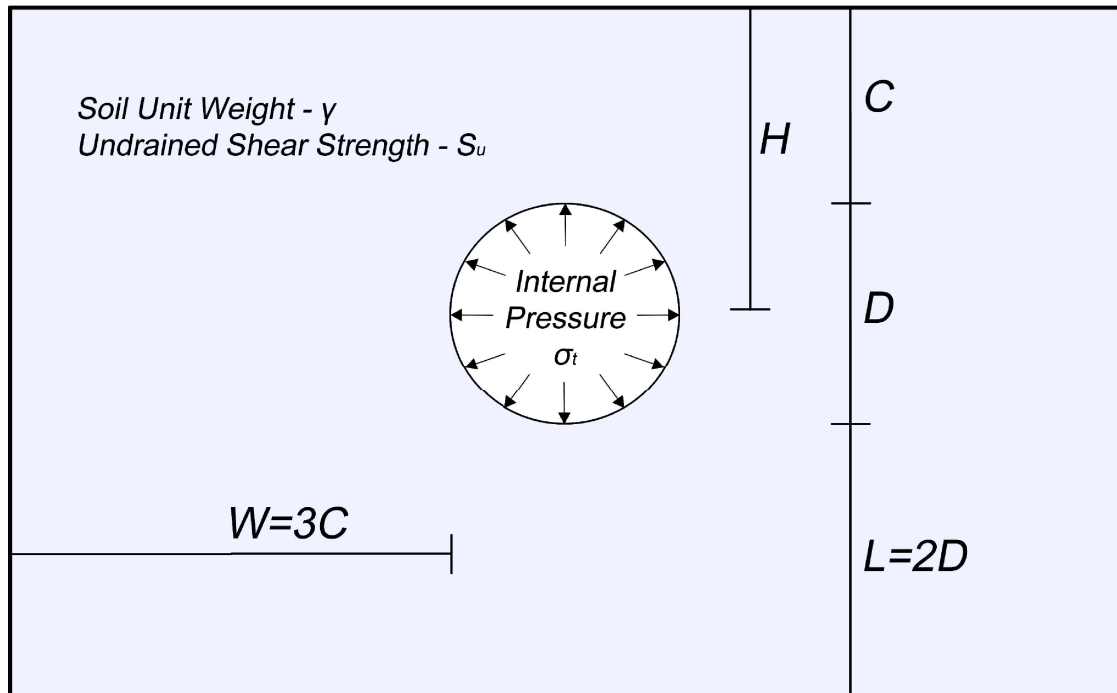


**Figure 4-1 Typical diagram of a single tunnel**

The circular tunnel problem is shown in figure 4-1. In this study, only greenfield settlement has been analysed. Thus, the surcharge load ( $\sigma_s$ ) is set to zero kPa. The soil is considered as homogenous undrained clay following the Mohr-Coulomb (MC) model. Despite the fact that other soil models, such as the modified cam-clay model may give a more accurate simulation of ground movements, the MC model has the practical advantages of fewer input parameters and greater familiarity for engineering practitioners. The system will be described in terms of dimensionless ratios: depth ratio  $C/D$ , soil strength ratio  $\gamma D/S_u$ , and Young's Modulus ratio  $E/S_u$ .

The general profile of tunnel settlement is shown in figure 4-2.  $D$  is the diameter of the tunnel,  $H$  is the ground surface to tunnel axis depth, and  $C$  is the overburden.  $S_x$  is the vertical settlement at distance,  $x$  at the surface,  $S_{max}$  is the maximum vertical settlement, and  $i_x$  is the trough width parameter, which, physically, is the distance from the tunnel axis to the point of inflection of the curve. The volume loss at the

surface  $V_s$ , is equal to the ground moving into the tunnel in this case, as clay is considered non-dilational. This volume loss is commonly given as a percentage of the tunnel cross section area.

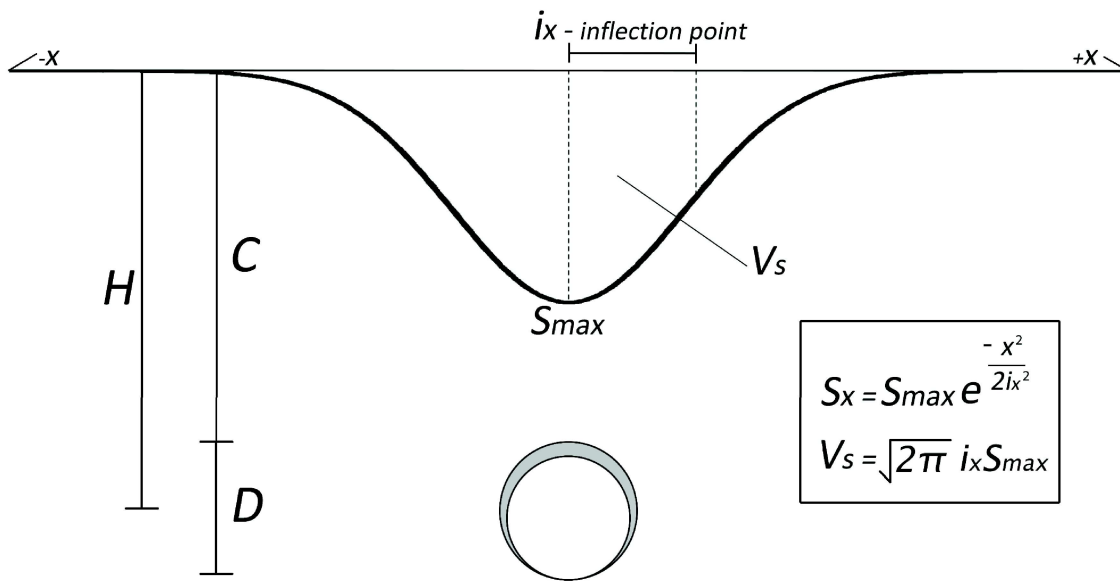


**Figure 4-2 Typical settlement induced by a single tunnel**

The most common method for describing this settlement profile is the empirical method. This estimation of surface settlements generally follows a Gaussian distribution curve, as in equation 4.1. This approach was first suggested by Martos (1958), who observed that it matched settlement patterns of deep excavations remarkably well. For the particular application to tunnels, research by Peck (1969) indicated a close fit with experimental and observational results. This method requires the input of a trough parameter ( $i_x$ ) which influences the physical width of the profile, and relates the volume loss ( $V_s$ ) and the maximum settlement ( $S_{max}$ ), as in equation 4.2 and figure 4-2.

$$S_x = S_{max} e^{-\frac{x^2}{2i_x^2}} \quad (4.1)$$

$$V_s = \sqrt{2\pi} \cdot i_x \cdot S_{max} \quad (4.2)$$

In practice, a target volume loss will likely be known, based on experience or client specified. This and the estimated  $i_x$  can be used to predict a  $S_{max}$ , which can then be

used in equation 4.1. This is the reason why the accurate estimation of  $i_x$  is important, as it heavily influences the predicted settlement profile.

This paper will study the following parametric range:  $C/D = 1 - 5$ ,  $\gamma D/s_u = 1.5 - 6$ , and  $E/s_u = 100 - 800$ . Using this approach, the results can be studied methodically, and practical design charts employing these ratios can be produced that should cover a practical range.

### 4.3 Method of Analysis

As previously discussed, these settlement profiles are commonly represented by the Gaussian equation, as in equation 4.1. In this study, this equation has been used for a regression with the data collected at the collapse and previous stages.

This has been done using *MATLAB*, and the curve fitting toolbox. In this analysis, the  $S_{max}$  parameter is fixed at the  $S_{max}$  of the data, and the trough width parameter is varied until the best solution is found. The curve-fitting toolbox uses robust bi-square regression combined with a trust-region algorithm. A typical example of this is shown in figure 4-3. It was found that using this equation to model settlement could be considered accurate, with  $r^2$  values of greater than 0.97 achieved for all cases, where an  $r^2$  of one would indicate a perfect fit. The example shown in figure 9 is for  $C/D = 4$ ,  $\gamma D/s_u = 3$ , and this particular example has an  $r^2 = 0.987$ . By curve fitting the equation to the *FLAC* data in this way,  $i_x$  values can be produced for each case reliably.

Figure 4-4 compares the settlement profiles obtained at the relaxation stages being analysed in this chapter. There is the point of collapse (PoC), 50% PoC, 25% PoC, and 10% PoC. For example, if the PoC was detected after 53% relaxation, then the pre-collapse stages being analysed would be 27%, 13%, and 5% relaxation. Note that in this figure (4-4), these profiles are of a particular case ( $C/D = 4$ ,  $\gamma D/s_u = 2$ ,  $E/s_u=400$ ). The deformation during the point of collapse (PoC) stage is very large and occurs abruptly at that stage. Observations of the deformation indicate that the change in movement amount for each relaxation step increases up to the PoC. A certain amount of heaving can also be observed at the surface, this is due to some squeezing effect of the tunnel. As the tunnel is ovalised, the sides push outwards and cause some slight blowout effects.

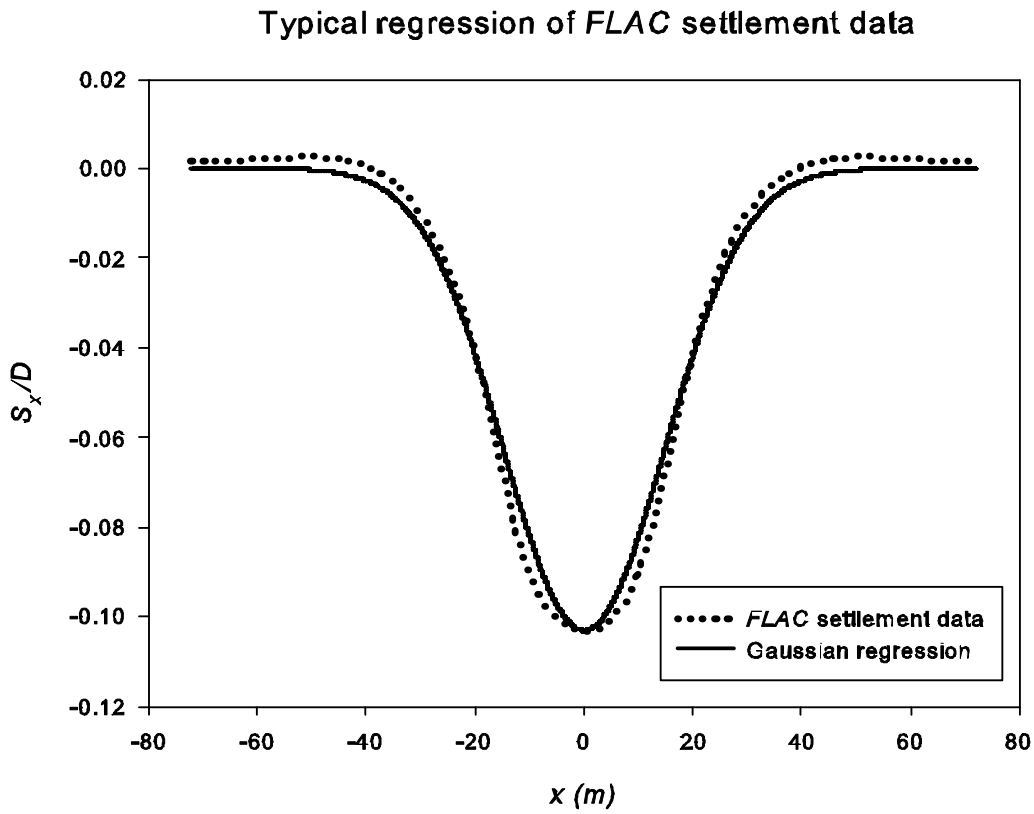


Figure 4-3 A typical regression of the Gaussian equation to the *FLAC* settlement data

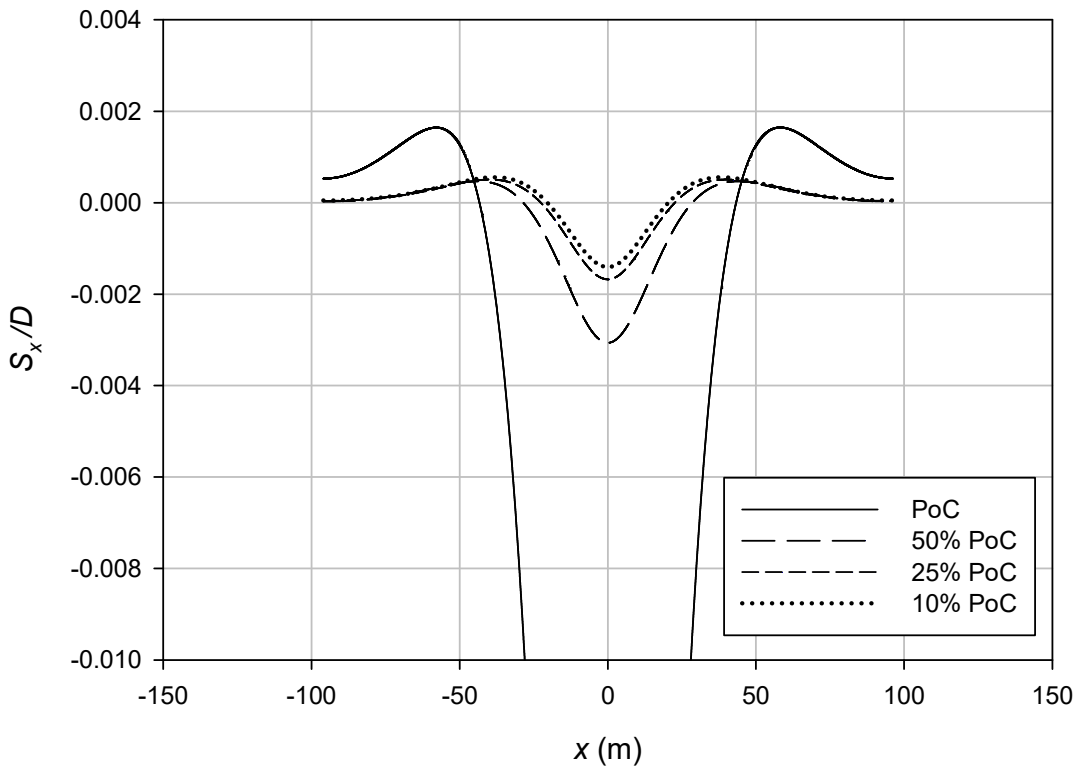


Figure 4-4 Settlement profiles at varying stages during relaxation ( $C/D=4$ ,  $\gamma D/s_u = 2$ ,  $E/s_u=400$ )

#### 4.4 Results – At Collapse

In figure 4-5, the depth ratio ( $C/D$ ) is varied and the strength ratio ( $\gamma D/S_u$ ) and Young's modulus ( $E$ ) are kept constant. The profiles are as expected, with the shallow case producing a narrow but deep trough, that become shallower and wider as  $C/D$  increases. In figure 4-6,  $C/D$  and  $E$  are kept constant, and  $\gamma D/S_u$  is varied. Once again, the trend is as expected, when the strength ratio is increased (i.e. soils become weaker), the settlement at the point of collapse is greater. Figure 4-7 similarly shows the impact of Young's modulus, with the stiffer soils (higher  $E$ ) having proportionately lower settlement.

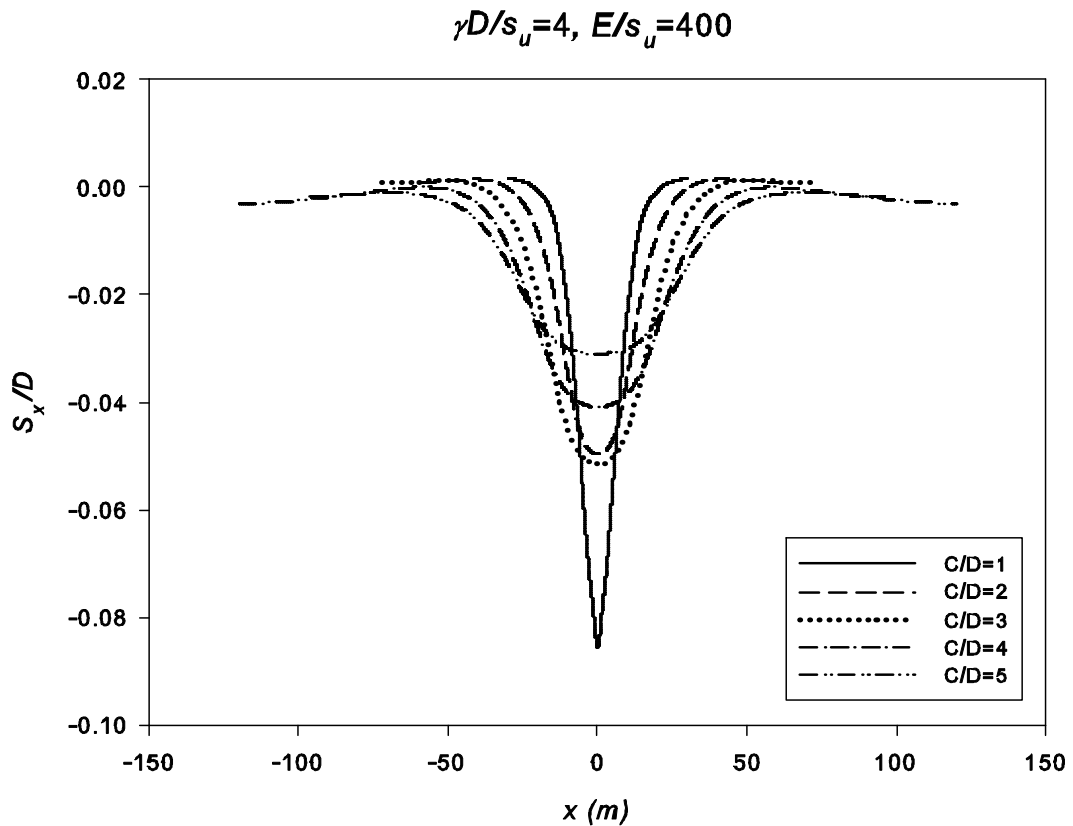


Figure 4-5 Typical settlement profiles with respect to  $C/D$

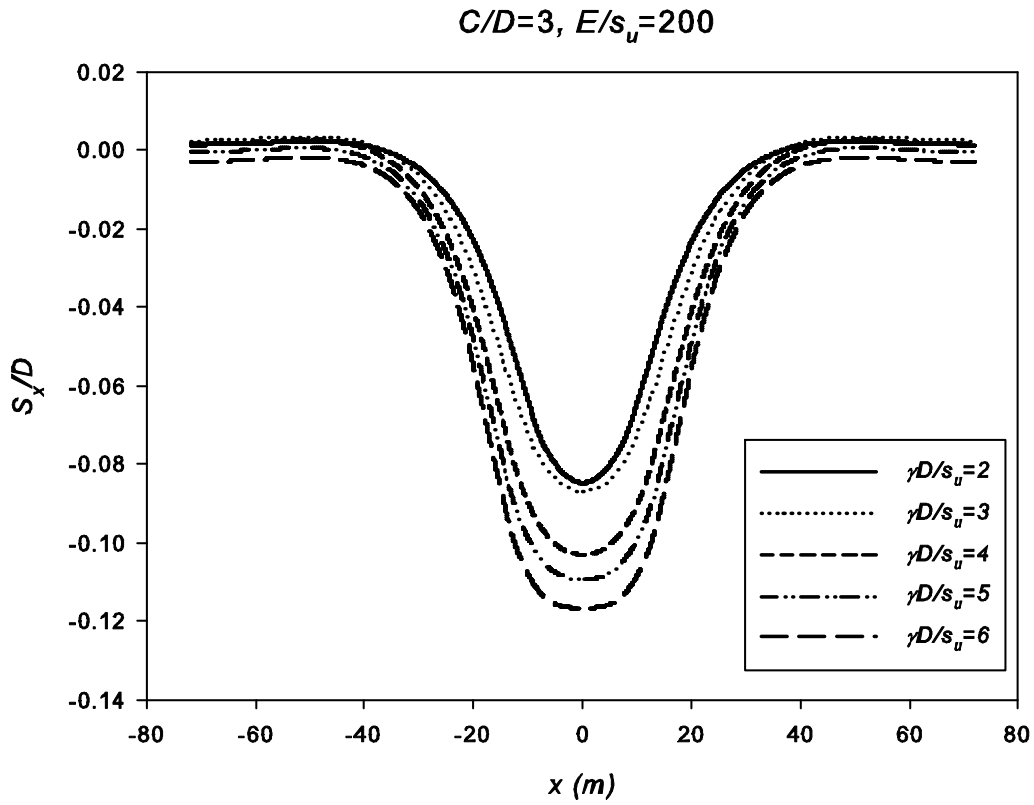


Figure 4-6 Typical settlement profiles with respect to  $\gamma D/S_u$

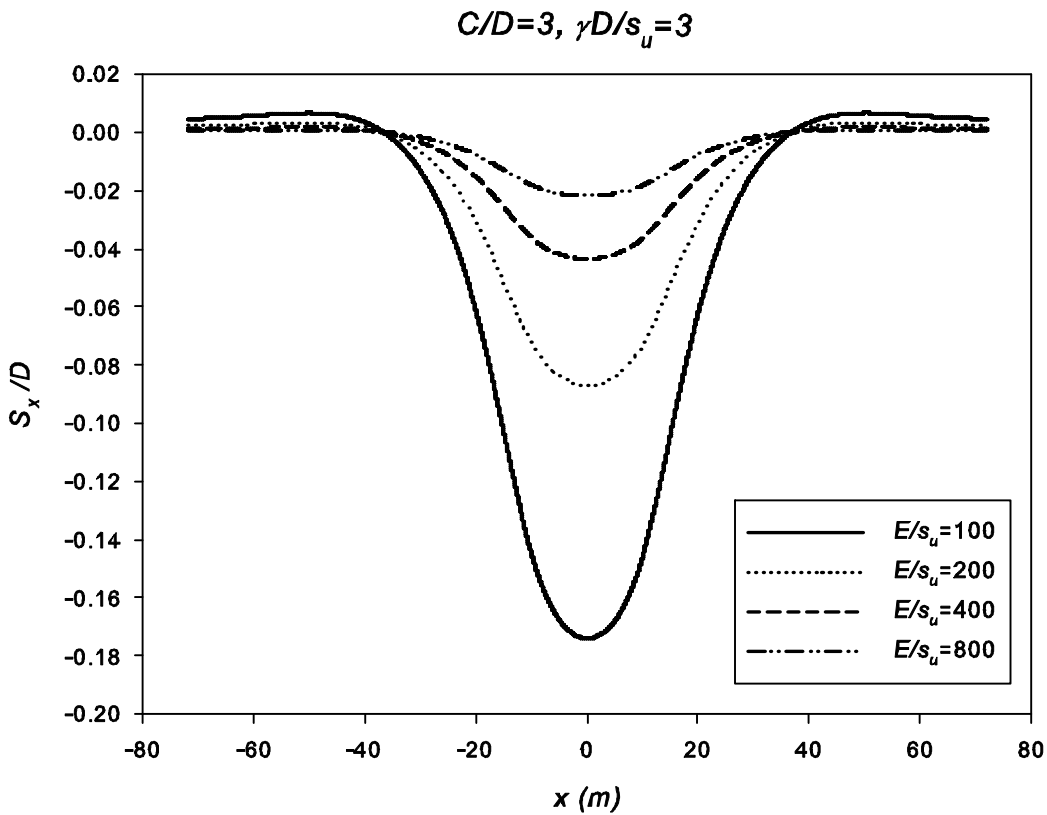


Figure 4-7 Typical settlement profiles with respect to  $E/S_u$



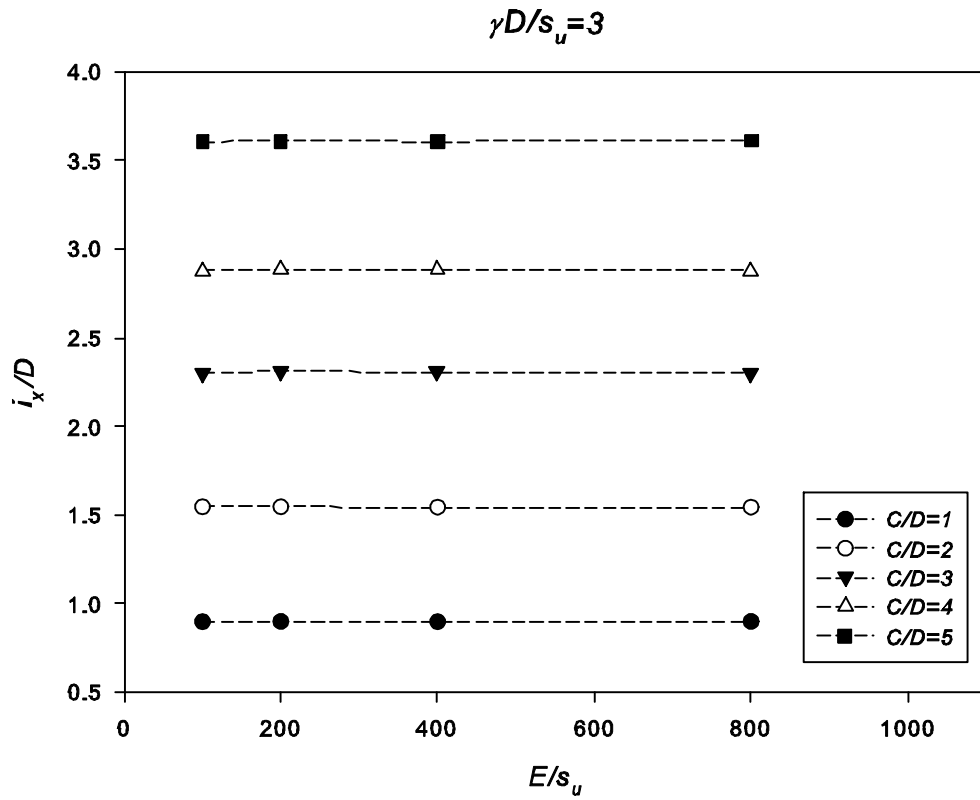


Figure 4-8  $E/s_u$  versus  $i_x/D$  with respect to  $\gamma D/s_u$

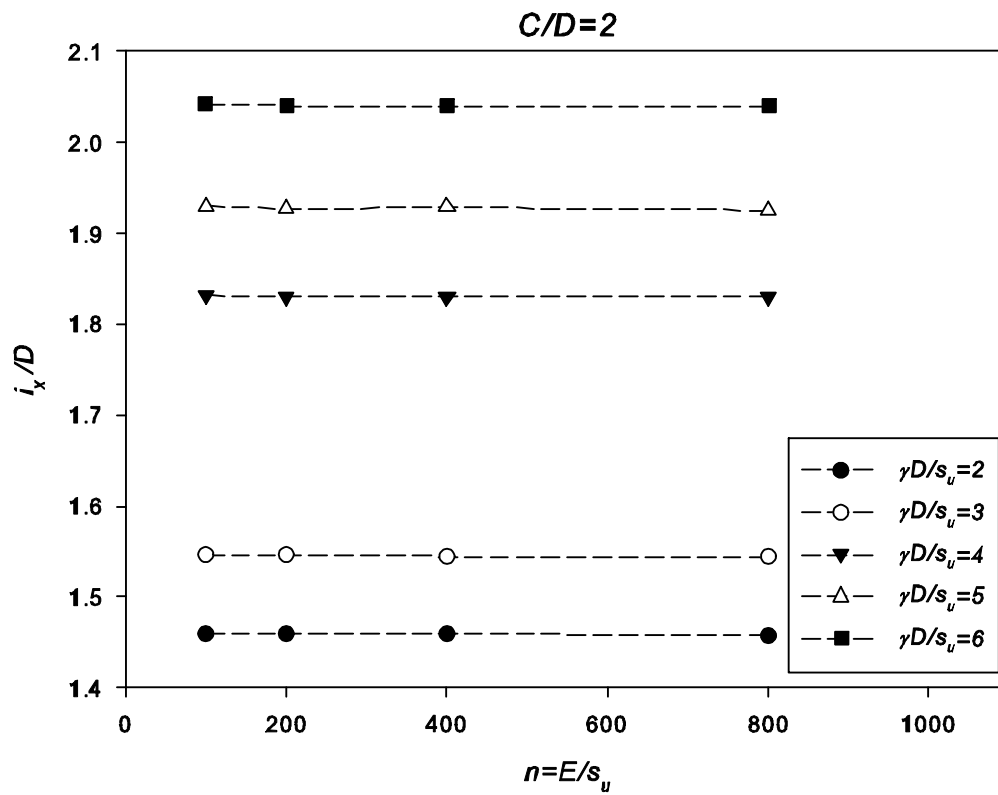


Figure 4-9  $E/s_u$  versus  $i_x/D$  with respect to  $C/D$

With  $i_x$  values obtained for the collapse stage, some observations can be made regarding the impact of the Young's modulus parameter. From figure 4-7, it is clear that this parameter will have significant effect on volume loss. However, in figures 4-8 and 4-9, the two graphs show that  $E$  has little to no impact on the  $i_x$  value obtained. So it is clear that the Young's Modulus ratio will have an impact on the magnitude of ground movement (at the same amount of pressure relaxation), but it won't have any impact on the shape factor.

With this established, the complete results can be presented with less confusion. Figure 4-10 is a graph showing the dimensionless trough parameter ( $i_x/D$ ) against  $H/D$  with various  $\gamma D/s_u$ . Presenting the results in this way allows them to be examined using O'Reilly and New's (1982) relationship, as in equation 2.8. From this relationship, the proportionality constant ( $k$ ) can be calculated for each case. As can be seen from the figure, the  $k$  values can be estimated reasonably based solely on  $\gamma D/s_u$ . Figure 4-11 shows this relationship; a linear regression can be applied to give a convenient expression for estimating  $k$ , and by extension  $i_x$ . This is given in equation 4.3. Mair and Taylor (1997) supported a recommendation that a  $k$  of 0.5 could be reasonably selected for undrained clay. This equation would tend to support this; in strong clays, it will approach 0.52.

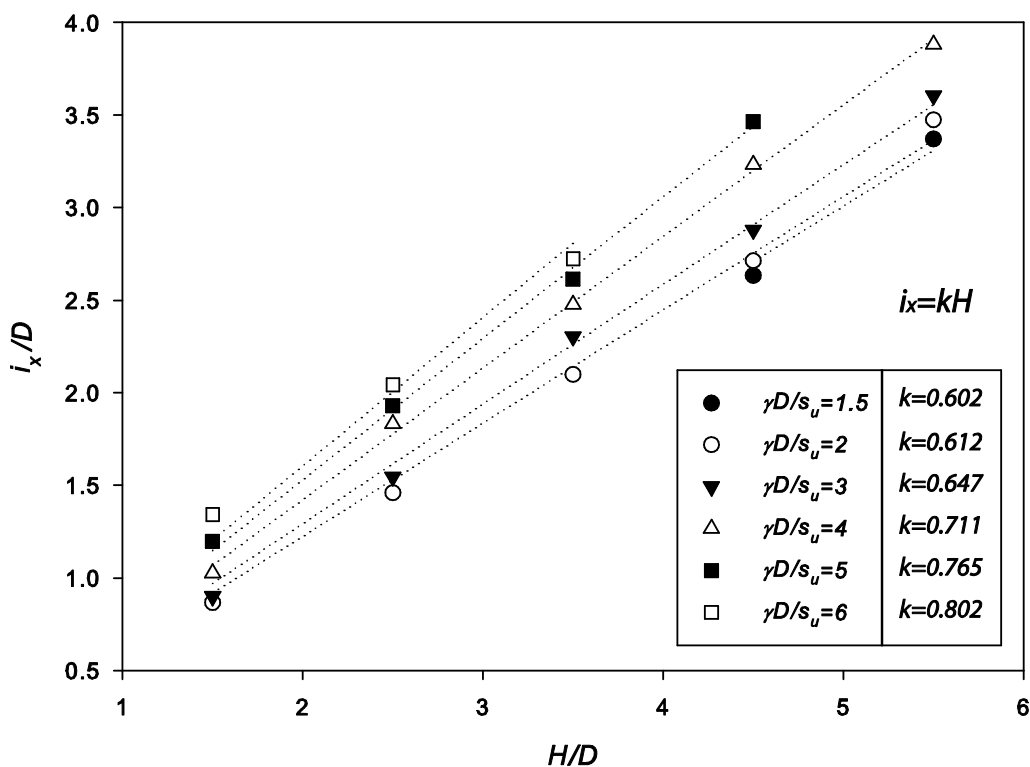


Figure 4-10 Results of regression analysis, with resulting normalised settlement parameter ( $k$ )

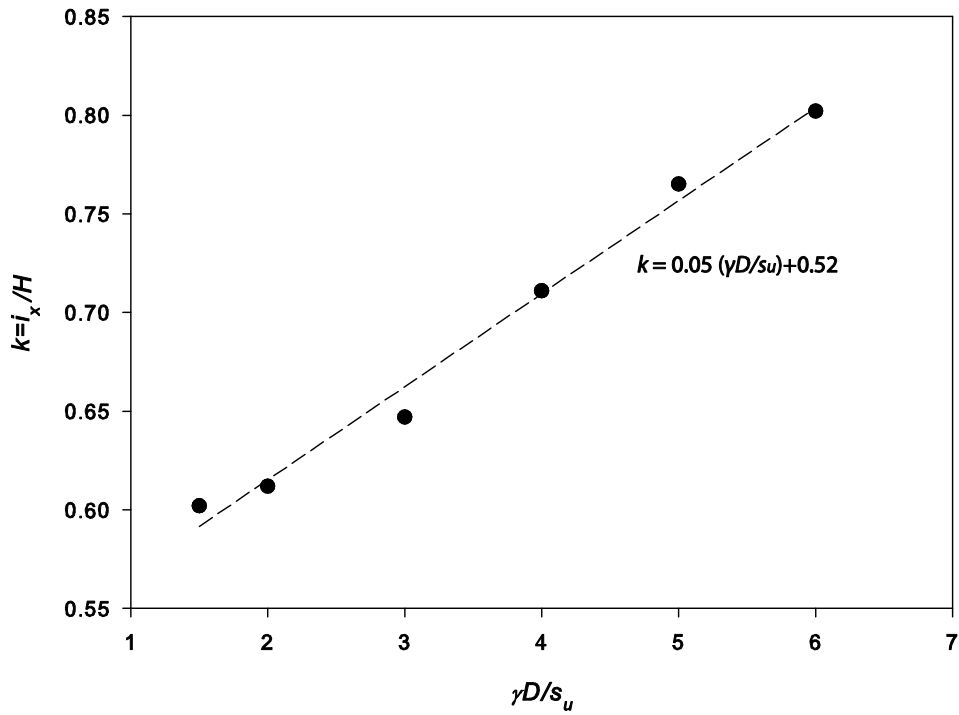


Figure 4-11 Relationship between  $k$  and  $\gamma D/S_u$

$$k = \frac{i_x}{H} = 0.05 \left( \frac{\gamma D}{s_u} \right) + 0.52 \quad (4.3)$$

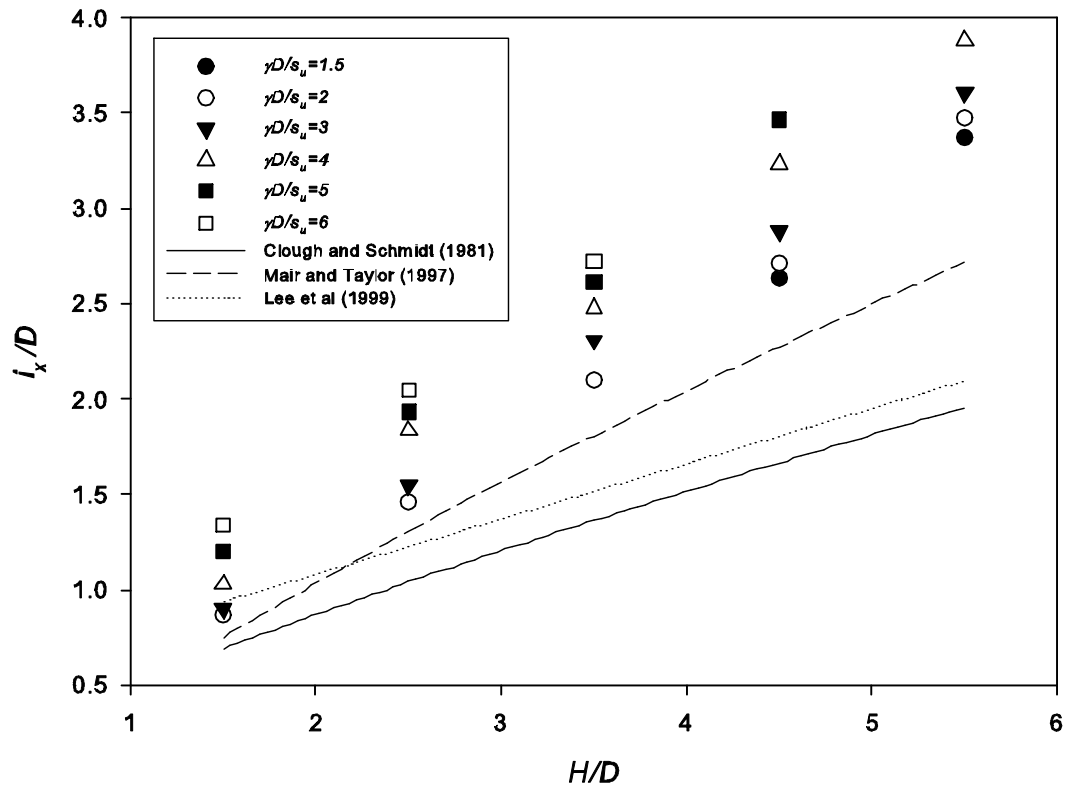


Figure 4-12 Results comparison with other suggested equations

Figure 4-12 shows the results of the regression in this study compared to suggested equations for  $i_x$  as listed in equations 2.5, 2.6, and 2.7. Note that equation 2.5 is based on  $\gamma D/S_u \approx 1.8$  (Clough and Schmidt, 1981), equation 2.6 is based on  $\gamma D/S_u \approx 2.6$  (Mair and Taylor, 1997), and equation 2.7 is based on  $\gamma D/S_u \approx 3$  (Lee et al. 1999). It can be understood that the results from this study do not match particularly well with these equations. This is due to the estimates in this study being based off the collapse stage where the volume loss is much higher. The equations are based off data where the tunnel was closer to working condition volume loss. If the settlement data was exported at an earlier relaxation stage (i.e. lower simulated volume loss), lower  $i_x$  values would be expected (Palmer and Mair, 2011). This the subject of section 4.5.

## 4.5 Results – Pre-collapse

The surface settlement data can be recorded for every relaxation of the pressure relaxation method. Thus, settlement analysis can be done for any arbitrary step. The previous section has analysed results from the collapse step. In this section, the analysis has been based on the relaxation steps of 10%, 25%, and 50% of the point of collapse (PoC). In other words, if the PoC was 52% relaxation; the stages being analysed are 5%, 13%, and 26%). This has been done such that an analysis of the settlement shape factor ( $i_x$ ) can be done at pre-collapse conditions, closer to ground loss levels experienced during construction. The volume loss can be back calculated by integrating the surface settlement data. It should be noted that this numerical model controls the internal tunnel pressure; the volume loss is not a controlled parameter.

Figures 4-13, 4-14, and 4-15 show settlement profiles with respect to specified variables. In figure 4-13, the depth ratio ( $C/D$ ) is varied and the strength ratio ( $\gamma D/S_u$ ) and Young's modulus ratio ( $E/S_u$ ) are kept constant, and the profiles are given for 50% of the point of collapse (PoC). The deeper cases consistently produce a deeper trough, which is not necessarily expected. Indeed, at the collapse stage, the opposite trend has been observed. In figure 4-14,  $C/D$  and  $E/S_u$  are kept constant, and  $\gamma D/S_u$  is varied. Once again, the trend is as expected; when the strength ratio is increased (i.e. soils become weaker), the settlement at the point of collapse is greater. Figure 4-15 similarly shows the impact of Young's modulus, with the stiffer soils (higher  $E$ ) having proportionately lower settlement.

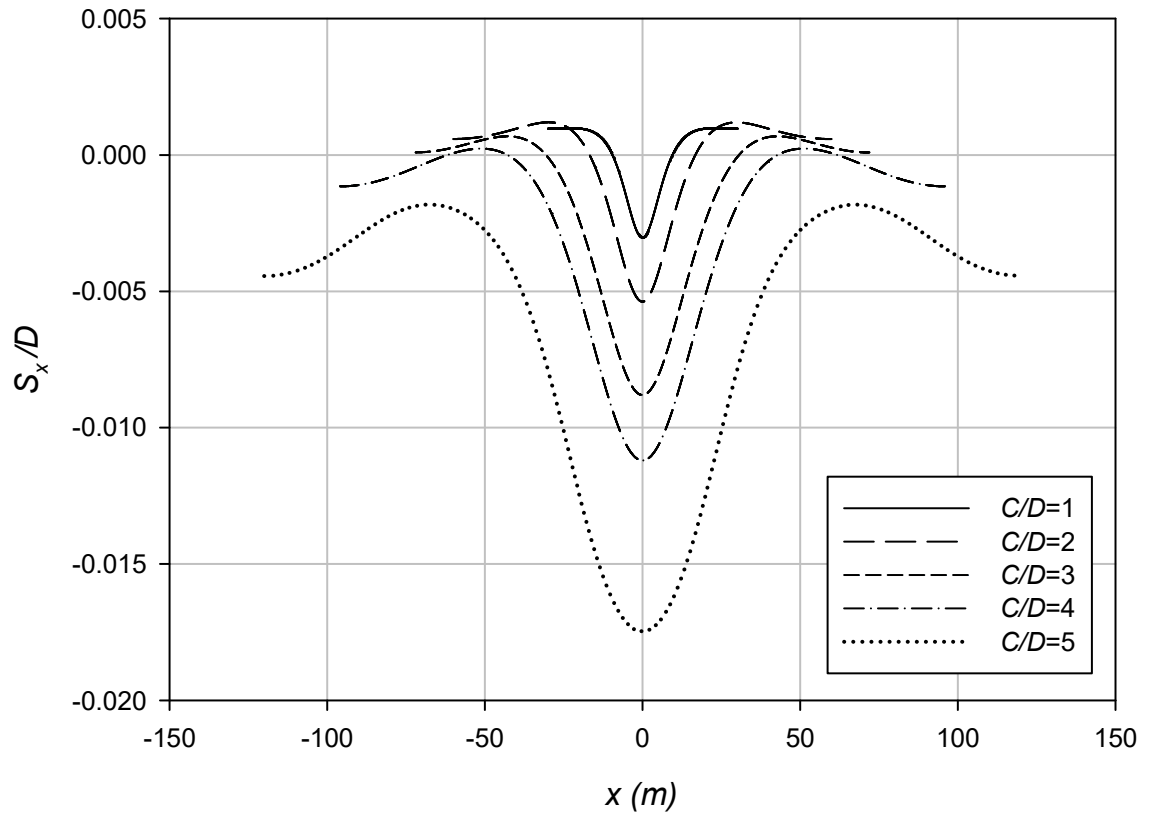


Figure 4-13 Settlement profiles with varying  $C/D$  ( $\gamma D/s_u = 3$ ,  $E/s_u=200$ , 50% PoC)

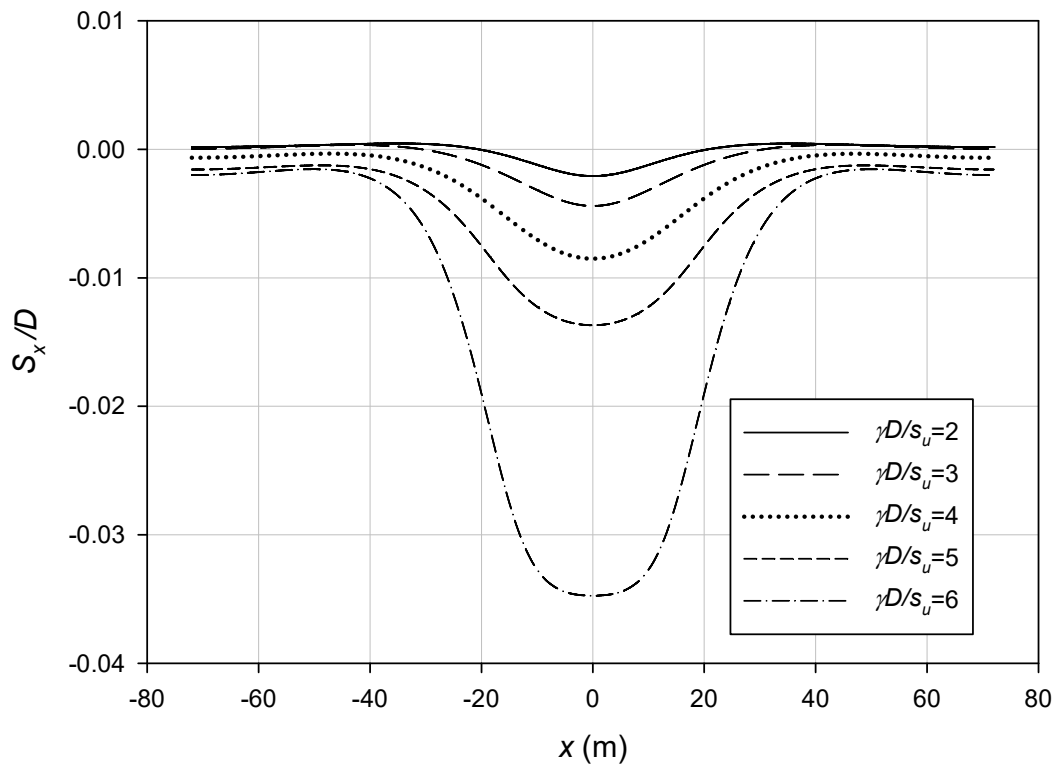
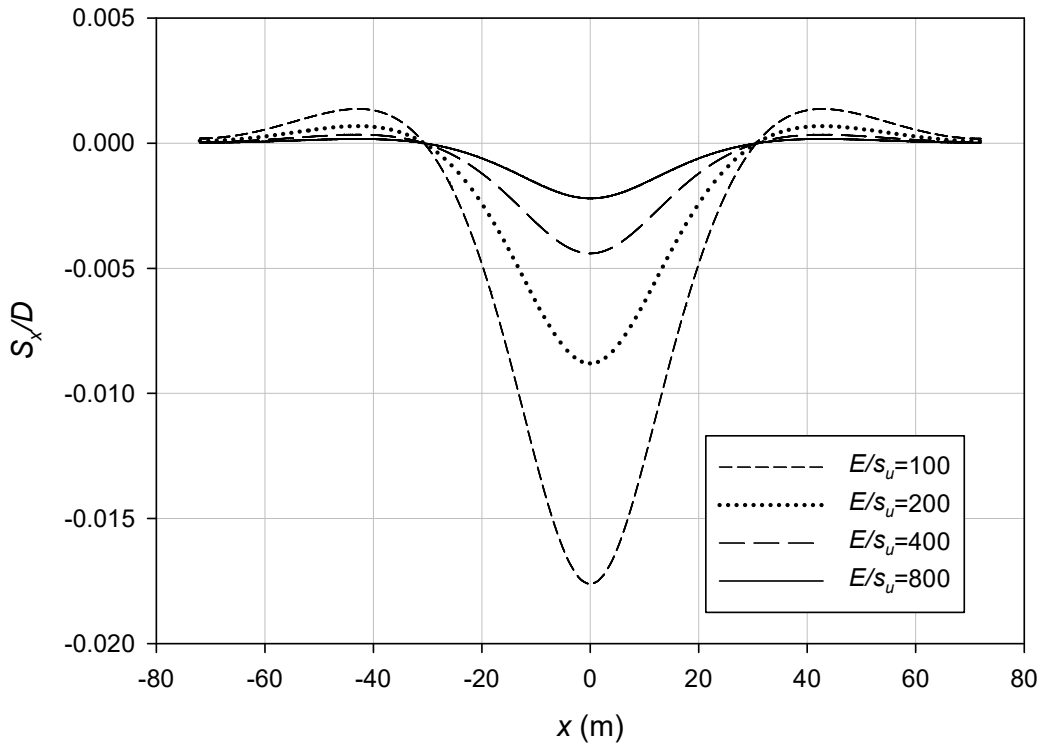


Figure 4-14 Settlement profiles with varying  $\gamma D/s_u$  ( $C/D = 3$ ,  $E/s_u=400$ , 50% PoC)



**Figure 4-15 Settlement profiles with varying  $E/s_u$  ( $C/D = 3$ ,  $\gamma D/s_u = 3$ , 50% PoC)**

Figure 4-16 shows the effect of volume loss and strength ratio on  $i_x/D$ . In general,  $i_x/D$  increases with volume loss. However, this effect seems to reduce with higher  $\gamma D/s_u$ , where the rate of change is smaller. Similarly, if  $\gamma D/s_u$  is always constant, the effect of  $C/D$  and volume loss can be examined, as in figure 4-17. This graph also shows a trend of increasing  $i_x/D$  with increasing volume loss for each case. Also,  $i_x/D$  increases with  $C/D$ , although this effect seems to diminish with higher depth ratio.

Figure 4-18 is a graph showing the effect of Young's Modulus ( $E$ ) on volume loss and  $i_x/D$ . It can be seen that the data is aligned in three groups, where the  $i_x/D$  remains the same. These represent the three relaxation stages (50%, 25%, and 10% of PoC) being analysed. This clearly shows that at a particular relaxation stage, the Young's modulus has no impact on  $i_x/D$ . However, Young's modulus has a strong impact on the amount of volume loss, as seen in figure 4-15.

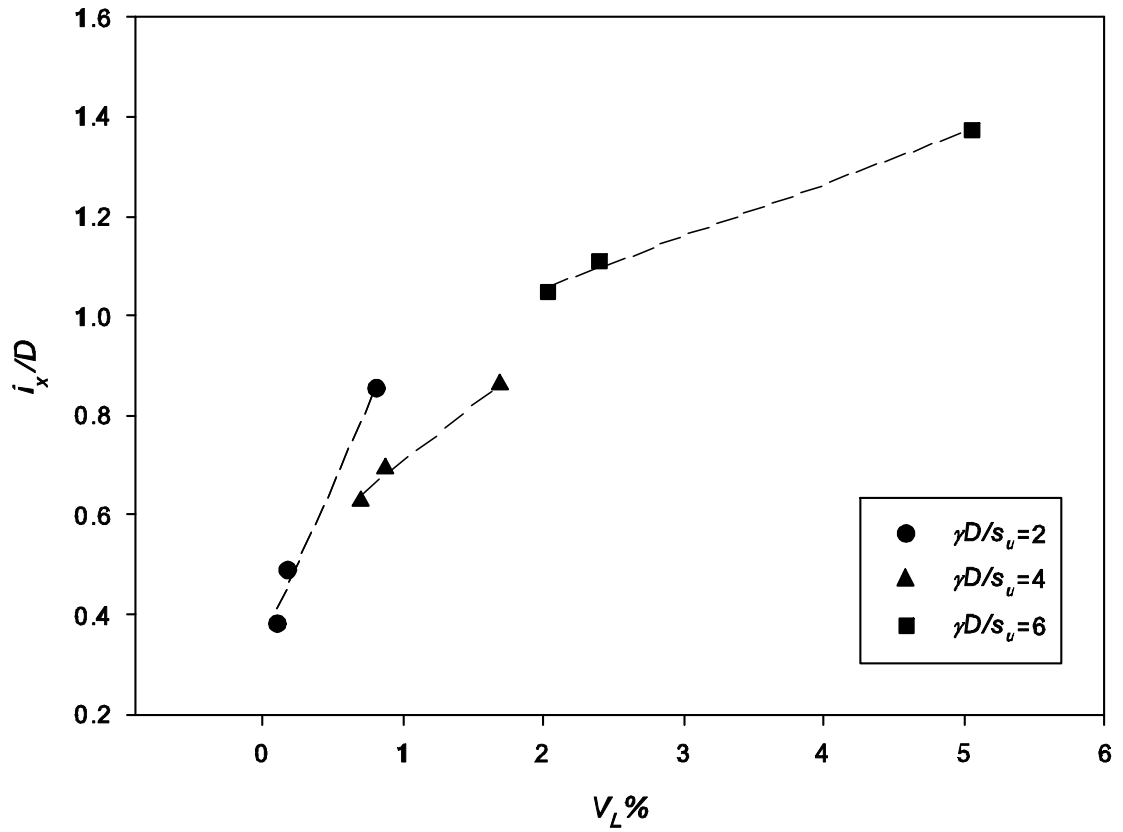


Figure 4-16 Impact of  $\gamma D/s_u$  on profile inflection point ( $C/D = 1, E/s_u=200$ )

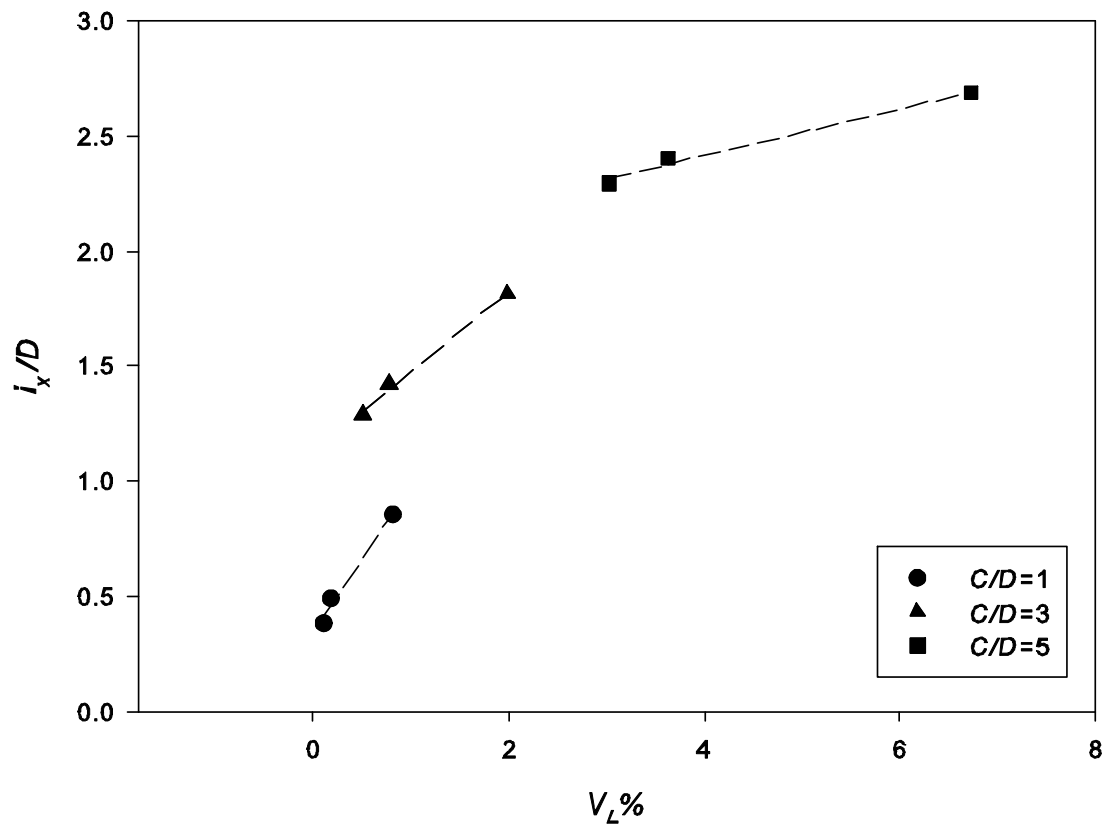


Figure 4-17 Impact of  $C/D$  on profile inflection point ( $\gamma D/s_u = 2, E/s_u=200$ )

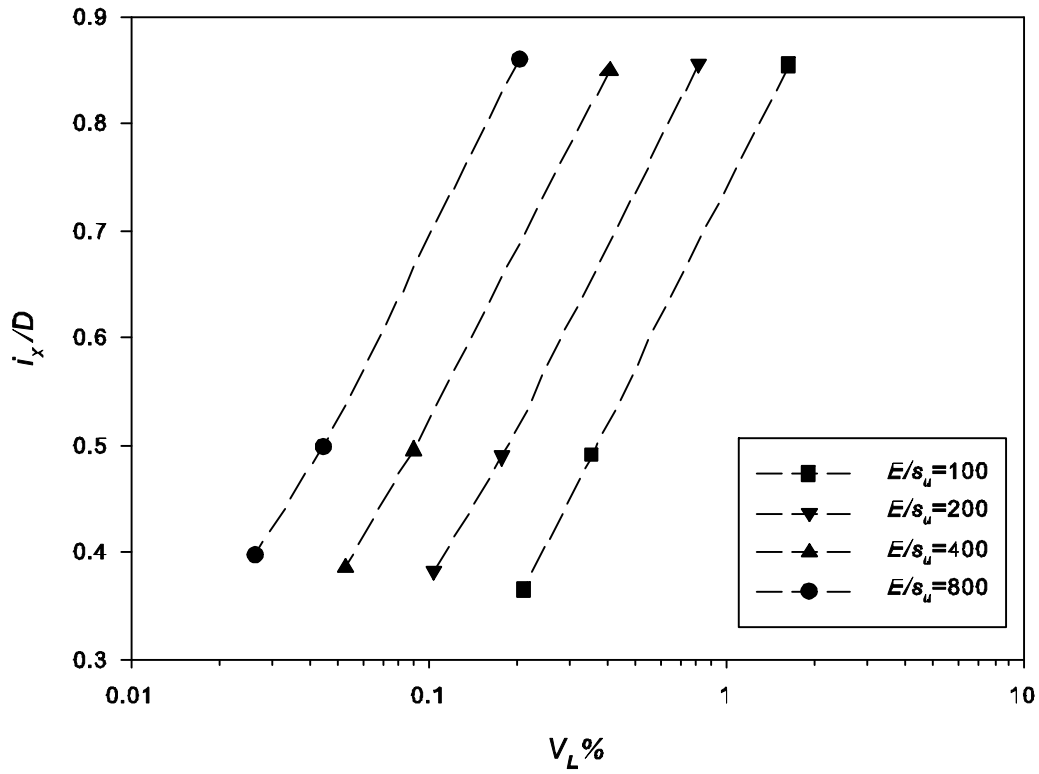


Figure 4-18 Impact of  $E/s_u$  on profile inflection point ( $C/D=1, \gamma D/s_u = 2$ )

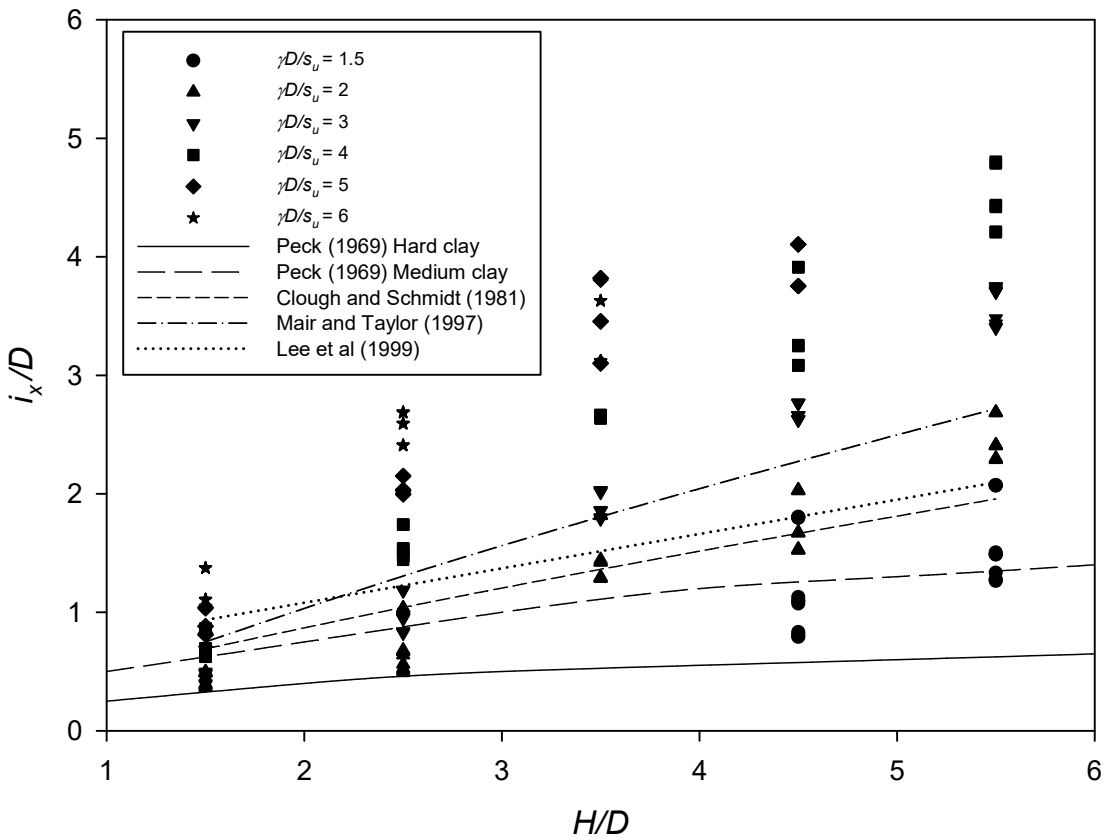


Figure 4-19 Comparison with previous results



Figure 4-19 contains all results from this study grouped with respect to soil strength ratio ( $\gamma D/s_u$ ), irrespective of the relaxation stage of the data (10%, 25%, 50% of PoC). This allows a comparison with experimental results by Peck (1969), and the suggested equations by Clough and Schmidt (1981), Mair and Taylor (1997), and Lee et al (1999), as given in equations 2.5 - 2.7. Note that equation 2.5 (Clough and Schmidt, 1981) is based on  $\gamma D/s_u \approx 1.8$ , equation 2.6 (Mair and Taylor, 1997) is based on  $\gamma D/s_u \approx 2.6$ , and equation 2.7 (Lee et al. 1999) is based on  $\gamma D/s_u \approx 2.7$ . Based on this, these equations appear to concur with the results from this study, as they are located in the position corresponding to their strength ratio.

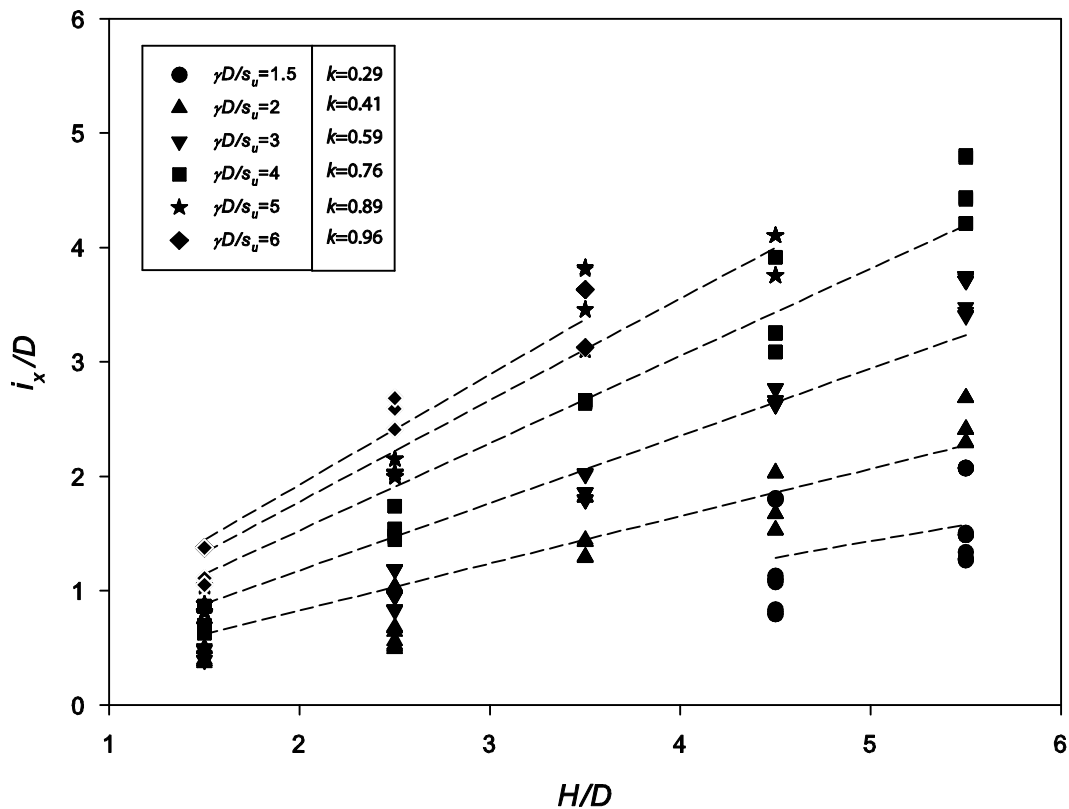
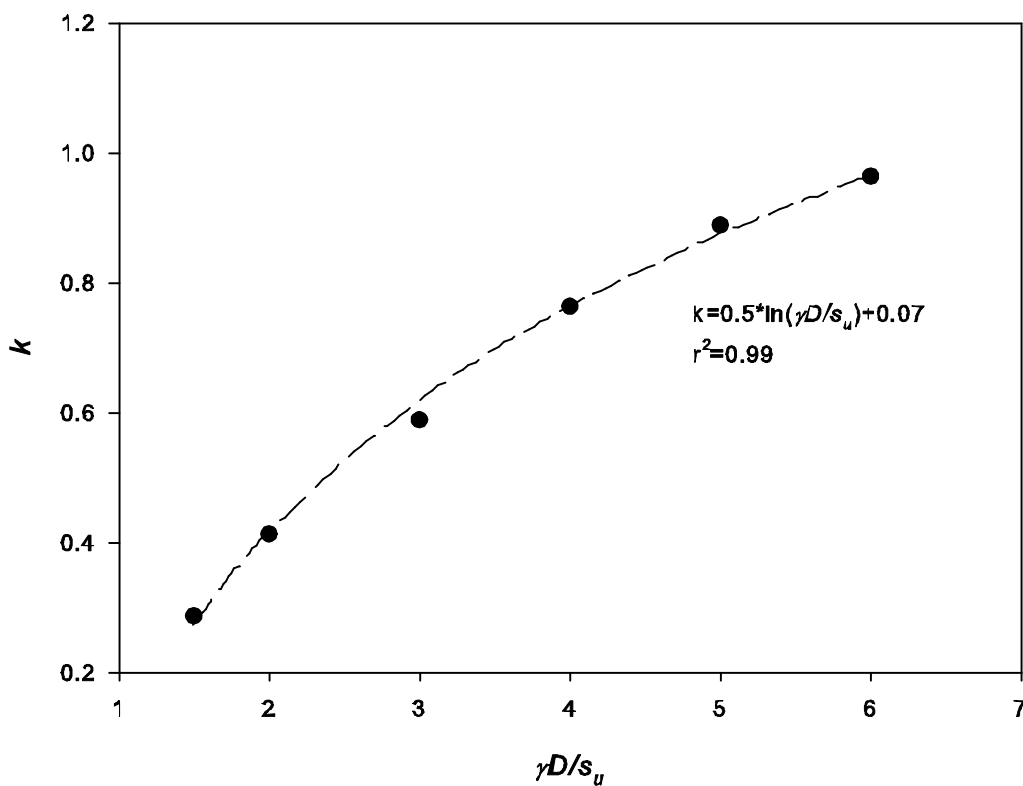


Figure 4-20 Results of this study with O'Reilly and New's equation (eq. 6)

These results are again shown in figure 4-20, this time with a linear regression which is equivalent to the commonly used equation 2.8 (O'Reilly and New, 1982). This approach allows an estimation of  $k$  for each  $\gamma D/s_u$ . These results show that the stronger soils achieving the lowest  $k$  (0.29 for  $\gamma D/s_u=1.5$ ), and the weaker soils achieving the highest  $k$  (0.96 for  $\gamma D/s_u=6$ ). This concurs with previous research about suggestions that the range is approximately 0.4 to 0.7. However, the general use of  $k = 0.5$  for clay may not be a good approach, as it will be conservative for strong soils and very un-conservative for weak soils.

From figure 15, it also becomes clear that a preliminary  $k$  value could be reasonably selected based solely on the soil strength ratio. The variation in results due to being from different stages of relaxation (10%, 25%, and 50% PoC) appears to be relatively small. These preliminary values of  $k$  are taken from figure 4-20, and graphed against  $\gamma D/s_u$ , as shown in figure 4-21. An equation describing the relationship between  $k$  and  $\gamma D/s_u$  can then be acquired. This equation is given in equation 4.4.

$$k = 0.5 \ln \left( \frac{\gamma D}{s_u} \right) + 0.07 \quad (4.4)$$



**Figure 4-21 Equation for practical estimation of  $k$ , ignoring volume loss effects**

However, it can be seen from figure 4-20 that there is some variation being caused by volume loss differences. Taking  $\gamma D/s_u = 4$  (solid square data) at  $H/D=5.5$  as an example, the difference in  $i_x/D$  is due to different volume loss levels of the relaxation stages (50%, 25%, 10% of PoC). For this reason, contour charts for the  $k$  parameter are provided in figures 4-22 – 4-27, which correspond to  $\gamma D/s_u = 1.5, 2, 3, 4, 5,$  and  $6$  respectively. These are dependent on Young's modulus ratio and volume loss % which are inextricably linked. These are based off a surface regression (figure 10-1

Appendix 1) of the corresponding data, with equation 8. The parameter  $c$  ranges from -2.07 to -1.54, and increases with  $\gamma D/s_u$  as seen in table 1. This regression achieved an  $r^2$  of greater than 0.85 in all cases.

$$k = \left( \frac{E}{s_u} \right)^{0.055} + (V_L \%)^{0.07} + c \quad (4.5)$$

Table 4-1 Parameters of volume loss general equation

$\gamma D/s_u$	1.5	2	3	4	5	6
$c$	-2.07	-2.04	-1.97	-1.86	-1.78	-1.54

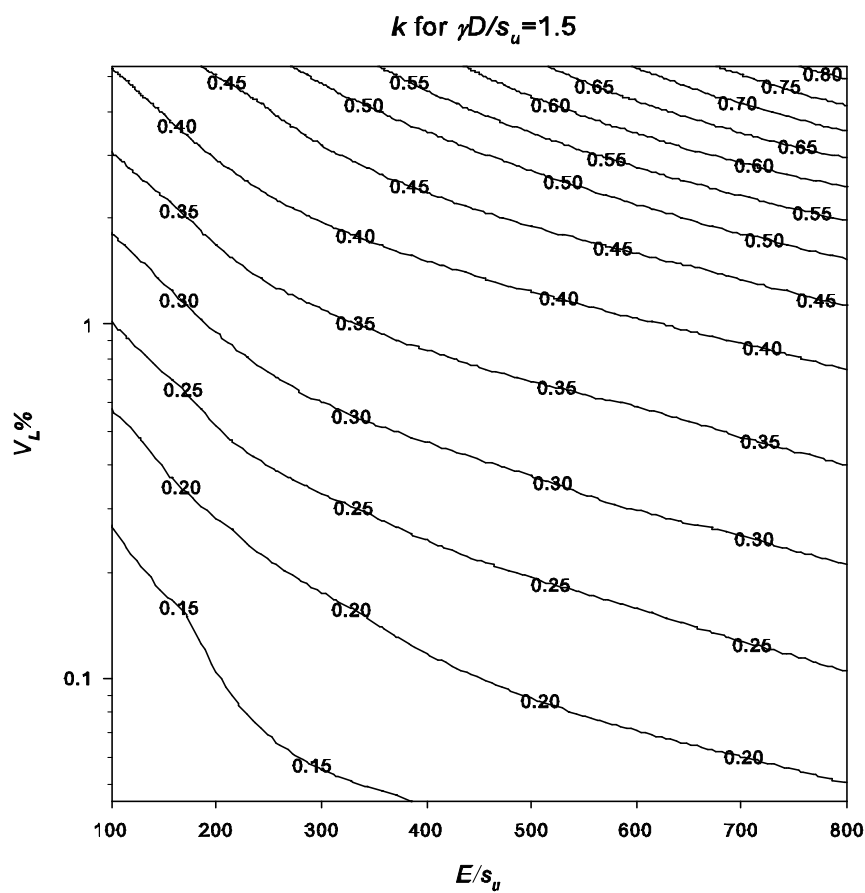


Figure 4-22 Contour plot of  $k$  for  $\gamma D/s_u = 1.5$

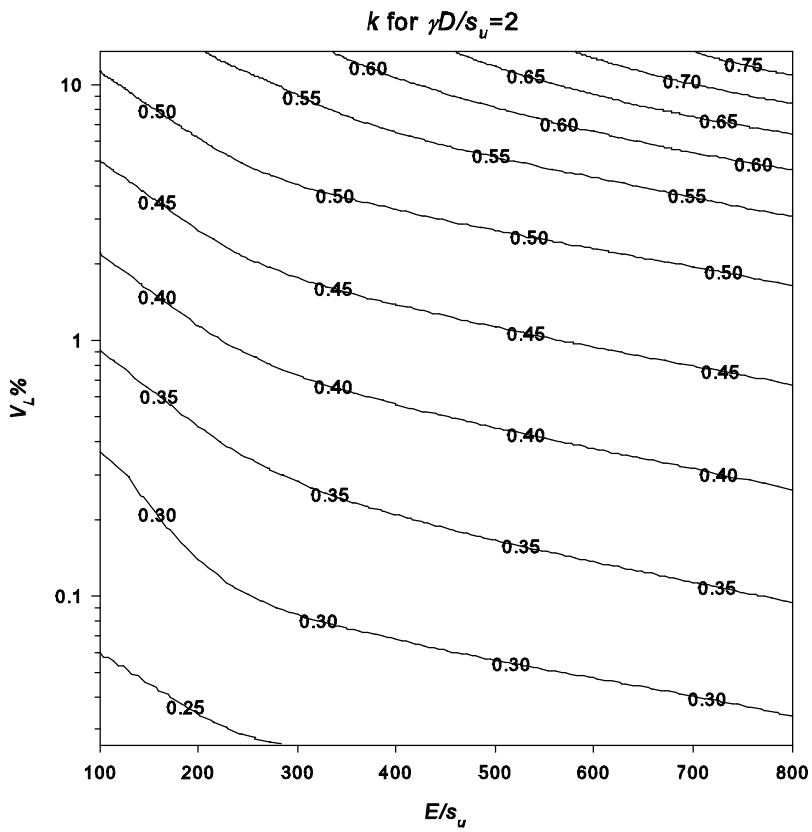


Figure 4-23 Contour plot of  $k$  for  $\gamma D/s_u = 2$

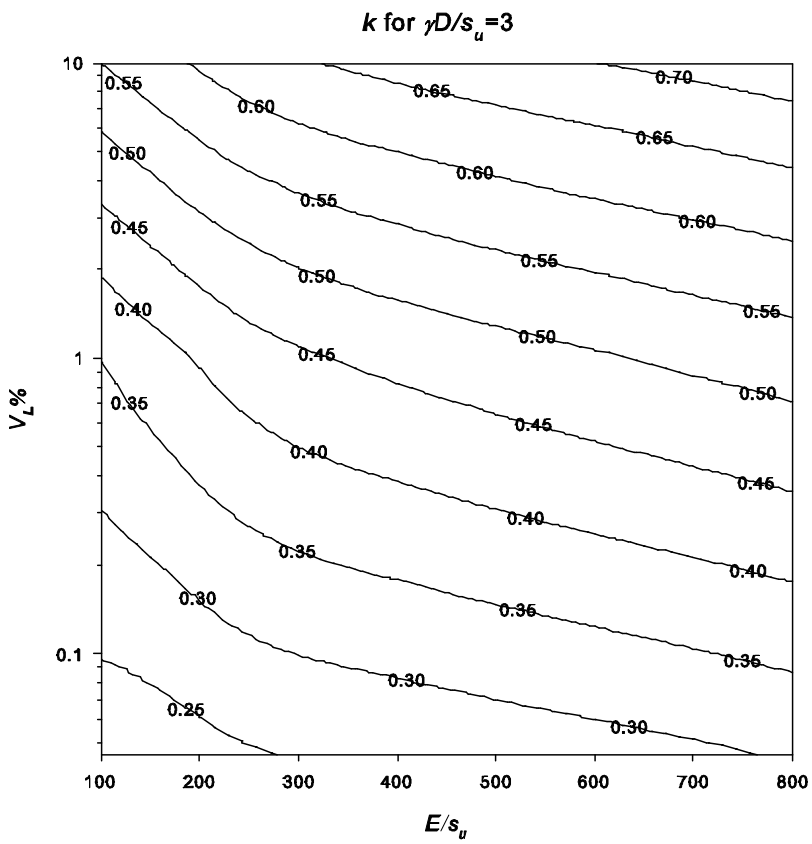
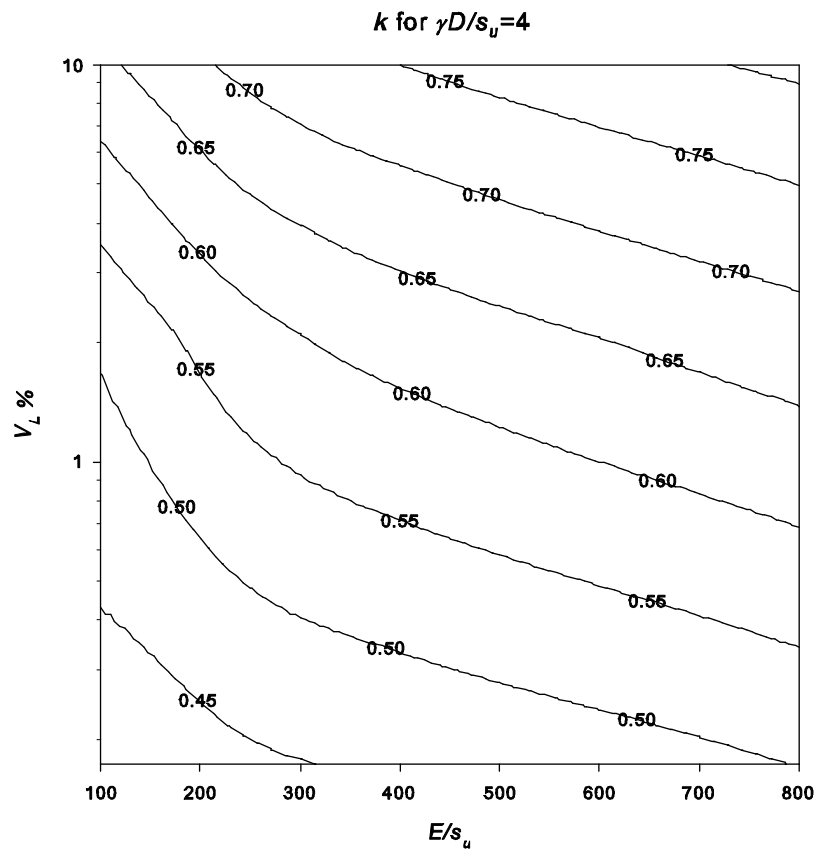
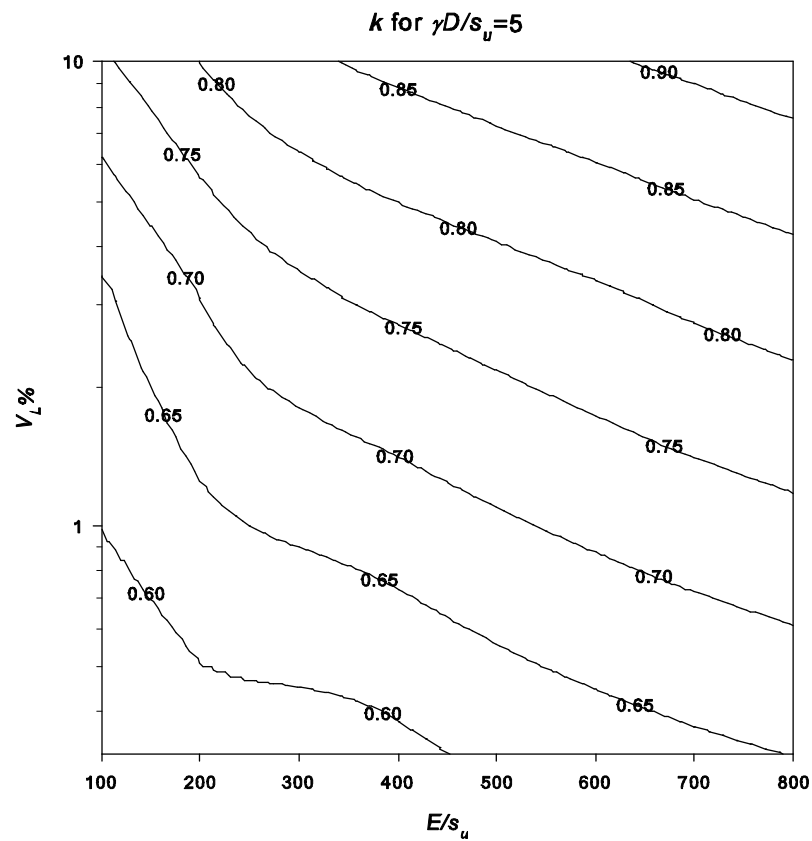


Figure 4-24 Contour plot of  $k$  for  $\gamma D/s_u = 3$

Figure 4-25 Contour plot of  $k$  for  $\gamma D/s_u = 4$ Figure 4-26 Contour plot of  $k$  for  $\gamma D/s_u = 5$

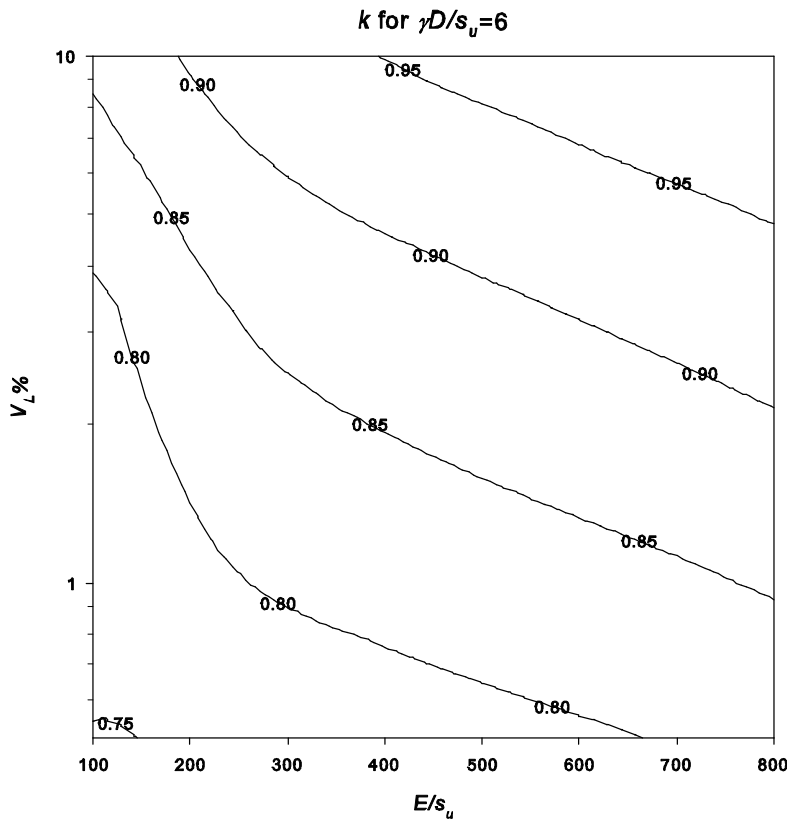


Figure 4-27 Contour plot of  $k$  for  $\gamma D/s_u = 6$

#### 4.5.1 Practical Example – Predicting Settlement Profile

The following example describes the procedure in using this semi-empirical method together with figures 4-22 – 4-27 equations 4.4 and 4.5.

A tunnel planned in clay soil will have an estimated volume loss of 2%. The soil has an undrained cohesion of 40 kPa, unit weight of 18 kN/m<sup>3</sup>, and a Young's modulus of 12 MPa. At this stage, the design indicates a preferred tunnel depth (to axis) of 20m, and a diameter of 6.7m. Calculating the dimensionless ratios gives:  $\gamma D/s_u = 3$ ,  $E/s_u = 300$ . A volume loss of 2% with a 6.7m tunnel corresponds to a contraction area of 0.7 m<sup>2</sup>.

Calculating a preliminary  $k$  value can be done using equation 4.4. By substituting in  $\gamma D/s_u = 3$ , it is found that  $k = 0.62$ . However, as more detail about the volume loss is known, equation 4.5 and figure 4-24 can be used. These should be both consistent, as the contour plots are based on the equation. They estimate a  $k$  value of 0.49. With a tunnel depth of 20m, this gives an inflection point distance,  $i_x$  of 9.8m.

Using equation 4.2, an estimated maximum settlement ( $S_{max}$ ) can be calculated by rearranging the equation. Doing this yields  $S_{max} = 0.0285$ m (Note that this assumes

that the contraction at the tunnel is equal to the ground loss at the surface, this is an assumption that the material is non-dilational which is reasonable for undrained clay, but not for drained soil or granular material.). Everything needed for equation 4.1 is now available. The predicted settlement profile is given by equation 4.6, where  $x$  is the distance from the tunnel axis.

$$S_x = 0.0285e^{-\frac{x^2}{2 \cdot 9.8^2}} \quad (4.6)$$

This 2% volume loss profile is shown in figure 4-28, alongside those for a hypothetical 1 and 3% volume loss, which have been determined using the same procedure.

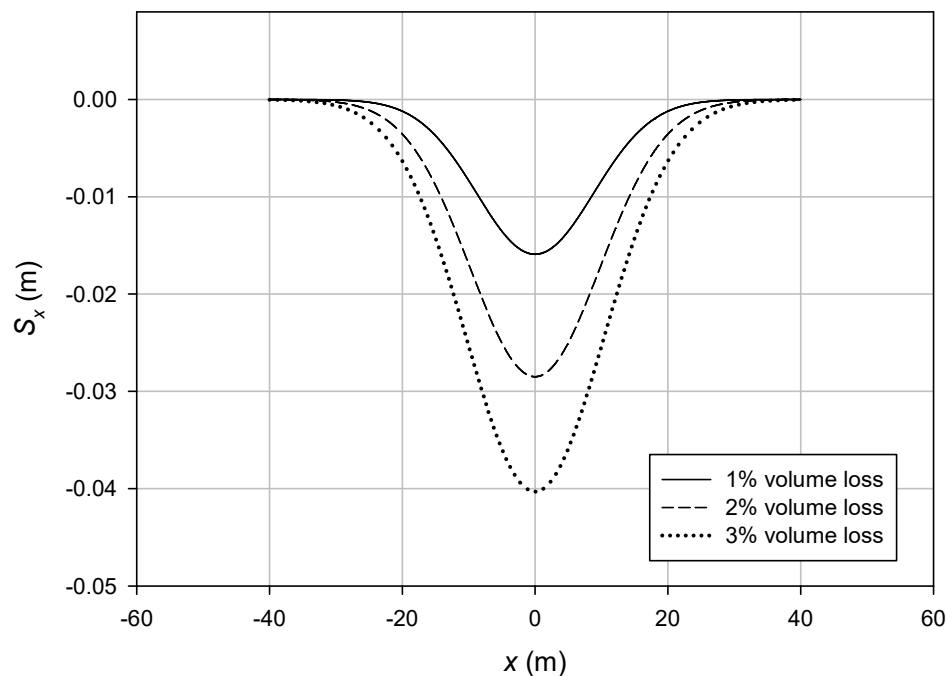


**Figure 4-28 Settlement profiles of example tunnel problem ( $H/D=3$ ,  $\gamma D/s_u=3$ ,  $E/s_u=300$ )**

## 4.6 Conclusion

A numerical procedure has been developed to simulate a circular tunnel and the relaxation of the soil that occurs during construction. This procedure is able to automatically generate the mesh based on a series of inputs and output the surface settlement data for each relaxation step. Using outputs from the model, the point of collapse step can be determined. The settlement data at this collapse stage and the data at three previous pre-collapse stages are exported and analysed in *MATLAB* by

doing a regression of the Gaussian equation. This allows reliable estimation of  $i_x$  for all cases.

Using this approach, a parametric study was undertaken in which a series of commonly used dimensionless ratios were controlled including  $C/D$ ,  $\gamma D/s_u$ , and  $E/s_u$ . The volume loss ( $V_L\%$ ) was calculated at the analysed stages by integrating the settlement data. A brief description of the effect of these parameters has been given. It is concluded that the  $i_x$  parameter always increases with volume loss, but that this rate of change reduces with increasing  $C/D$  and  $\gamma D/s_u$ . The Young's modulus ratio ( $E/s_u$ ) has little impact on  $i_x$ , but clearly does have a big impact on volume loss.

The calculated settlement parameters of this study were then compared to several suggested equations which are based on observations and centrifuge modelling. This comparison was quite positive, with the suggested lines falling approximately into the correct corresponding position, based on the strength ratio of the soil used in those studies. The linear relationship of O'Reilly and New (1982) is also used, which involves a coefficient of linear proportionality ( $k$ ) which is the ratio of  $i_x$  and the tunnel depth ( $H$ ). It is found that this coefficient increases with soil strength ratio, and a relationship describing this is suggested.

Further investigation of this  $k$  parameter and the variations being caused by volume loss led to a 3D regression being conducted with respect to  $E/s_u$  and the volume loss %. Another more comprehensive equation is suggested which is presented alongside its consequent design contour charts. The combination of these and the general procedure of this semi-empirical method are demonstrated in a practical example.

The great similarity between the *FLAC* modelled settlement and the Gaussian curve indicates that this empirical method is still suitable to be applied in the industry as a preliminary tool. This research suggests that at high volume loss and/or at collapse, the constant  $k$  should be approximately between 0.52 - 0.75 for undrained clays. A new equation is proposed for estimating the  $k$  value at the collapse stage. It is concluded that this is a reliable method for preliminary analysis and prediction.



# 5 SINGLE TUNNEL STABILITY

## 5.1 Introduction

This chapter describes the verification and use of a numerical model for investigating single circular tunnels in cohesive soils. The model aims to simulate the movement and relaxation of the soil around the shield and lining annulus that occurs due to the overcutting and grouting of the tunnel void by a tunnel-boring machine (TBM). To achieve this, the model uses a pressure relaxation technique that progressively reduces the tunnel support pressure from an initial condition until a point of failure is detected. At each of these relaxation steps, the stability number (equation 5.1) is calculated, and can be later analysed. This is done for a range of geometry and soil ratios that will cover most practical cases for soft cohesive soils.

In this study, both the point of collapse (PoC) and three stages before this point have been analysed. The stability numbers calculated at the determined PoC are compared to rigorous upper and lower bound solutions, and can be used as boundaries for design purposes. The results of this study are quite positive, with the stability results from this study remaining within 5% of the upper and lower bound solutions. Design charts using dimensionless ratios have therefore been presented. The pre-collapse 'working condition' results have been correlated with volume loss that has been back calculated from surface settlement as stated in chapter 4, and the results of this has been discussed. Design charts have also been produced for these cases.

## 5.2 Problem Definition

Managing the system stability during tunnel construction is essential. This is most often done by using the stability number ( $N$ ), as in equation (5.1). This formulation is an approach followed by the finite element limit analysis (FELA) studies of Wilson et al (2011), where  $\sigma_s$  is the surface surcharge pressure,  $\sigma_t$  is the internal tunnel pressure, and  $s_u$  is the undrained shear strength. Figure 5-1 also shows this problem definition. This stability number is a function of the depth ratio  $C/D$  and the soil shear-strength ratio  $\gamma D/S_u$ . It will be once again used in this study, in conjunction with the developed model.

$$N = \frac{\sigma_s - \sigma_t}{s_u} = f\left(\frac{C}{D}, \frac{\gamma D}{s_u}\right) \quad (5.1)$$

By formulating the equation to the problem in this way, it allows for the creation of practical stability charts, which are useful for design. These dimensionless ratios allow the results of this study to be used in scenarios that are physically different, but where the soil strength ratio and the depth ratio still fall in the parametric domain. The parameters used in this study are  $\gamma D/S_u = 1 - 5$  and  $C/D = 1 - 5$ . This is to cover most of the realistic values to give a comprehensive analysis, and to ensure that the design charts produced can be applicable to many different tunnel design and analysis problems.

Using this internal pressure relaxation method, and a small relaxation interval (amount relaxed each step); the stability number (equation 5.1) that induces collapse can be calculated with reasonable accuracy. It should be noted that the pressure relaxation method would always slightly overestimate the stability number at collapse, as the internal pressure is reduced in discrete steps, not continuously. The internal pressure at the 'collapse stage' will have been relaxed slightly more than needed, unless the internal pressure at that stage coincides exactly with the actual collapse stability number. However, this problem is reduced significantly by reducing the size of the relaxation interval (reducing internal pressure by 1% each stage is far more accurate than 5% etc.).

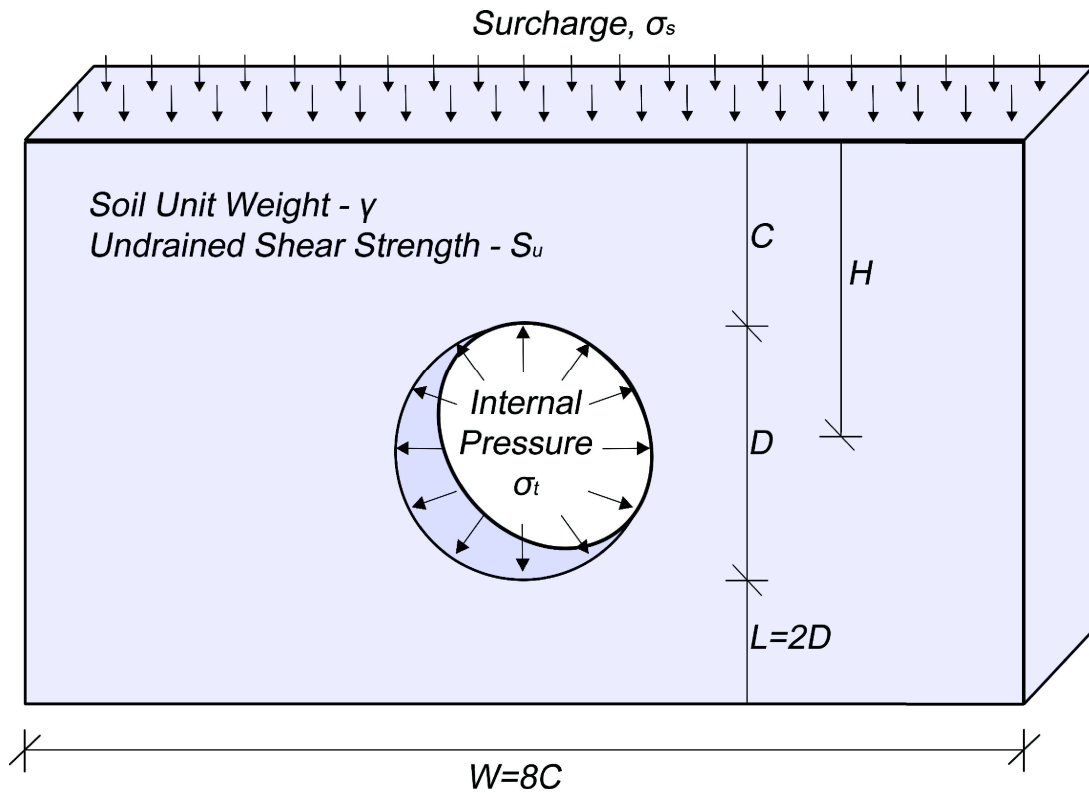
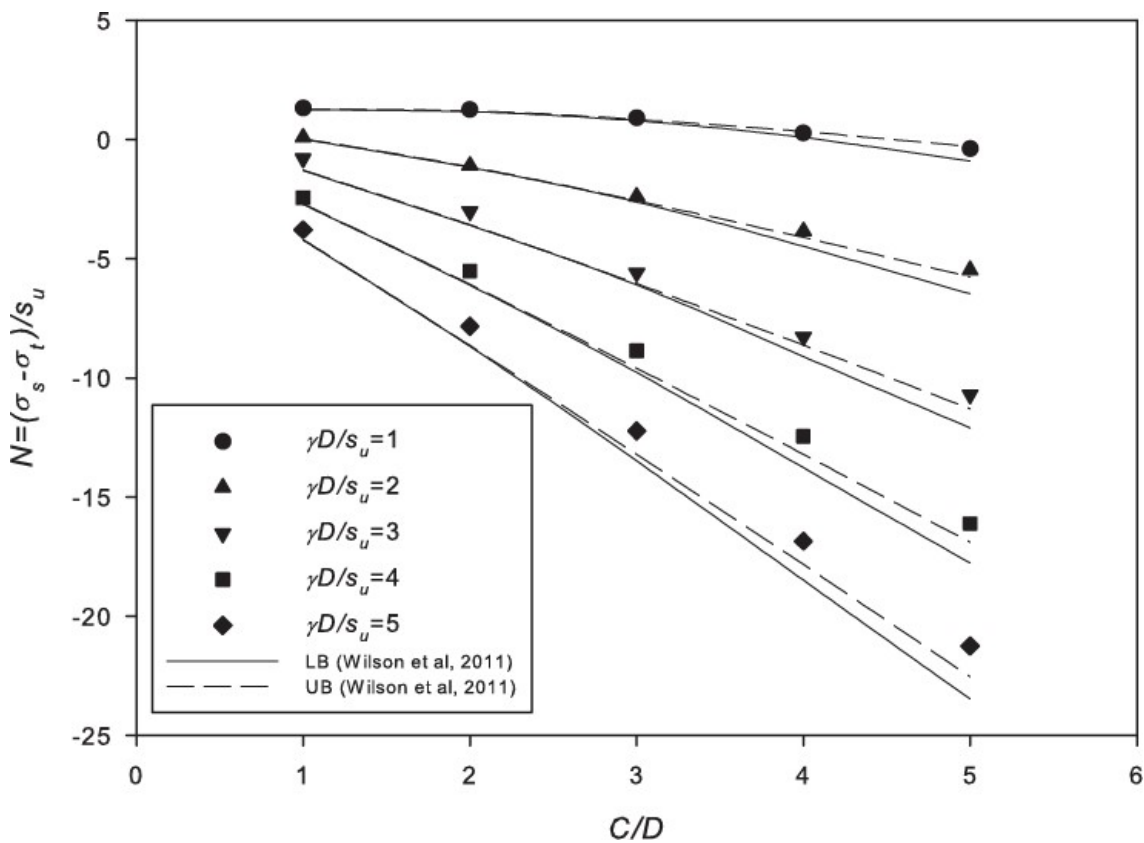


Figure 5-1 Single tunnel problem definition

### 5.3 Results – At Collapse

Figure 5-2 shows a graphical comparison of stability numbers ( $N$ ) at collapse using the pressure relaxation method and the rigorous upper and lower bounds. In general, the finite difference results using pressure relaxation method are in good agreement with FELA solutions (Wilson et al. 2011). It should be noted that the positive values of stability number, such as those with  $\gamma D/S_u = 1$  for  $C/D = 1, 2, 3$  suggest that the tunnel would require a theoretical negative internal pressure  $\sigma_t$  (a suction pressure) to reach the point of collapse. In other words, scenario such as these will avoid the PoC with a stability of number of zero – no internal or surcharge pressure. As  $\gamma D/S_u$  increases (decrease in soil strength) negative values of stability number are obtained. From the equation  $(\sigma_s - \sigma_t)/S_u$ , it is known that for a negative stability number, the value of  $\sigma_t$  must be positive i.e. a positive “pushing” pressure is required to prevent imminent collapse.



**Figure 5-2 Comparison of stability number at collapse with Wilson et al (2011)**

Note that given a constant value of  $\gamma D/S_u$ , the stability number ( $N$ ) decreases with increasing  $C/D$ . It can also be seen that, for a constant  $C/D$ , the stability number  $N$  decreases with increasing strength ratio  $\gamma D/S_u$ . These results indicate that greater internal pressure control would be needed for larger value of depth ratio  $C/D$  and larger values of strength ratio  $\gamma D/S_u$  (softer soils).

A design chart has been produced, as shown in figure 5-3. Given values of strength ratio ( $\gamma D/S_u$ ) and depth ratio ( $C/D$ ), users can easily identify the critical stability number  $N = (\sigma_s - \sigma_t)/S_u$  for their design purposes. This can be useful, as it describes the collapse bound, where a hypothetical factor of safety would be one. A surface regression of this data (figure 10-2 in Appendix 1) is given in equation 5.2, which represents this data with an  $r^2 = 0.97$ .

$$N_c = 3 - \left(\frac{C}{D}\right)^{1.15} \left(\frac{\gamma D}{s_u}\right)^{0.82} \quad (5.2)$$

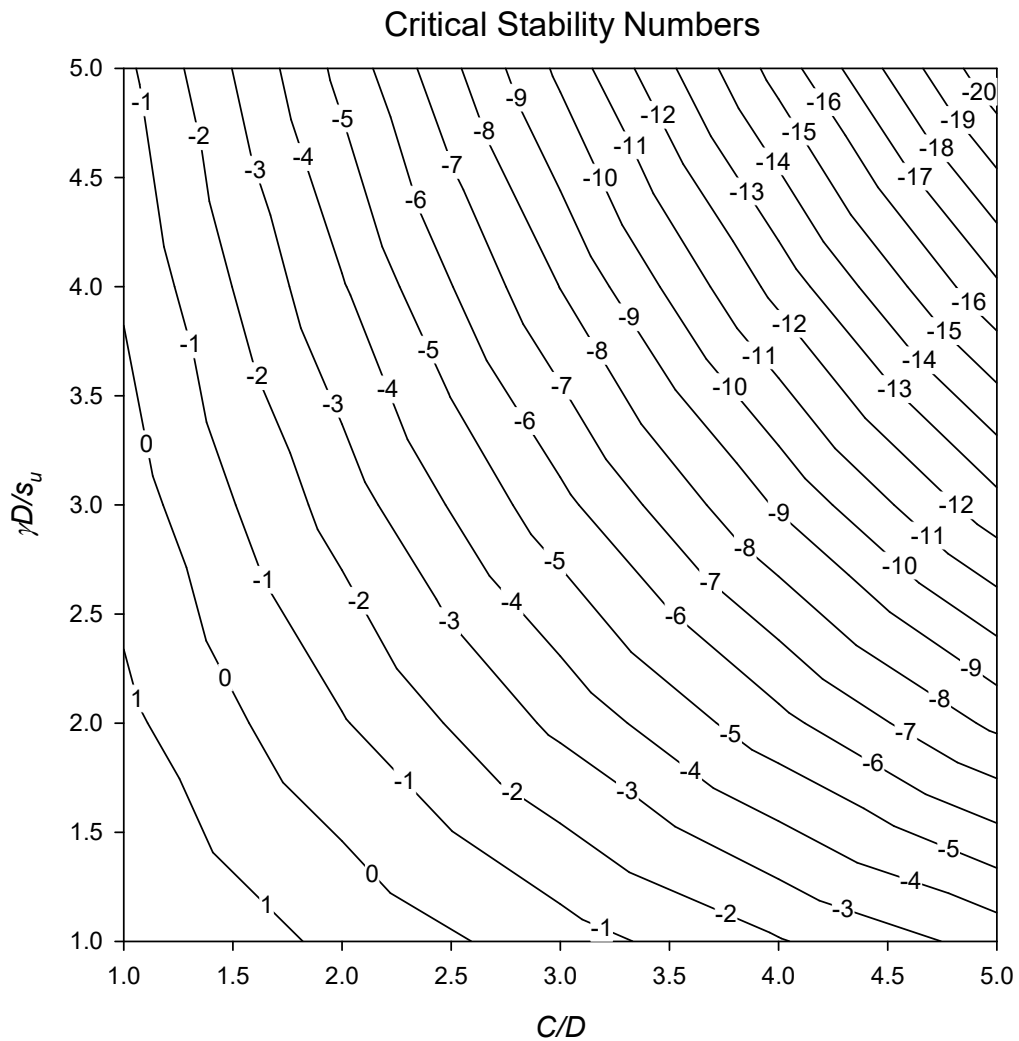


**Figure 5-3 Stability numbers at the point of collapse design chart**

### 5.3.1 Practical Examples

The following examples are used to demonstrate the potential of this chart in design and analysis scenarios.

#### **Stability in soft soil**

A tunnel boring machine has a diameter ( $D$ ) of 6.0 m and is buried at a depth of 18 m ( $C$ ) in an undrained clayey material with properties  $S_u = 27kPa$ ,  $\phi_u = 0^\circ$  and  $\gamma = 18 \text{ kN/m}^3$ . The site is assumed to be a Greenfield so no surface pressure is assumed ( $\sigma_s = 0$ ). The following procedures can be used to determine the absolute minimum tunnel internal pressure ( $\sigma_t$ ) to prevent collapse.

1. Calculate dimensionless ratios from the known data.  $C/D = 3$ .  $\gamma D/S_u = 4$

2. For a 2D circular tunnel problem with  $C/D = 3$ ,  $\gamma D/S_u = 4.0$ , figure 5-3 returns a value of  $N = -8.1$ . Equation 5.2 yields  $-8.03$  for the same conditions.
3. Using equation 5.1 ( $N = (\sigma_s - \sigma_t)/S_u$ ),  $\sigma_t$  can then be computed as  $\sigma_t \approx 0 - (-8.1 * 27) = 219 \text{ kPa}$ . A positive value of  $\sigma_t$  indicates that an internal pushing pressure is required to maintain tunnel stability and prevent reaching the PoC.

### Stability in stiff soil

Similar to Practical Example 1, if we assume that a tunnel boring machine has a diameter ( $D$ ) of 6.0 m and is buried at a depth of 12 m ( $C$ ) in an undrained clayey material with properties  $S_u = 80 \text{ kPa}$ ,  $\phi_u = 0^\circ$  and  $\gamma = 18 \text{ kN/m}^3$ . The following procedures can be used to determine the required tunnel internal pressure  $\sigma_t$  to maintain the tunnel stability.

1. Calculate dimensionless ratios from the known data.  $C/D = 2$ .  $\gamma D/S_u = 1.35$ .
2. Figure 5-3 returns a value of  $N = 0.35$ . Equation 5.2 yields  $N=0.30$ .
3. Using equation 5.1 ( $N = (\sigma_s - \sigma_t)/S_u$ ),  $\sigma_t$  can then be computed as  $\sigma_t \approx 0 - (0.5 * 80) = -40 \text{ kPa}$ . A negative value of  $\sigma_t$  such as this indicates that the tunnel actually requires a pulling pressure to reach a collapse state. In other words, the tunnel will remain stable without any internal pressure.

### Depth determination

A 6m tunnel is proposed in soil with an undrained clayey material with properties  $S_u = 40 \text{ kPa}$ , and  $\gamma = 18 \text{ kN/m}^3$ . If the proposed TBM has the capacity to provide an internal pressure ( $\sigma_t$ ) of  $300 \text{ kPa}$ , and the surface surcharge pressure ( $\sigma_s$ ) is found to be  $100 \text{ kPa}$ . The maximum allowable depth can be back-calculated using figure 5-3 and equation 5.2.

1. Calculate dimensionless ratios from the known data.  $N = (\sigma_s - \sigma_t)/S_u = -5$ ,  $\gamma D/S_u = 2.7$ .
2. Using figure 5-3 and these parameters, the maximum allowable depth ratio ( $C/D$ ) is approximately 3.1. With a specified tunnel diameter of 6m, this results in a maximum depth of 18.6m. If the tunnel is placed any deeper than this, a collapse will be induced. Using equation 5-2, a  $C/D$  value of 3.0 is obtained.

### 5.3.2 Failure Mechanism

Shear strain rate (*SSR*) plots can be useful to give an indication of failure mechanism. Figures 5-4 to 5-7 show *SSR* plots for  $C/D = 1$  and 3, each with  $\gamma D/S_u = 1$ , and 5. For all  $C/D$ , the failure zone gets wider for decreasing soil strength. Floor heaving is most severe for the deep, soft cases, but reduces for shallow and strong cases. At the surface of all cases, two 'arms' are visible with an elastic zone in between. A similar observation is presented in the power dissipation charts by Wilson et al. (2011).

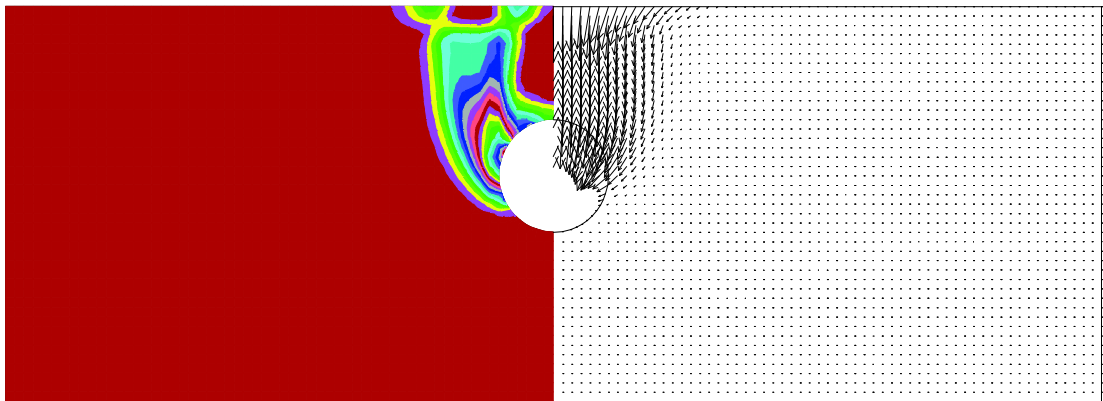


Figure 5-4 Shear strain rate (*SSR*) and velocity plot for  $C/D=1$  and  $\gamma D/S_u =1$

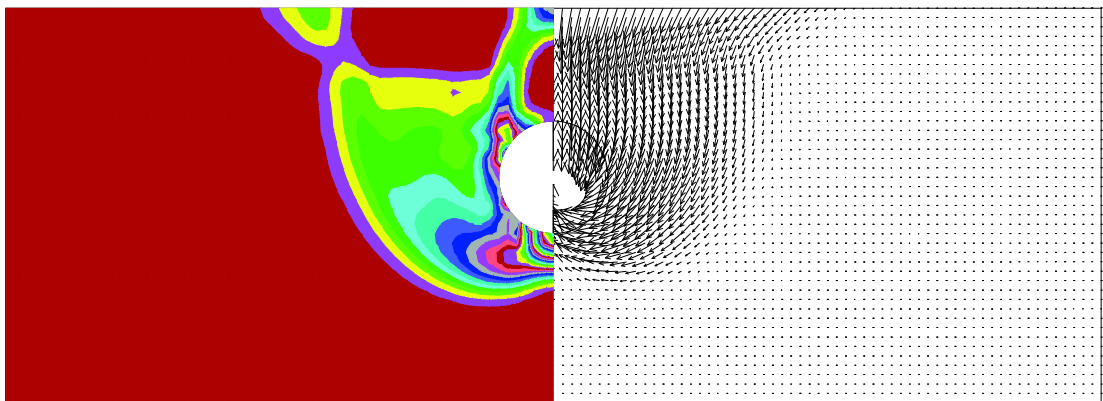


Figure 5-5 Shear strain rate (*SSR*) and velocity plot for  $C/D=1$  and  $\gamma D/S_u =5$

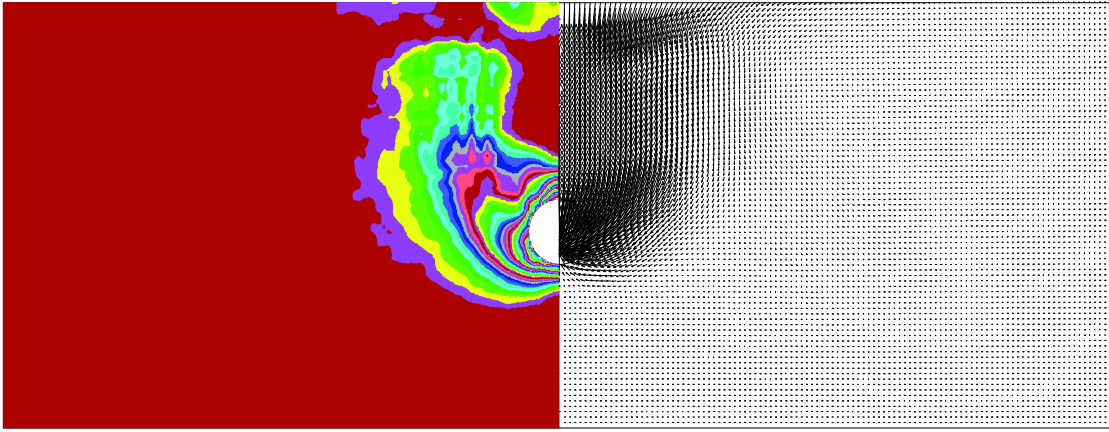


Figure 5-6 Shear strain rate (SSR) and velocity plot for  $C/D=3$  and  $\gamma D/S_u = 1$

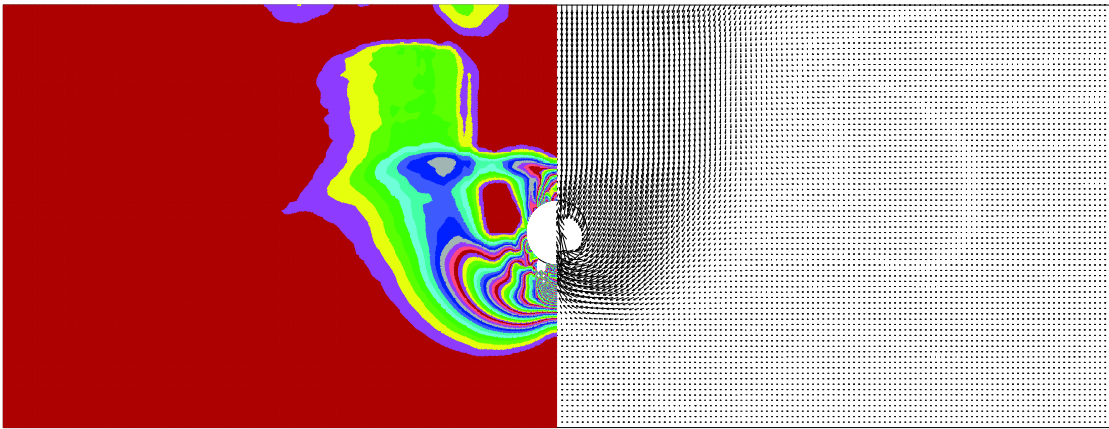


Figure 5-7 Shear strain rate (SSR) and velocity plot for  $C/D=3$  and  $\gamma D/S_u = 5$

## 5.4 Results – Pre-collapse

Using the pressure relaxation method, the model can be run until a point of collapse (PoC) is detected. This section will analyse stability numbers and volume loss at the three points before the PoC, at the so-called pre-collapse ‘working conditions’. These points will be 0.5PoC, 0.25PoC, and 0.1PoC. So, if the PoC occurs at 53% relaxation, then the points being analysed are 27%, 13%, and 5%. These stability numbers are defined in equation 5.1, and the volume loss is back calculated by integrating the surface settlement as discussed in the settlement chapter 4. All results presented in this section are for  $E/s_u=200$  only, for simplicity. Also note that for less confusion, it will be taken that an increasing  $N$  will mean becoming ‘more negative’, and a reducing  $N$  will mean becoming ‘less negative’.



Figures 5-8 and 5-9 show the relationship between stability number  $N$  (pressure ratio) and volume loss. It can be seen that  $N$  always reduces with volume loss. This seems a reasonable conclusion – as the support is reduced (i.e.  $N$  reducing), the volume loss increases. It can also be seen that both soil strength ratio ( $\gamma D/s_u$ ) and depth ratio ( $C/D$ ) have a significant impact on the  $N$ -volume loss relationship. In figure 5-8, it is shown that stronger soils (lower  $\gamma D/s_u$ ) require less support (smaller  $N$ ) to maintain the same volume loss, which is as expected. In figure 5-9, it is shown that shallower tunnels (smaller  $C/D$ ) require less support (smaller  $N$ ) to maintain the same volume loss than deeper cases. This seems to indicate that the widely held truth that stability is easier to attain in deeper tunnels does not hold with clay soils. Based on these results, *MATLAB* surface regressions for this data have been done (figure 10-3 in Appendix 1) and using this, the following contour charts for stability number  $N$  have been produced in figures 5-8 to 5-14. These allow a user to relate volume loss and  $N$  for any single tunnel stability problem in clay, and for a given  $C/D$  and  $\gamma D/s_u$ .

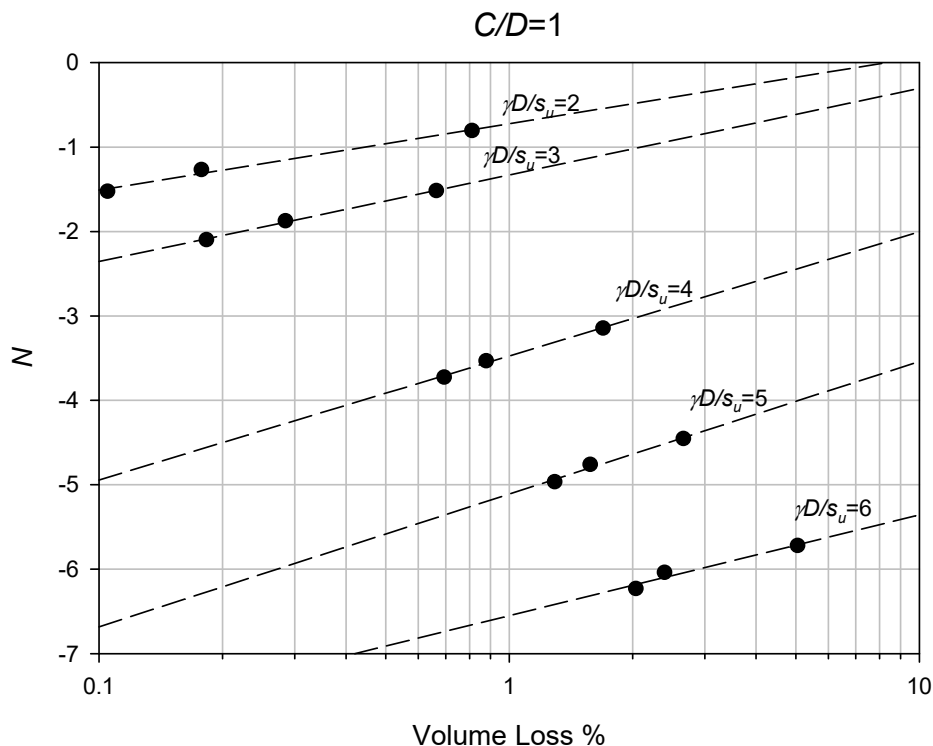


Figure 5-8 Stability number  $N$  versus volume loss % for varying  $\gamma D/s_u$  but constant  $C/D=1$

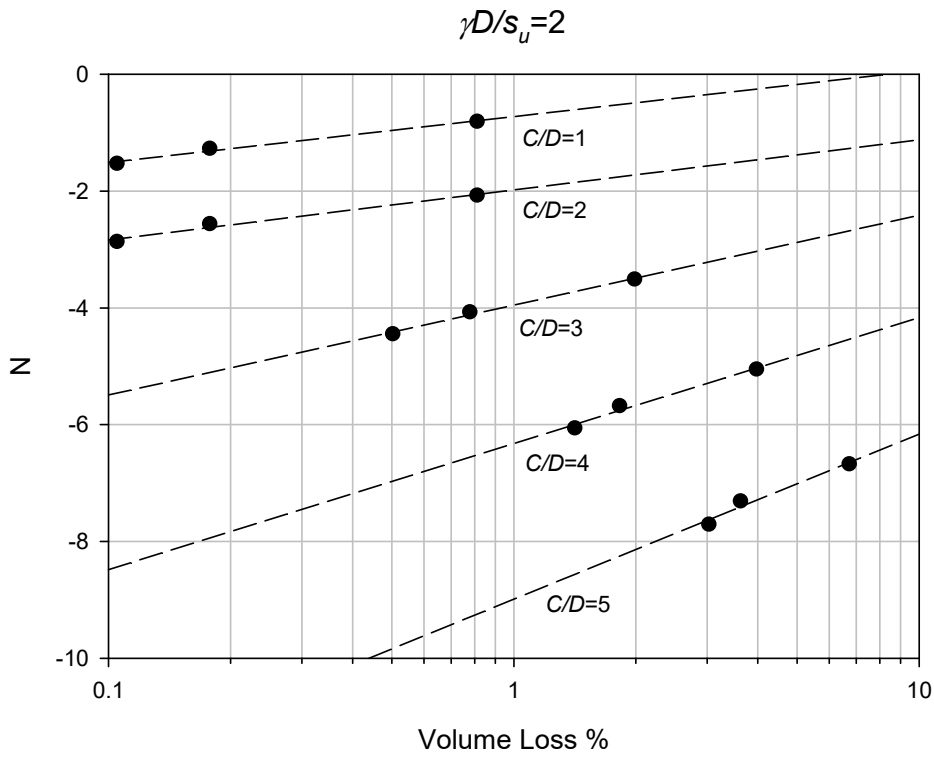


Figure 5-9 Stability number N versus volume loss % for varying C/D but constant  $\gamma D/s_u = 2$

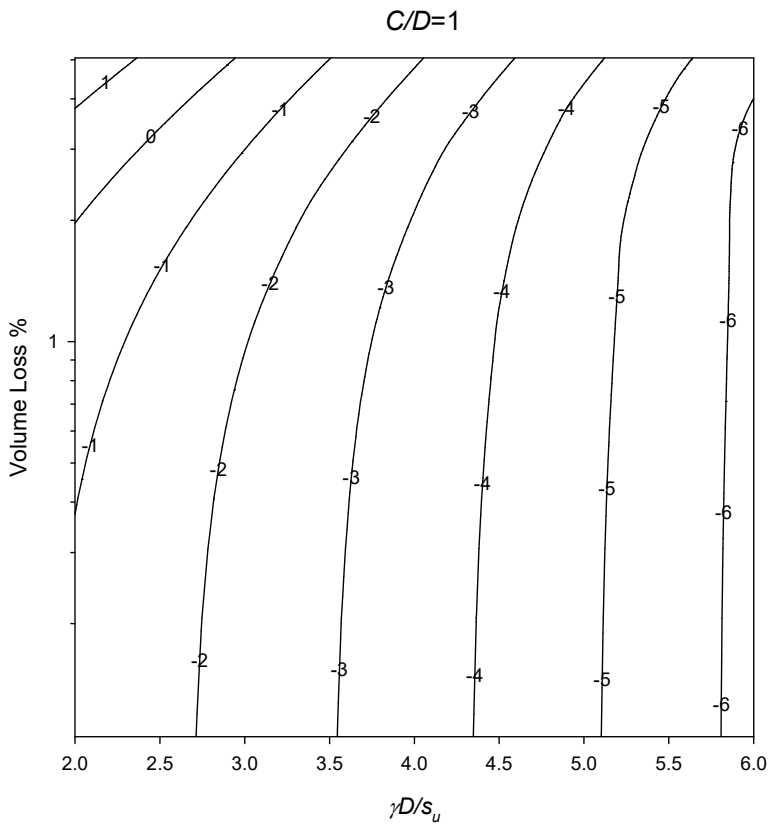


Figure 5-10 Stability numbers and volume loss design chart for  $C/D=1$

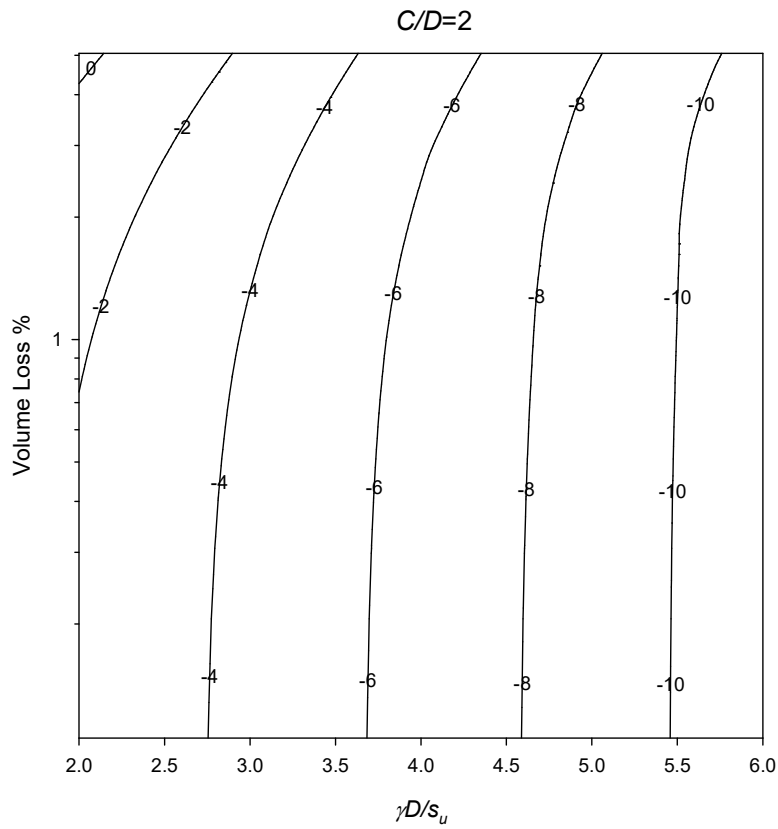


Figure 5-11 Stability numbers and volume loss design chart for  $C/D=2$

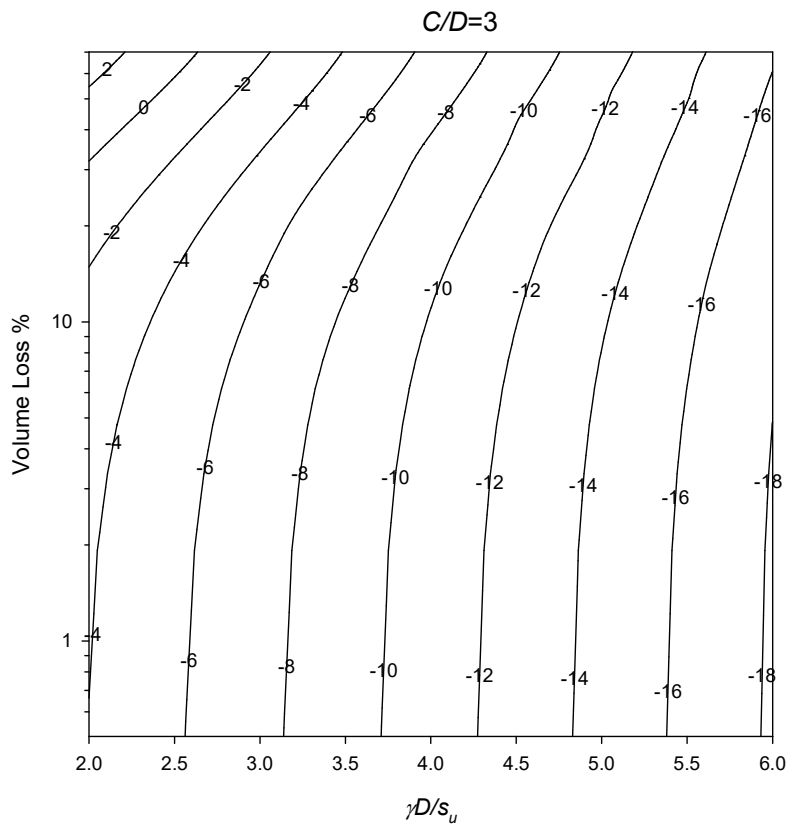
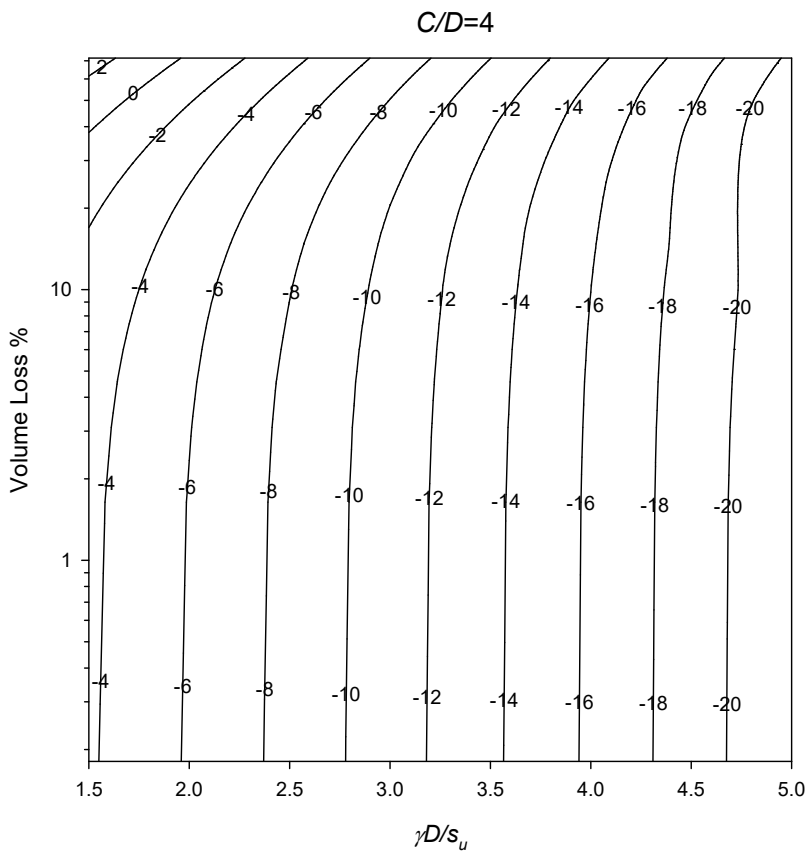
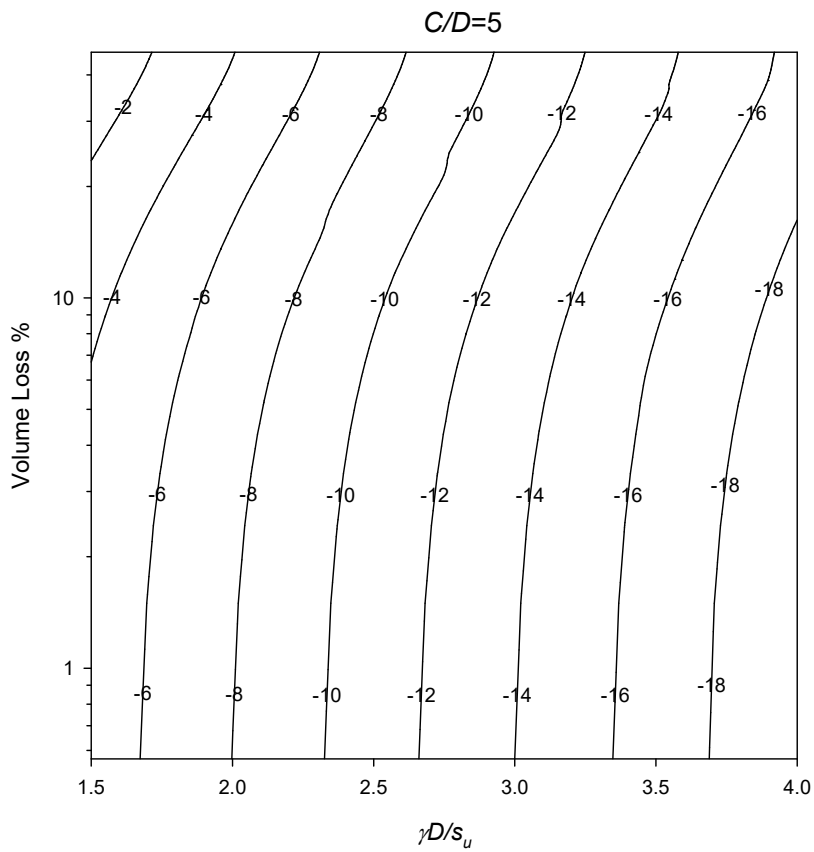


Figure 5-12 Stability numbers and volume loss design chart for  $C/D=3$



**Figure 5-13 Stability numbers and volume loss design chart for  $C/D=4$**



**Figure 5-14 Stability numbers and volume loss design chart for  $C/D=5$**

### 5.4.1 Practical Example

To demonstrate the potential usefulness of these charts, a practical example will be given.

#### **Evaluating TBM operations in terms of ground movement**

A planned tunnel is going to have a diameter of 6m, and a cover depth of 18m. The soil is found to be clay with a unit weight of 18 kN/m<sup>3</sup>, and an undrained shear strength of 27 kPa. Therefore, some of the dimensionless ratios can be calculated –  $C/D = 3$  and  $\gamma D/s_u = 4$ .

The question could then be – what pressure ratio ( $N$ ) is required to limit the volume loss to 2%? To answer this, figure 5-12 can be used. With this chart, it is found that a pressure ratio of approximately -11.1 will satisfy this condition. Referring to equation 5.1, if the surcharge pressure ( $\sigma_s$ ) is zero (greenfield conditions), then this will require an internal pressure ( $\sigma_t$ ) of 299.7 kPa.

## 5.5 Conclusion

This study has completed an analysis on the stability of circular tunnels in undrained clay, over a practical range of parameter ratios:  $C/D$ ,  $\gamma D/s_u$ ,  $N$ , and volume loss %. Stability has been analysed with the stability number (or pressure ratio,  $N$ ) at the detected stage of collapse, where the stability number represents the minimum to avoid collapse. Several pre-collapse ‘working conditions’ stages have also been analysed with this ratio, with the aim of establishing a stability-volume loss relationship.

The collapse stability results are compared with rigorous upper and lower bound results of Wilson et al (2011). The effect of the parameters is also shown. It is clear that the soil strength ratio has a big impact on the collapse stability number; in cases with strong clay, this number remains almost constant with increasing depth ratio. As the strength ratio increases (i.e. soil becomes weaker), the rate at which this stability number changes with  $C/D$  becomes greater. These conclusions concur with the comparison, which is quite positive, and shows that the results using the current pressure relaxation method are accurate. Therefore, it is believed that these results could be used with confidence as a potential design tool in practice. A design chart is developed and a number of practical examples are given.

The results for the pre-collapse stages have also been analysed. The stability numbers obtained from these stages are then related to their respective volume losses, which is obtained by integrating the settlement profile, as from chapter 4. It is found that volume loss increases as stability number reduces (i.e. becomes less negative). This is expected; reducing stability number theoretically reduces tunnel support and increases surcharge pressure. Soil strength ratio and depth ratio also have a big impact here – softer and deeper cases require higher pressure ratio (more negative) to maintain the same level of volume loss. Based on these reasonable conclusions and validation of previous results, contour charts have been produced for stability number  $N$ , which can be used to relate it to volume loss for any  $C/D$  and  $\gamma D/s_u$ .

# 6 TWIN TUNNEL SETTLEMENT

## 6.1 Introduction

This chapter describes the verification and use of a numerical model for investigating the settlement of twin circular tunnels in cohesive soils at the point of collapse, and at the preceding 'working condition' stage. The model aims to simulate the movement and relaxation of the soil around the shield and lining annulus that occurs due to the overcutting and grouting of the tunnel void by a tunnel-boring machine (TBM). To achieve this, the model uses a pressure relaxation technique that progressively reduces the tunnel support pressure from an initial condition until any points of interest, such as the point of collapse. At these stages, the surface settlement data is exported for analysis. In this chapter, data is exported for the collapse stage, and three previous 'working condition' stages.

The surface settlement data from these stages is exported for analysis using a regression of the commonly used Gaussian equation on the settlement data. Doing this allows accurate determination of  $i_x$  values for each case. This is done for a number of geometry and soil ratios, which will cover the most practical range for soft cohesive soils. The results of this study are quite positive, settlement results compare well with previous experimental and observational results. Design charts using dimensionless ratios have therefore been presented.

## 6.2 Problem Definition

Surface settlement caused by tunnelling is a complex soil-mechanics problem that is dependent on a number of a geometry and material properties, as well as the excavation operations themselves. Estimating surface settlement for twin tunnel activity adds many more variables, and thus adds extra complexity. For this reason, a careful scope of research must be detailed. In this study, the problem has been defined using parameters as shown in figure 6-1.  $C$  and  $H$  describe the overburden depth,  $D$  is the tunnel diameter (it is assumed that both tunnels will be the same diameter), and  $S$  is the centre-to-centre spacing.

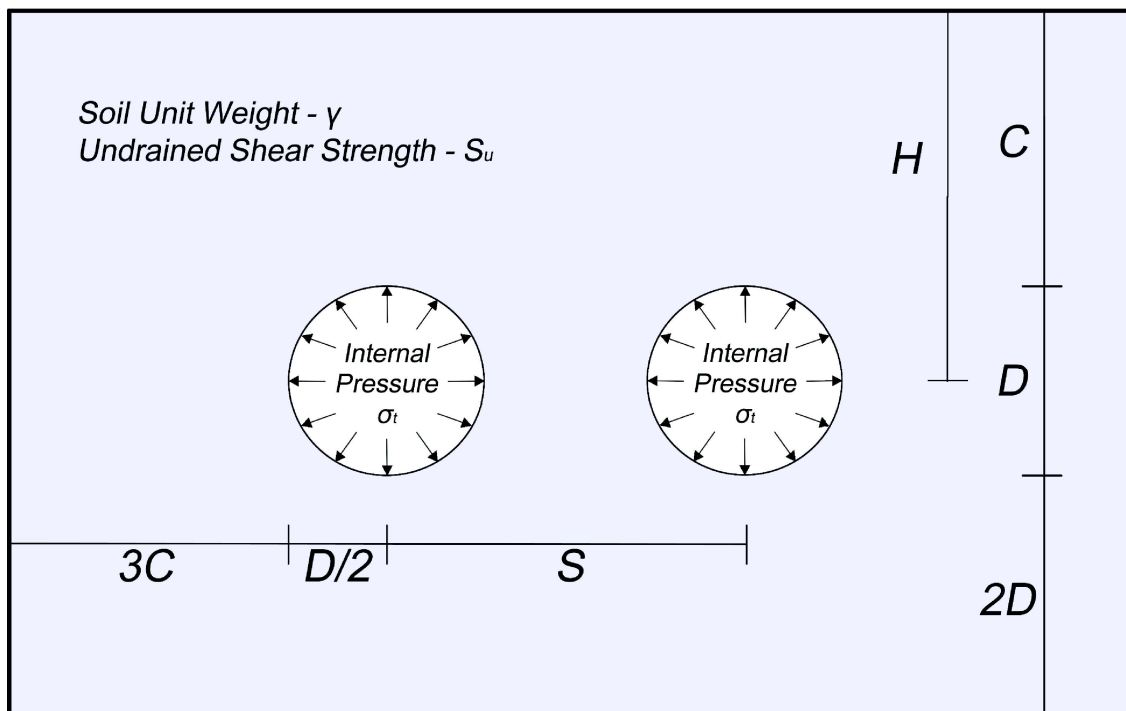


**Figure 6-1 Demonstration of the different categories used in this study (not to scale)**

These parameters are then combined to form some easy to use, easy to understand dimensionless ratios:  $C/D$  as the depth ratio,  $\gamma D/S_u$  as the soil strength ratio, and  $S/D$  for the tunnel spacing ratio. For simplicity, the Young's modulus ratio ( $E/S_u$ ) has been set to 200. Only greenfield settlement is being analyzed, and the surcharge is therefore is set to zero. It is also important to mention another simplification in this study, that is the tunnels are being modelled as being excavated simultaneously, and thus a symmetrical settlement profile will be expected.

The soil is a homogenous Mohr-Coulomb clay (Tresca) with assumed plane strain conditions. This is despite the fact that other models such as the modified cam-clay may be superior for simulating soil movement. However, the Tresca model has the



practical advantage, and given the number of assumptions and variables in practice, it will still provide useful results.

During the study, it became clear that the profiles were categorically different depending on the spacing ratio ( $S/D$ ). At lower  $S/D$ , the profiles became merged into something resembling a single tunnel profile. There were also other cases at higher  $S/D$  that had only partially merged profiles. The cases that are fully merged will be referred to as 'method 1' and the cases that are partially merged will be referred to as 'method 2'. The cases with the profiles, which could be considered as two separate tunnels, were termed 'method 3'. The latter category was designated as such if the spacing was more than eight times the inflection point parameter. These can be analysed using chapter 4.

An example of this categorization has been given in figure 6-2 for the case of  $C/D=3$ ,  $\gamma D/s_u=2$ . This also shows typical settlement profiles obtained in this study. As the method 3 case essentially depicts two independent tunnels with very little to no interaction, this case is more stable, which allows more soil movement to occur before a collapse occurs. The method 1 and 2 cases with interaction effects are more sensitive and thus the failure occurs at lower levels of deformation.

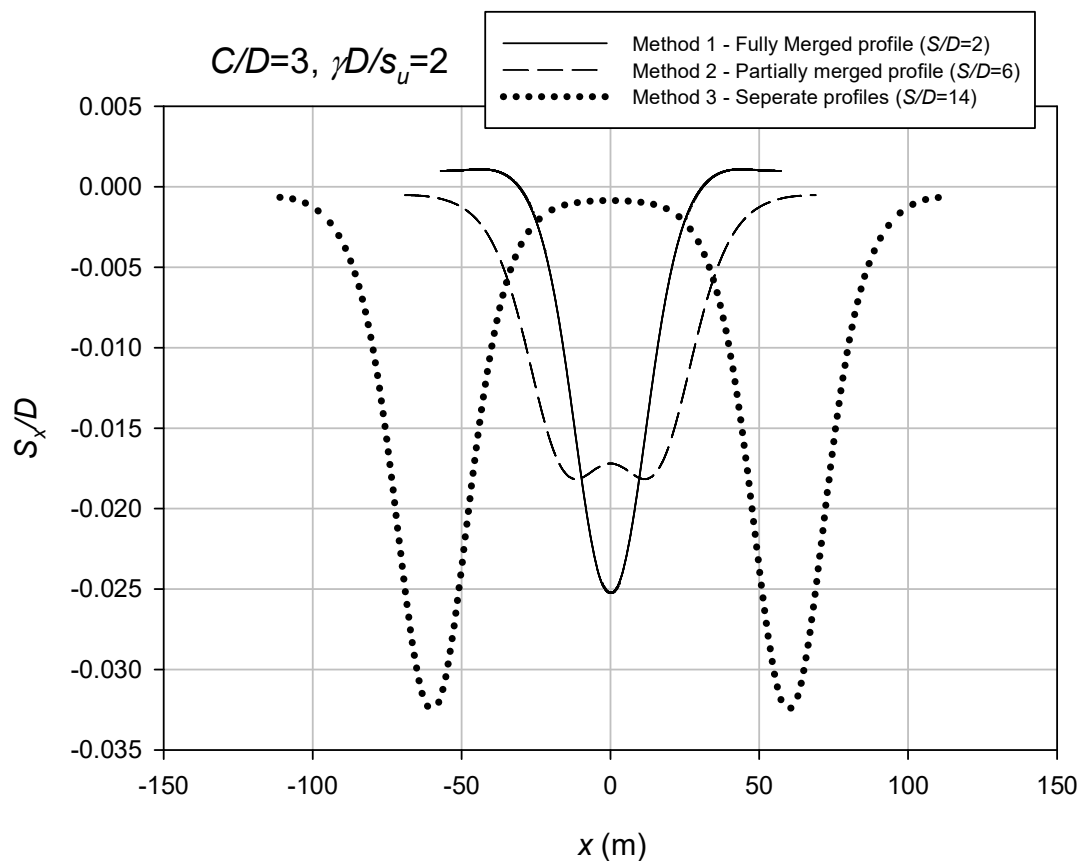


**Figure 6-2 Demonstration of the different categories used in this study**

Given the profiles are different, they are also analysed differently. Method 1 uses the commonly known Gaussian equation, as shown in equation 6.1 from Martos (1958) and Peck (1969). In this equation,  $S_{max}$  is the maximum settlement, and  $i_x$  is the inflection point parameter, which controls the shape of the settlement profile. Method 2 uses superimposed Gaussian equations that take the form of equation 6.2 (New and O'Reilly, 1991). In this equation, there is the additional variable  $s$ , which is the centre-to-centre spacing of the tunnels. As stated, method 3 cases can be analysed as two separate tunnels, and thus readers can refer to chapter 4 for these cases.

$$S_x = S_{max} e^{-\frac{x^2}{2i_x^2}} \quad (6.1)$$

$$S_x = S_{max} \left( e^{-\frac{(x-0.5s)^2}{2i_x^2}} + e^{-\frac{(x+0.5s)^2}{2i_x^2}} \right) \quad (6.2)$$

### 6.3 Method of Analysis

As previously discussed, the 'method 1' settlement profiles are commonly represented by equation 6.1, and the 'method 2' profiles can be represented using equation 6.2. In this study, these equations have been used for a regression with the data collected at the collapse and previous 'working condition' stages. This has been done using *MATLAB*, and the curve fitting toolbox. In this analysis, the  $S_{max}$  parameter is fixed at the  $S_{max}$  of the data, and the trough width parameter is varied until the best solution is found. The curve-fitting toolbox uses robust bi-square regression combined with a trust-region algorithm.

A typical example of this is shown in figure 6-3. It was found that using this equation to model settlement could be considered accurate, with  $r^2$  values of greater than 0.97 achieved for all cases, where an  $r^2$  of one would indicate a perfect fit. The examples shown in figure 6-3 demonstrate the curve fitting for methods 1 and 2. They are once again for the  $C/D=3$ ,  $\gamma D/s_u=2$  case for  $S/D=2$  and 6. Using this approach is quite accurate; in all cases, an  $r^2 > 0.95$  can be achieved. By curve fitting

the equation to the *FLAC* data in this way,  $i_x$  values can be produced for each case reliably.

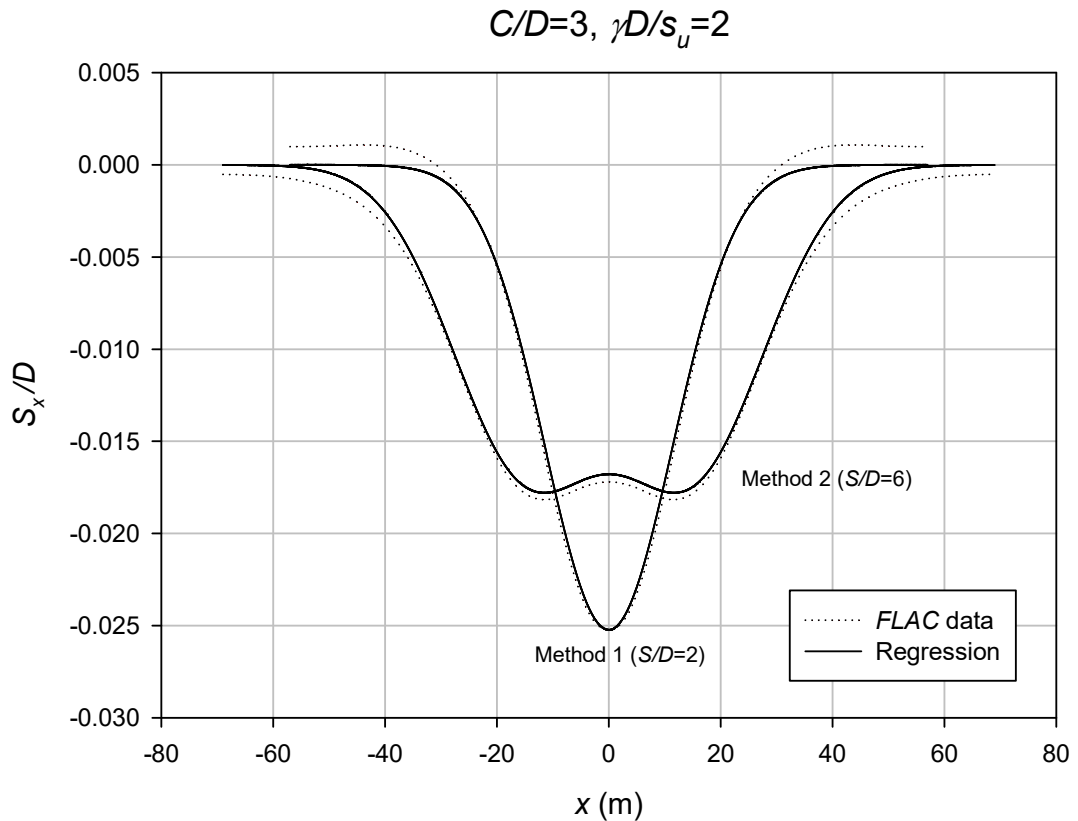


**Figure 6-3 Demonstration of the different categories used in this study**

As mentioned previously, the type of settlement profile produced for twin tunnels can be categorically different depending on the spacing ratio. Figures 6-4 to 6-8 are charts that provide an estimate of which method will be required depending on depth ratio, soil strength ratio, and spacing ratio. There is immediately some interesting trends with these figures – cases with stronger soils (lower  $\gamma D/s_u$ ) tend to become defined by method 2 sooner with increasing  $S/D$ , they also become method 3 sooner as well. Increasing depth ratio ( $C/D$ ) results in the transition from method 2 to method 3 being delayed until larger spacing ratios.

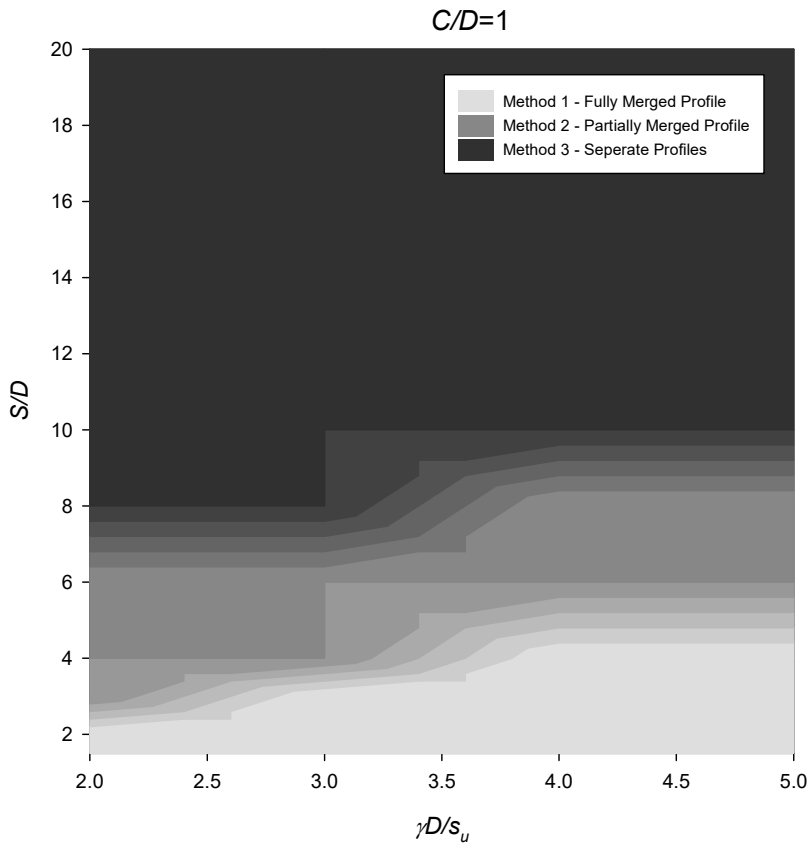


Figure 6-4 Contour plot for  $C/D=1$  which indicates the method of settlement analysis to use

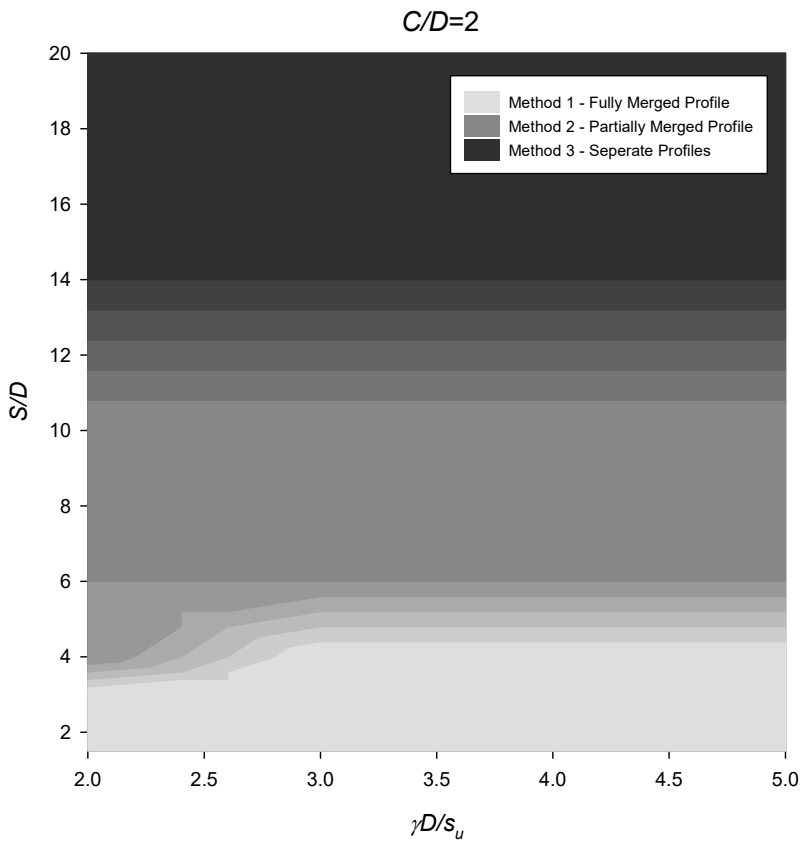
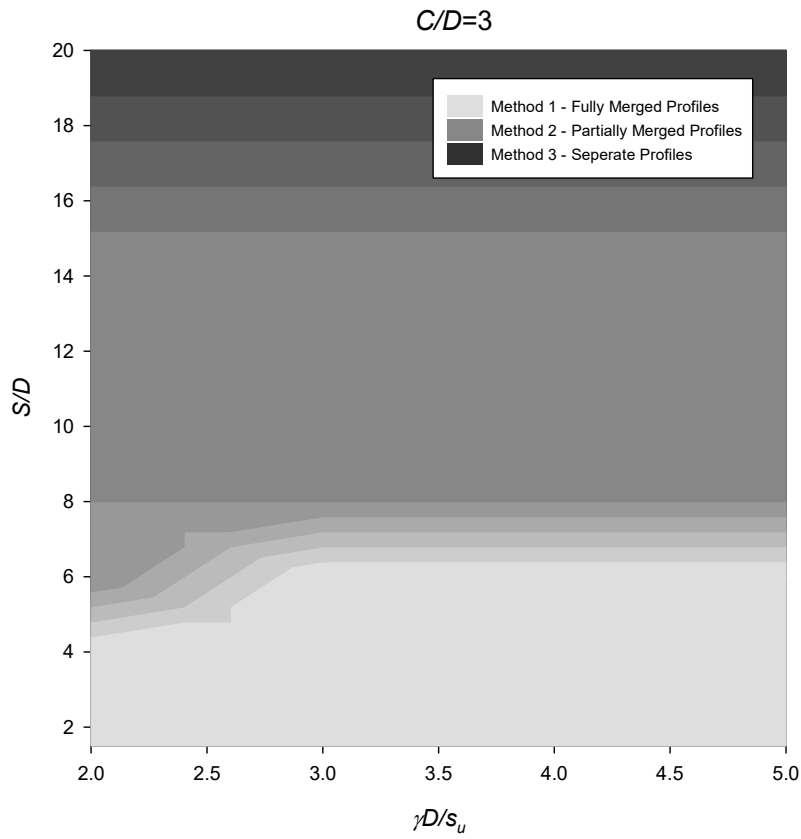
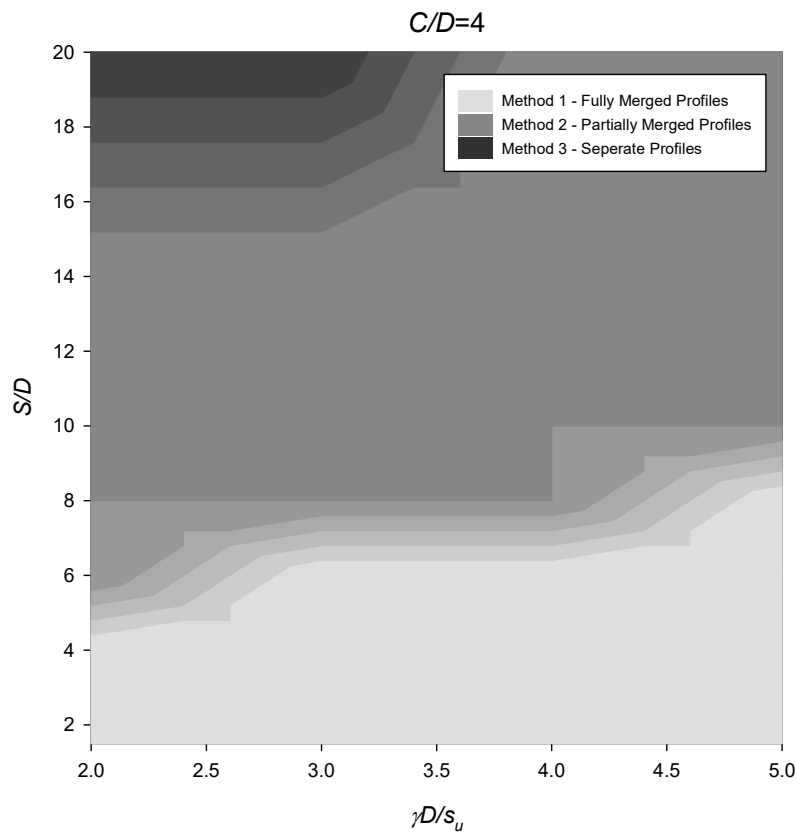
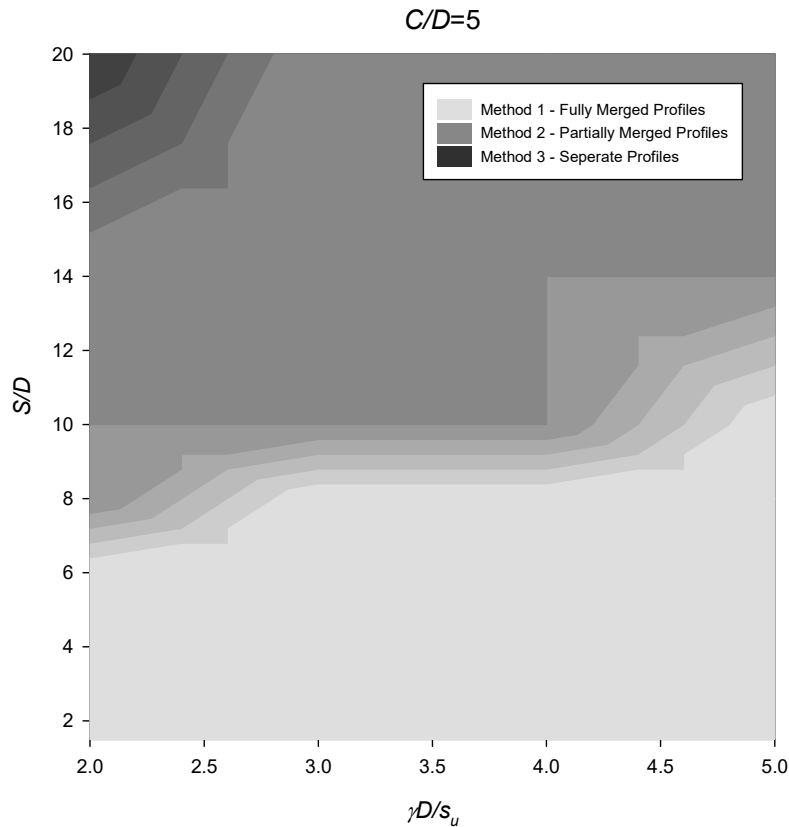


Figure 6-5 Contour plot for  $C/D=2$  which indicates the method of settlement analysis to use



**Figure 6-6 Contour plot for  $C/D=3$  which indicates the method of settlement analysis to use**



**Figure 6-7 Contour plot for  $C/D=4$  which indicates the method of settlement analysis to use****Figure 6-8 Contour plot for  $C/D=5$  which indicates the method of settlement analysis to use**

## 6.4 Results - At Collapse

This section discusses results for twin tunnel settlement at the collapse stage. For convenience, subsections will be used for each of the settlement profile 'methods'.

### 6.4.1 Method 1 – Fully Merged Profiles

In figure 6-9, settlement profiles are presented for method 1 where the depth ratio ( $C/D$ ) is varied and the strength ratio ( $\gamma D/s_u$ ) and spacing ratio ( $S/D$ ) are kept constant. The profiles are as expected, with the shallow case producing a narrow but deep trough, that become shallower and wider as  $C/D$  increases. Note that this is consistent with the equivalent method 2 chart (fig 6-13) in section 6.4.2.

Figure 6-10 shows settlement profiles where  $C/D$  and  $S/D$  are kept constant, and  $\gamma D/s_u$  is varied. In this chart, the weaker case has a larger maximum settlement at collapse. This seems reasonable, it would be expected that the weaker soil would have higher movement during a collapse. However, this result is inconsistent with

the equivalent chart (fig 6-14) in section 6.4.2. This may be due to increased interaction effects in that case.

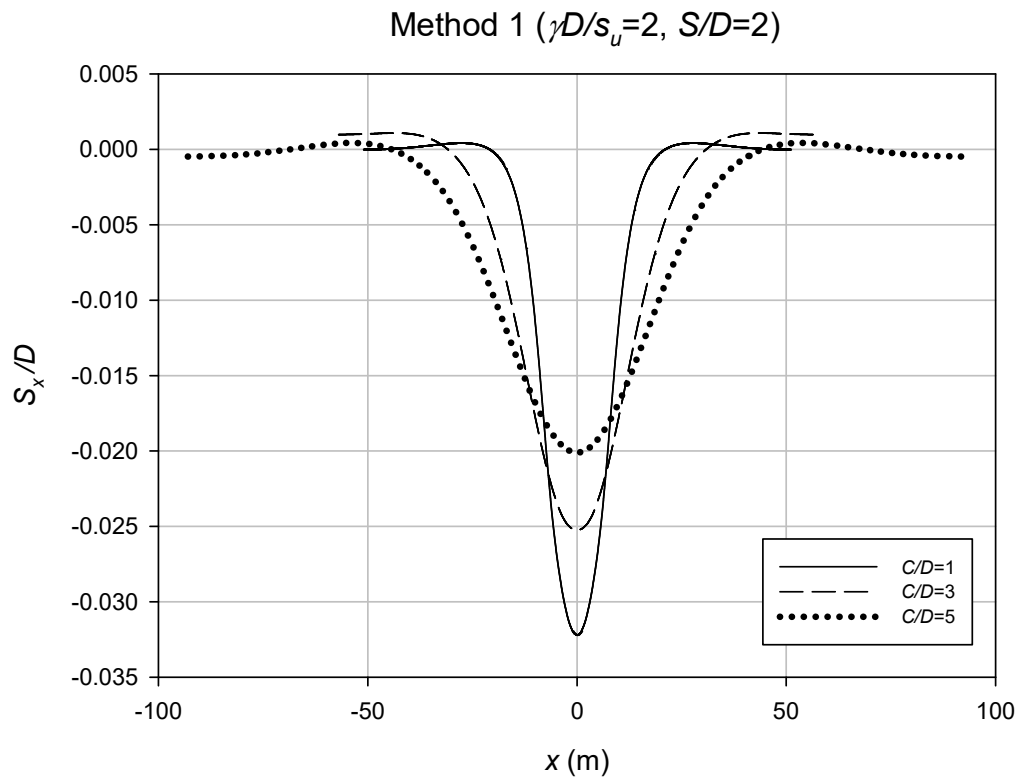


Figure 6-9 Settlement profiles with varying  $C/D$  for a typical method 1 case

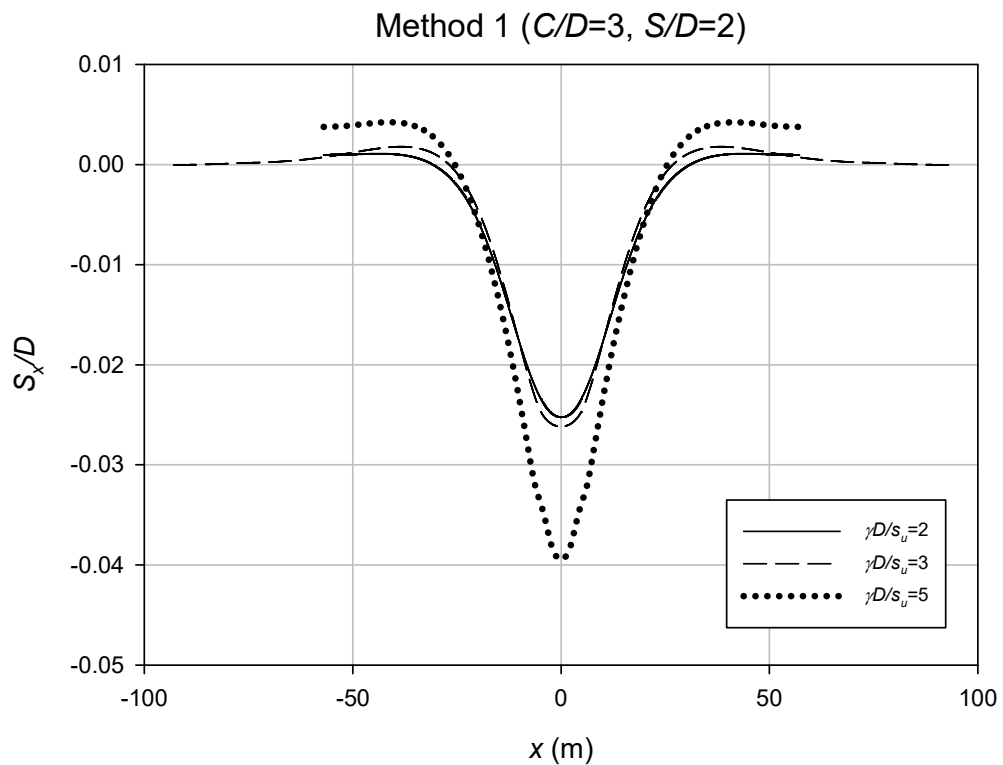
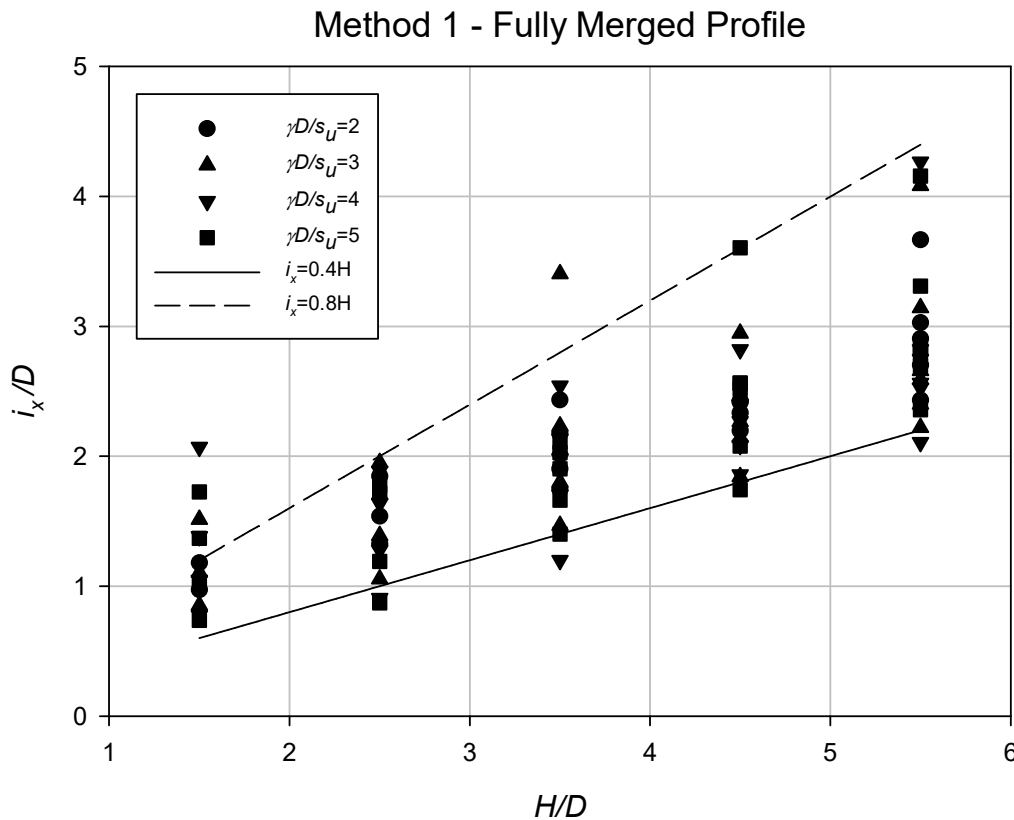


Figure 6-10 Settlement profiles with varying  $\gamma D/s_u$  for a typical method 1 case



**Figure 6-11  $i_x/D$  vs  $H/D$  with varying  $\gamma D/s_u$  for all method 1 data**

Once the settlement data has been analysed using the regression approach, as described in section 6.3, an  $i_x$  is generated for each case. Figures 6-11 and 6-12 display some analysis of these results. Note that  $i_x$  has been normalised with the diameter  $D$ , to increase its usefulness.

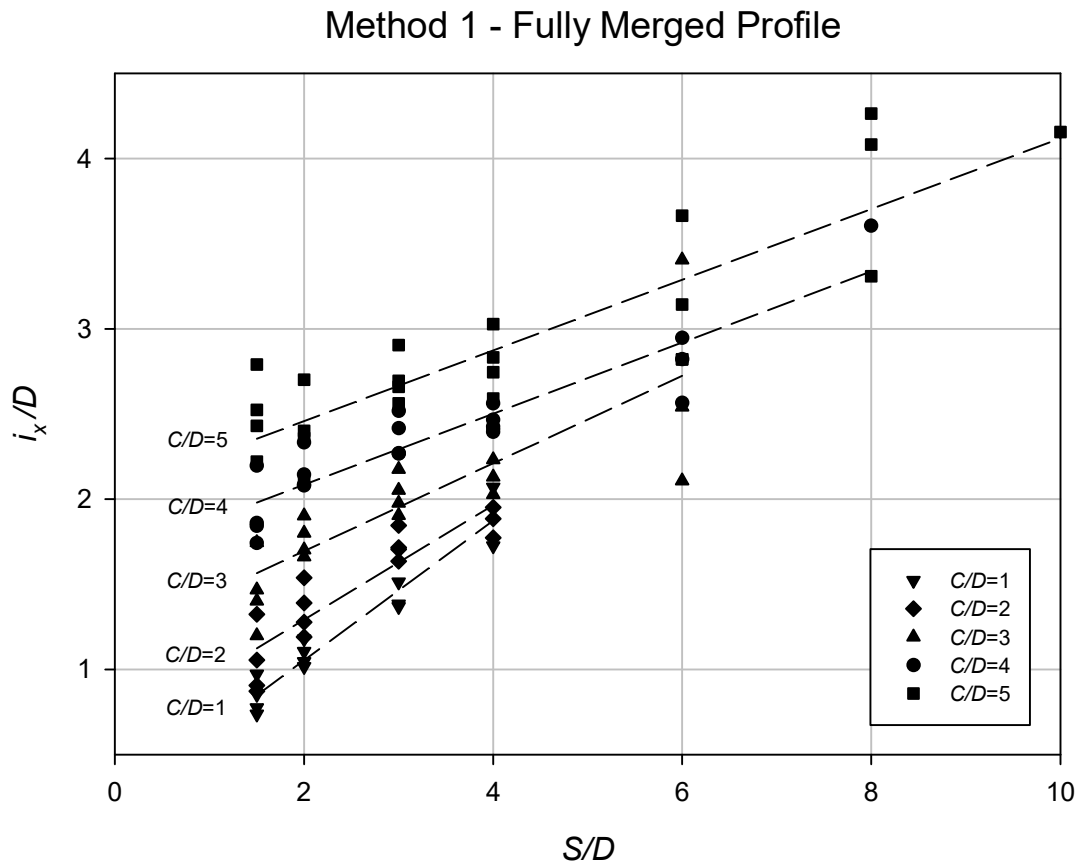
In these figures,  $i_x/D$  is heavily dependant on both  $C/D$  and  $S/D$ . Figure 6-11 shows the relationship with respect to the depth ratio variable  $H/D$  (note that  $H = C+D/2$ ,  $H$  and  $C$  are effectively the same) and the soil strength variable  $\gamma D/s_u$ . It can be seen that O'Reilly and New's relationship (1982) still seems to hold -  $i_x/D$  is linear with  $H/D$ , and the data points fit approximately within a  $k$  range of 0.4 - 0.7, as shown. However, it seems that there is no identifiable relationship with respect to  $\gamma D/s_u$ . The data points are spread rather randomly.

Figure 6-12 shows the relationship between  $i_x/D$  and the spacing ratio  $S/D$  with varying  $C/D$ . In this chart, a convincing relationship can be seen, that  $i_x/D$  is also linearly related to  $S/D$ . It also appears that the gradient of this relationship is steepest in the shallower cases. From these two charts, equation 6.3 is developed



which estimates  $i_x/D$  at collapse for any 'method 1' twin tunnel case based on the  $C/D$  and  $S/D$ .

$$\frac{i_x}{D} = \left(\frac{C}{D}\right) \left[ -0.05 \left(\frac{S}{D}\right) + 0.47 \right] + 0.44 \left(\frac{S}{D}\right) - 0.25 \quad (6.3)$$



**Figure 6-12  $i_x/D$  vs  $S/D$  with varying  $C/D$  for all method 1 data**

#### 6.4.2 Method 2 – Partially Merged Profiles

In figure 6-13, settlement profiles are presented for method 2 where the depth ratio ( $C/D$ ) is varied and the strength ratio ( $\gamma D/s_u$ ) and spacing ratio ( $S/D$ ) are kept constant. The trend is as expected, with the profiles of the deeper cases producing a smaller maximum settlement but being wider than the shallow cases. Note that this is consistent with the equivalent method 2 chart (fig 6-9) in section 6.4.1.

Figure 6-14 shows settlement profiles where  $C/D$  and  $S/D$  are kept constant, and  $\gamma D/s_u$  is varied. In this chart, the weaker case has a smaller maximum settlement at collapse. This is opposite to the equivalent figure for the method 1 results (fig 6-10). The reason for this is most likely some increased interaction effects in this case,

leading to the cases with the stronger soils being able to be relaxed further and tolerate more ground movement before failure occurs.

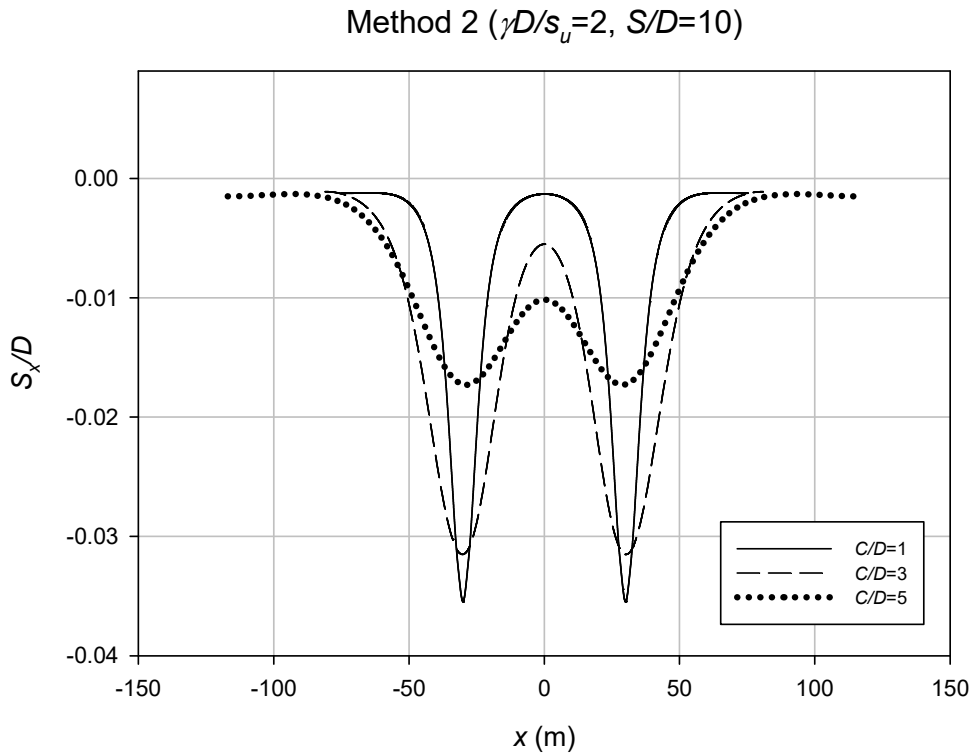


Figure 6-13 Settlement profiles with varying  $C/D$  for a typical method 2 case

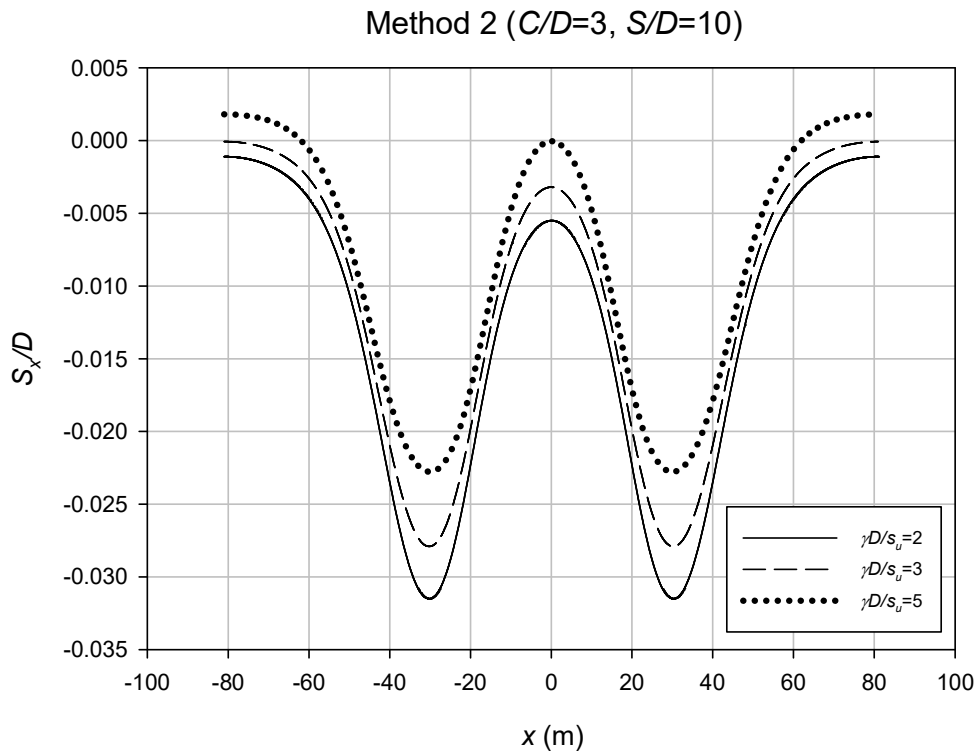


Figure 6-14 Settlement profiles with varying  $\gamma D/s_u$  for a typical method 2 case

The settlement data from these profiles is then used in a regression, which allows the generation of an  $i_x$  value for each case accurately and reliably. Figures 6-15 and 6-16 show some analysis of these  $i_x$  results. Note that this value has been normalised with tunnel diameter,  $D$  to make the results dimensionless.

Figure 6-15 shows the relationship between  $i_x/D$  and  $H/D$  for varying  $\gamma D/s_u$ . This shows that the relationship between  $i_x/D$  and  $H/D$  is linear, and therefore O'Reilly and New's relationship seems to hold. Comparing to the method 1 equivalent chart (fig 6-11), the data is tighter, with the  $k$  range being approximately between 0.5 – 0.7. However, it is also seen that there is no notable trend with  $\gamma D/s_u$ .

In figure 6-16, the relationship between  $i_x/D$  and  $S/D$  is shown for varying  $C/D$ . This chart again shows the importance of the depth ratio, but seemingly shows that  $S/D$  has a minimal impact as the data grouping and the regression lines are approximately horizontal. Based on these results, equation 6.4 has been developed, which can approximately estimate an  $i_x/D$ , for any  $C/D$ .

$$\frac{i_x}{D} = 0.49 \left( \frac{C}{D} \right) + 0.81 \quad (6.4)$$

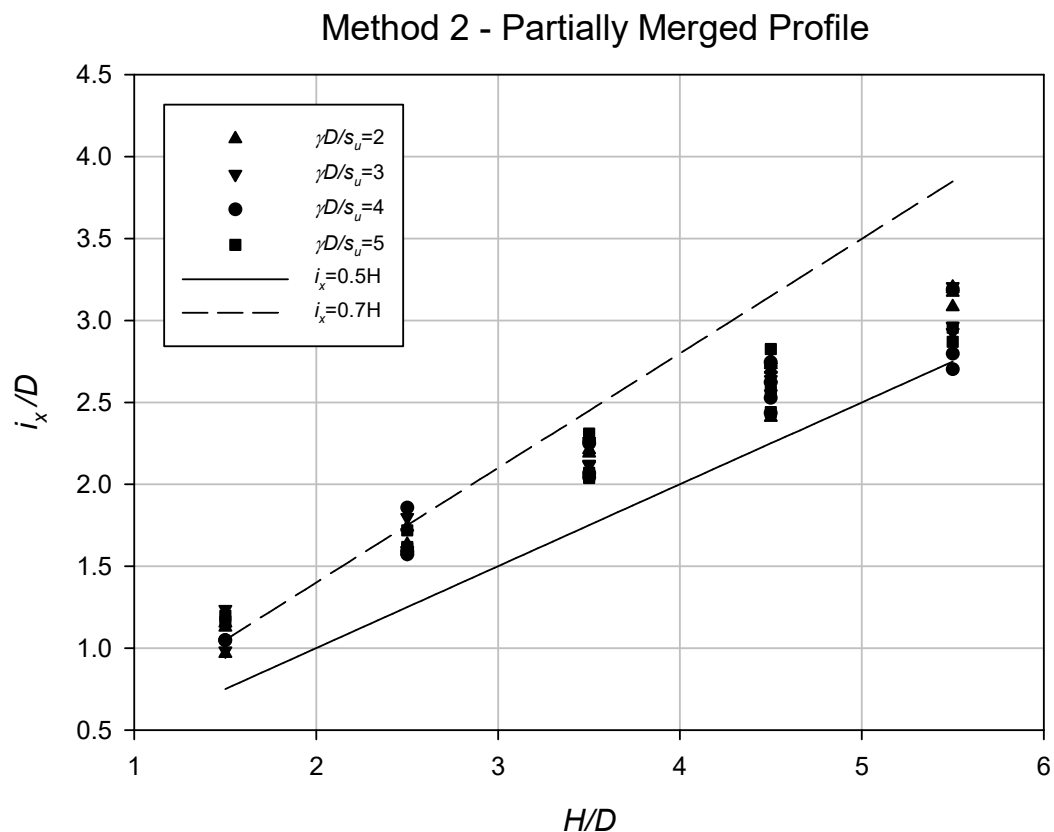


**Figure 6-15  $i_x/D$  vs  $H/D$  with varying  $\gamma D/s_u$  for all method 2 data**

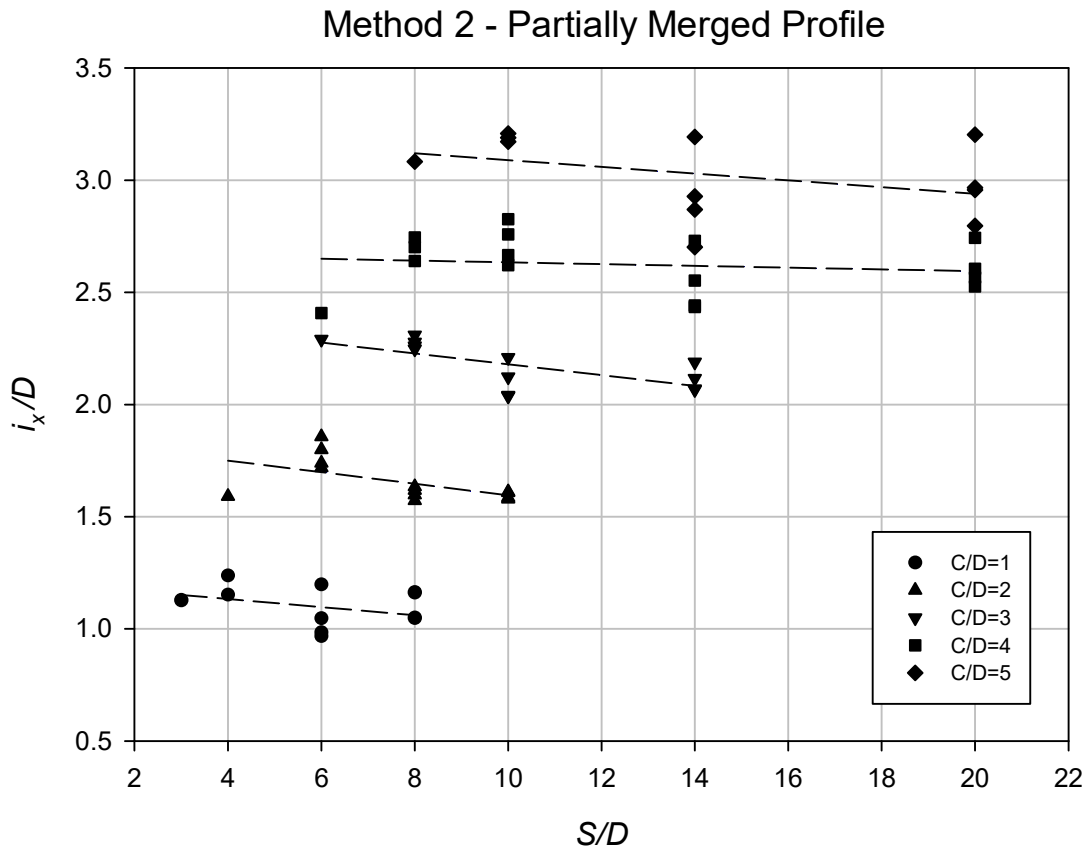


**Figure 6-16**  $i_x/D$  vs  $S/D$  with varying  $C/D$  for all method 2 data

### 6.4.3 Method 3 – Separate profiles

The settlement of twin tunnels in this category can simply be analysed using two single tunnels as in chapter 4. As discussed in section 6.2, the two tunnels will be far enough apart that the impact they have on each other will be negligible.

## 6.5 Results – Pre-Collapse

The previous section has analysed results from the collapse step. In this section, the analysis has been based on the three relaxation steps before the point of collapse (PoC). In other words, if the PoC was 52% relaxation; the stages being analysed are 49%, 50%, and 51%).

This has been done such that an analysis of the settlement shape factor ( $i_x$ ) can be done at pre-collapse conditions, closer to ground loss levels experienced during construction. The volume loss can then be back calculated by integrating the surface settlement data. It should be noted that this numerical model controls the internal tunnel pressure; the volume loss is not a controlled parameter. In the following, section 6.5.1 deals with the results and analysis of method 1 type settlement, section

6.5.2 deals with method 2 type settlement, and 6.5.3 briefly discusses how to handle method 3 type settlement.

### 6.5.1 Method 1 – Fully Merged Profiles

Figure 6-17 shows  $i_x/D$  against  $H/D$ . From this chart, it can be concluded that O'Reilly and New's relationship still holds, the relationship is approximately linear, with a  $k$  range between 0.3 – 0.7. It can also be concluded that the soil strength ratio ( $\gamma D/s_u$ ) seems to be relatively unimportant, as there is no noticeable trend. This is consistent with the PoC results. However, it is clear that depth ratio is important, and that the variations are being caused by either or both volume loss % or  $S/D$ , the two variables that are not distinguished in this chart.

From figures 6-18 and 6-19, volume loss ( $VL\%$ ) is graphed against  $i_x/D$  for varying  $S/D$  for  $C/D=1$  and  $C/D=5$  respectively. It can be seen that  $i_x/D$  increases with volume loss; the rate of increase is high at low  $VL\%$ , but appears to plateau at higher  $VL\%$ , which may indicate a logarithmic relationship. It also seems that spacing ratio does not have much impact on this relationship. The range of  $i_x/D$  in the two charts is also important to note – the  $C/D=1$  chart (figure 6-18) has a range of 0.7-1.5, and the  $C/D=5$  chart (figure 6-19) has a range of 1.2-3. This is a consequence of the relationship previously identified in figure 6-17.

These charts conclude that the parameters influencing  $i_x/D$  are depth ratio  $C/D$ , and volume loss. The spacing ratio  $S/D$  and soil strength ratio  $\gamma D/s_u$  seem to have little impact.

Further to this point, figure 6-20 shows  $i_x/D$  against  $S/D$ , which after some examination reinforces the conclusion that  $S/D$  appears unimportant. The graph shows the data separated by  $C/D$  and their attempted regression lines. However, it is observed to be a poor fit, and the only clear trend is the regression lines getting 'higher' with  $C/D$  is a consequence of the same trend previously identified. Therefore, it is understood that the variations in this chart are being caused by differing levels of volume loss.

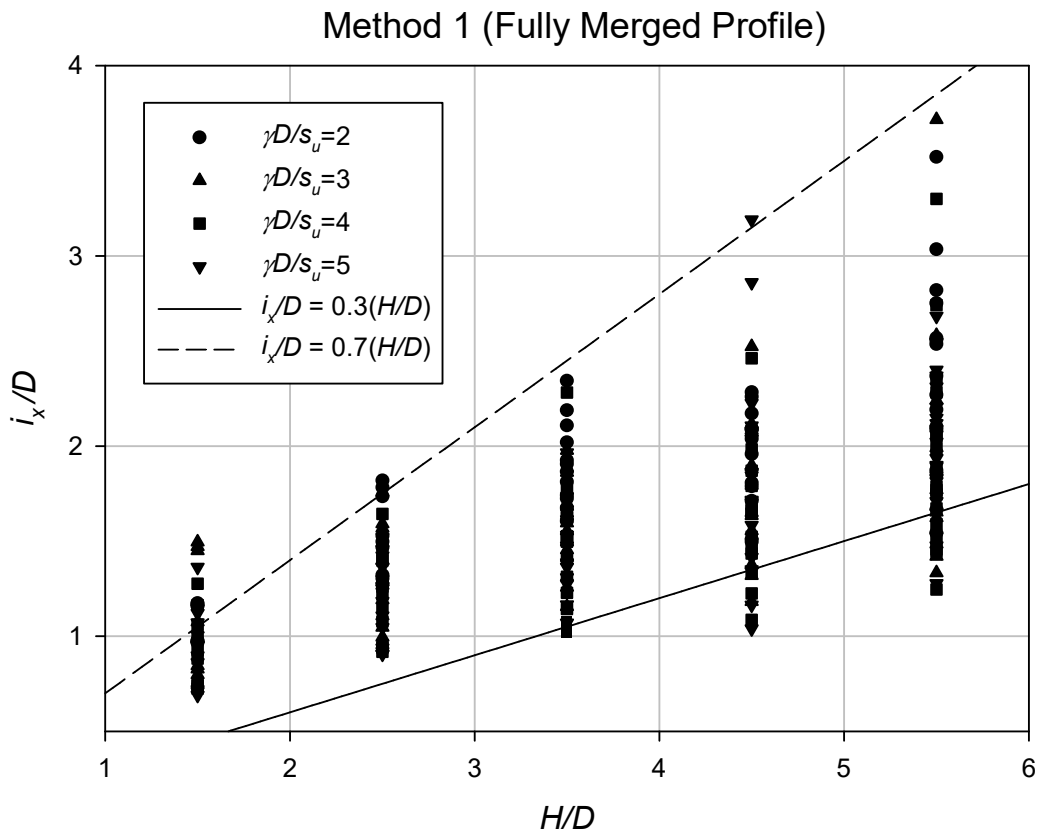


Figure 6-17  $i_x/D$  vs  $H/D$  with varying  $\gamma D/s_u$  for all method 1 data

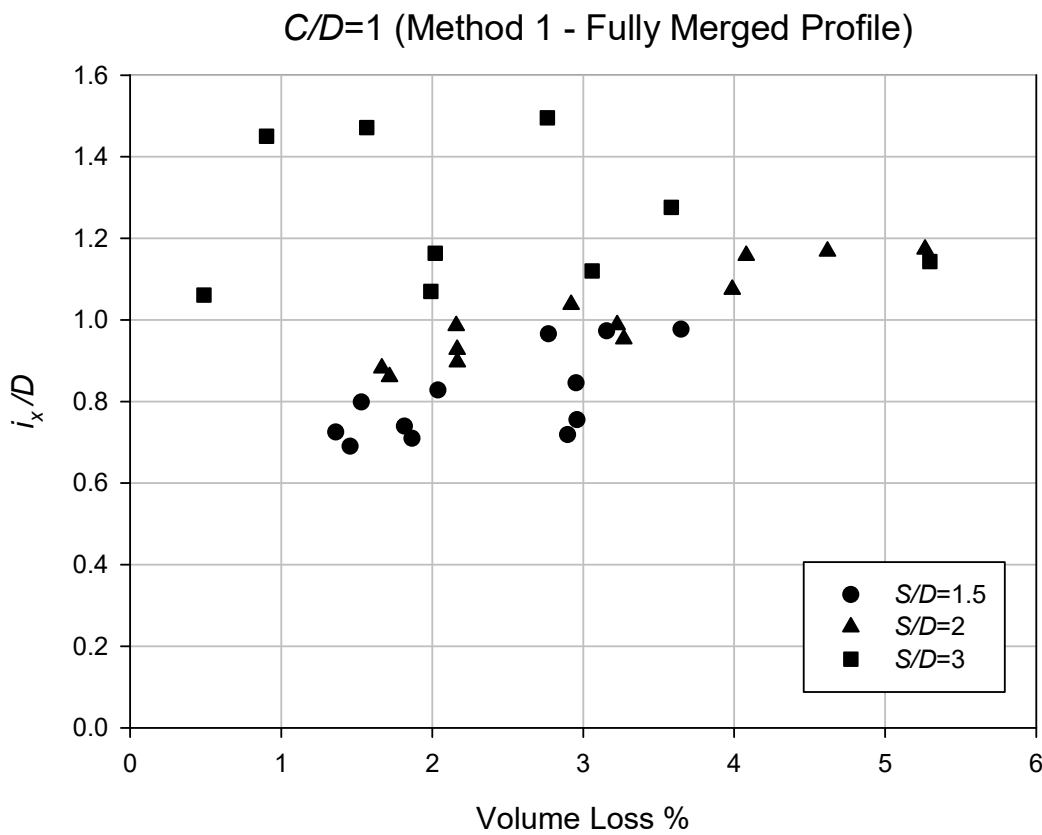


Figure 6-18  $i_x/D$  vs volume loss % with varying  $S/D$  for  $C/D=1$  method 1 data

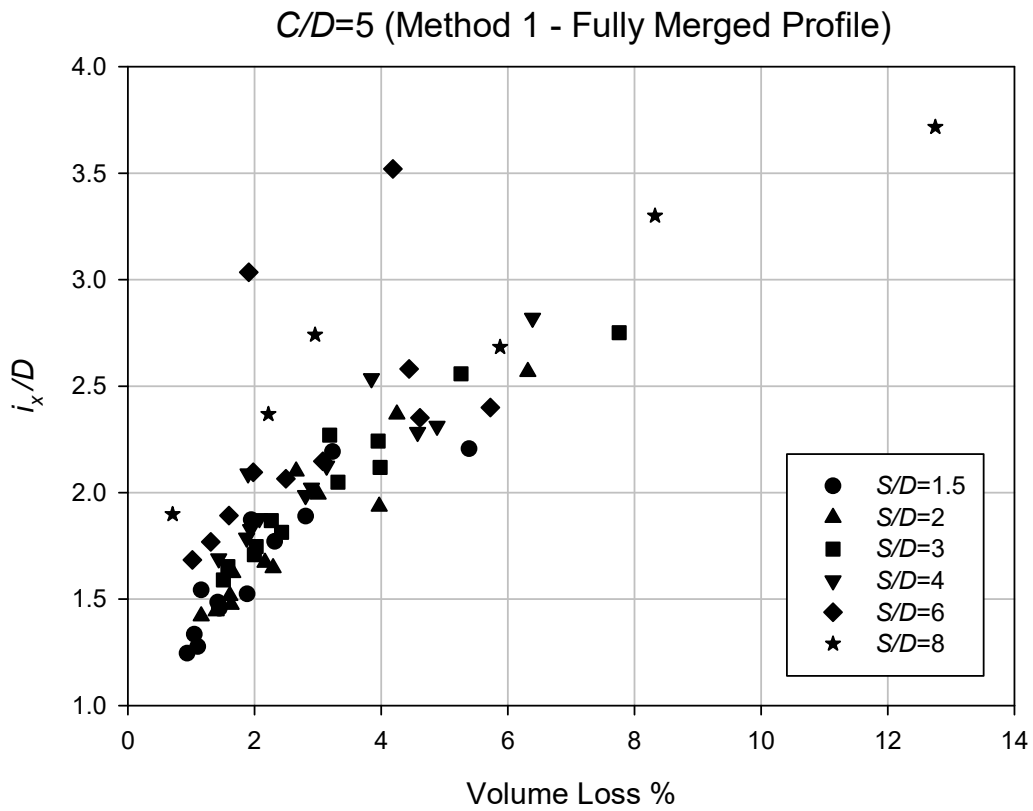


Figure 6-19  $i_x/D$  vs volume loss % with varying  $S/D$  for  $C/D=5$  method 1 data

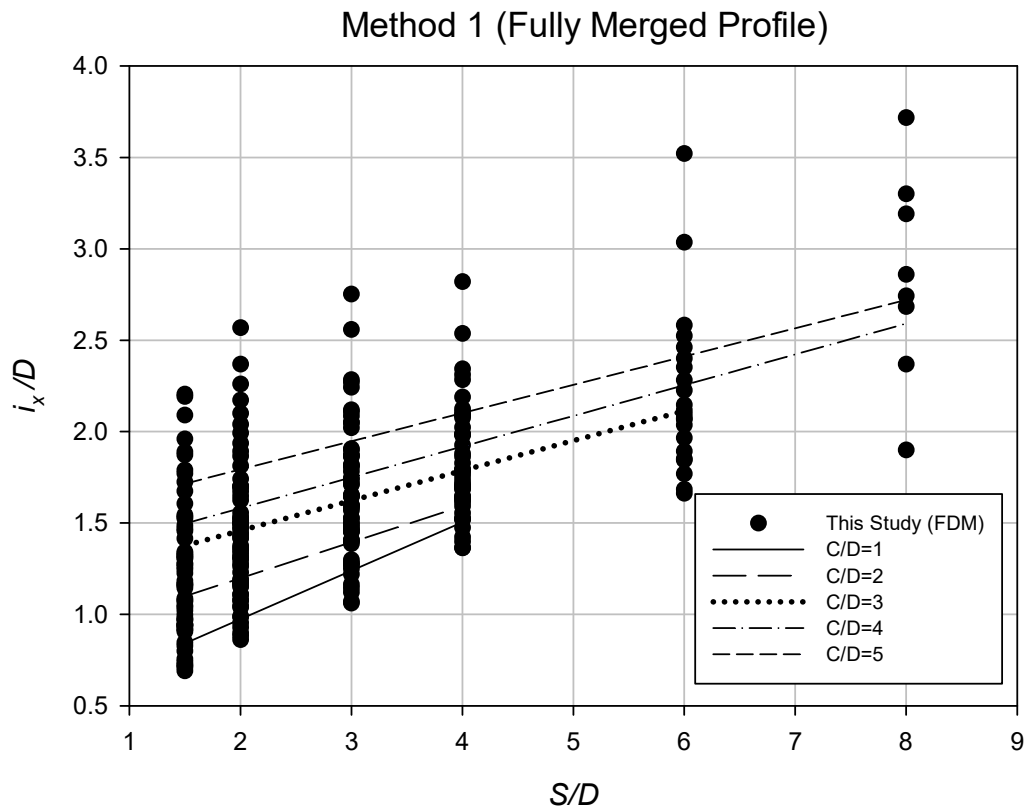


Figure 6-20  $i_x/D$  vs  $S/D$  with varying  $C/D$  for all method 1 data

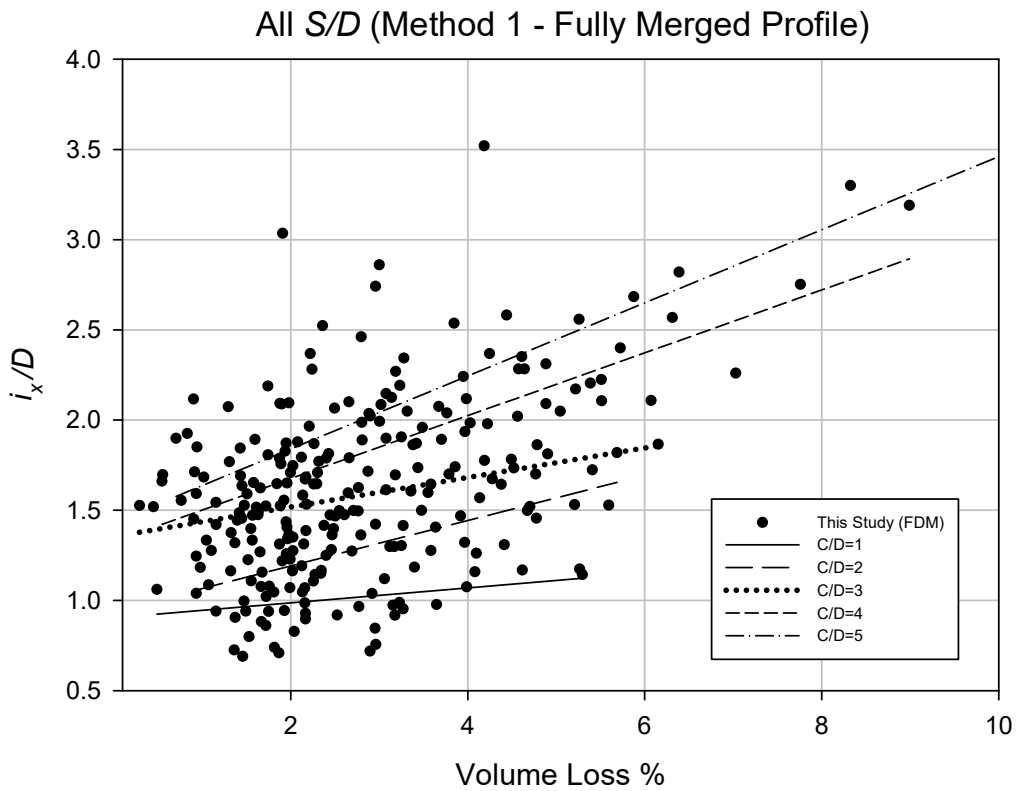


Figure 6-21  $i_x/D$  vs volume loss % with varying  $C/D$  for all method 1 data (All S/D)

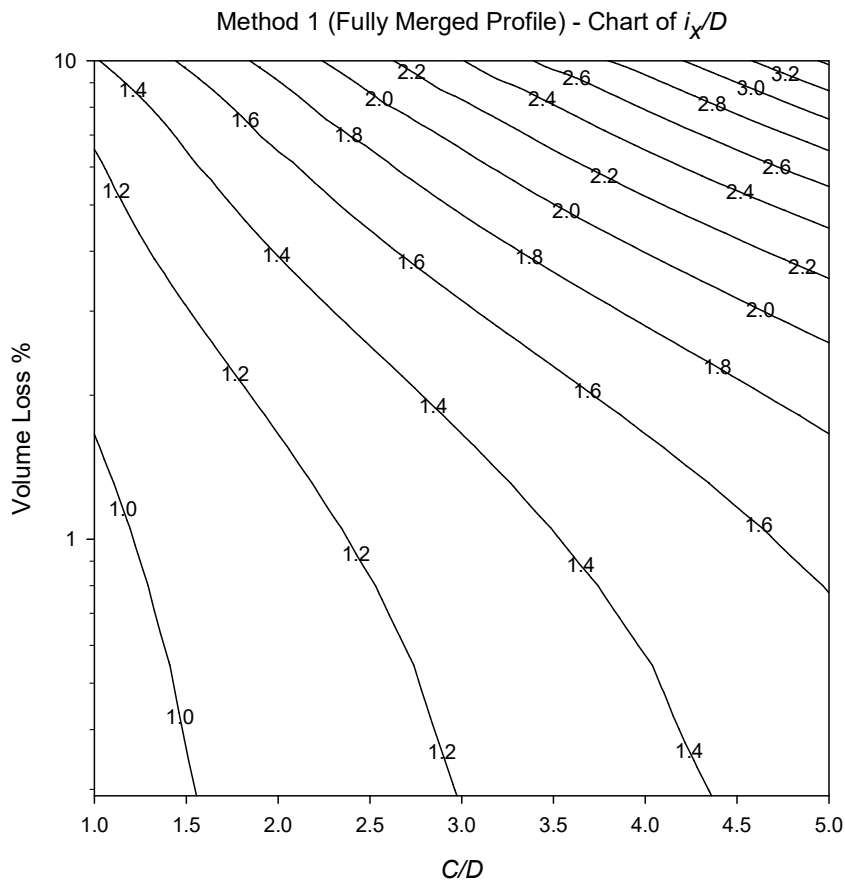


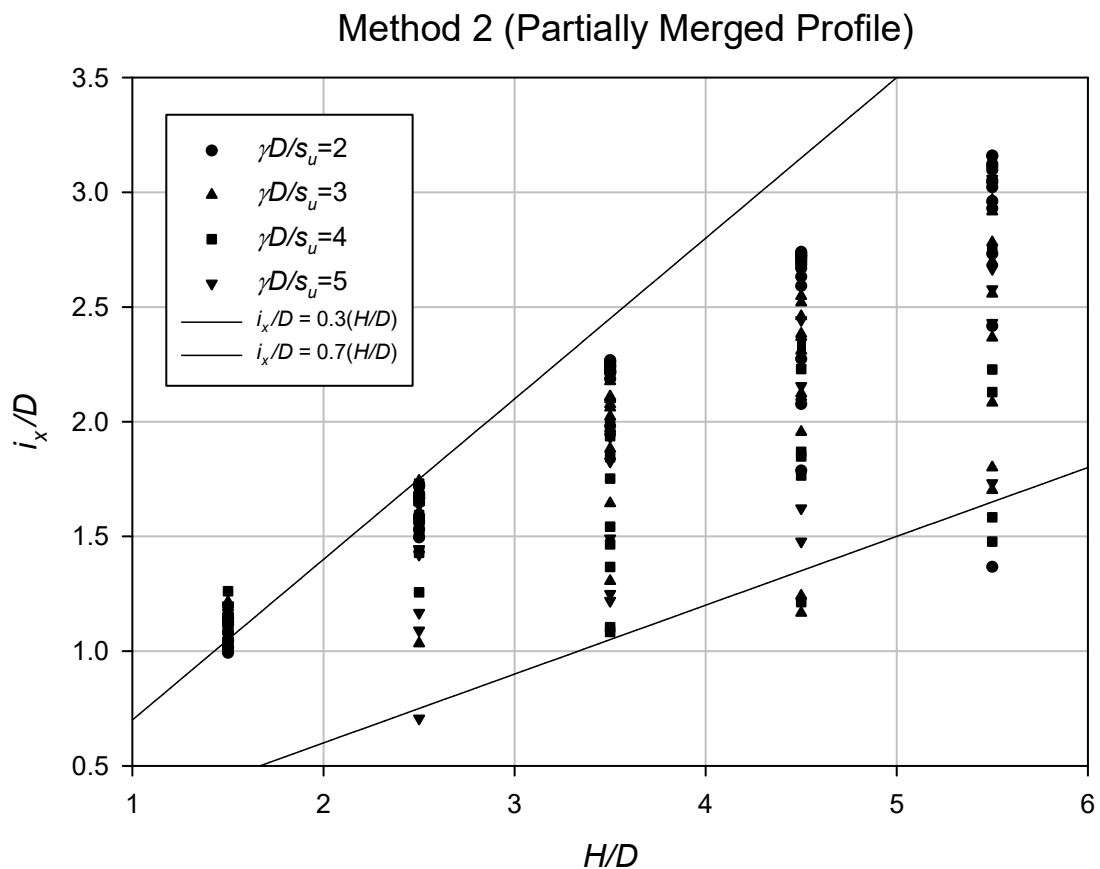
Figure 6-22 Design chart for  $i_x/D$  against VL% with varying  $C/D$  for all method 1 data (All S/D)



Figure 6-21 is a chart incorporating all of the variables that appear to have a significant trend with  $i_x/D$ , that is  $C/D$  and  $VL\%$ . It can be seen in this figure, that the data grouping for each  $C/D$  shows a convincing trend, with relatively minimal outliers. From this a *MATLAB* surface fit can be done (figure 10-4 in Appendix 1). This surface has an  $r^2=0.86$ , and is a good fit. Therefore, a design chart has been produced in figure 6-22, that can be used to predict  $i_x/D$  for any method 1 twin tunnel settlement profile according to its depth ratio  $C/D$  and volume loss  $VL\%$ .

### 6.5.2 Method 2 – Partially Merged Profiles

A similar procedure is followed for the analysis of the ‘method 2’ partially merged profile results. Figure 6-23 once again shows that  $i_x/D$  is linearly related to  $H/D$ , as per the O’Reilly and New relationship equation (eq. 2.8). The  $k$  range is approximately 0.3 - 0.7. However, this relationship is not distinguished by strength ratio ( $\gamma D/s_u$ ), as there is no trend. Therefore, the variation is caused by  $S/D$  and/or volume loss.



**Figure 6-23  $i_x/D$  vs  $H/D$  with varying  $\gamma D/s_u$  for all method 2 data (All  $S/D$ )**

The two graphs, shown in figures 6-24 and 6-25 show  $i_x/D$  and volume loss for various  $S/D$ . The first is for  $C/D=1$ , and the other is for  $C/D=5$ . The graphs display all the data ignoring strength ratios, as per the conclusions of figure 6-23. In both figures, the data forms a line regardless of  $S/D$ . Thus, it is concluded that the spacing ratio appears to make little difference to the volume loss- $i_x/D$  relationship. This point is reinforced by figure 6-26, which shows  $S/D$  against  $i_x/D$  with varying  $C/D$ . The data is very spread, and because of conclusions from previous figures, the observable trends can be attributed to  $C/D$  and volume loss.

With the conclusion that volume loss and  $C/D$  are the dominant factors in affecting  $i_x/D$ , figure 6-27 presents these variables together and disregards the unimportant variables ( $S/D$  and  $\gamma D/s_u$ ). This chart shows a convincing  $i_x/D$ -volume loss trend for each  $C/D$ . This is then used as the basis for the final chart. A *MATLAB* surface fit is completed, as shown in figure 10-5 appendix 1 with an  $r^2=0.95$ . Using this surface equation, a design chart is produced in figure 6-28, which can estimate an  $i_x/D$  value for any twin tunnel settlement situation falling in the 'method 2' section, based on  $C/D$  and volume loss.

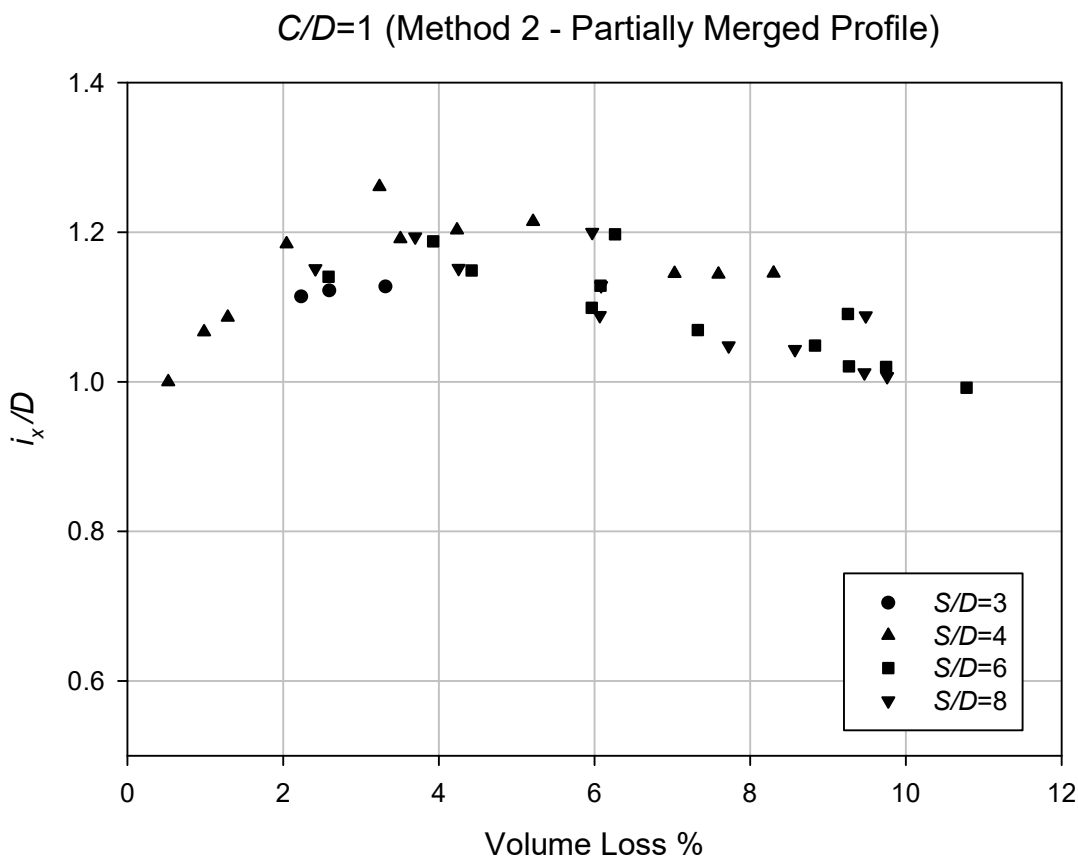


**Figure 6-24  $i_x/D$  vs volume loss % with varying  $S/D$  for  $C/D=1$  method 2 data**

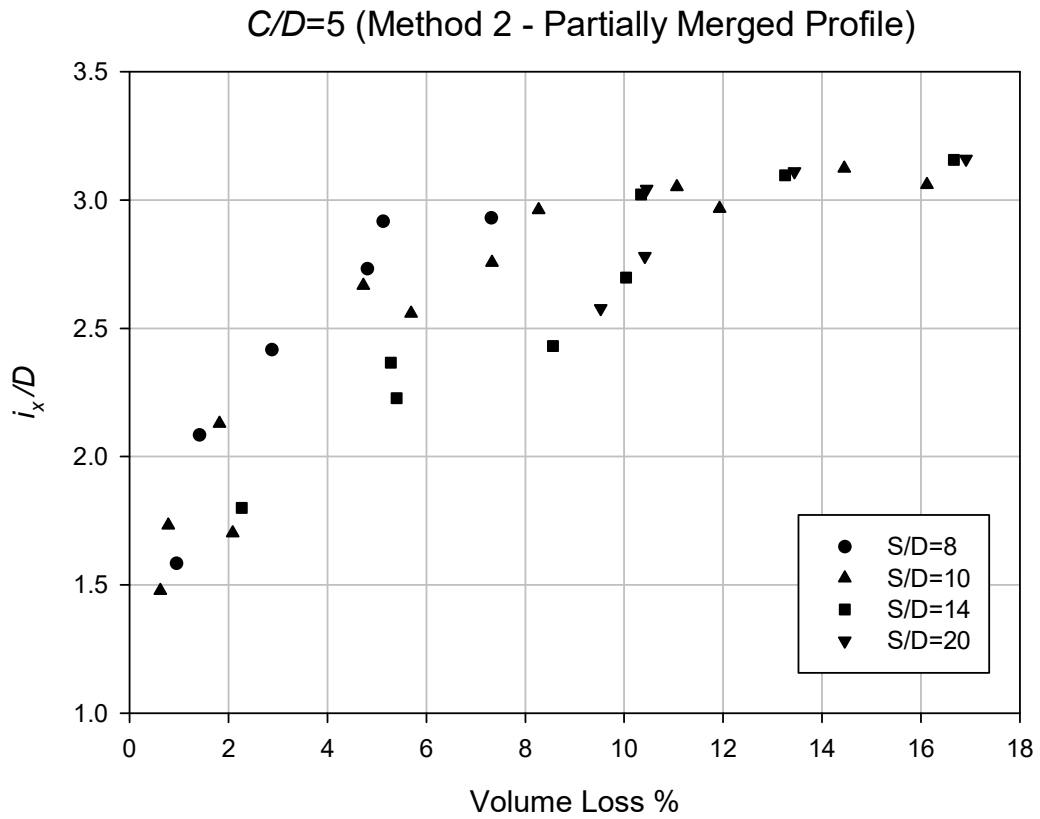


Figure 6-25  $i_x/D$  vs volume loss % with varying  $S/D$  for  $C/D=5$  method 2 data

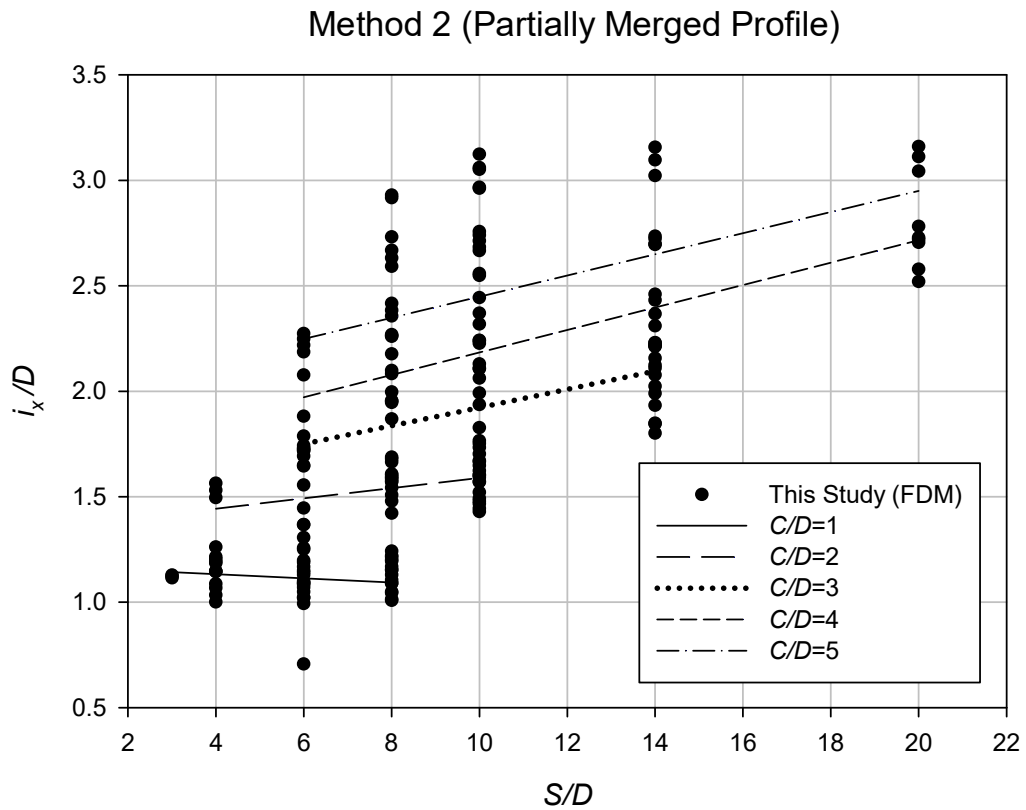


Figure 6-26  $i_x/D$  vs  $S/D$  with varying  $C/D$  for all method 2 data

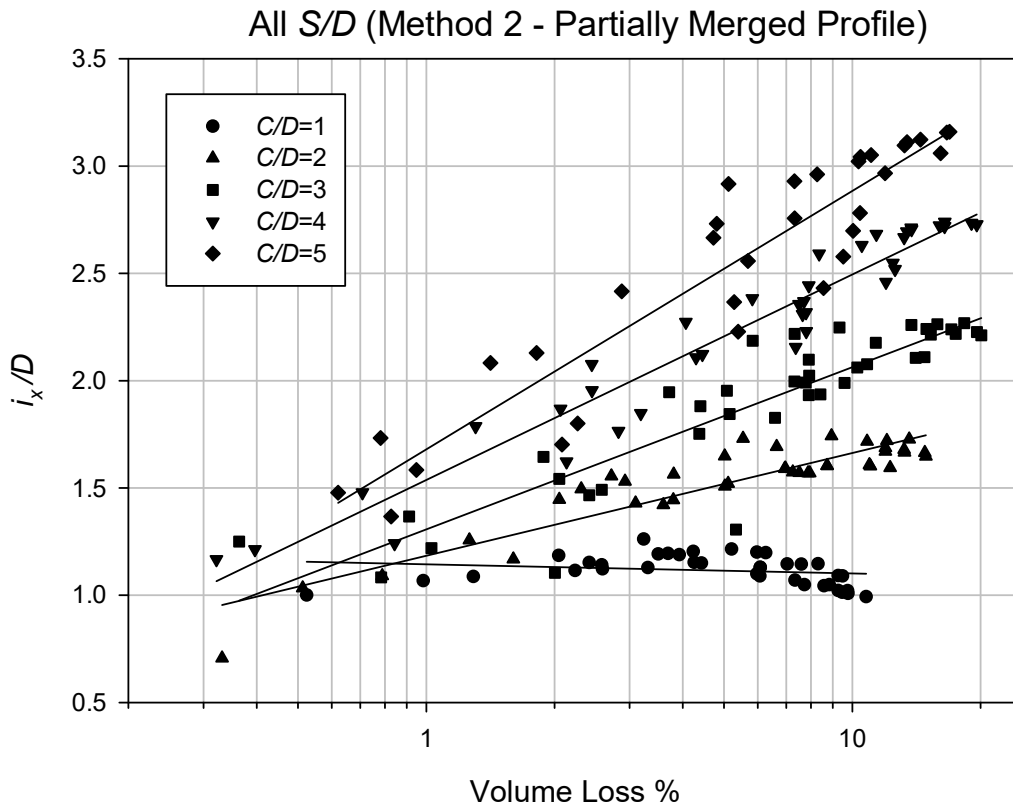


Figure 6-27  $i_x/D$  vs volume loss % with varying  $C/D$  for all method 2 data (All  $S/D$ )

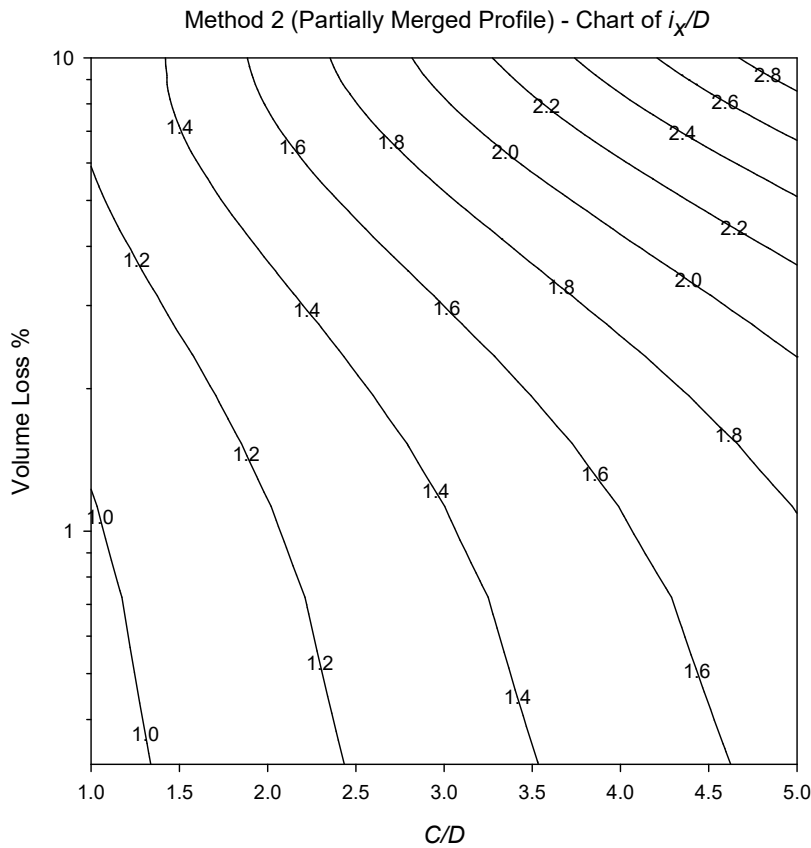


Figure 6-28 Design chart for  $i_x/D$  against VL % with varying  $C/D$  for all method 2 data (All  $S/D$ )

### 6.5.3 Method 3 – Separate Profiles

The settlement of twin tunnels in this category can simply be analysed using two single tunnels as in chapter 4. As discussed in section 6.2, the two tunnels will be far enough apart that the impact they have on each other will be negligible.

### 6.5.4 Practical Example

The following example is intended to demonstrate how these results could be useful.

#### **Prediction of Settlement of Twin Tunnels**

A pair of 5m tunnels are to be constructed with a cover depth of 20m. They are to be bored simultaneously at a centre-to-centre spacing of 20m. After some testing, the soil is found to have a unit weight of 18 kN/m<sup>3</sup>, and an undrained shear strength of 27 kPa. The constructors have been set and agreed to a volume loss limit of 2% per tunnel. Using these,  $C/D = 4$ ,  $S/D = 4$ , and  $\gamma D/s_u = 3.33$ .

The challenge is to generate a prediction of the equation which could be used to estimate the resultant settlement profile. Using figure 6-7, it can be seen that this situation will require analysis using ‘Method 1 – Fully Merged Profiles’, and the standard single Gaussian equation. Then from figure 6-22, the  $i_x/D$  value is found to be approximately 1.6, and then  $i_x$  is 8m. A volume loss of 2% for each tunnel then means a total contraction area of 0.79 m<sup>2</sup>. Using equation 2.4,  $S_{max}$  can be calculated by rearranging volume loss and  $i_x$ , it is found to be 0.039m.

Note this equation 2.4 is an approximate integral of the single Gaussian equation, and will not be compatible with method 2 calculations. Estimating  $S_{max}$  based on volume loss and  $i_x$  for method 2 cases is more complicated and requires further investigation, which is an area for future work to improve the usefulness of these results.

Equation 6.1 can now be used to generate an equation for the settlement profile. This is given in equation 6.4.

$$S_x = 0.039e^{-\frac{x^2}{2 \times 8^2}} \quad (6.5)$$

## 6.6 Conclusion

A numerical procedure has been developed to simulate twin circular tunnels and the relaxation of the soil that occurs during construction. This procedure is able to automatically generate the mesh based on a series of inputs and output the surface settlement data for each relaxation step. Using outputs from the model, the point of collapse step can be determined. The settlement data at the collapse and three previous pre-collapse stages are exported to *MATLAB* where either a standard Gaussian or modified twin-Gaussian curve is fitted. This is due to a merging effect when the tunnels are relatively close. If they are close enough, the profiles completely merge and can be treated as a single tunnel. As the spacing continues to be increased, the profiles will start to diverge, and a superimposed twin Gaussian equation must be used. Charts have been provided (figure 6-4 to 6-8) which indicate which method is appropriate.

Following this approach allows reliable estimation of  $i_x$  for all cases. A parametric study was undertaken in which a series of commonly used dimensionless ratios were controlled including  $C/D$ ,  $\gamma D/s_u$ , and  $S/D$ . The volume loss ( $V_L\%$ ) was calculated at the analysed stages by integrating the settlement data. A brief description of the effect of these parameters has been given. It is concluded that the  $i_x$  parameter always changes with volume loss, but that this rate of change becomes increasingly positive with increasing  $C/D$ . The spacing ratio ( $S/D$ ) and the soil strength ratio ( $\gamma D/s_u$ ) have little impact on  $i_x$ .

Further investigation of this  $i_x$  parameter and the variations being caused by volume loss led to 3D regressions being conducted with respect to  $C/D$  and the volume loss for both the collapse and pre-collapse conditions. From this, design contour charts are presented which can be used for prediction purposes. The great similarity between the *FLAC* modelled settlement and the Gaussian and twin-Gaussian curves indicate that this empirical method is still suitable to be applied in the industry as a preliminary tool. It is concluded that this is a reliable method for preliminary analysis and prediction.

# 7 TWIN TUNNEL STABILITY

## 7.1 Introduction

This chapter describes the verification and use of a numerical model for investigating twin circular tunnels in cohesive soils. The model aims to simulate the movement and relaxation of the soil around the shield and lining annulus that occurs due to the overcutting and grouting of the tunnel void by a tunnel-boring machine (TBM). To achieve this, the model uses a pressure relaxation technique that progressively reduces the tunnel support pressure from an initial condition until a point of failure is detected. At each of these relaxation steps, the stability number (equation 7.1) is calculated, and can be later analysed. This is done for a range of geometry and soil ratios that will cover most practical cases for soft cohesive soils.

In this study, both the point of collapse (PoC) and three stages before this point have been analysed. The stability numbers calculated at the determined PoC are compared to rigorous upper and lower bound solutions as well as previous physical modelling research. These can be useful as they provide a boundary for design purposes. The results of this study are quite positive, with the stability results from this study remaining within 5% of the upper and lower bound solutions. Design charts using dimensionless ratios have therefore been presented. The three pre-collapse stages are closer to a 'working condition'; results have been considered with volume loss that has been back calculated from surface settlement as stated in chapter 6.

## 7.2 Problem Definition

Managing the system stability during tunnel construction is essential. This is most often done by using the stability number ( $N$ ), as in equation (5.1). This formulation is an approach followed by the finite element limit analysis (FELA) studies of Wilson et al (2014), where  $\sigma_s$  is the surface surcharge pressure,  $\sigma_t$  is the internal tunnel pressure, and  $s_u$  is the undrained shear strength. Figure 7-1 also shows this problem definition. This stability number is a function of the depth ratio  $C/D$ , the soil shear-strength ratio  $\gamma D/s_u$ , and the spacing ratio  $S/D$ . It will be once again used in this study, in conjunction with the developed model.

$$N = \frac{\sigma_s - \sigma_t}{s_u} = f\left(\frac{C}{D}, \frac{\gamma D}{s_u}, \frac{S}{D}\right) \quad (7.1)$$

By formulating the equation to the problem in this way, it allows for the creation of practical stability charts, which are useful for design. These dimensionless ratios allow the results of this study to be used in scenarios that are physically different, but where the soil strength ratio, depth ratio, and spacing ratio still fall in the parametric domain. The parameters used in this study are  $\gamma D/s_u = 1 - 5$ ,  $C/D = 1 - 5$ , and  $S/D = 1.5 - 20$ . This is to cover most of the realistic values to give a comprehensive analysis, and to ensure that the design charts produced can be applicable to many different tunnel design and analysis problems.

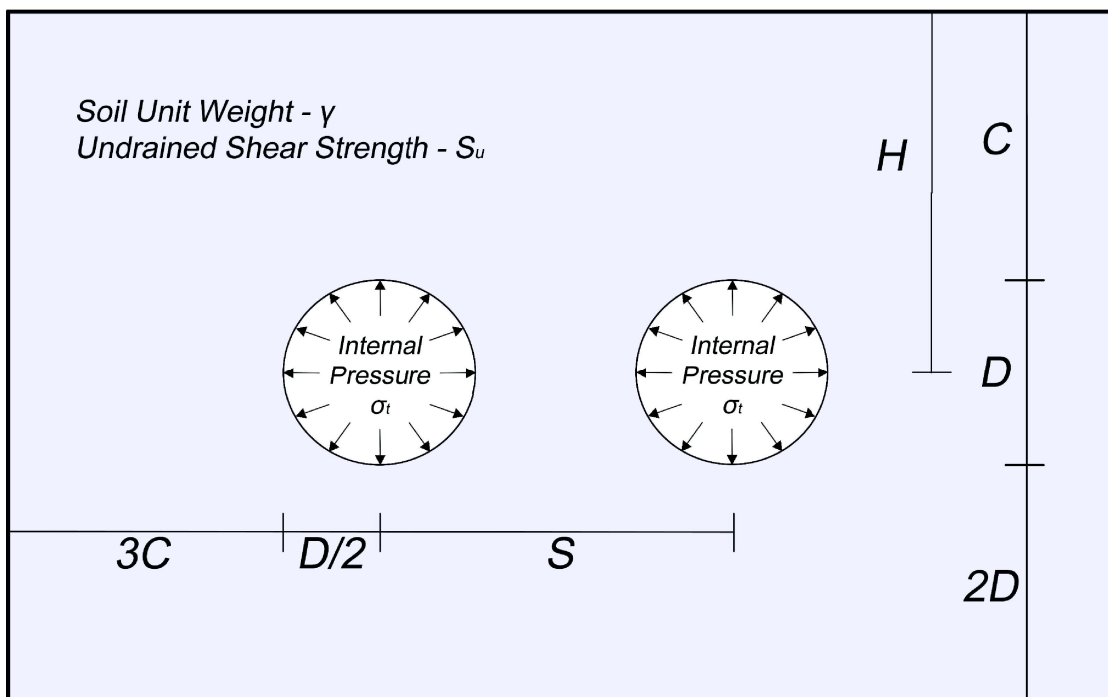


Figure 7-1 Typical schematic diagram of the problem



The internal pressure relaxation method will again be used, and it is important to note that the simulation is such that both tunnels are excavated and relaxed at the same time and rate respectively. By using this approach and a small relaxation interval (amount relaxed each step), the stability number (equation 7.1) that induces collapse can be calculated with reasonable accuracy. It should be noted that the pressure relaxation method would always slightly overestimate the stability number at collapse, as the internal pressure is reduced in discrete steps, not continuously. The internal pressure at the ‘collapse stage’ will have been relaxed slightly more than needed, unless the internal pressure at that stage coincides exactly with the actual collapse stability number. However, this problem is reduced significantly by reducing the size of the relaxation interval (reducing internal pressure by 1% each stage is far more accurate than 5% etc.).

### 7.3 Results – At Collapse

This section will discuss the stability numbers that were calculated at the collapse stage, as identified as discussed in section 3.5. Figures 7-2 and 7-3 show results from this study compared to the upper and lower bounds calculated using the rigorous FELA approach of Wilson et al (2014). Figure 7-2 is for  $\gamma D/s_u=2$ , and it is observed that the comparison is quite positive. It can be seen that when the tunnels are close the required pressure ratio is high (i.e. more negative, indicating a larger  $\sigma_t$ ), and eventually plateaus as the spacing increases. On this chart, the single tunnel critical stability number has also been indicated, i.e. the white circular symbol at  $S/D=0$ . Then it seems that the plateauing of the twin tunnel critical stability number approximately coincides with these points.

So, it can be concluded that when the tunnels are very close, i.e. with an  $S/D$  between 1 and 0 (where at  $S/D=1$  the tunnels would be exactly adjacent, and at  $S/D<1$  the tunnels would be hypothetically intersecting), the mechanics of the ground movement would be similar to that of a single tunnel. That is, with the ground moving to a single point, and with a collapse inducing pressure ratio of close to that of a single tunnel. When the tunnel spacing ratio is slightly bigger, the interaction effects become more substantial, and the collapse will occur at a greater  $N$  (more negative). If the spacing ratio continues to increase, then the interaction will be reduced again, and the two tunnels will behave as individual tunnels, and thus the similar collapse point as in the single tunnel study.

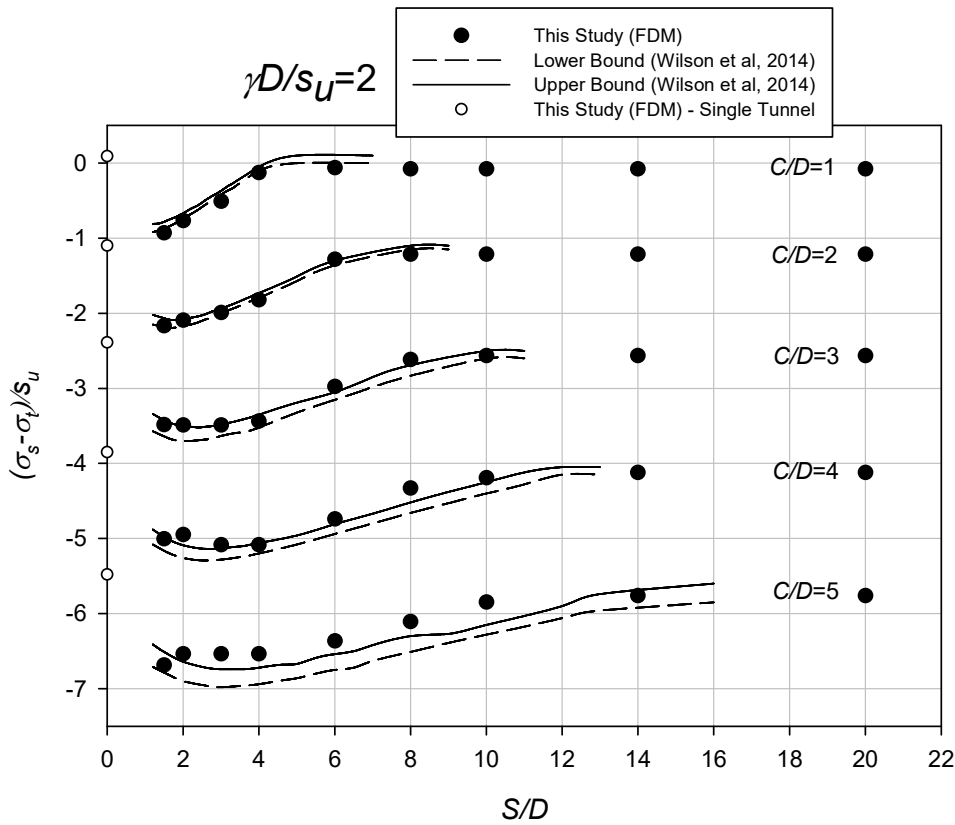


Figure 7-2 Comparison of results with Wilson et al (2014) for  $\gamma D / s_u = 2$

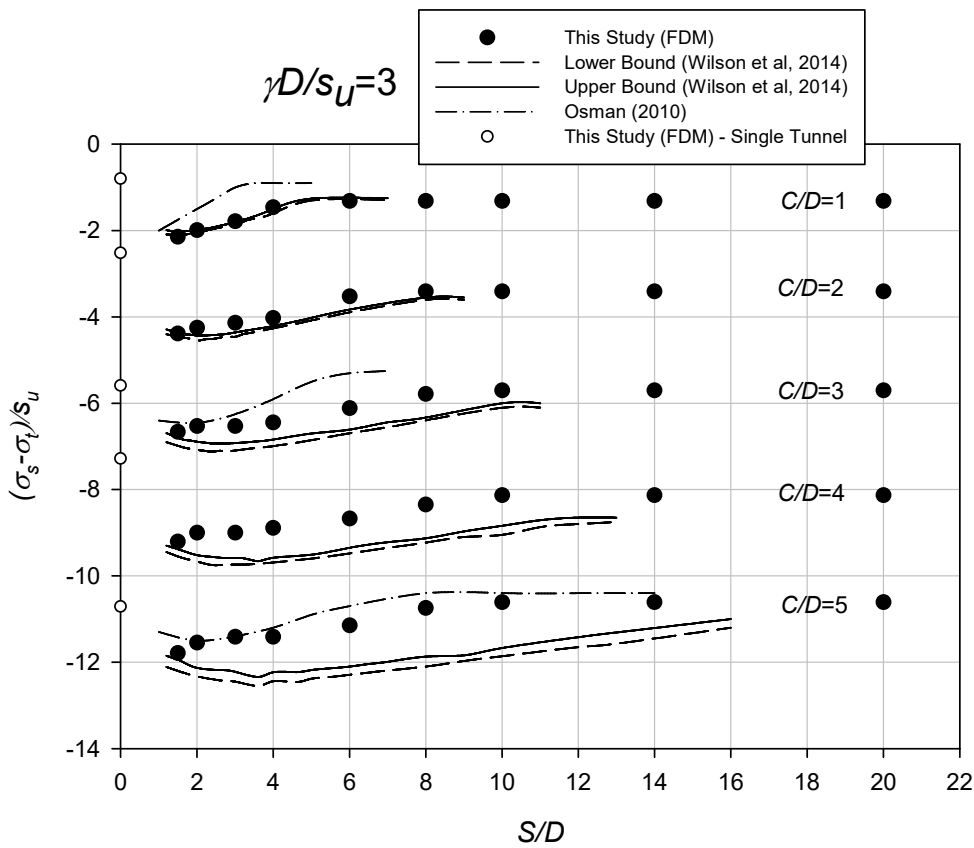
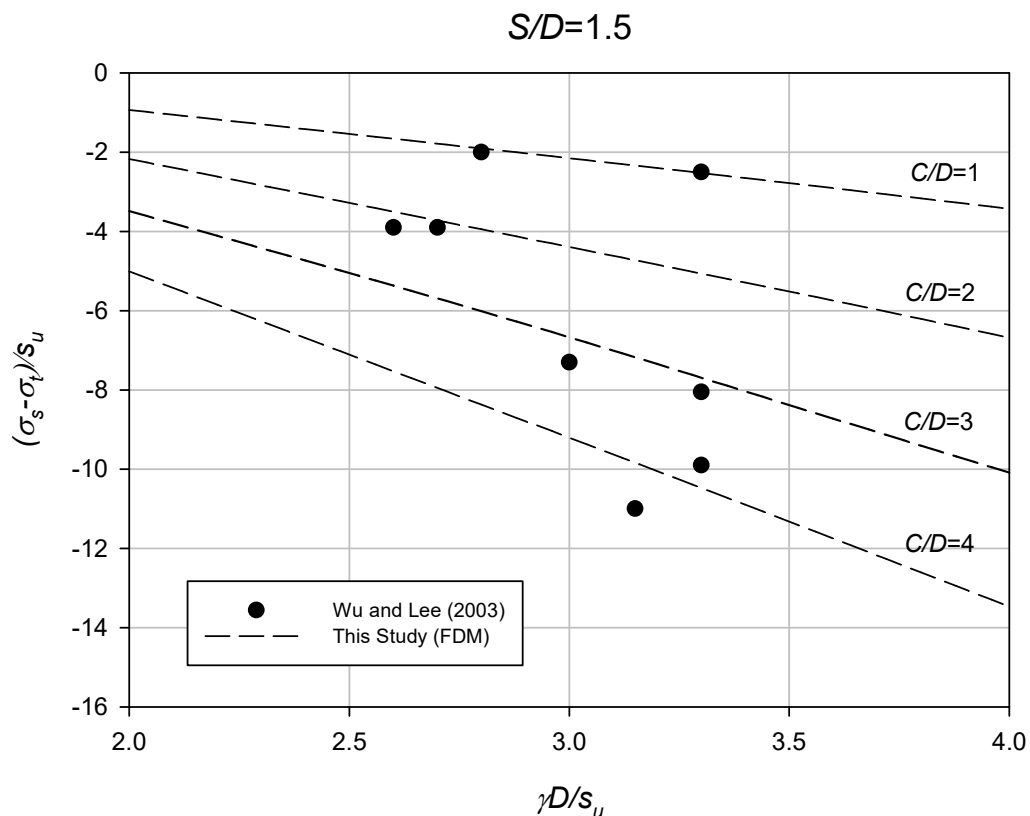


Figure 7-3 Comparison of results with Wilson et al (2014) and Osman (2010) for  $\gamma D / s_u = 3$

Figure 7-3 is a similar chart, however it is for  $\gamma D/s_u=3$ . This allows a comparison with the experimental results of Osman (2010), who only conducted a study using this clay. The FELA upper and lower bounds are also included in this chart. Once again, the single tunnel critical pressure ratio is a white dot, and similar observations can be made as in figure 7-2. A key point to observe in figure 7-3 is the comparisons. It can be seen that with the  $C/D=1$  results, the FELA bounds (Wilson et al 2014) correspond very well, but in the deeper cases (higher  $C/D$ ), they and the results of this study diverge. At the same time, the results of Osman (2010) appear to do the reverse – they do not match well in the shallow cases, but match very well in the deep cases. This is unusual and further investigations are required to clarify this inconsistency.

Figure 7-4 is also a comparison chart. It shows the results from this study for  $S/D=1.5$  compared with the experimental results of Wu and Lee (2003), shown as dots in the chart. There are two dots for each  $C/D$ , and they correspond approximately to the dashed line which represents the numerical results from this study. As the comparisons are quite positive, design charts have been produced in figures 7-5 to 7-9 for  $C/D = 1 - 5$  respectively.



**Figure 7-4 Comparison of results with Wu and Lee (2003) for  $S/D=1.5$**

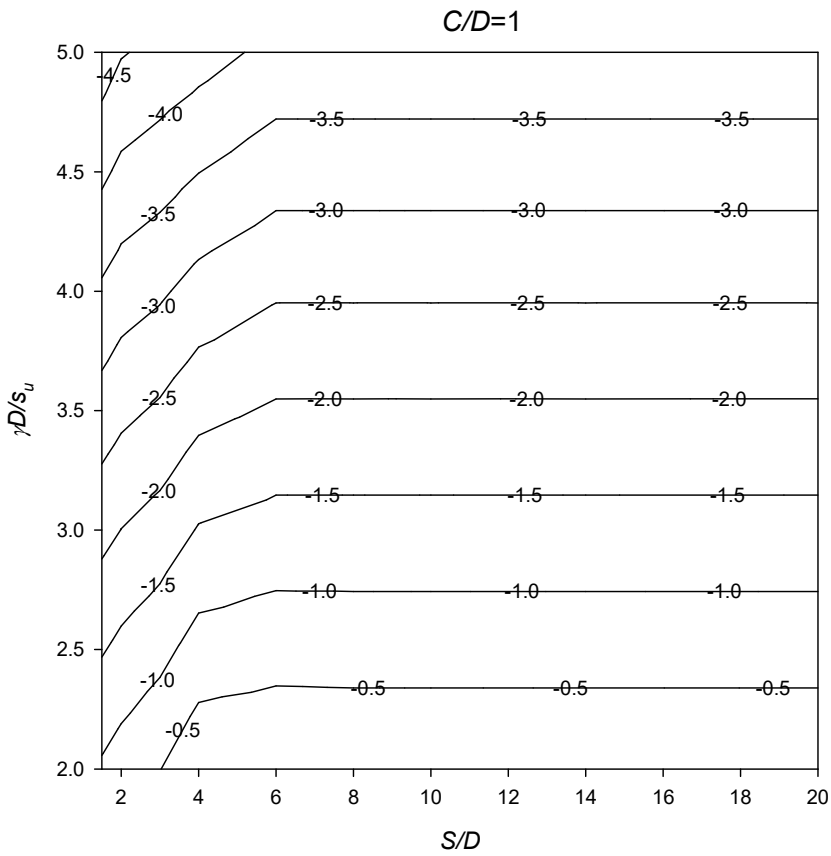


Figure 7-5 Design Chart for the critical stability number  $N$  for  $C/D=1$

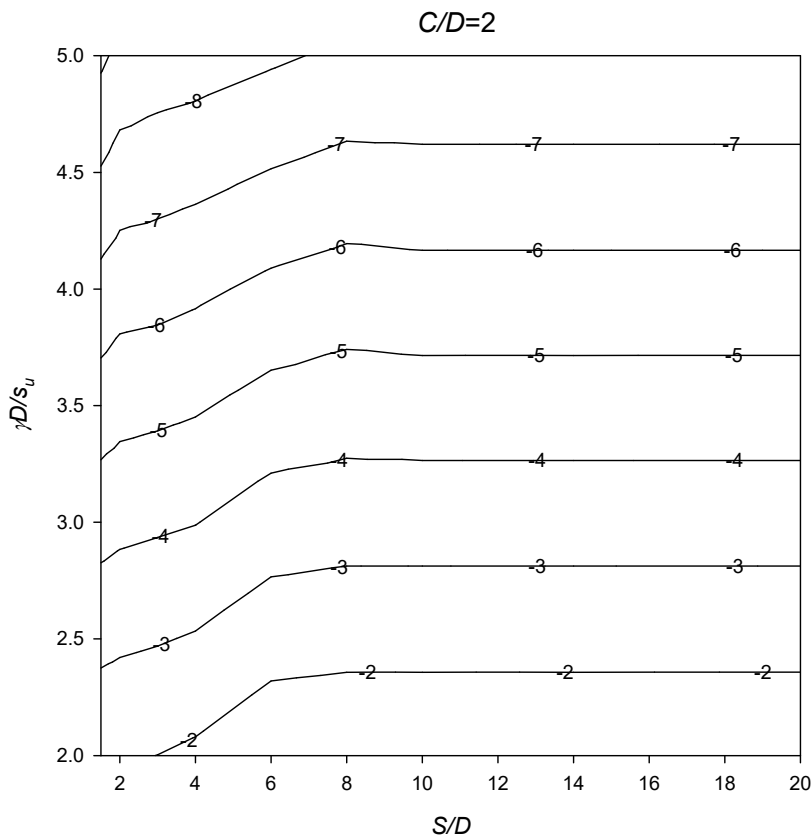
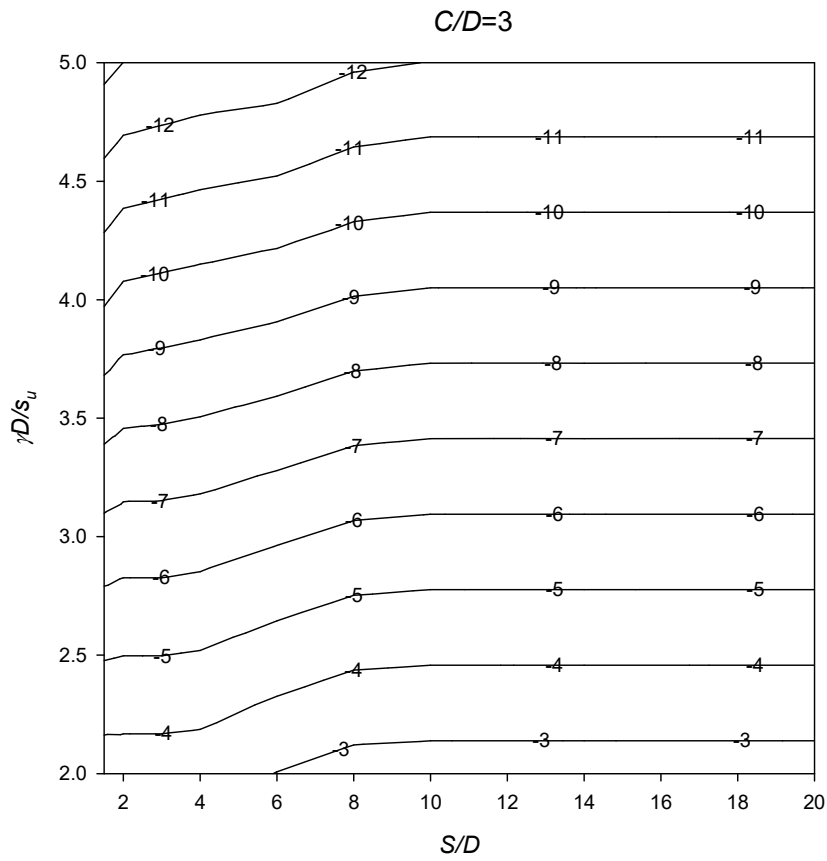
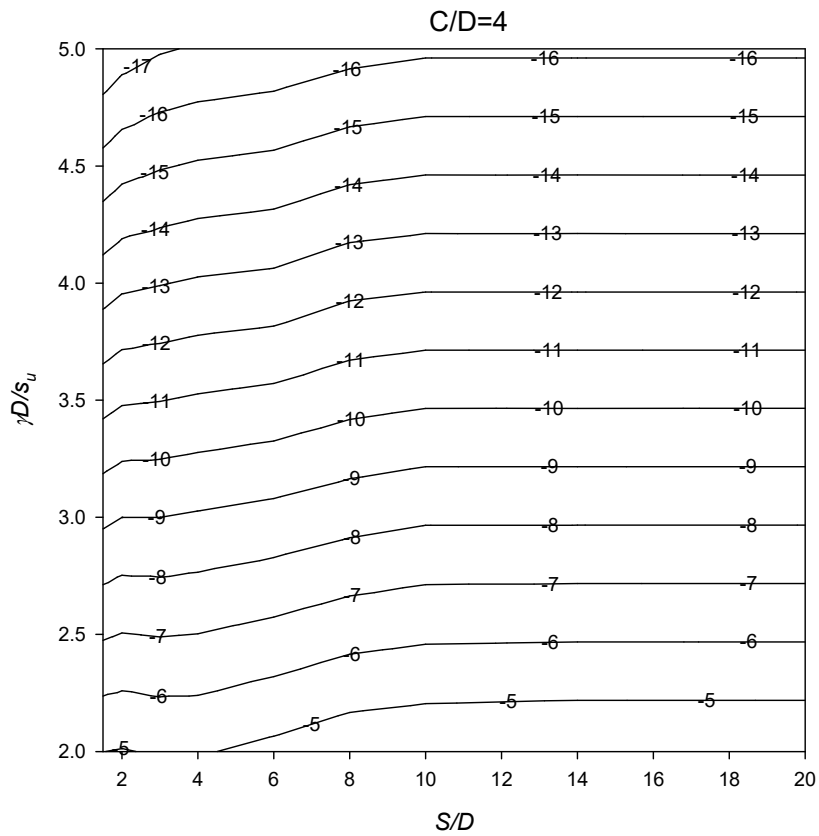


Figure 7-6 Design Chart for the critical stability number  $N$  for  $C/D=2$



**Figure 7-7 Design Chart for the critical stability number  $N$  for  $C/D=3$**



**Figure 7-8 Design Chart for the critical stability number  $N$  for  $C/D=4$**

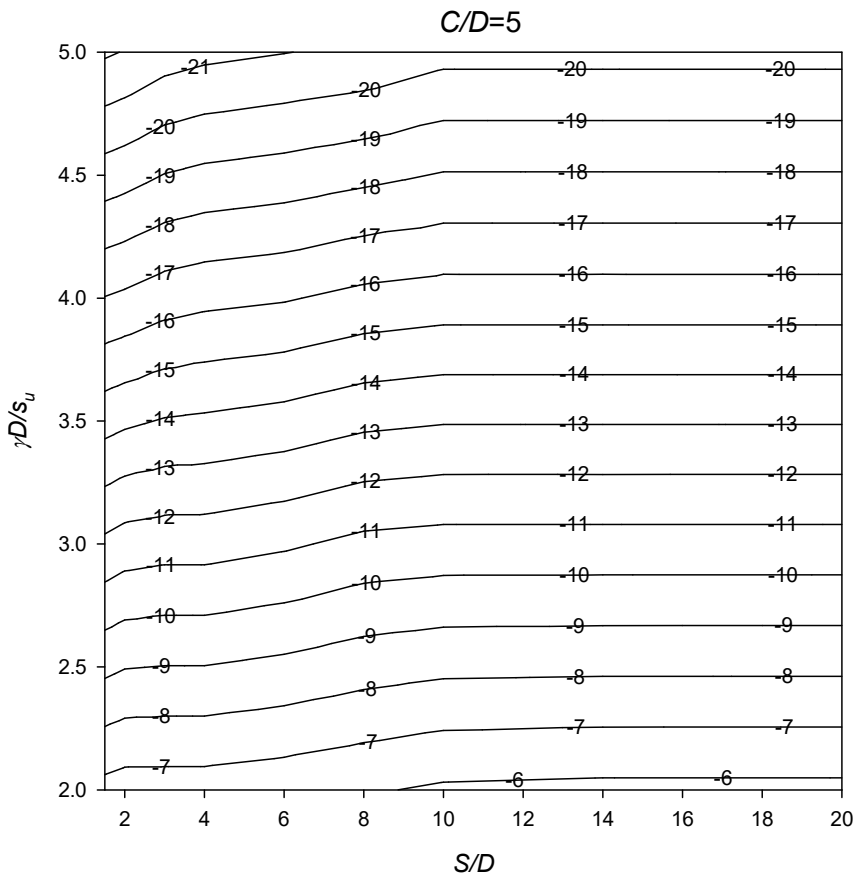


Figure 7-9 Design Chart for the critical stability number  $N$  for  $C/D=5$

### 7.3.1 Practical Examples

An example using these results will be given to demonstrate how these results can be used.

#### Determine critical internal pressure

Two side-by-side tunnels are planned to be 40 metres apart (centre-to-centre), and are assumed to be bored simultaneously. The tunnel boring machines have a diameter ( $D$ ) of 6.0 m and are buried at a depth of 18 m ( $C$ ) in an undrained clayey material with properties  $S_u = 27\text{ kPa}$ ,  $\phi_u = 0^\circ$  and  $\gamma = 18\text{ kN/m}^3$ . The site is assumed to be a Greenfield so no surface pressure is assumed ( $\sigma_s = 0$ ). The following procedures can be used to determine the absolute minimum tunnel internal pressure ( $\sigma_t$ ) to prevent collapse.

Calculate dimensionless ratios -  $C/D = 3$ ,  $\gamma D/S_u = 4$ ,  $S/D = 6.67$ . With figure 7-7, it is found that the critical stability number for this scenario is approximately -9.2. By rearranging equation 7.1, the minimum internal tunnel pressure to avoid collapse will be 248.4 kPa.

### 7.3.2 Failure Mechanism

Shear strain rate (*SSR*) plots can be useful to give an indication of failure mechanism. Figures 7-10 to 7-17 show *SSR* plots for  $C/D = 1$  and 3,  $\gamma D/S_u = 2$ , and 5, and  $S/D = 2$  and 8, as labelled. For all  $C/D$ , the failure zone gets wider for decreasing soil strength. Floor heaving is most severe for the deep, soft cases, but reduces for shallow and strong cases. When the tunnels are closer, there is significant interaction between the tunnels – an *SSR* band can be seen connecting the two tunnels. However, when the spacing ratio is increased this interaction reduces, and the plots resemble those of a single tunnel, as in section 5.3.2.

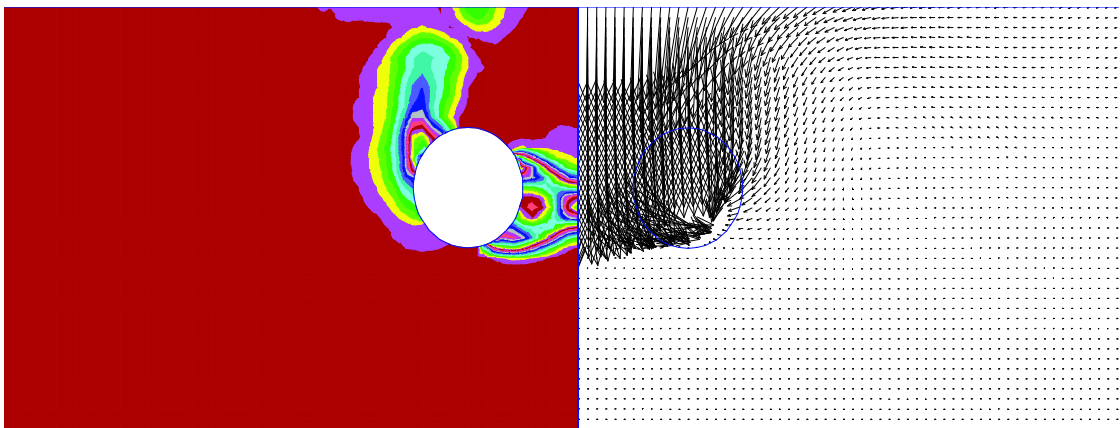


Figure 7-10 *SSR* plot (left) and velocity vectors (right) at the PoC ( $C/D=1$ ,  $\gamma D/s_u=2$ ,  $S/D=2$ )

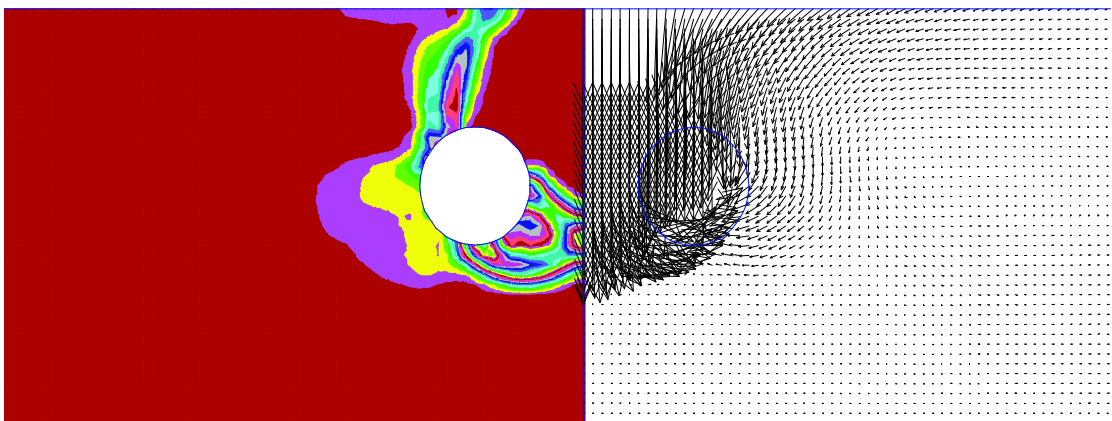


Figure 7-11 *SSR* plot (left) and velocity vectors (right) at the PoC ( $C/D=1$ ,  $\gamma D/s_u=5$ ,  $S/D=2$ )

Some of the *SSR* plots show some discontinuous contours, i.e. ‘spikes’, figure 7-15 and 7-16 in particular. This is due to the model not being fully converged. As discussed in section 3.5, the model has been run allowing 5000 steps per relaxation stage. These results indicate that more steps may be required per stage in order to reach better solution convergence.

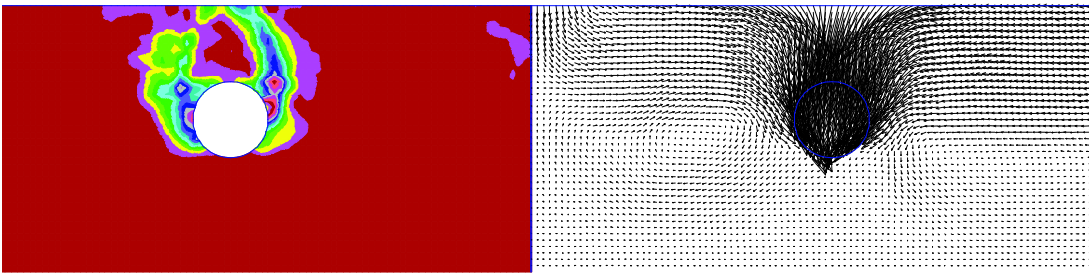


Figure 7-12 SSR plot (left) and velocity vectors (right) at the PoC ( $C/D=1$ ,  $\gamma D/s_u=2$ ,  $S/D=8$ )

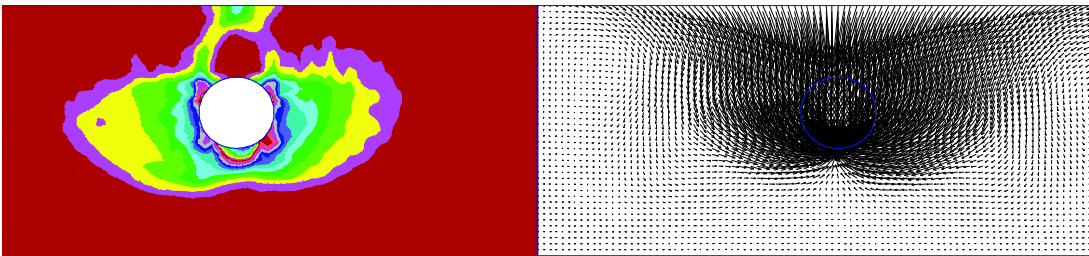


Figure 7-13 SSR plot (left) and velocity vectors (right) at the PoC ( $C/D=1$ ,  $\gamma D/s_u=5$ ,  $S/D=8$ )

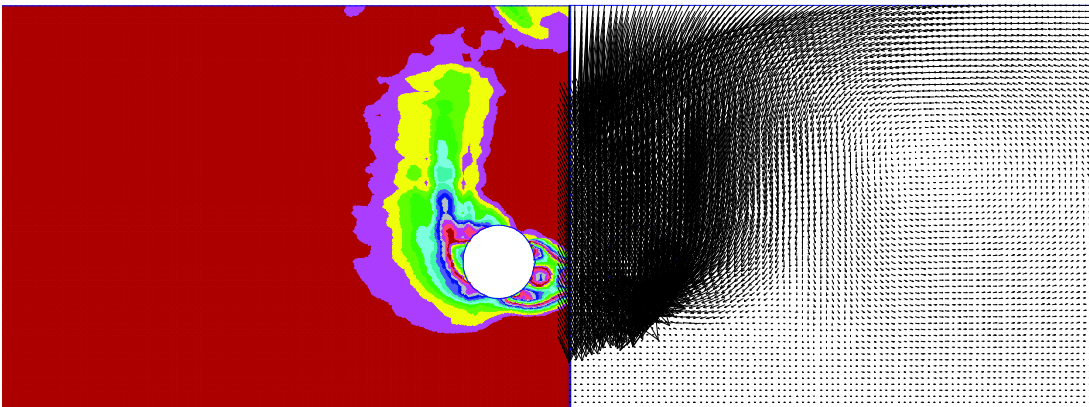


Figure 7-14 SSR plot (left) and velocity vectors (right) at the PoC ( $C/D=3$ ,  $\gamma D/s_u=2$ ,  $S/D=2$ )

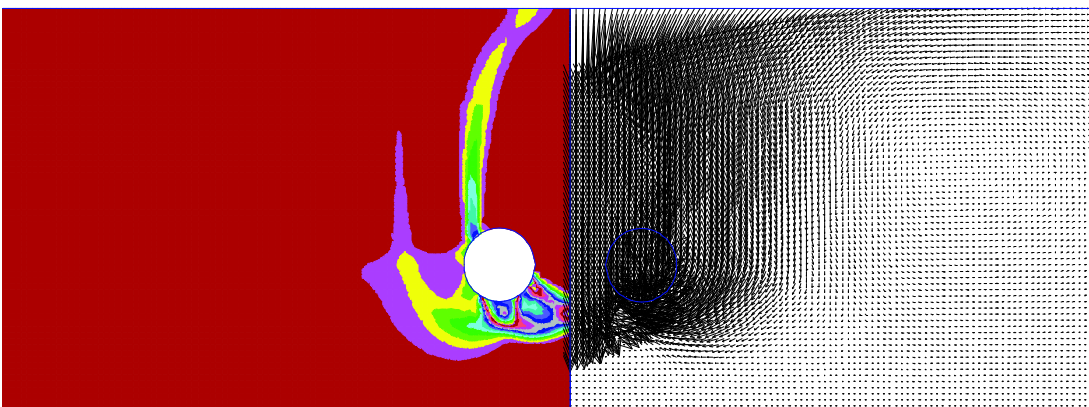


Figure 7-15 SSR plot (left) and velocity vectors (right) at the PoC ( $C/D=3$ ,  $\gamma D/s_u=5$ ,  $S/D=2$ )



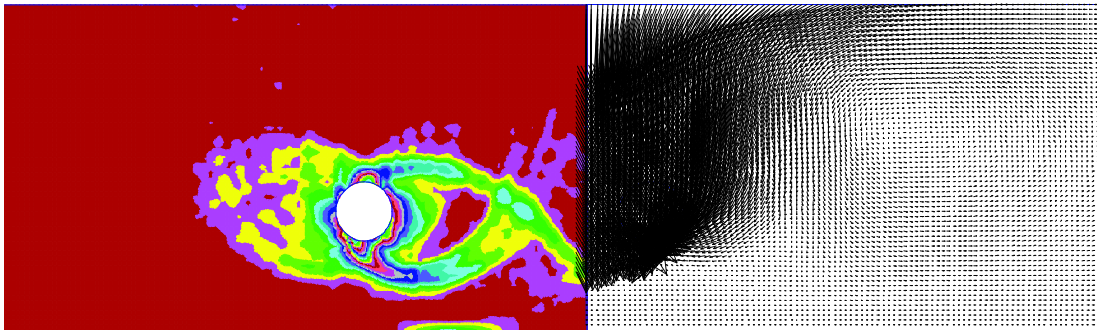


Figure 7-16 SSR plot (left) and velocity vectors (right) at the PoC ( $C/D=3$ ,  $\gamma D/s_u=2$ ,  $S/D=8$ )

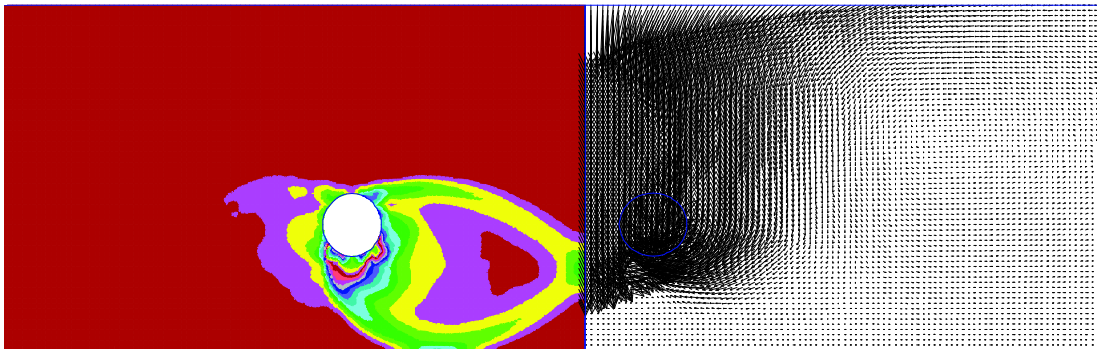


Figure 7-17 SSR plot (left) and velocity vectors (right) at the PoC ( $C/D=3$ ,  $\gamma D/s_u=5$ ,  $S/D=8$ )

## 7.4 Results – Pre-Collapse

This section will discuss the volume loss and stability numbers that were calculated at three stages prior to the collapse stage. In this case, the three are the ones immediately before collapse. For example, if the collapse stage was 53%, then the stages being analysed in this section would be 50, 51, and 52% relaxation. The stability number is calculated at every stage of relaxation, and the volume loss is back calculated using the settlement data as from chapter 6.

Figures 7-18 and 7-19 show stability number ( $N$ ) against volume loss for varying strength ratio ( $\gamma D/s_u$ ). They are for  $C/D=1$  and  $C/D=5$  respectively, and both include data for all  $S/D$ . This represents the conclusion that the spacing ratio seems to make little difference to the volume loss-stability number relationship. The effect of soil strength ratio is significant here though; the weaker clays (higher  $\gamma D/s_u$ ) require greater internal pressure (where  $N$  is therefore more negative) to maintain the same level of volume loss as stronger clay. This seems a reasonable conclusion.

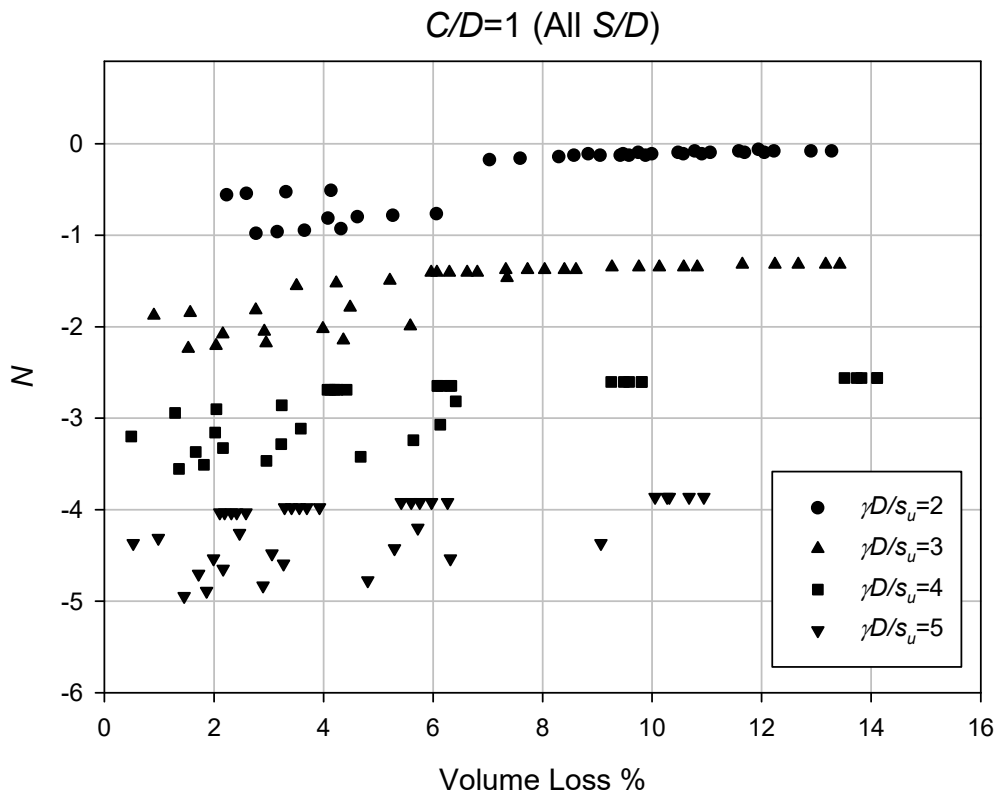


Figure 7-18 Chart showing N with respect to volume loss % for various  $\gamma D/ s_u$  ( $C/D=1$ , All  $S/D$ )

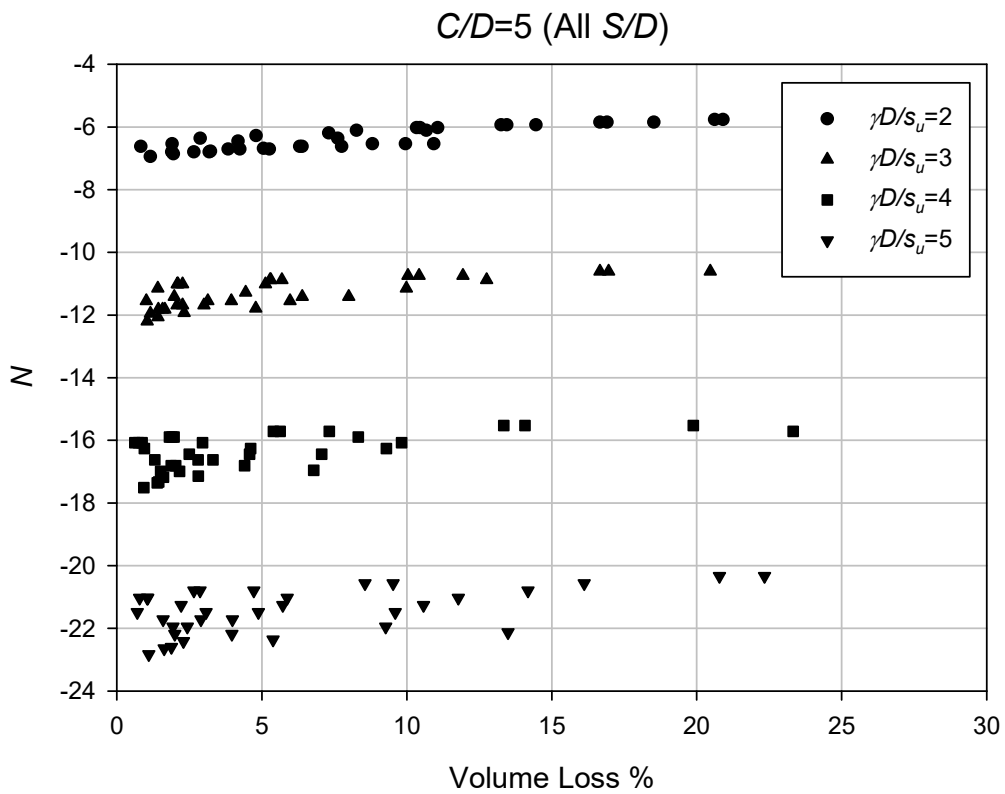
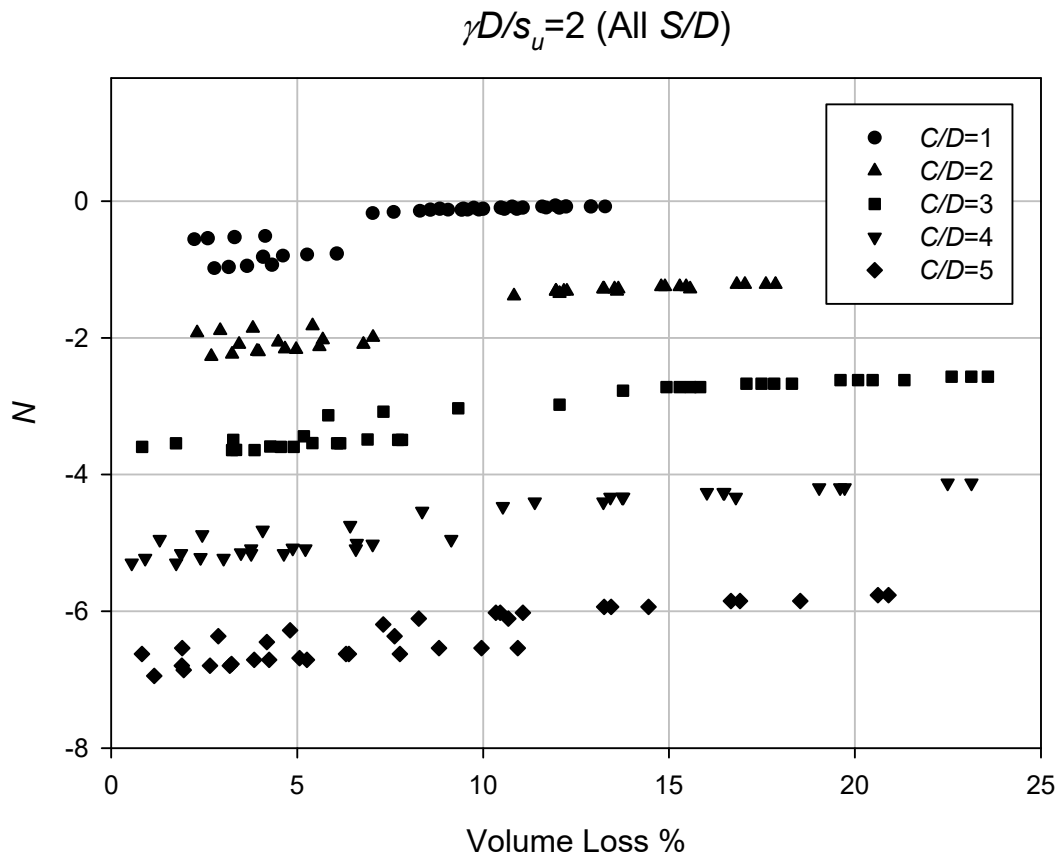


Figure 7-19 Chart showing N with respect to volume loss % for various  $\gamma D/ s_u$  ( $C/D=5$ , All  $S/D$ )



**Figure 7-20** Chart showing  $N$  with respect to volume loss % for various  $C/D$  ( $\gamma D/s_u=2$ , All  $S/D$ )

It also seems that there is greater scatter in the data points at low volume loss %, which in some ways reflects the uncertainty in choosing an internal pressure for low volume loss. Comparing figures 7-18 and 7-19 ( $C/D=1$  vs  $C/D=5$ ), the deeper case requires greater  $N$ , which may be counter-intuitive to some, as it seems opposite to the widely known fact that stability is easier to attain at greater depth. However, it seems that with pure clay this may not be true. Figure 7-20 is a similar chart that has the  $C/D$  and  $\gamma D/s_u$  positions reversed (for  $\gamma D/s_u=2$ , with varying  $C/D$ ). This demonstrates in a way, that the  $N$ -volume loss relationship is equally dependant on depth ratio and soil strength ratio. In any case, the conclusions for practical purposes are that  $C/D$ ,  $\gamma D/s_u$ , and volume loss are significantly related to pressure ratio ( $N$ ), while  $S/D$  seems to make little difference.

Using this data, and these conclusions from analysis, contour charts of  $N$  have been produced in figures 7-21 to 7-25 based on a polynomial surface fitting in *MATLAB*. A typical example of this is shown in figure 10-6 in appendix 1. These can be used to relate volume loss and  $N$  for a twin tunnel scenario for any given  $C/D$  and  $\gamma D/s_u$ .

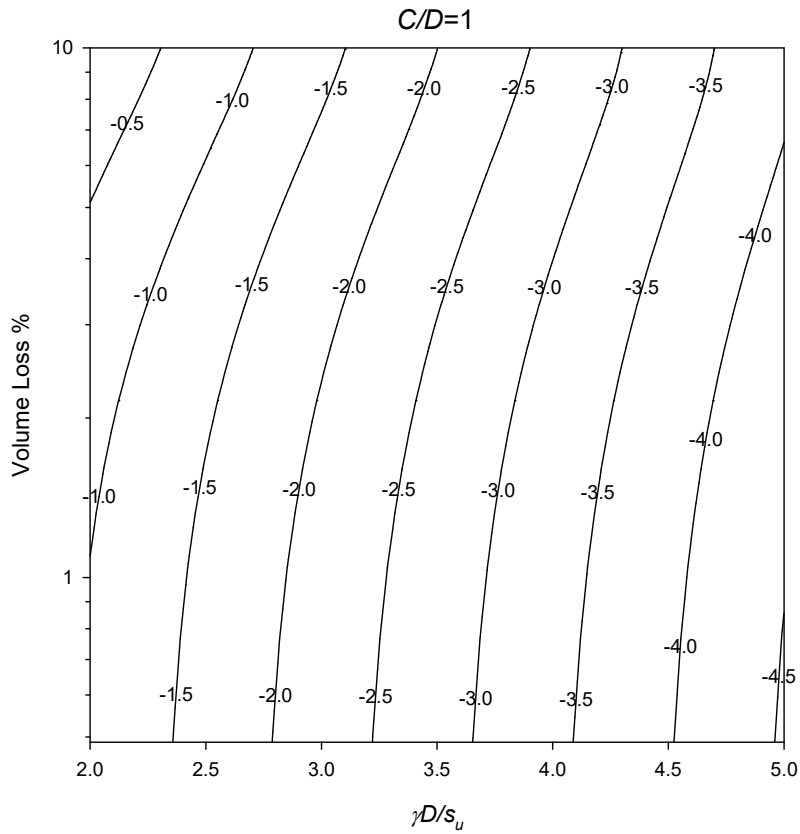


Figure 7-21 Design chart for  $N$  with respect to volume loss % and  $\gamma D / s_u$  ( $C/D=1$ )

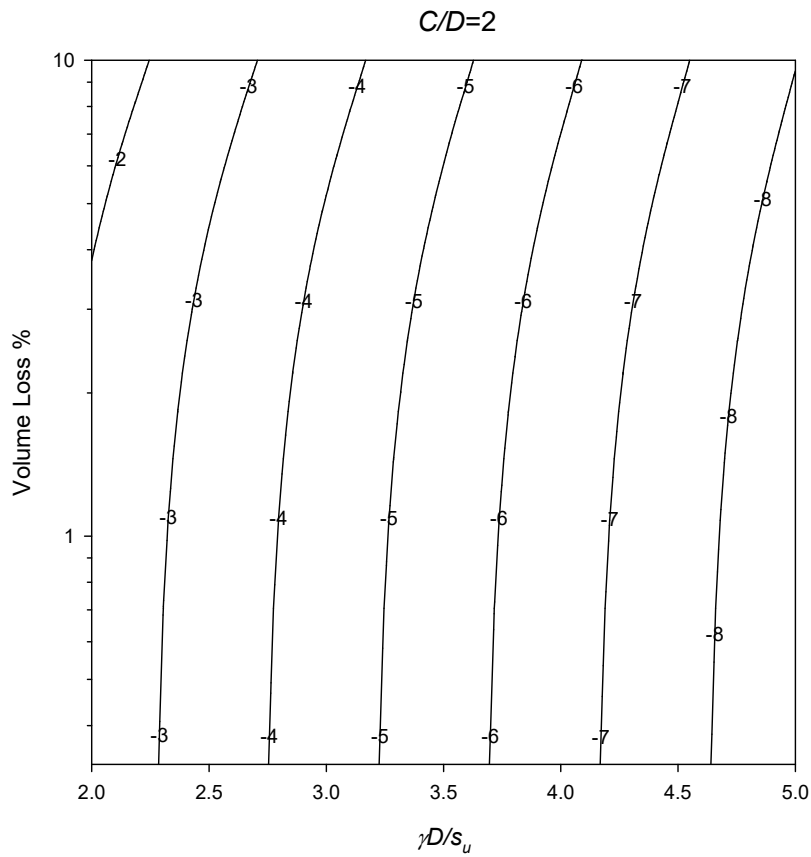


Figure 7-22 Design chart for  $N$  with respect to volume loss % and  $\gamma D / s_u$  ( $C/D=2$ )

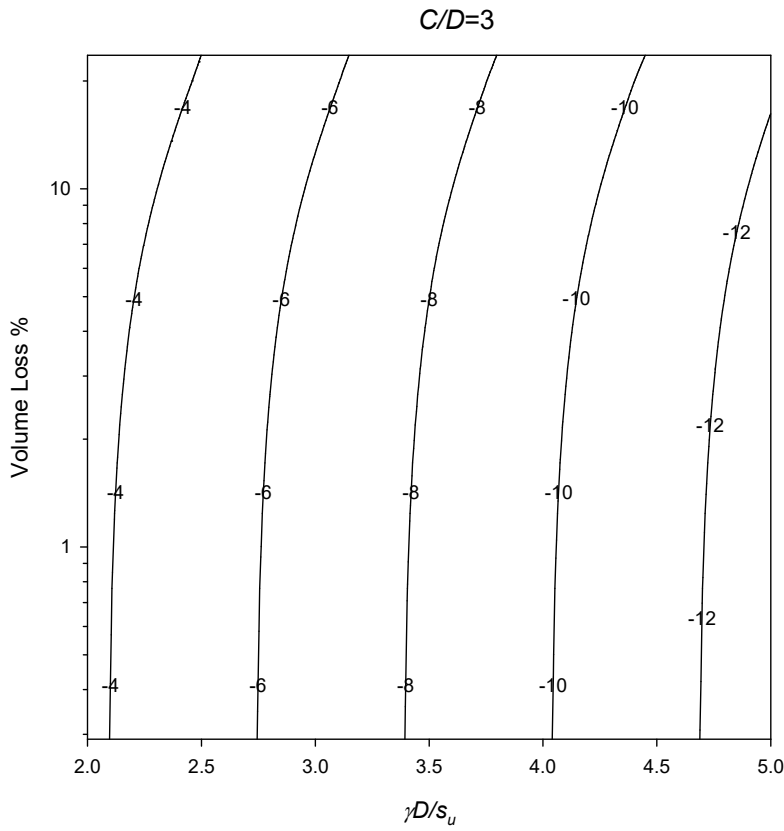


Figure 7-23 Design chart for  $N$  with respect to volume loss % and  $\gamma D / s_u$  ( $C/D=3$ )

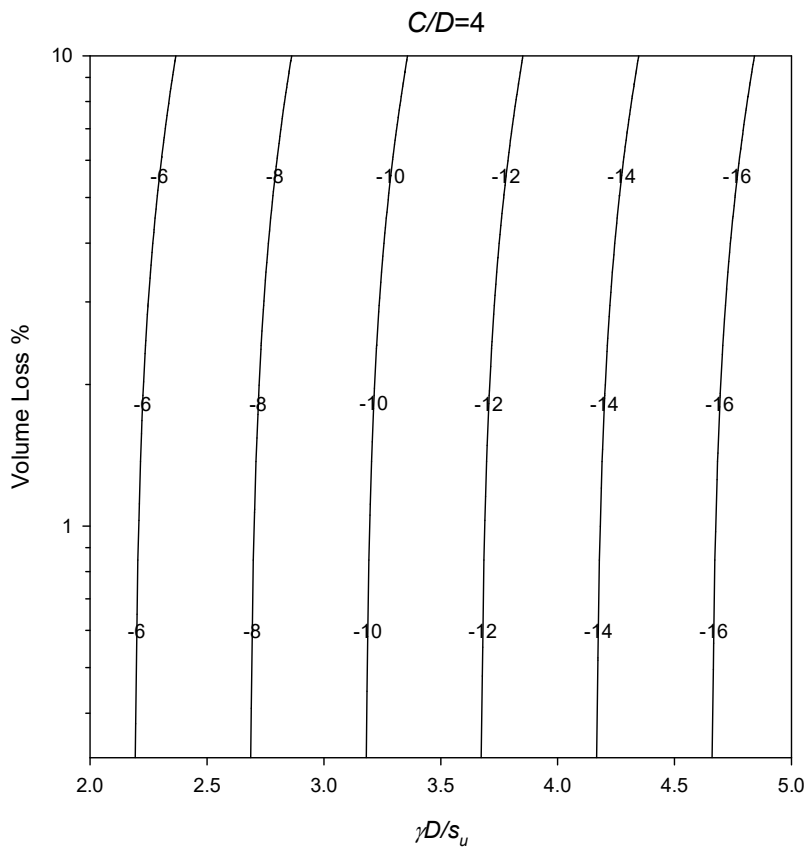


Figure 7-24 Design chart for  $N$  with respect to volume loss % and  $\gamma D / s_u$  ( $C/D=4$ )

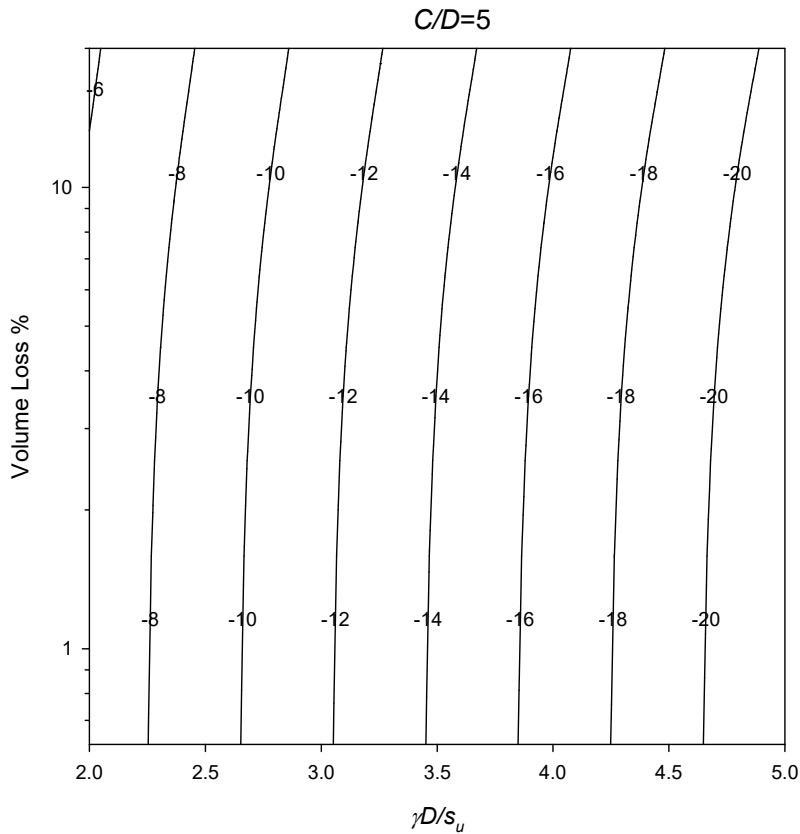


Figure 7-25 Design chart for  $N$  with respect to volume loss % and  $\gamma D / s_u$  ( $C/D=5$ )

### 7.4.1 Practical Examples

To demonstrate the potential usefulness of these charts, a practical example will be given.

#### Evaluating TBM operations in terms of ground movement

Two planned tunnels with centre-to-centre spacing of 60m are being constructed simultaneously have a diameter of 6m, and a cover depth of 18m. The soil is found to be clay with a unit weight is  $18 \text{ kN/m}^3$ , and an undrained shear strength of 27 kPa. Therefore, some of the dimensionless ratios can be calculated –  $C/D = 3$  and  $\gamma D / s_u = 4$ , and  $S/D = 6.67$ .

The question could then be – what pressure ratio ( $N$ ) is required to limit the volume loss of each tunnel to 2%? To answer this, figure 7-23 can be used. With this chart, it is found that a pressure ratio of approximately -9.5 will satisfy the conditions. Referring to equation 7.1, if the surcharge pressure ( $\sigma_s$ ) is zero (greenfield conditions), then this will require an internal pressure ( $\sigma_t$ ) of 256.5 kPa in both tunnels.

## 7.5 Conclusion

This chapter has studied the parameters of stability for twin circular tunnels in undrained clay, over a practical range of dimensionless ratios:  $C/D$ ,  $\gamma D/S_u$ ,  $S/D$ , and volume loss. Stability has been analyzed at the stage of collapse and at three previous pre-collapse 'working condition' states. Comparison with rigorous FELA upper and lower bounds and previous experimental research of the collapse results is quite positive. They show that the current approach using the pressure relaxation method is accurate and could be used with confidence as a design tool in practice. Based on a parametric study, design charts have been developed and a number of practical examples are given.

The three stages before the collapse have ground movements more similar to a realistic working condition. Therefore, stability conditions at these points have also been analysed. In the case of the volume loss-stability relationship, the conclusions are that the spacing ratio is actually mostly irrelevant; the dominant parameters are depth and soil strength ratio. The general trends are: as pressure ratio (or stability number  $N$ ) is reduced (made less negative), volume loss increases, and that the stronger and shallower cases require less internal pressure (less negative stability ratio) to achieve the same volume loss as weaker and/or deeper twin tunnel scenarios. On this basis, design charts have been produced which can be conveniently used to relate volume loss and stability number, with respect to strength and depth ratio. A number of examples have been given to highlight the purpose and potential usefulness of these charts.

# 8 CONCLUSIONS AND RECOMMENDATIONS

## 8.1 Summary

This study has investigated the stability and settlement problems of tunnelling in soft clay. A *FLAC* model has been developed which makes use of a pressure relaxation approach. It simulates the short-term soil relaxation that occurs at the tail void, due to the overcutting and time delay occurring between boring and liner and grout installation. The pressure relaxation method slowly reduces the internal pressure in the tunnel from the equivalent in-situ pressure until collapse is detected.

This study assumed a homogenous Tresca material, and plane strain conditions. The study was parametric, making use of dimensionless ratios – depth ratio  $C/D$ , soil strength ratio  $\gamma D/s_u$ , Young's modulus ratio  $E/s_u$ , volume loss %, and the spacing ratio  $S/D$  in the twin tunnel cases. Both single and twin tunnel scenarios were modelled. The twin tunnel cases were modelled as if they were being excavated simultaneously. During each relaxation step of the model, the surface settlement data was exported and the pressure ratio (stability number) was calculated.

Using this settlement data, a settlement parameter ( $i_x$ ) can be estimated reliably and accurately by using a regression. This approach can be used for both single and twin tunnels by using the Gaussian equation and twin-Gaussian equation. Settlement was analysed at the detected collapse stage (a worst case scenario), and also at pre-collapse stages, which represent working construction conditions. Volume loss



could also be back-calculated by integrating this settlement data. However, it is really only meaningful at the pre-collapse stages; the collapse state occurs very quickly, and will only be a practical account of the collapse shape, not the magnitude. The stability numbers have been calculated using the Broms-Bennermark equation, which is essentially an expression of the difference between the surface surcharge and internal tunnel pressure. These can then be analysed independently against the dimensionless ratios. This is a useful approach for generating a boundary at which collapse occurs. This is something that has been extensively done using FELA methods (University of Newcastle group – Sloan, Lyamin, Wilson, Abbo), and is a useful comparison. However, it is also useful at pre-collapse conditions, as it can be correlated with volume loss. This can then be effectively used to evaluate TBM performance based on the stability number.

**Some key conclusions of the single settlement chapter 4 are:**

1. It is concluded that the  $i_x$  parameter always increases with volume loss, but that this rate of change reduces with increasing  $C/D$  and  $\gamma D/s_u$ . The Young's modulus ratio ( $E/s_u$ ) has little impact on  $i_x$ , but clearly does have a big impact on volume loss.
2. Comparisons with previous work were quite positive, with the suggested equations falling approximately into the correct position, based on the soil used in those studies.
3. The linear relationship of O'Reilly and New (1982) is also used, which involves a coefficient of linear proportionality ( $k$ ) which is the ratio of  $i_x$  and the tunnel depth ( $H$ ). It is found that this coefficient increases with soil strength ratio, and an initial relationship describing this is suggested.
4. Further investigation of this  $k$  parameter and the variations being caused by volume loss led to a 3D regression being conducted with respect to  $E/s_u$  and the volume loss %. A more comprehensive equation is suggested which is presented alongside its consequent design charts.
5. The combination of these and the general procedure of this semi-empirical method are demonstrated in a practical example.
6. The great similarity between the *FLAC* modelled settlement and the Gaussian curve indicates that this empirical method is still suitable to be applied in the industry as a preliminary tool.

7. This research suggests that at very high volume loss and/or at collapse, the constant  $k$  should be approximately between 0.52 - 0.75 for undrained clays. A new equation is proposed for estimating the  $k$  value at the collapse stage.

**Some key conclusions of the single stability chapter 5 are:**

1. Stability has been analysed with the stability number (or pressure ratio,  $N$ ) at the detected stage of collapse, where the stability number represents the minimum to avoid collapse.
2. The collapse stability results are compared with rigorous upper and lower bound results of Wilson et al (2011). The effect of the parameters is also shown. It is clear that the soil strength ratio has a big impact on the collapse stability number; in cases with strong clay, this number remains almost constant with increasing depth ratio. As the strength ratio increases (i.e. soil becomes weaker), the rate at which this stability number changes with  $C/D$  becomes greater. These conclusions concur with the comparison, which is quite positive, and shows that the results using the current pressure relaxation method are accurate.
3. It is believed that these results could be used with confidence as a potential design tool in practice. A design chart is developed and a number of practical examples are given.
4. Several pre-collapse 'working conditions' stages have also been analysed with this ratio, with the aim of establishing a stability-volume loss relationship.
5. It is found that volume loss increases as stability number reduces (i.e. becomes less negative). This is expected; reducing stability number is effectively reducing tunnel support and increasing surcharge pressure, more ground movement would be expected with either of these.
6. Soil strength ratio and depth ratio also have a big impact here – softer and deeper cases require higher pressure ratio (more negative) to maintain the same level of volume loss.
7. Based on these conclusions and validation of previous results, contour charts have been produced for stability number  $N$ , which can be used to relate it to volume loss for any  $C/D$  and  $\gamma D/S_u$ .

**Some key conclusions of the twin settlement chapter 6 are:**

1. Studying twin tunnel settlement has provided some interesting results. If the tunnels are close enough, the profiles completely merge and can be treated as a single tunnel. As the spacing continues to be increased, the profiles will start to diverge, and a superimposed twin Gaussian equation must be used. If the spacing increases even more, it is determined that single tunnel settlement profiles can be used individually for each tunnel as interaction effects are minimal. Charts have been provided which indicate which method is appropriate.
2. Following the regression approach allows reliable estimation of  $i_x$  for all cases. A parametric study was undertaken in which a series of commonly used dimensionless ratios were controlled including  $C/D$ ,  $\gamma D/s_u$ , and  $S/D$ . The volume loss ( $V_L\%$ ) was calculated at the analysed stages by integrating the settlement data.
3. It is concluded that the  $i_x$  parameter always changes with volume loss, but that this rate of change becomes increasingly positive with increasing  $C/D$ . The spacing ratio ( $S/D$ ) and the soil strength ratio ( $\gamma D/s_u$ ) have little impact on  $i_x$ .
4. Further investigation of this  $i_x$  parameter and the variations being caused by volume loss led to 3D regressions being conducted with respect to  $C/D$  and the volume loss for both the collapse and pre-collapse conditions. From this, design contour charts are presented which can be used for prediction purposes.
5. The great similarity between the *FLAC* modelled settlement and the Gaussian and twin-Gaussian curves indicate that this empirical method is still suitable to be applied in the industry as a preliminary tool.

**Some key conclusions of the twin stability chapter 7 are:**

1. This chapter has studied the stability for twin circular tunnels in undrained clay at the stage of collapse and at three previous pre-collapse 'working condition' states. This has been done over a practical range of dimensionless ratios:  $C/D$ ,  $\gamma D/s_u$ ,  $S/D$ , and volume loss %.
2. The results at the stage of collapse represent a failure envelope. This is compared with rigorous FELA upper and lower bounds and previous

experimental research. This comparison is quite positive and shows that the current approach using the pressure relaxation method is accurate and could be used with confidence as a design tool in practice. Based on a parametric study, design charts have been developed and a number of practical examples are given.

3. The three stages before the collapse have ground movements more similar to a realistic working condition. This allows the development of a volume loss-stability relationship.
4. The conclusions are that the spacing ratio is actually mostly irrelevant; the dominant parameters are depth and soil strength ratio. The general trends are as pressure ratio (or stability number  $N$ ) is reduced (made less negative), volume loss increases, and that the stronger and shallower cases require less internal pressure (less negative stability ratio) to achieve the same volume loss as weaker and/or deeper twin tunnel scenarios.
5. On this basis, design charts have been produced which can be conveniently used to relate volume loss and stability number, with respect to strength and depth ratio. A number of examples have been given to highlight the purpose and potential usefulness of these charts.

## 8.2 Future Work and Closing Comments

As with all geotechnical modelling, complexity is especially high because of the number of amount of variables and amount of uncertainty. When it comes to research, simplifications are always necessary to develop the model with confidence. This is especially true with tunnel modelling, where there are a huge number of possibilities. Not only is there the geometry, material properties and the complexity of simulating the tunnel, but also the possibility of many other complications such as: surface surcharges (buildings, roads), sub-surface structures (pipelines, piles, other tunnels), and complex geology (layers).

This likely means that practical design of tunnels will always be complicated and will need to be tailored to each scenario. However, parametric studies are still useful to study the response to changing variables. It provides insight into likely behaviour, and allows the development of some useful and simple design tools for preliminary work that are useful, and desired by industry.

Following the research achievements in this study, and the knowledge and experience gained by the author throughout its duration, some important areas have been identified for future investigation. These will enhance the results of this study, but would also expand the scope and allows these approaches to be used in a greater number of possible scenarios.

**Some important future work following this study:**

- 2D plane strain modelling of tunnelling in sand. This would include a parametric study of settlement, and an investigation of the influence of dilation. Is the empirical method (Gaussian equation) still usable? It is widely reported that O'reilly and New's relationship ( $i_x=kH$ ) does not work well in sand, are there others that could work. Stability analysis in sand could also be an interesting area, in terms of comparing the stability envelope to clay.
- An investigation into the effectiveness of the empirical method (Gaussian equation) to represent settlement in layered soils is another interesting area. How different do the soil layers need to be before it is unusable? Some general conclusions about stability could also be interesting - if you have sand over clay are the stability conditions better or worse?
- Twin tunnel sequential construction. As mentioned, this study modelled the twin tunnels as if they were bored simultaneously, which is unlikely in reality. However, modelling them as if they bored with a delay involves some extra complications – the amount of time delay is another parameter, the settlement profile will be unsymmetrical. There have been many suggestions as to how the empirical method can be used to cope with this problem such as modifiers etc. A review of these approaches is needed, to determine which will be best. Aside from settlement, there is also the stability problem. The first tunnel will have the same stability characteristics as a single tunnel, but the second will be quite different as the soil conditions have changed – is this dependant on the amount of delay?
- Vertical twin tunnels. All of the previous areas of interest for side-by-side twin tunnels with the new arrangement. Particular research questions are – can the empirical method be used, what is the influence of the vertical

spacing? Stability analysis is also interesting, what is the difference between the top and bottom tunnel for the stability envelope.

- 3D modelling of tunnel to simulate heading. The internal pressure in TBMs isn't actually controlled at the annulus, but at the cutting face. Also, the heading is a 3D problem (plane strain is generally inadequate), it is much more realistic to model the internal pressure at the heading, and in three dimensions. For this research, both stability and settlement could be studied. With a parametric study, the stability envelope for headings could be found, and the longitudinal settlement could also be studied – particularly ahead of the TBM.
- Modelling of the tunnel lining to determine stresses. Using a parametric study in 2D plane strain, the research could develop design charts for tunnel linings in particular soils. These results could also be compared to semi-analytical bedded-beam method which is currently popular in industry.

# REFERENCES

- Abbo, A. J., Wilson, D. W., Sloan, S. W., & Lyamin, A. V. (2013). Undrained stability of wide rectangular tunnels. *Computers and Geotechnics*, 53, 46-59.
- Addenbrooke, T. I., & Potts, D. M. (2001). Twin tunnel interaction: surface and subsurface effects. *International Journal of Geomechanics*, 1(2), 249-271.
- Ahmed, M. and Iskander, M., (2010). Analysis of tunneling-induced ground movements using transparent soil models. *Journal of Geotechnical and Geoenvironmental Engineering*, 137(5), pp.525-535.
- Anagnostou, G. and Kovari, K., (1996). Face stability conditions with earth-pressure-balanced shields. *Tunnelling and Underground Space Technology*, 11(2), pp.165-173.
- Ang, W.T., (2007). *A beginner's course in boundary element methods*. Universal-Publishers.
- Assadi, A., & Sloan, S. W. (1991). Undrained stability of shallow square tunnel. *Journal of Geotechnical Engineering*, 117(8), 1152-1173.
- Atkinson, J., & Cairncross, A. (1973). "Collapse of a shallow tunnel in a Mohr-Coulomb material". Paper presented at the Proceedings of the Symposium on the Role of Plasticity in Soil Mechanics, Cambridge, UK.
- Atkinson, J.H. and Mair, R.J., (1981). Soil mechanics aspects of soft ground tunnelling. *Ground Engineering*, 14(5).
- Atkinson, J. H., & Potts, D. M. (1977). "Subsidence above shallow tunnels in soft ground". *Journal of the geotechnical engineering division*, 103(4), 307-325.
- Attewell, P., & Farmer, I. (1974). "Ground deformations resulting from shield tunnelling in London Clay". *Canadian Geotechnical Journal*, 11(3), 380-395.
- Attewell, P.B. and Woodman, J.P., (1982). Predicting the dynamics of ground settlement and its derivatives caused by tunnelling in soil. *Ground engineering*, 15(8).
- Attewell, P.B., Yeates, J. and Selby, A.R., (1986). Soil movements induced by tunnelling and their effects on pipelines and structures.

- Augarde, C. E., Lyamin, A. V., & Sloan, S. W. (2003). Stability of an undrained plane strain heading revisited. *Computers and Geotechnics*, 30(5), 419-430.
- Bartlett, J.V. and Bubbers, B.L., (1970). Surface movements caused by bored tunnelling. In *Conference on Subway Construction* (Vol. 539). sl]: Budapest-Balatonfured.
- Brinkgreve, R.B., (2005). Selection of soil models and parameters for geotechnical engineering application. In *Soil Constitutive Models@ sEvaluation, Selection, and Calibration* (pp. 69-98). ASCE
- Broms, B. B., & Bennermark, H. (1967). "Stability of clay at vertical openings". *Journal of Soil Mechanics & Foundations Div., ASCE*, 193, SMI, 71-94
- Chakeri, H., Ozcelik, Y., & Unver, B. (2013). Effects of important factors on surface settlement prediction for metro tunnel excavated by EPB. *Tunnelling and Underground Space Technology*, 36, 14-23.
- Chakeri, H., & Ünver, B. (2014). A new equation for estimating the maximum surface settlement above tunnels excavated in soft ground. *Environmental earth sciences*, 71(7), 3195-3210.
- Chakeri, H., Ozcelik, Y., & Unver, B. (2015). Investigation of ground surface settlement in twin tunnels driven with EPBM in urban area. *Arabian Journal of Geosciences*, 8(9), 7655-7666.
- Chambon, P. and Corté, J.F., (1994). Shallow tunnels in cohesionless soil: stability of tunnel face. *Journal of Geotechnical Engineering*.
- Chapman, D. N., Rogers, C. D. F., & Hunt, D. V. L. (2004). Predicting the settlements above twin tunnels constructed in soft ground. *Tunneling and Underground Space Technology*, 19(4/5), 378-380.
- Chapman, D.N., Ahn, S.K. and Hunt, D.V., (2007). Investigating ground movements caused by the construction of multiple tunnels in soft ground using laboratory model tests. *Canadian Geotechnical Journal*, 44(6), pp.631-643.
- Chapman, D., Metje, N., & Stärk, A. (2010). Introduction to tunnel construction (Vol. 3). CRC Press.
- Chen, S. L., Gui, M. W., & Yang, M. C. (2012). Applicability of the principle of superposition in estimating ground surface settlement of twin-and quadruple-tube tunnels. *Tunnelling and Underground Space Technology*, 28, 135-149.
- Chi, S.-Y., Chern, J.-C., & Lin, C.-C. (2001). Optimized back-analysis for tunneling-induced ground movement using equivalent ground loss model. *Tunnelling and Underground Space Technology*, 16(3), 159-165.
- Chou, W.I. and Bobet, A., (2002). Predictions of ground deformations in shallow tunnels in clay. *Tunnelling and Underground Space Technology*, 17(1), pp.3-19.
- Chow, L., (1994). The prediction of surface settlements due to tunnelling in soft ground. *M. Sc.*
- Clough, G. W., & Schmidt, B. (1977). "Design and performance of excavations and tunnels in soft clay". In *Soft Clay Engineering*, Elsevier, 569-634
- Cording, E. J., and Hansmire, W. H. (1975). "Displacement around soft ground tunnels". General Report: Session IV, Tunnels in soil. In Proc., 5th Panamerican Congr. on Soil Mech. and Found. Engrg.



- Crouch, S.L., Starfield, A.M. and Rizzo, F.J., (1983). Boundary element methods in solid mechanics. *Journal of Applied Mechanics*, 50, p.704.
- Cundall, P. A. (1976). Explicit Finite Difference Method in Geomechanics: Numerical Methods in Engineering. In Proc. EF Conference on Numerical Methods in Geomechanics. Blacksburg, VA. Pp. 132-150
- Davis, E., Gunn, M., Mair, R., & Seneviratine, H. (1980). "The stability of shallow tunnels and underground openings in cohesive material". *Geotechnique*, 30(4), 397-416.
- Devriendt, M., (2010). Risk analysis for tunnelling ground movement assessments. *Proceedings of the Institution of Civil Engineers-Geotechnical Engineering*, 163(3), pp.109-118.
- Divall, S. and Goodey, R.J., (2015). Twin-tunnelling-induced ground movements in clay. *Proceedings of the Institution of Civil Engineers-Geotechnical Engineering*, 168(3), pp.247-256.
- Do, N. A., Dias, D., & Oreste, P. (2015). 3D numerical investigation on the interaction between mechanized twin tunnels in soft ground. *Environmental Earth Sciences*, 73(5), 2101-2113.
- Eisenstein, Z., El-Nahhas, F., & Thompson, S. (1981). Strain field around a tunnel in stiff soil. In *Proceedings of the International Conference on Soil Mechanics and Foundation Engineering*, 10th. (Vol. 1, No. Conf Paper).
- Ercelebi, S. G., Copur, H., & Ocak, I. (2011). Surface settlement predictions for Istanbul Metro tunnels excavated by EPB-TBM. *Environmental Earth Sciences*, 62(2), 357-365.
- Fattah, M.Y., Shlash, K.T. and Salim, N.M., (2013). Prediction of settlement trough induced by tunneling in cohesive ground. *Acta Geotechnica*, 8(2), pp.167-179.
- Federal Highway Administration, USA. (2009). Road Tunnel Manual – Chapter 7: Soft Ground Tunnelling. FHWA-NHI-09-010.
- Ghaboussi, J., & Ranken, R. E. (1977). Interaction between two parallel tunnels. *International Journal for Numerical and Analytical Methods in Geomechanics*, 1(1), 75-103.
- Ghaboussi, J., Ranken, R. E., & Karshenas, M. (1978). "Analysis of subsidence over soft-ground tunnels". Paper presented at the International conference on Evaluation and Prediction of Subsidence.
- Gioda, G. and Swoboda, G., (1999). Developments and applications of the numerical analysis of tunnels in continuous media. *International Journal for Numerical and Analytical Methods in Geomechanics*, 23(13), pp.1393-1405.
- Grant, R.J. and Taylor, R.N., (2000). Tunnelling-induced ground movements in clay. *Proceedings of the ICE-Geotechnical Engineering*, 143(1), pp.43-55.
- Guglielmetti, V., Grasso, P., Mahtab, A., & Xu, S. (Eds.). (2008). "Mechanized tunnelling in urban areas: design methodology and construction control". Taylor and Francis. Ch. 5.
- Gunn, M. J. (1993). "The prediction of surface settlement profiles due to tunneling". In Predictive Soil Mechanics. Proceedings of the Wroth Memorial Symposium, 27-29 July, St Catherines College, Oxford.

- Hajjar, M., Nemati Hayati, A., Ahmadi, M. M., & Sadrnejad, S. A. (2014). Longitudinal Settlement Profile in Shallow Tunnels in Drained Conditions. *International Journal of Geomechanics*, 15(6), 04014097.
- Hughes, T.J., (2012). *The finite element method: linear static and dynamic finite element analysis*. Courier Corporation.
- Itasca Consulting Group Inc (2003). "FLAC2D User's Manual". Minneapolis, USA.
- Kim, S. H., Burd, H. J., & Milligan, G. W. E. (1998). Model testing of closely spaced tunnels in clay. *Geotechnique*, 48(3), 375-388.
- Krabbenhoft, K., Lyamin, A.V., Hjiiaj, M. and Sloan, S.W., (2005). A new discontinuous upper bound limit analysis formulation. *International Journal for Numerical Methods in Engineering*, 63(7), pp.1069-1088.
- Krabbenhøft, K., Lyamin, A.V. and Sloan, S.W., (2007). Formulation and solution of some plasticity problems as conic programs. *International Journal of Solids and Structures*, 44(5), pp.1533-1549.
- Kuesel, T. R., King, E. H., & Bickel, J. O. (2012). Tunnel engineering handbook. Springer Science & Business Media.
- Leca, E. and Dormieux, L., (1990). Upper and lower bound solutions for the face stability of shallow circular tunnels in frictional material. *Géotechnique*, 40(4), pp.581-606.
- Leca, E., Leblais, Y. and Kuhnhenh, K., (2000), November. Underground works in soils and soft rock tunneling. In *ISRM International Symposium*. International Society for Rock Mechanics.
- Leca, E. and New, B., (2007). Settlements induced by tunneling in soft ground. *Tunnelling and Underground Space Technology*, 22(2), pp.119-149.
- Lee, C.J., Wu, B.R., Chiou, S.Y., (1999). "Soil movements around a tunnel in soft soils". Proceedings of the National Science Council, Part A: Physical Science and Engineering 23 (2), 235-247.
- Lee, C.J., Wu, B.R., Chen, H.T. and Chiang, K.H., (2006). Tunnel stability and arching effects during tunneling in soft clayey soil. *Tunnelling and Underground Space Technology*, 21(2), pp.119-132.
- Lee, F.H., (2008). How useful is numerical analysis in geotechnical engineering?. In *Proc., Int. Conf. on Deep Excavation (ICDE) 2008*. Singapore: Land Transport Authority.
- Lee, K.M. and Rowe, R.K., (1990a). Finite element modelling of the three-dimensional ground deformations due to tunnelling in soft cohesive soils: Part I—Method of analysis. *Computers and Geotechnics*, 10(2), pp.87-109.
- Lee, K.M. and Rowe, R.K., (1990b). Finite element modelling of the three-dimensional ground deformations due to tunnelling in soft cohesive soils: Part 2—results. *Computers and Geotechnics*, 10(2), pp.111-138.
- Lee, K., Rowe, R. K., & Lo, K. (1992). Subsidence owing to tunnelling. I. Estimating the gap parameter. *Canadian Geotechnical Journal*, 29(6), 929-940.
- Li, Y., Emeriault, F., Kastner, R., & Zhang, Z. (2009). Stability analysis of large slurry shield-driven tunnel in soft clay. *Tunnelling and Underground Space Technology*, 24(4), 472-481.

- Loganathan, N., & Poulos, H. G. (1998). "Analytical prediction for tunneling-induced ground movements in clays". *Journal of Geotechnical & Geoenvironmental Engineering*, 124(9), 846.
- Lyamin, A., & Sloan, S. (2000). *Stability of a plane strain circular tunnel in a cohesive-frictional soil*. Paper presented at the Proceedings of the JR Booker memorial symposium, Sydney.
- Lyamin, A., & Sloan, S. (2000). "Stability of a plane strain circular tunnel in a cohesive-frictional soil". Paper presented at the Proceedings of the JR Booker memorial symposium, Sydney.
- Lyamin, A.V., & Sloan, S. (2002a). "Lower bound limit analysis using non-linear programming". *International Journal for Numerical Methods in Engineering*, 55(5), 573-611.
- Lyamin, A. V., & Sloan, S. (2002b). "Upper bound limit analysis using linear finite elements and non-linear programming". *International journal for numerical and analytical methods in geomechanics*, 26(2), 181-216.
- Mair, R. J. (1979). "Centrifugal modelling of tunnel construction in soft clay". PhD Thesis. University of Cambridge, Cambridge, UK
- Mair, R.J. (2008). "Tunnelling and geotechnics: new horizons". *Geotechnique*, 58(9), 695-736.
- Mair, R.J., Gunn, M.J. and O'REILLY, M.P., (1982). Ground movement around shallow tunnels in soft clay. *Tunnels & Tunnelling International*, 14(5).
- Mair, R. J., and Taylor, R. N. (1997). "Theme lecture: Bored tunnelling in the urban environment". In Proc., 14th Int. Conf. on Soil Mechanics and Foundation Engineering, Hamburg, Balkema, Rotterdam, Netherlands, 2353-2385.
- Mair, R., Taylor, R., & Bracegirdle, A. (1993). Subsurface settlement profiles above tunnels in clays. *Geotechnique*, 43(2).
- Martos, F. (1958). "Concerning an approximate equation of the subsidence trough and its time factors". In International strata control congress, Leipzig, 191-205.
- Meguid, M.A., Saada, O., Nunes, M.A. and Mattar, J., (2008). Physical modeling of tunnels in soft ground: a review. *Tunnelling and Underground Space Technology*, 23(2), pp.185-198.
- Moh, Z.C., Ju, D.H. and Hwang, R.N., (1996). Ground movements around tunnels in soft ground. In Proceedings of the International Symposium on Geotechnical Aspects of Underground Construction in Soft Ground. London: Balkema AA (pp. 725-730).
- Mollon, G., Dias, D. and Soubra, A.H., (2009a). Face stability analysis of circular tunnels driven by a pressurized shield. *Journal of geotechnical and geoenvironmental engineering*, 136(1), pp.215-229.
- Mollon, G., Dias, D. and Soubra, A.H., (2009b). Probabilistic analysis and design of circular tunnels against face stability. *International Journal of Geomechanics*, 9(6), pp.237-249.
- New, B. M., & O'Reilly, M. P. (1991). Tunnelling induced ground movements; predicting their magnitude and effects. In Proceedings of the 4th International

- Conference on Ground Movements and Structures, invited review paper, Cardiff, Pentech Press, London (pp. 671-697).
- Ng, C.W., Simons, N.E. and Menzies, B.K., (2004). A short course in soil-structure engineering of deep foundations, excavations and tunnels. Thomas Telford.
- Ocak, I. (2014). A new approach for estimating the transverse surface settlement curve for twin tunnels in shallow and soft soils. *Environmental Earth Sciences*, 72(7), 2357-2367.
- O'reilly, M. P., & New, B. M. (1982). "Settlements above tunnels in the United Kingdom-their magnitude and prediction". In *Tunneling '82*. 173-181.
- Osman, A. S. (2010). Stability of unlined twin tunnels in undrained clay. *Tunnelling and Underground Space Technology*, 25(3), 290-296.
- Osman, A. S., Mair, R. J., & Bolton, M. D. (2006a). "On the kinematics of 2D tunnel collapse in undrained clay". *Géotechnique*, 56(9), 585-595.
- Osman, A.S., Bolton, M.D. and Mair, R.J., (2006b). Predicting 2D ground movements around tunnels in undrained clay. *Geotechnique*, 56(9), pp.597-604.
- Palmer, A. C., & Mair, R. J. (2011). Ground movements above tunnels: a method for calculating volume loss. *Canadian Geotechnical Journal*, 48(3), 451-457.
- Panet, M., & Guenot, A. (1983). "Analysis of convergence behind the face of a tunnel". *Tunnelling 82*, proceedings of the 3rd international symposium, Brighton, 7-11 June 1982, P197-204.
- Park, K.-H. (2005). Analytical solution for tunnelling-induced ground movement in clays. *Tunnelling and Underground Space Technology*, 20(3), 249-261.
- Peck, R.B., (1969). "Deep Excavations and Tunneling in Soft Ground". In: *Proceedings of the 7th International Conference on Soil Mechanics and Foundation Engineering*, Mexico City, State-of-the-art Volume, pp. 225-290.
- Phienweij, N. (1997). "Ground movements in shield tunneling in Bangkok soils". *Proceedings of the 14th International Conference on Soil Mechanics and Foundation Engineering*. Hamburg, Vol. 3, pp. 1469-1472.
- Pinto, F., & Whittle, A. J. (2013). "Ground movements due to shallow tunnels in soft ground. I: Analytical solutions". *Journal of Geotechnical and Geoenvironmental Engineering*, 140(4), 04013040.
- Potts, D.M., and Zdravković, L., (2001). *Finite element analysis in geotechnical engineering: application* (Vol. 2). Thomas Telford.
- Rankin, W. (1988). "Ground movements resulting from urban tunnelling: predictions and effects". Geological Society, London, *Engineering Geology Special Publications*, 5(1), 79-92.
- Romo, M.P. and Diaz, M., (1981). Face stability and ground settlement in shield tunneling. In *Proceedings of the Tenth International Conference on Soil Mechanics and Foundation Engineering*, Stockholm..
- Rowe, R. K., Lo, K. Y., & Kack, G. J. (1983). "A method of estimating surface settlement above tunnels constructed in soft ground". *Canadian geotechnical journal*, 20(1), 11-22.

- Sagaseta, C. (1987). "Analysis of undrained soil deformation due to ground loss". *Geotechnique*, 37(3), 301-320.
- Seneviratne, H. (1979). "Deformations and pore-pressures around model tunnels in soft clay". Ph. D. thesis, University of Cambridge, Cambridge, UK.
- Sloan, S. (1988). "Lower bound limit analysis using finite elements and linear programming". *International journal for numerical and analytical methods in geomechanics*, 12(1), 61-77.
- Sloan, S. (1989). "Upper bound limit analysis using finite elements and linear programming". *International journal for numerical and analytical methods in geomechanics*, 13(3), 263-282.
- Sloan, S. (2013). "Geotechnical stability analysis". *Geotechnique*, 63(7), 531-571.
- Sloan, S., & Assadi, A. (1991). Undrained stability of a square tunnel in a soil whose strength increases linearly with depth. *Computers and Geotechnics*, 12(4), 321-346.
- Sloan, S., & Assadi, A. (1993). *Stability of shallow tunnels in soft ground*. Paper presented at the PREDICTIVE SOIL MECHANICS. PROCEEDINGS OF THE WROTH MEMORIAL SYMPOSIUM, 27-29 JULY 1992, ST CATHERINE'S COLLEGE, OXFORD.
- Sloan, S., & Assadi, A. (1994). Undrained stability of a plane strain heading. *Canadian Geotechnical Journal*, 31(3), 443-450.
- Soubra, A.H., (2000), November. Three-dimensional face stability analysis of shallow circular tunnels. In *ISRM International Symposium*. International Society for Rock Mechanics.
- Soubra, A.H., Dias, D., Emeriault, F. and Kastner, R., (2008). Three-dimensional face stability analysis of circular tunnels by a kinematical approach. *Geotechnique*, 30(5), pp.894-901.
- Sugiyama, T., Hagiwara, T., Nomoto, T., Nomoto, M., Ano, Y., Mair, R. J., Bolton, M. D. & Soga, K. (1999). Observations of ground movements during tunnel construction by slurry shield method at the Docklands Light Railway Lewisham extension – east London. *Soils Found.* 39, No. 3, 99–112.
- Suwansawat, S., & Einstein, H. H. (2007). Describing settlement troughs over twin tunnels using a superposition technique. *Journal of geotechnical and geoenvironmental engineering*, 133(4), 445-468.
- Tan, W. L., & Ranjith, P. G. (2003). Parameters and considerations in soft ground tunneling. *Electronic Journal of Geotechnical Engineering*, 8, 1.
- Taylor, R. (1998). "Modelling of Tunnel Behaviour". *Proceedings of the ICE-Geotechnical Engineering*, 131(3), 127-132.
- Terzaghi, K., (1950). *Geologic aspects of soft-ground tunneling*.
- Verruijt, A., & Booker, J. (1996). "Surface settlements due to deformation of a tunnel in an elastic half plane". *Geotechnique*(46), 753-756.
- Ward, W., & Pender, M. (1981). "Tunnelling in soft ground: general report". Paper presented at the Proceedings of the 10th International Conference on Soil Mechanics and Foundation Engineering, Stockholm.
- Whittaker B.N. and Frith R.C. (1990). *Tunnelling Design Stability and Construction*, Institution of Mining and Metallurgy, London.

- Wilson, D.W., Abbo, A.J., Sloan, S.W. and Lyamin, A.V., (2008). Undrained stability of dual square tunnels. *Acta Geotechnica*, pp.1-18.
- Wilson, D. W., Abbo, A. J., Sloan, S. W., & Lyamin, A. V. (2011). "Undrained stability of a circular tunnel where the shear strength increases linearly with depth". *Canadian Geotechnical Journal*, 48(9), 1328-1342.
- Wilson, D. W., Abbo, A. J., Sloan, S. W., & Lyamin, A. V. (2013). "Undrained stability of a square tunnel where the shear strength increases linearly with depth". *Computers and Geotechnics*, 49, 314-325.
- Wilson, D. W., Abbo, A. J., Sloan, S. W., & Lyamin, A. V. (2014). "Undrained stability of dual circular tunnels". *International Journal of Geomechanics*, 14(1), 69-79.
- Wu, B.R. and Lee, C.J., (2003). Ground movements and collapse mechanisms induced by tunneling in clayey soil. *International Journal of Physical Modelling in Geotechnics*, 3(4), pp.15-29.
- Yamamoto, K., Lyamin, A. V., Wilson, D. W., Sloan, S. W., & Abbo, A. J. (2011). "Stability of a circular tunnel in cohesive-frictional soil subjected to surcharge loading". *Computers and Geotechnics*, 38(4), 504-514.
- Yamamoto, K., Lyamin, A.V., Wilson, D.W., Sloan, S.W. and Abbo, A.J., (2013). Stability of dual circular tunnels in cohesive-frictional soil subjected to surcharge loading. *Computers and Geotechnics*, 50, pp.41-54.
- United Nations – Department of Economic and Social Affairs, Population Division. (2015) "World Population Prospects – The 2015 Revision". New York, ESA/P/WP.241.  
<<http://esa.un.org/unpd/wpp/Publications>>
- Zienkiewicz, O.C., Taylor, R.L. and Too, J.M., (1971). Reduced integration technique in general analysis of plates and shells. *International Journal for Numerical Methods in Engineering*, 3(2), pp.275-290.
- Zienkiewicz, O.C., Taylor, R.L. (1977). *The finite element method* (Vol. 3). London: McGraw-hill.

# APPENDIX 1

## A1 MATLAB Surface Fits

The following are MATLAB surface fits of data in this study.

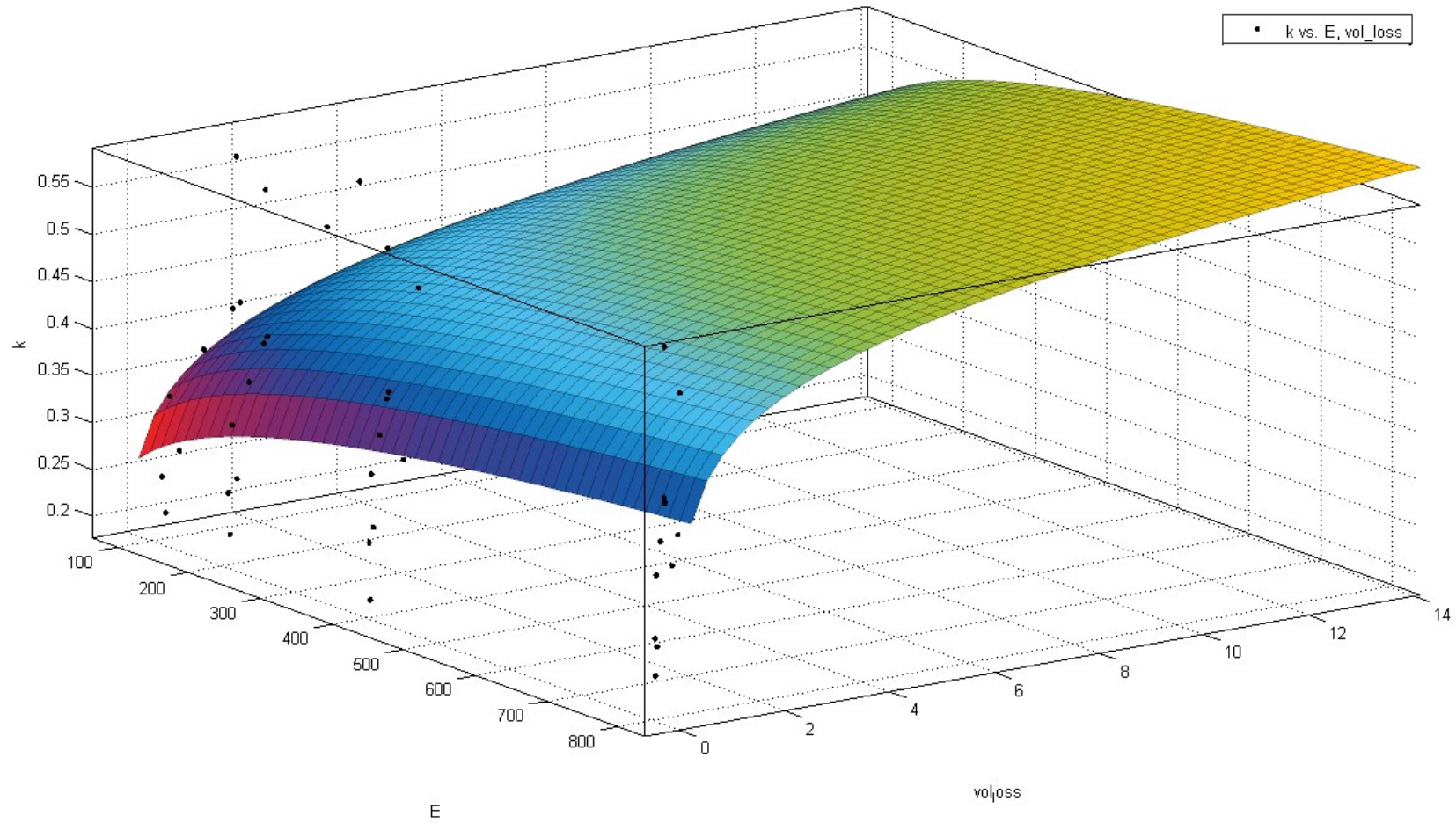


Figure 0-1 Typical *MATLAB* surface fit for single tunnel settlement at pre-collapse ( $\gamma D/s_u=2$ )



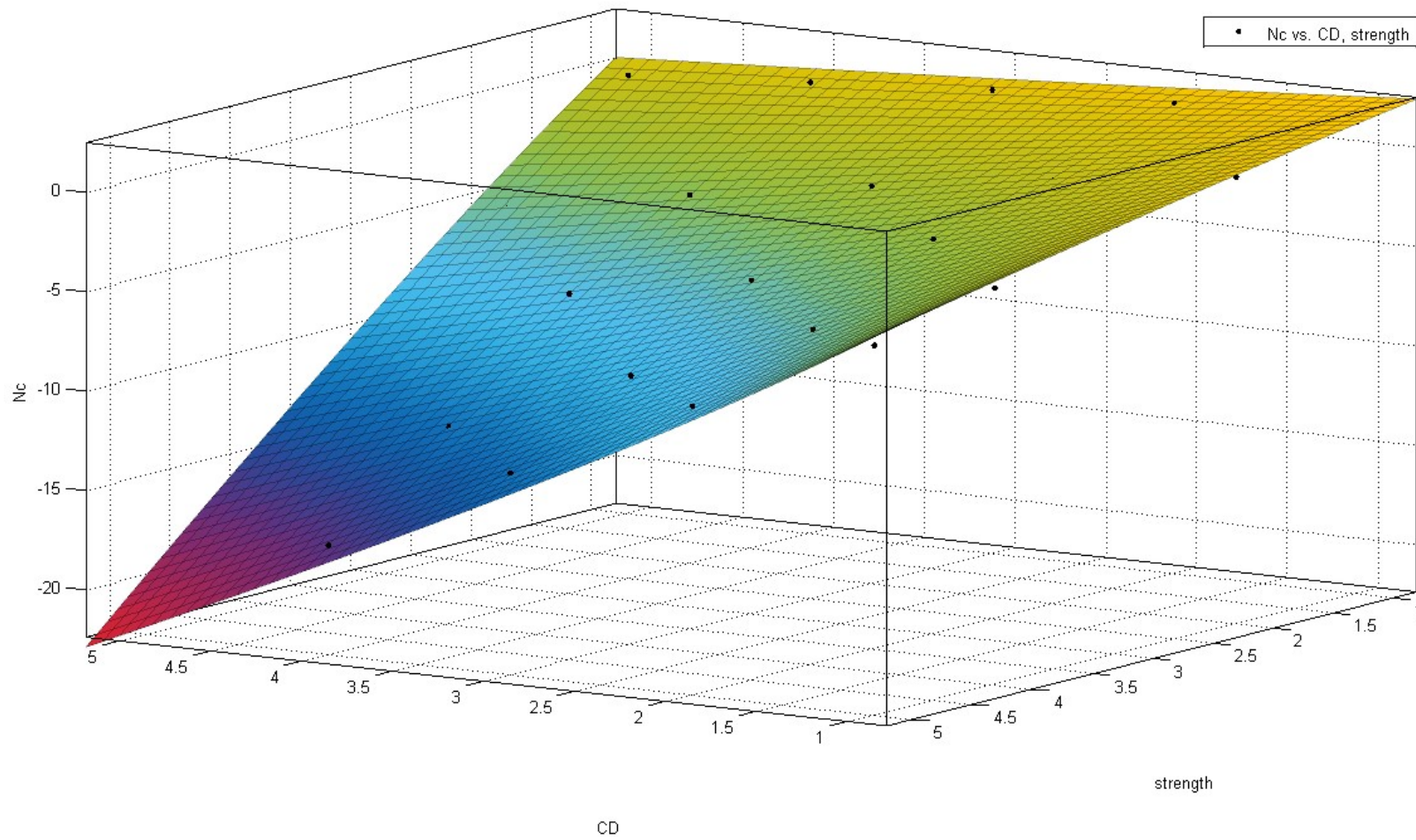


Figure 0-2 *MATLAB* surface fit for single tunnel critical stability number at collapse

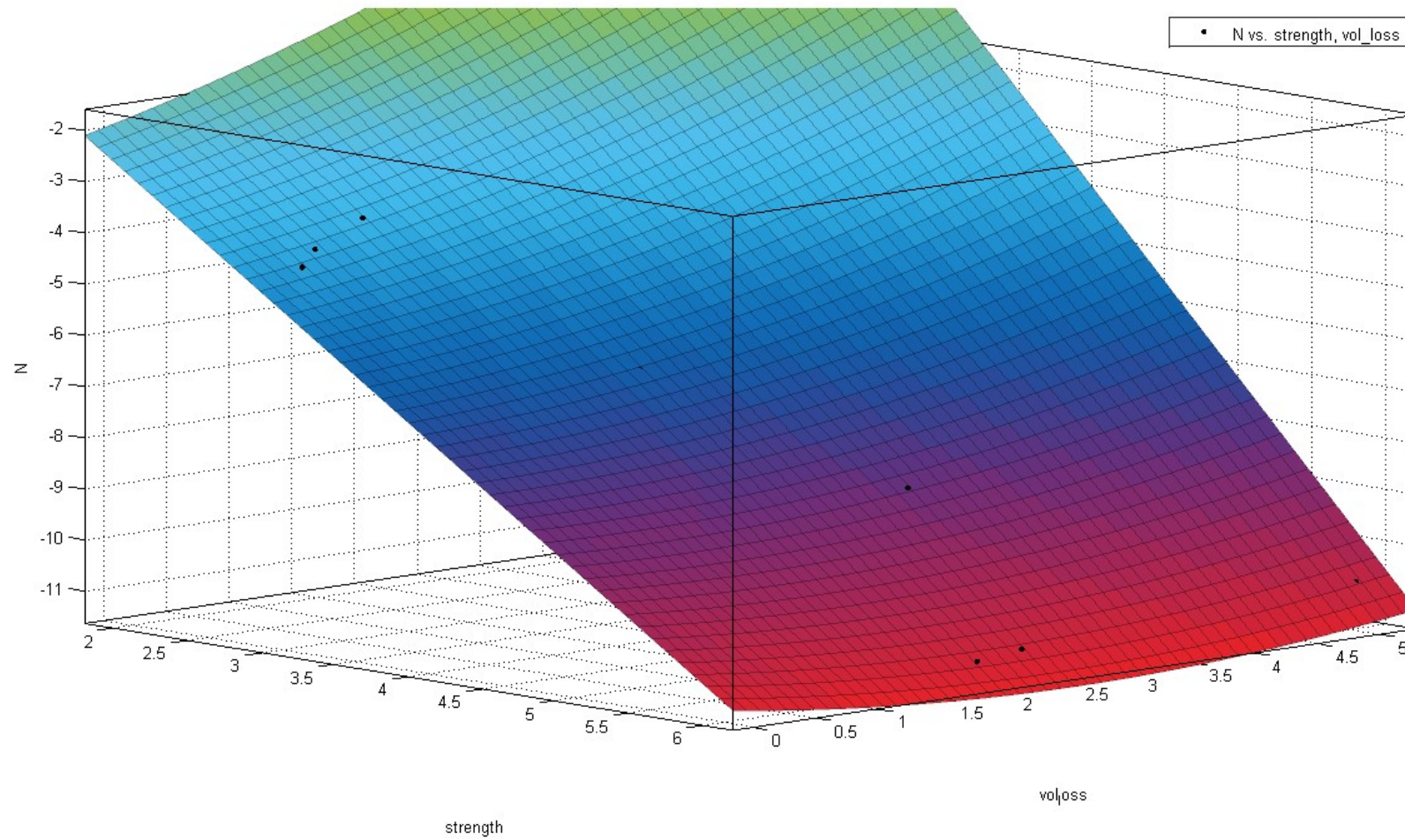


Figure 0-3 Typical *MATLAB* surface fit for single tunnel stability at pre-collapse ( $C/D=2$ )

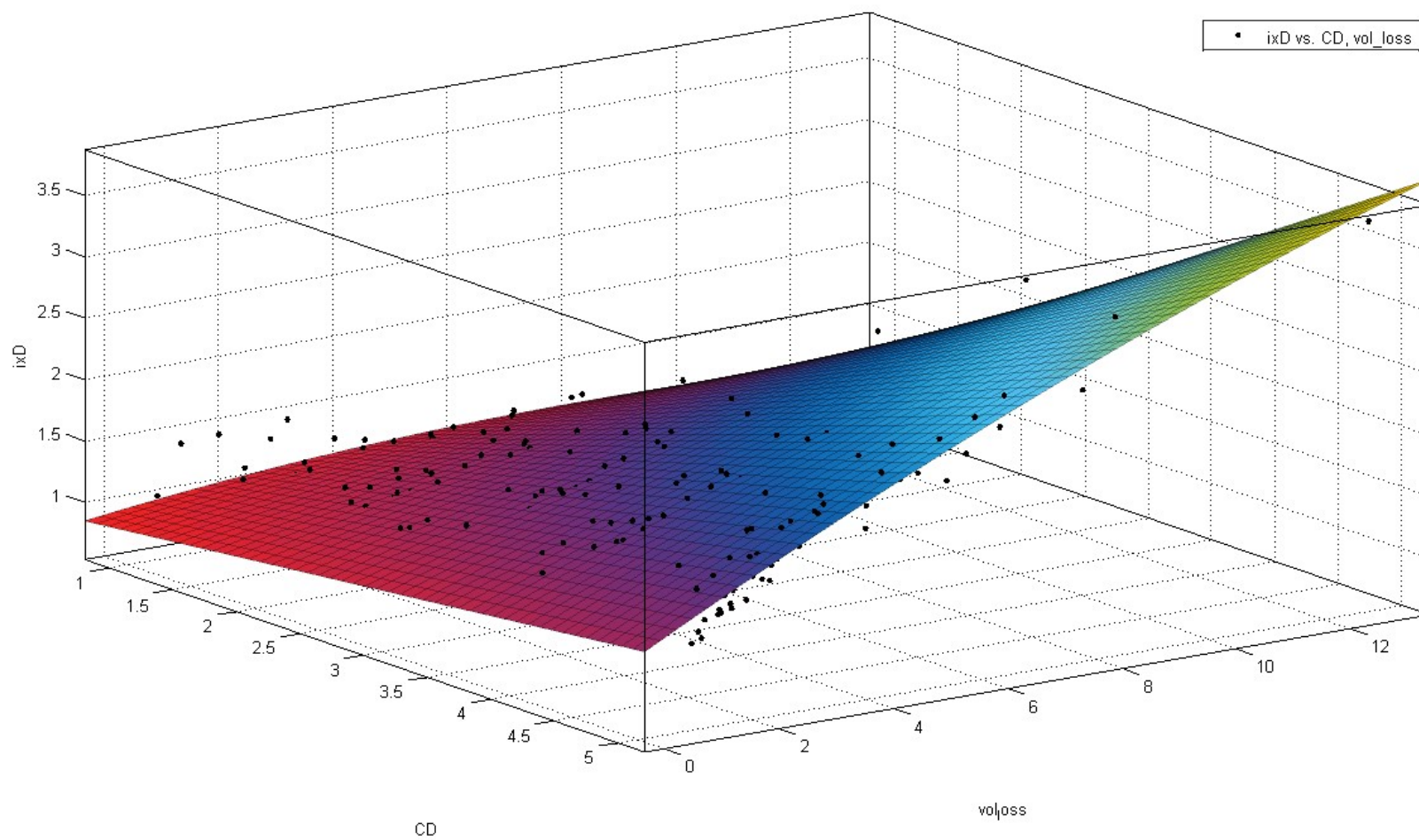


Figure 0-4 *MATLAB* surface fit for method 1 twin tunnel settlement at pre-collapse

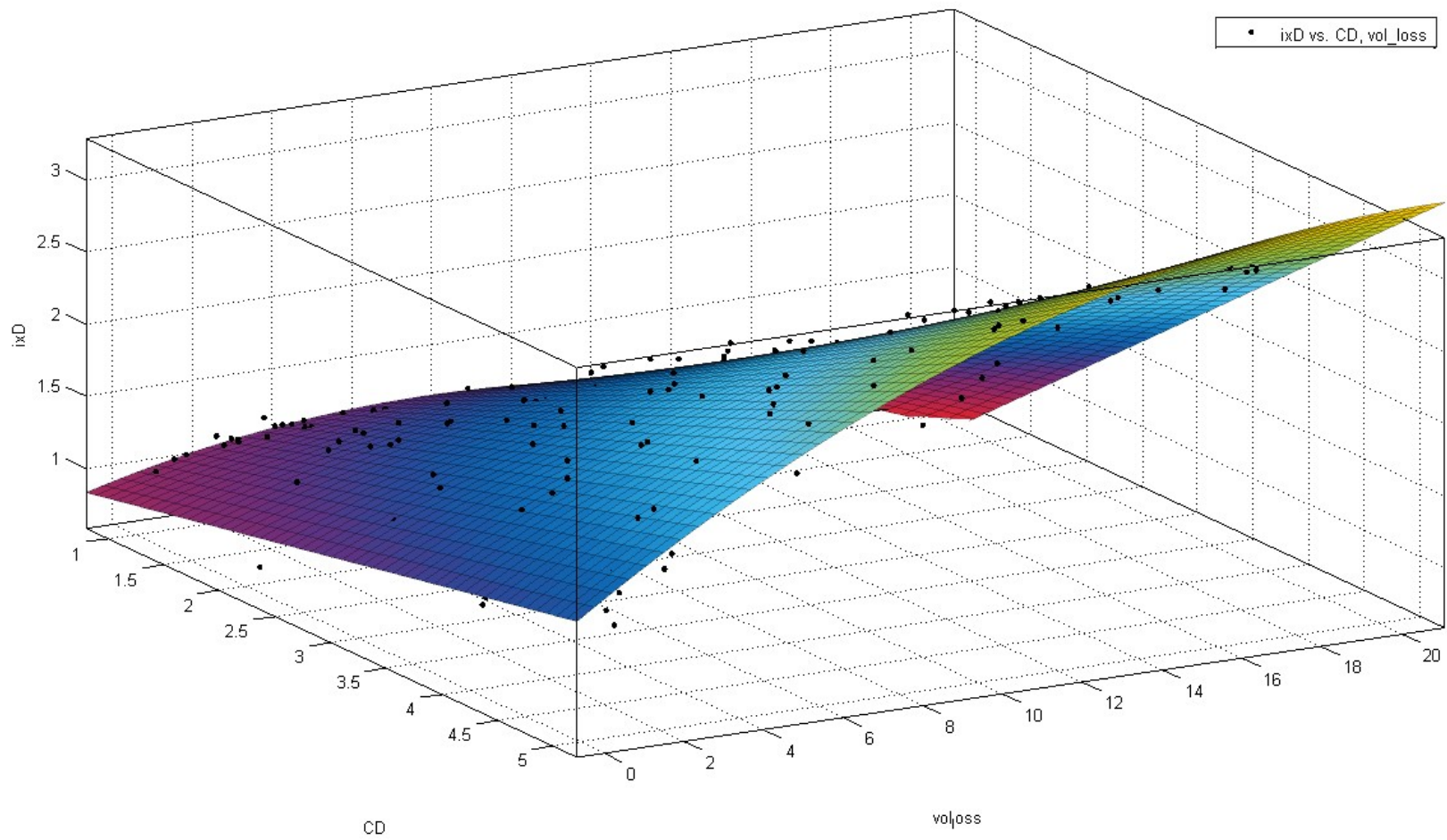


Figure 0-5 *MATLAB* surface fit for method 2 twin tunnel settlement at pre-collapse

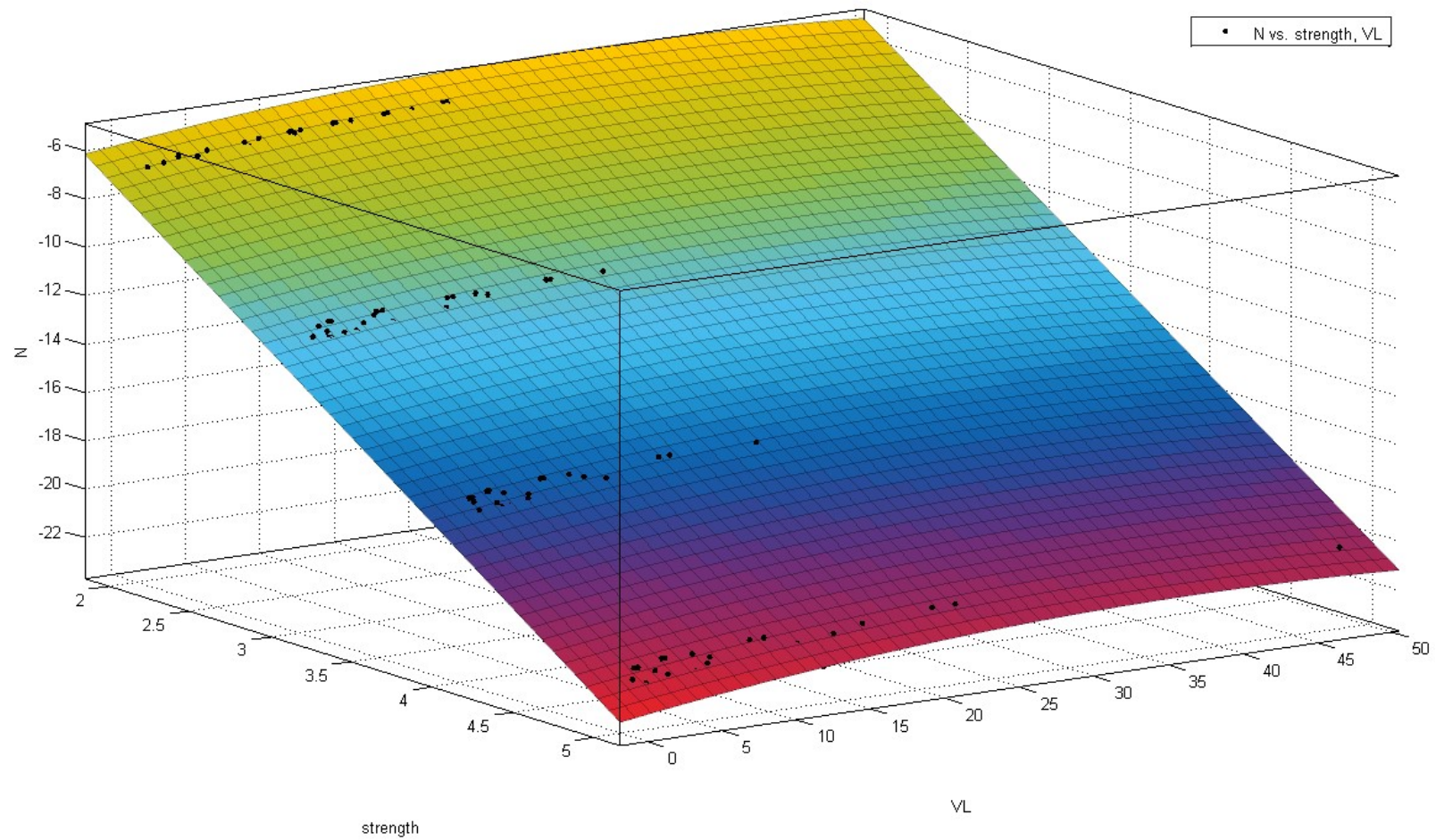


Figure 0-6 Typical *MATLAB* surface fit for twin tunnel stability at pre-collapse ( $C/D=5$ )